VOLUME 78 NOVEMBER 7, 1974 NUMBER 23

JPCHAx

THE JOURNAL OF PHYSICAL CHEMISTRY

PUBLISHED BIWEEKLY BY THE AMERICAN CHEMICAL SOCIETY

THE JOURNAL OF

PHYSICAL CHEMISTRY

AMERICAN CHEMICAL SOCIETY, *1155 Sixteenth St., N.W., Washington, D. C. 20036*

Books and Journals Division

JOHN K CRUM *Director*
RUTH REYNARD *Assistant to the Director*

CHARLES R. BERTSCH *Head, Editorial Processing Department*
D. H. MICHAEL BOWEN *Head, Journals Department*
BACIL GUILEY *Head, Graphics and Production Department*
SELDON W. TERRANT *Head, Research and Development Department*

 Published biweekly by the American Chemical Society at 20th and Northampton Sts., Easton, Pa. 18042. Second-class postage paid at Washington, D. C., and at additional mailing offices.

All manuscripts should be sent to *The Journal of Physical Chemistry*, Department of Chemistry, University of Minnesota, Minneapolis, Minn. 55455.

Additions and Corrections are published once yearly in the final issue. See Volume 77, Number 26 for the proper form.

Extensive or unusual alterations in an article after it has been set in type are made at the author's expense, and it is understood that by requesting such alterations the author agrees to defray the cost thereof.

The American Chemical Society and the Editor of *The Journal of Physical Chemistry* assume no responsibility for the statements and opinions advanced by contributors.

Correspondence regarding accepted copy, proofs, and reprints should be directed to Editorial Processing Department, American Chemical Society, 20th and Northampton Sts., Easton, Pa. 18042. Department Head: CHARLES R. BERTSCH. Assistant Department Head: MARIANNE C. BROGAN. Assistant Editor: CELIA B. MCFARLAND. Editorial Assistant: JOSEPH E. YURVATI.

Advertising Office: Centcom, Ltd., 50 W. State St., Westport, Conn. 06880.

Business and Subscription Information

Send all new and renewal subscriptions *with payment* to: Office of the Controller, 1155 16th Street, N.W., Washington, D. C. 20036. Subscriptions should be renewed promptly to avoid a break in your series. All correspondence and telephone calls regarding changes of address, claims for missing issues, subscription service, the status of records, and accounts should be directed to Manager, Membership and Subscription Services, American Chemical Society, P.O. Box 3337, Columbus, Ohio 43210. Telephone (614) 421-7230.

On changes of address, include both old and new addresses with ZIP code numbers, accompanied by mailing label from a recent issue. Allow four weeks for change to become effective.

Claims for missing numbers will not be allowed (1) if loss was due to failure of notice of change in address to be received before the date specified, (2) if received more than sixty days from date of issue plus time normally required for postal delivery of journal and claim, or (3) if the reason for the claim is "issue missing from files."

Subscription rates (1974): members of the American Chemical Society, $20.00 for 1 year; to nonmembers, $60.00 for 1 year. Those interested in becoming members should write to the Admissions Department, American Chemical Society, 1155 Sixteenth St., N.W., Washington, D. C. 20036. Postage to Canada and countries in the Pan-American Union, $5.00; all other countries, $6.00. Air freight rates available on request. Single copies for current year: $3.00. Rates for back issues from Volume 56 to date are available from the Special Issues Sales Department, 1155 Sixteenth St., N.W., Washington, D. C. 20036.

Subscriptions to this and the other ACS periodical publications are available on microfilm. Supplementary material not printed in this journal is now available in microfiche form on a current subscription basis. For information on microfilm or microfiche subscriptions, write Special Issues Sales Department at the address above.

Notice to Authors last printed in the issue of June 6, 1974

THE JOURNAL OF

PHYSICAL CHEMISTRY

Volume 78, Number 23 November 7, 1974

JPCHAx 78(23) 2309-2416 (1974)

ISSN 0022-3654

COMMUNICATIONS TO THE EDITOR

■ Supplementary and/or miniprint material for this paper is available separately, in photocopy or microfiche form. Ordering information is given in the paper.

* In papers with more than one author, the asterisk indicates the name of the author to whom inquiries about the paper should be addressed.

AUTHOR INDEX

ANNOUNCEMENT

On the last two pages of this issue you will find reproduced the table of contents of the October 1974 issue of the Journal of Chemical and Engineering Data.

THE JOURNAL OF
PHYSICAL CHEMISTRY

VOLUME 78, NUMBER 23 NOVEMBER 7, 1974

Rice–Ramsperger–Kassel–Marcus Theory Applied to Decomposition of Hot Atom Substitution Products. c-C_4H_7T and c-C_4D_7T

C. C. Chou

Department of Chemistry, University of California, Irvine, California 92664

and William L. Hase*[1]

Department of Chemistry, Wayne State University, Detroit, Michigan 48202

(Received January 31, 1974; Revised Manuscript Received July 25, 1974)

Publication costs assisted by the Petroleum Research Fund

The RRKM theory has been used to interpret experimental measurements of the decomposition of excited c-C_4H_7T and c-C_4D_7T following T-for-H and T-for-D substitution in recoil tritium experiments. An expression is obtained for calculating the pressure dependence of decomposition to stabilization. It is found that (1) rotational effects are unimportant for either c-C_4H_7T or c-C_4D_7T decomposition; (2) when the excitation function for T-for-H substitution in c-C_4H_8 is approximated by one derived from molecular beam experiments, the displaced H atoms carry on the average 40% or more of the incident T translational energy; (3) for similar T-for-H and T-for-D excitation functions, displaced H and D atoms have nearly the same average kinetic energies.

Introduction

The decomposition of excited molecules and radicals formed by hot atom substitution and addition reactions has been widely observed and has provided valuable information about the preceding hot atom reactions.[2] Measurements of the pressure dependence of the decomposition to stabilization ratios for hot atom substitution products have been combined with the RRKM (Rice-Ramsperger-Kassel-Marcus) theory to yield values for the median excitation energies of the hot substitution products.[2,3] It has been found that more than 250 kcal/mol may be deposited on the substitution product and the median excitation energies for the different systems are not identical. A detailed explanation of those observations requires an understanding of the dynamics of the substitution process. For the molecular dynamics of T-for-H and T-for-D substitution reactions of recoil tritium atoms with c-C_4H_8 and c-C_4D_8, Rowland and coworkers[4,5] have made the following conclusions and hypotheses from the pressure dependence of product distributions and RRKM calculations: (a) a broad excitation with a median energy of 115 ± 23 kcal/mol for both c-C_4H_7T and c-C_4D_7T, (b) the kinetic energies of the displaced H and D atoms are nearly equivalent, and (c) the displaced and D atoms emerge from the substitution reaction with small amounts of energy.

Bunker[6] has shown hot atom substitution may produce a species with large amounts of angular momentum, and the RRKM expression appropriate for thermal systems must be modified for treating the decomposition of hot atom substitution products. He found inclusion of rotational effects (angular momentum) in the RRKM calculations could in some cases greatly change the calculated rates and explain some seemingly paradoxical experimental observations. In particular he found the secondary decomposition of CH_2TNC[7] and $CH_3CF_2{}^{18}F$,[3] which appeared to display non-RRKM behavior, is in accord with the RRKM theory if rotational effects are included. Bunker also found under certain circumstances the RRKM calculations may be a useful source of information about the dynamics of primary substitution and addition reactions.

In this paper we have extended Bunker's formulation so the decomposition to stabilization ratio of the substitution product may be calculated as a function of pressure. An analysis is then made of experimental measurements of c-C_4H_7T decomposition. This molecule has provided one of

the best and most important examples of unimolecular reaction following hot atom substitution.

The original motivation for this study was to see if a more complete analysis, one which includes rotational effects, would alter any of the earlier conclusions reached regarding the cyclobutane systems. However, it was also found that specific information about the substitution reaction, gained from molecular beam experiments,[8] could be used to correlate the experimental data for c-C_4H_7T decomposition with several dynamical quantities.

Theory

The theoretical formulation we use is an extension of the one presented by Bunker.[6] Parts of it are described below for completeness and clarity.

In a hot atom substitution reaction the average angular momentum and resulting rotational energy retained on each molecular axis of the polyatomic product are

$$L_i = b(E_s/2)^{1/2}\left\{m_R^{1/2} - [(1-f)m_A m_P/(m_A + m_P)]^{1/2}\right\}$$
$$E_{ri} = L_i^2/2L_i \quad i = x, y, \text{ or } z \tag{1}$$

where b is the impact parameter, E_s is the translational energy of the hot atom, m_R, m_A, and m_P are the masses of the hot atom, displaced atom, and product, respectively, and f is the fraction of E_s left behind on the product. If there is no A–P relative translation, $f = f_{max} = 1 - m_R/(m_A + m_P)$.

The vibrational-internal rotational energy of the energized molecule (*) and critical configuration (+) are

$$E_{vr}^{*} = fE_s + E_{vr}^{th} - \sum_i E_{ri}^{*}$$
$$E_{vr}^{+} = fE_s + E_{vr}^{th} - \sum_i E_{ri}^{+} - E_0 \tag{2}$$

with E_0 the threshold energy for the unimolecular decomposition of the energized molecule and E_{vr}^{th} the thermal vibrational energy of the product molecule. Substituting eq 1 into 2 yields

$$E_{vr}^{*} = fE_s + E_{vr}^{th} - b^2E_s(1/I_x^{*} + 1/I_y^{*} + 1/I_z^{*})\alpha/4$$
$$E_{vr}^{+} = fE_s + E_{vr}^{th} - E_0 - b^2E_s(1/I_x^{+} + 1/I_y^{+} + 1/I_z^{+})\alpha/4$$
$$\alpha^{1/2} = m_R^{1/2} - [(1-f)m_A m_P/(m_A + m_P)]^{1/2} \tag{3}$$

These energies were inserted into standard RRKM expressions[9] to calculate unimolecular rate constants. The semiclassical Whitten–Rabinovitch approximation was employed to calculate the necessary sum and density terms.[10]

The total decomposition (D) and stabilization (S) of the product molecule (P*) depends on the competition between the processes

$$P^* \xrightarrow{k(f,b,E_s)} \text{decomposition (D)} \quad \text{fragments}$$
$$\xrightarrow{\omega} P \quad (S) \tag{4}$$

where ω is the collision deactivation probability. For a fixed value of f, the ratio of decomposition to stabilization is

$$D/S = \left[\int_{E_s}\int_b \frac{k(b,E_s)}{k(b,E_s)+\omega} P_r(b)P(b)dbP(E_s)\sigma(E_s)v(E_s)dE_s\right] / \left[\int_{E_s}\int_b \frac{\omega}{k(b,E_s)+\omega} P_r(b)P(b)dbP(E_s)\sigma(E_s)v(E_s)dE_s\right] \tag{5}$$

where $P_r(b)$ and $P(b)$ are the reaction probability (opacity function) and collision probability, and $P(E_s)$, $\sigma(E_s)$, and $v(E_s)$ are the relative translational energy distribution, excitation function, and velocity, respectively. This expression was used to calculate the theoretical D/S values.

Lin and Laidler[11] have performed an extensive RRKM analysis of the thermal decomposition of cyclobutane. Using energetic and mechanistic arguments they hypothesized that cyclobutane decomposes *via* a tetramethylene diradical. A recent *ab initio* calculation[12] also suggests that this is the reaction path. There is some question as to the location of the critical configuration along the reaction coordinate. Thermodynamic arguments have been presented which suggest that the critical configuration is located between the biradical and the two ethylene product molecules.[13] However, earlier thermodynamic arguments[14] and extended Hückel calculations[15] indicate that the location of the critical configuration is between the molecule and biradical.

The structure for the critical configuration used in our calculations is intermediate of those of the molecule and biradical. The four C atoms lie in a plane with one C–C bond extended; *i.e.*, a trapezoidal structure similar to that of eclipsed n-butane. The three unextended C–C bonds have a length of 1.55 Å. The two expanded C–C–C angles are 110°. Skeletal deformations and CH_2 motions were lowered in the critical configuration to yield Arrhenius parameters in agreement with the measured ones.[16] Therefore, the RRKM model is calibrated to the thermal decomposition rates. A ring deformation was taken as the reaction coordinate. The frequencies for c-C_4H_7T and c-C_4D_7T were derived from those of c-C_4H_8 and c-C_4D_8[17] by an approximate application of the Teller–Redlich product rule.[18] Frequencies for c-C_4H_8 and c-C_4D_8 were grouped according to the type of mode (stretch, bend, wag, twist, etc.) so the geometric mean of the frequencies remained the same. The C–T stretching frequency was then derived from the C–H (or C–D) stretch group by the square root of the C–T to C–H (or C–D) reduced mass ratios. A CH_2 (or CD_2) wag, twist, rock, and deformation were then varied proportionally to account for the remaining frequency difference specified by the Teller–Redlich product rule. In Table I are presented the molecular and critical configuration frequencies and other pertinent structural and energy parameters.

Cyclobutane may also decompose by the simultaneous cleavage of two C–C bonds to produce two ethylene molecules. The importance of this process was estimated by using the critical configuration structures in Table I and the activation energy of 156 kcal/mol, which was determined by *ab initio* calculations.[12] It was found that decomposition by the simultaneous cleavage of two C–C bonds is slower than decomposition *via* the tetramethylene diradical by 10, 7, 4, and 3 orders of magnitude at 200, 250, 300, and 350 kcal/mol of vibrational excitation of the cyclobutane molecules, respectively. These numbers should be representative since there is little reason to expect a significantly looser critical configuration structure (larger A factor) for the mechanism involving simultaneous cleavage of the two C–C bonds. In fact, one might expect a tighter crit-

TABLE I: Energy and Structural Parameters for the Decomposition of c-C_4H_7T and c-C_4D_7T

Frequencies[a]	
Molecule	Critical configuration
c-C_4H_7T	
2935(7)	2935(7)
1695(1)	1695(1)
1450(3)	1450(3)
1245(3)	1245(1), *628*(2)
1230(3)	1230(1), *624*(2)
1150(1)	1150(1)
1010(1)	*508*(1)
990(1)	990(1)
975(1)	975(1)
926(4)	926(3), rc[b]
720(3)	720(1), *364*(2)
570(1)	570(1)
193(1)	*96*(1)
$I_x^* = 48.6$[c] $I_y^* = 54.5$ $I_z^* = 87.2$	
$I_x^+ = 81.3$ $I_y^+ = 48.9$ $I_z^+ = 113.8$	
$E_0 = 59.5$ kcal/mol $E_a = 63.2$ kcal/mol[d]	
$A = 7.0 \times 10^{15}$ sec^{-1}	
c-C_4D_7T	
2170(7)	2170(7)
1770(1)	1770(1)
1070(3)	1070(3)
1060(3)	1060(1), *521*(2)
980(1)	980(1)
970(1)	970(1)
900(3)	900(1), *443*(2)
873(1)	*428*(1)
825(1)	825(1)
790(4)	790(3), rc[b]
545(3)	545(1), *267*(2)
500(1)	500(1)
151(1)	*74*(1)
$I_x^* = 66.3$[c] $I_y^* = 69.2$ $I_z^* = 107.6$	
$I_x^+ = 98.8$ $I_y^+ = 66.1$ $I_z^+ = 136.3$	
$E_0 = 60.6$ kcal/mol $E_a = 64.1$ kcal/mol[d]	
$A = 9.4 \times 10^{15}$ sec^{-1}	

[a] Frequencies are in cm^{-1}. Those that change in the critical configuration are italicized. [b] rc = reaction coordinate. [c] Moments of inertia in units of amu Å^2. [d] The Arrhenius parameters are calculated for 722°K.

ical configuration structure due to the simultaneous formation of two C=C bonds and the above factors would then represent lower limits. Therefore, since the largest degree of internal excitation of the cyclobutane molecules considered in this paper is less than 350 kcal/mol only the biradical mechanism was included in the calculations.

In the derivation of eq 5 it was assumed the collision deactivation probabilities can be calculated from gas kinetic cross sections. Data collected from thermal[19] and chemical activation experiments[20-24] indicate that this assumption is valid for molecules as large as cyclobutane. The chemical activation studies show that C_4 hydrocarbons and halocarbons transfer on the average ~10 kcal/mol from molecules which contain ~90–115 kcal/mol[20-22] of vibrational excitation. Though this amount of energy transfer only reduced the unimolecular rate constants by an order of magnitude, it was sufficient to yield a unit gas kinetic collisional deactivation efficiency at pressures where stabilization competes with decomposition. Only at lower pressures when decomposition overwhelmed stabilization (D/S > 10) did collisional inefficiency become evident.

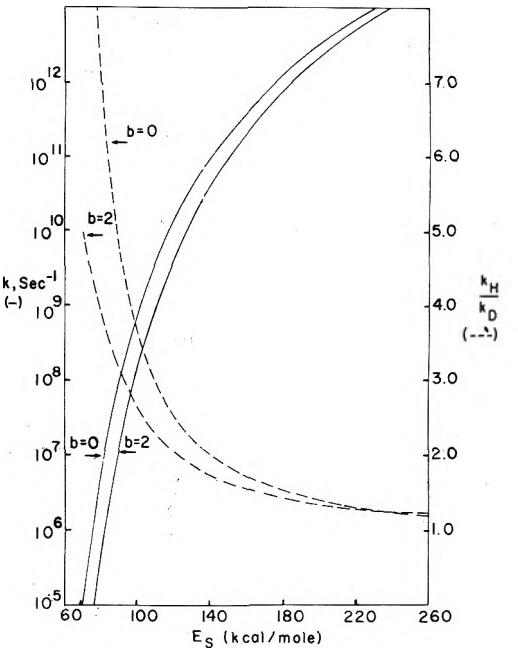

Figure 1. $k_{c\text{-}C_4H_7T}$ (—) and k_H/k_D (- - -) *vs.* E_s for $f = f_{max}$.

Nevertheless, there remains an uncertainty in using collision frequencies in eq 5 even if comparisons are made with experiments where decomposition and stabilization are competitive which is the case for this study. As the degree of internal excitation is increased the decrease in the unimolecular rate constant is smaller for equal amounts of energy transfer. For cyclobutane the rate constant changes by a factor of 8 at 100 kcal/mol but by only a factor of 1.5 at 200 kcal/mol, for an energy change of 10 kcal/mol (Figure 1). Though a factor of 8 is sufficient for a unit deactivation efficiency 1.5 is not. However, there is little justification for assuming the average amount of energy transferred remains constant for all excitation energies. Since vibrational levels become denser at greater degrees of excitation the probability of energy transfer should increase. This effect is seen when the chemical activation studies[20-24] are compared with photochemical experiments[25,26] which produce molecules with much smaller amounts of vibrational excitation. This result combined with that of the chemical activation experiments suggests the unit deactivation efficiency may be physically realistic for this cyclobutane study. However, even if not completely valid, it provides the only tractable approach, since very little is known about intermolecular energy transfer at energies as high as those attained in hot atom substitution reactions. The effect of using other deactivation models on the calculational results is discussed later.

That hot atom substitution products can possess significant amounts of rotational energy may add an additional complication for some studies since less is known about rotational energy transfer than vibrational energy transfer at large degrees of excitation. This problem has recently been discussed in reference to the isomerization of CH_2TNC.[27] However, for cyclobutane decomposition this complication is not important since the substitution reaction produces only a small amount of rotational excitation (see the following section).

In calculating the collision deactivation probabilities a diameter of 5.0 Å was used for all isotopic cyclobutanes. The oxygen and helium present in the experiments (less

than 20%) were assumed to make no contribution to the collision deactivation probability. The resulting values at 300 K are $\omega_{c\text{-}C_4H_7T} = 1.18 \times 10^7$ Torr^{-1} sec^{-1} and $\omega_{c\text{-}C_4D_7T} = 1.14 \times 10^7$ Torr^{-1} sec^{-1}.

Results and Discussion

A. Unimolecular Rate Constants. Calculated rate constants for the decomposition of c-C_4H_7T for $f = f_{max}$ and $f = 0.5$ are displayed in Figures 1 and 2, respectively. Also shown are the ratios of the decomposition rate constants for c-C_4H_7T and c-C_4D_7T, k_H/k_D.

In contrast to the calculations for CH_2TNC isomerization,[6] the rate constants for c-C_4H_7T and c-C_4D_7T are only slightly dependent on the impact parameter. Experimental values of D/S for c-C_4H_7T and c-C_4D_7T have been measured in the 50–850-Torr pressure range.[5] Over this range, rate constants of 6×10^8–1×10^{10} sec^{-1} will be competitive with collisional stabilization. For this large variance in rate constants, $k(b = 0)/k(b = 2$ Å) for c-C_4H_7T only varies from 5 to 3 for $f = f_{max}$ and 3.5 to 2.5 for $f = 0.5$. In the liquid phase where only molecules with rate constants $>10^{12}$ sec^{-1} decompose, rotational effects are minimal; $k(b = 0)/k(b = 2$ Å) is <1.6 for both $f = f_{max}$ and $f = 0.5$. This insensitivity to b is primarily a result of the small amount of rotational excitation. The percentage of fE_s which is converted to rotational excitation is as follows for $b = 2$ Å: c-C_4H_7T, 12.1% ($f = f_{max}$) and 10.7% ($f = 0.5$); c-C_4D_7T, 8.4% ($f = f_{max}$) and 4.3% ($f = 0.5$).

The k_H/k_D ratio shows a normal isotope effect; *i.e.*, decreasing with increasing energy. However, the ratio is dependent on the choice of f and b, and is smallest for $f = 0.5$ and $b = 2$ Å.

By fitting a monoenergetic RRKM calculation to the experimental results for c-C_4H_7T at D/S = 1,[2b] a median excitation energy of 115 ± 23 kcal/mol was derived for c-C_4H_7T molecules formed by hot atom substitution. This calculation neglected rotational effects and can be compared with ours at $b = 0$. By the above definition, we find a median excitation energy of 100 kcal/mol at $b = 0$ independent of f. This result is in essential agreement with the earlier calculation.[28] There is very little change in the median excitation energy when substitution occurs at $b = 2$ Å; the median excitation energies are 107 and 106 kcal/mol for f equal to f_{max} and 0.5, respectively. The difference between the result at $b = 0$ and $b = 2$ Å arises from the fact rotational excitation is not as effective as vibrational excitation in inducing unimolecular decomposition. That the difference is only minor, results from the small fraction of rotational energy present in the excited molecules.

The median excitation energy is determined by the excitation function, opacity function, translational energy distribution of the hot atoms, and the fraction of energy carried by the displaced atoms. In the following sections those quantities are discussed with respect to the pressure dependence of decomposition to stabilization in the T + c-C_4H_8 and T + c-C_4D_8 systems.

B. Dynamics of T-for-H Substitution in Cyclobutane. An exact calculation of D/S requires an integration over b, E_s, and f. For a fixed value of f the form of the integration is given by eq 5, in which information is required about $\sigma(E_s)$, $P(E_s)$, and $P_r(b)$. The function $\sigma(E_s)P(E_s)$ defines the relative yield of hot atom substitution product as a function of E_s and $P_r(b)$ determines how the internal energy of the substitution product is partitioned between external rotational and vibrational energy.

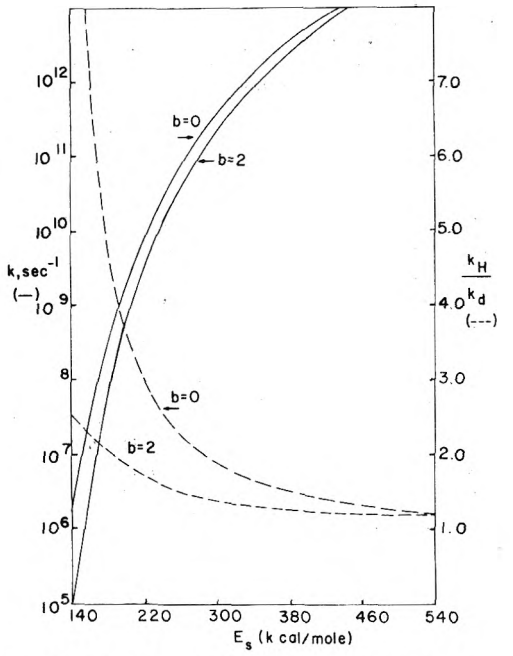

Figure 2. $k_{c\text{-}C_4H_7T}$ (—) and k_H/k_D (- - -) *vs.* E_s for $f = 0.5$.

Excitation functions for T-for-H substitution have recently been determined by different techniques. Using six-body Monte Carlo trajectory methods, there have been two separate determinations of the T + CH_4 and CD_4 excitation functions.[29,30] Though there are several differences between the results of these two investigations, they both show that the T-for-H substitution excitation function peaks between 150 and 200 kcal/mol and is still appreciable at $E_s = 300$ kcal/mol. From molecular beam studies LeRoy, *et al.*,[8] found excitation functions of similar shape for T-for-H substitution in cyclopentane, cyclohexane, *n*-hexane, and *n*-butane. Specifically, they found a reaction threshold at 35 ± 10 kcal/mol,[31] a maximum in $\sigma(E_s)$ at 210–280 kcal/mol, and a slow decline at higher energies. Though substitution still appeared to be appreciable at 350–460 kcal/mol, the scatter of the data was such that this also represents a lower bound at which substitution no longer occurs.

Unfortunately, there have not been any determinations of the T-for-H or T-for-D excitation function for cyclobutane. However, the above studies indicate that the substitution excitation functions are similar for different reactant molecules. In particular, those for cyclopentane and cyclohexane are nearly identical in shape. Therefore, the cyclopentane and cyclohexane excitation functions should provide a meaningful form for the cyclobutane excitation function, and were fitted to give the following expression for $\sigma(E_s)$ in cyclobutane

$$\sigma(E_s) \propto (E_s - 35.0)\exp[0.0049(35.0 - E_s)] \qquad 35.0 \leq E_s \leq E_s^{max} \tag{6}$$

$$\sigma(E_s) = 0.0 \qquad E_s^{max} < E_s < 35.0$$

Values for E_s^{max} equal to 350 and 700 kcal/mol were chosen in accord with the molecular beam results and in order to interpret the D/S measurements with different energy ranges.

Using results from neutron slowing theory, Estrup and Wolfgang[32] formulated the kinetic theory of hot reactions to interpret product yields in nuclear recoil studies. For

this theory, the relative translational energy distribution is

$$P(E_s) \propto 1/E_s^{3/2} \quad (7)$$

in the limiting case of no hot atom reaction. For a reactive system, such as T + c-C_4H_8, there is a depletion of hot atoms at large values of E_s which decreases $P(E_s)$ at small E_s. In addition to this effect, the above form of $P(E_s)$ is altered by the high probability of grazing collisions[33] which results in very little energy transfer. Since the kinetic theory assumes a hard sphere model for energy moderation the effect of near elastic grazing collisions will be to enhance $P(E_s)$ at large E_s. Both the hot atom depletion and grazing collisions will cause a net flattening or leveling of the distribution given in (7). Therefore (7) provides a limit for our calculations and other forms were chosen for $P(E_s)$ using

$$P(E_s) \propto 1/E_s^n \qquad n < 3/2 \quad (8)$$

When a more precise excitation function has been determined and the nature of energy moderation has been evaluated, an exact form for $P(E_s)$ may be used.[34]

The opacity function, $P_r(b)$, is related to the excitation function by

$$\sigma(E_s) = 2\pi \int_0^{b_{max}} P_r(b) b \, db \quad (9)$$

where b_{max} is the impact parameter where $P_r(b)$ falls to zero. The molecular beam experiments are unable to provide information about $P_r(b)$. However, the weak dependence of the unimolecular rate constants on b suggests that the actual form of $P_r(b)$ is not important in fitting the experimental D/S values.[35] The plots in Figure 3 show this is true. Representing $P_r(b)$ by a δ function at 2 Å,[36] an excellent fit to the experimental data is given by $P(E_s) = 1/E_s$, E_s^{max} = 350 kcal/mol, and f = 0.53. Varying the form of $P_r(b)$ has only a very small effect on the calculated curve. The forms

$$P_r(b) = 1.0 \qquad 0 < b \leq 2.0 \text{ Å}$$
$$= 0 \qquad 2.0 \text{ Å} < b \quad (10)$$

and $P_r(b)$ equal to a δ function at 1 Å give nearly identical results and will fit the experimental points by decreasing f by only 10%. As shown in the following paragraphs, this uncertainty in f is very small given the uncertainties in $P(E_s)$ and $\sigma(E_s)$. Therefore, the actual form of $P_r(b)$ and magnitude of $\sigma(E_s)$ are unimportant in fitting the experimental results. As discussed previously, this is due to the small amount of rotational excitation produced in the substitution reaction.

In Figure 4 are displayed results using different forms for $P(E_s)$, where E_s^{max} = 350 kcal/mol and f is varied in order to fit the data. It is seen that the experimental data are precise enough to allow one to distinguish between the fit for the different $P(E_s)$ expressions. At E_s^{max} = 700 kcal/mol, $P(E_s) = 1.0$ gives a fit to the data nearly identical with the one provided by $P(E_s) = 1/E_s$ at E_s^{max} = 350 kcal/mol. That the relative translational energy distributions which give the best fit are flatter than $1/E_s^{3/2}$ agrees with the previous discussion. In Table II are listed the values of f which fit the experimental c-C_4H_7T D/S values for $P(E_s)$ equal to $1/E_s^{3/2}$, $1/E_s$, and 1.0. Since the shape of the calculated D/S curves is not significantly changed for alternative $P_r(b)$ formulations, varying the yield, $P(E_s)\cdot\sigma(E_s)v(E_s)$, *vs.* E_s is the important adjustment in fitting the experimental data. Therefore, if a complete and exact excitation function was available, these calculations would provide a value for f and a general form of the hot atom translational energy distribution which best fits the data.

TABLE II: Values of the Parameter f that Fit the Experimental Values of D/S for c-C_4H_7T[a]

E_s^{max}, kcal/mol	f		
	$P(E_s) = 1/E_s^{3/2}$	$P(E_s) = 1/E_s$	$P(E_s) = 1.0$
350	0.62	0.53[b]	0.45
700	0.48	0.39	0.28[b]

[a] Calculations were performed with $P_r(b)$ represented by a δ function peaked at 2 Å. If $P_r(b)$ is represented by a δ function at 1 Å or a step function, eq 10, the values for f are approximately 10% smaller. [b] Best fit.

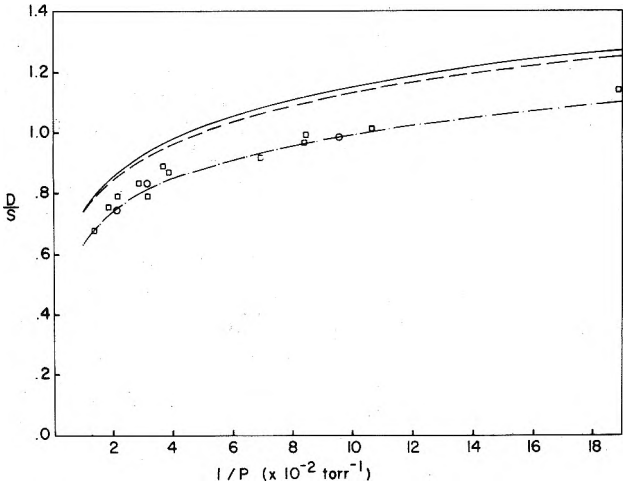

Figure 3. Calculated curves of D/S *vs.* $1/P$ for c-C_4H_7T. f = 0.53, $P(E_s) = 1/E_s$, and E_s^{max} = 350 kcal/mol for each of the curves. $P_r(b)$ given by eq 10 (—), $P_r(b) = \delta$ function at b = 1 Å (- - -), and $P_r(b) = \delta$ function at b = 2 Å (- · - ·): O, c-C_4H_7T from c-C_4H_8 and c-C_4D_8 mixtures, ref 5; □, c-C_4H_7T from c-C_4H_8, ref 4.

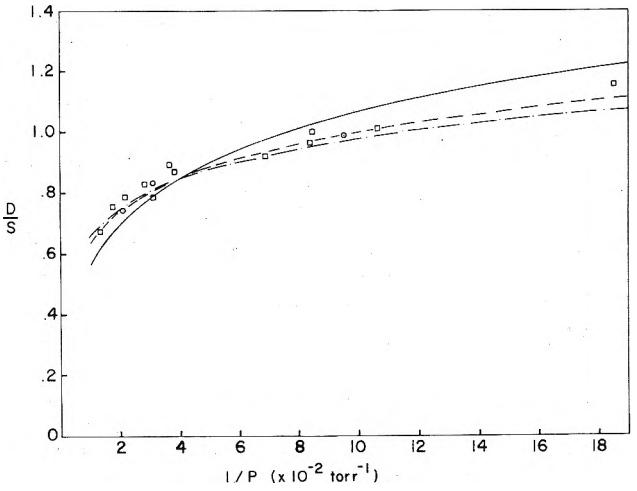

Figure 4. Best fit curves to D/S *vs.* $1/P$ for c-C_4H_7T by varying f. $P_r(b) = \delta$ function at b = 2 Å and E_s^{max} = 350 kcal/mol for each of the curves. $P(E_s) = 1.0$ (—), $P(E_s) = 1/E_s$ (- - -), and $P(E_s) = 1/E_s^{3/2}$ (- · - ·). Experimental points same as Figure 3.

The above calculations show that the displaced H atom carries on the average 40% or more of the incident T translational energy. This result is contrary to the hypothesis that H and D atoms emerge from T substitution reactions in cyclobutane with low translational energies.[5] However, it

appears to be consistent with two recent studies. An RRKM analysis of CH_2TNC isomerization data indicated that the substituted H atom in the T + CH_3NC reaction carries ~25% of the incident translational energy.[6] Results from a Monte Carlo trajectory study of the T + CH_4 reaction show that at an incident translational energy of 200 kcal/mol the average fraction of this energy carried by the displaced H atom is 0.24, with a largest fraction of 0.62.[37] H-atom substitution in CH_4 and CH_3NC should entail considerably more coupling between the internal modes than in *c*-C_4H_8 due to its rigid ring structure; *e.g.*, the configuration of the saddle point in the T + CH_4 substitution is thought to be trigonal bipyramid, while such a structure is impossible for H-atom substitution in T + c-C_4H_8. This increased coupling may result in a greater amount of energy deposition in the hot-atom product, resulting in the displaced atom carrying a smaller fraction of the incident translational energy. It should be noted that the calculated f values for T-for-H substitution in cyclobutane are similar to those derived from a three-body T + CH_4 trajectory study in which CH_3 is represented by an atom of mass 15 amu.[38]

In addition to the uncertainty in $\sigma(E_s)$ the remaining major uncertainty is in the model for collisional deactivation. For the calculations presented here a model assuming unit deactivation efficiencies was used. The effect of using a model which yields less than unit efficiencies would be to increase decomposition relative to stabilization. Therefore, in order to fit the D/S experimental data the parameter f would have to be decreased with respect to the values derived here (Table II).

The results of calculations assuming an identical excitation function for T-for-D substitution in c-C_4D_8 as that used above for T-for-H substitution in *c*-C_4H_8 are shown in Figure 5. It is seen the value of f which fits the T-for-H data overestimates the *c*-C_4D_7T experimental D/S values by only 10% and if f is lowered by a small fraction from 0.53 to 0.51 the calculated curve gives an excellent fit to the experimental data. Therefore, we find, as did Hosaka and Rowland,[5] if T-for-H and T-for-D substitution in cyclobutane have similar excitation functions the H and D atoms displaced by the recoil tritium atoms have nearly the same average kinetic energies. A verification of this assumption awaits a determination of the T-for-D excitation function in *c*-C_4D_8. However, nuclear recoil moderator studies[39] and Monte Carlo trajectory studies[29,30] suggest that T-for-H and T-for-D substitution processes may have similar excitation functions.

Summary

We have presented an RRKM analysis of cyclobutane hot atom chemistry which is more comprehensive than previous studies. The calculations show that experimental measurements of decomposition and stabilization of hot substitution products can provide new and important information about the dynamics of hot atom substitution reactions. The results of this study support some conjectures which have been made about the dynamics and mechanisms of recoil tritium atom substitution reaction with c-C_4H_8 and *c*-C_4D_8, but raise some serious questions about other earlier conjectures.

Specifically, the results of our study support the following: (1) c-C_4H_7T is formed with a broad spectrum of excitation energies; (2) 60% or less of the T energy is deposited on *c*-C_4H_7T product molecules (This percentage is smaller than that found for T-for-H substitution in CH_4 and CH_3NC and is probably due to a smaller vibrational disturbance of the *c*-C_4H_8 molecular structure.); (3) *c*-C_4H_7T and *c*-C_4D_7T decompositions are not centrifugally controlled (This is a result of the small amount of rotational excitation found in *c*-C_4H_7T and *c*-C_4D_7T (less than 15%).); (4) when T-for-H and T-for-D substitution are assumed to have identical excitation functions, it is found the displaced H and D atoms have nearly the same average energies. However, this does not require the average energies be small.

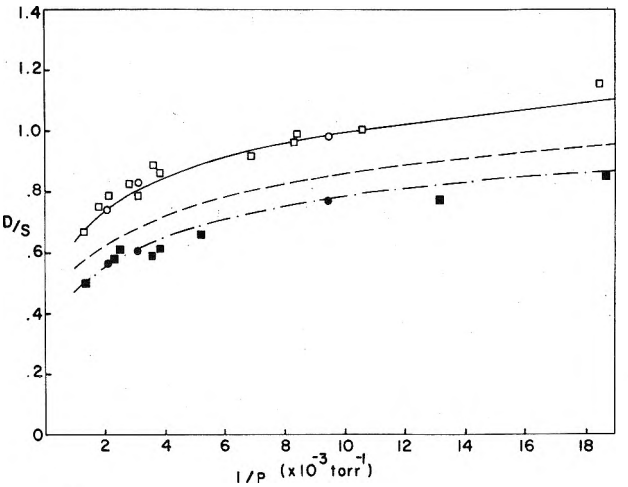

Figure 5. Calculated curves of D/S *vs.* 1/*P*. *c*-C_4H_7T: $\sigma(E_s)$ from beam experiments, $f = 0.53$, $P(E_s) = 1/E_s$, $E_s^{max} = 350.0$ kcal/mol^{-1}, and $P_f(b) = \delta$ function at $b = 2$ Å (—). *c*-C_4D_7T: same parameters as above (- - -). *c*-C_4D_7T: same parameters as above except $f = 0.51$ (- · - ·): O and □, experimental points same as in Figure 3; ●, *c*-C_4D_7T from *c*-C_4H_8–*c*-C_4D_8 mixtures, ref 5; ■ *c*-C_4D_7T from *c*-C_4D_9, ref 4.

Acknowledgment. This work was supported by the National Science Foundation and AEC Contract No. AT(04-3)-34, Agreement 126. Partial support was also provided by the donors of the Petroleum Research Fund, administered by the American Chemical Society, and the Research Corporation. W.L.H. wishes to thank the Wayne State University for a Summer Research Fellowship.

References and Notes

(1) Part of this research was performed while W. L. Hase was at the University of California, Irvine.
(2) (a) F. S. Rowland, *MTP (Med. Tech. Publ. Co.) Int. Rev. Sci., Phys. Chem.*, **9**, 109 (1972); (b) F. S. Rowland, *Proc. Int. Sch. Phys. "Enrico Fermi,"* **No. 44**, 127 (1970).
(3) K. A. Krohn, N. J. Parks, and J. W. Root, *J. Chem. Phys.*, **55**, 5785 (1971).
(4) E. K. C. Lee and F. S. Rowland, *J. Amer. Chem. Soc.*, **85**, 897 (1963).
(5) A. Hosaka and F. S. Rowland, *J. Phys. Chem.*, **75**, 3781 (1971).
(6) D. L. Bunker, *J. Chem. Phys.*, **57**, 332 (1972).
(7) C. T. Ting and F. S. Rowland, *J. Phys. Chem.*, **74**, 4080 (1970).
(8) R. L. LeRoy, A. J. Yencha, M. Menzinger, and R. Wolfgang, *J. Chem. Phys.*, **58**, 1741 (1973).
(9) P. J. Robinson and K. A. Holbrook, "Unimolecular Reactions," Wiley, New York, N.Y., 1972, p 74.
(10) D. C. Tardy, B. S. Rabinovitch, and G. Z. Whitten, *J. Chem. Phys.*, **48**, 1427 (1968), and references therein.
(11) M. C. Lin and K. J. Laidler, *Trans. Faraday Soc.*, **64**, 927 (1968).
(12) J. S. Wright and L. Salem, *J. Amer. Chem. Soc.*, **94**, 322 (1972).
(13) P. C. Beadle, D. M. Golden, K. D. King, and S. W. Benson, *J. Amer. Chem. Soc.*, **94**, 2943 (1972).
(14) S. W. Benson and P. S. Nangia, *J. Chem. Phys.*, **38**, 18 (1963).
(15) R. Hoffman, S. Swaminathan, B. Odel, and R. Gleiter, *J. Amer. Chem. Soc.*, **92**, 7091 (1970).
(16) R. W. Carr and W. D. Walters, *J. Phys. Chem.*, **67**, 1370 (1963); R. W. Vreeland and D. F. Swinehart, *J. Amer. Chem. Soc.*, **85**, 3349 (1963); R. W. Carr and W. D. Walters, *ibid.*, **88**, 884 (1966). The *A* factors and

activation energies for c-C_4H_7T and c-C_4D_7T were assumed to be the same as for c-C_4H_8 and c-C_4D_8.
(17) R. C. Lord and I. Nakagawa, *J. Chem. Phys.*, **39**, 2951 (1963).
(18) E. B. Wilson, Jr., J. C. Decius, and P. C. Cross, "Molecular Vibrations," McGraw-Hill, New York, N.Y., 1955, p 182.
(19) S. C. Chan, B. S. Ravinovitch, J. T. Bryant, L. D. Spicer, T. Fujimoto, Y. N. Lin, and S. P. Pavlou, *J. Phys. Chem.*, **74**, 3160 (1970).
(20) J. D. Rynbrandt and B. S. Rabinovitch, *J. Phys. Chem.*, **74**, 1679 (1970).
(21) D. W. Setser and E. E. Siefert, *J. Chem. Phys.*, **57**, 3623 (1972).
(22) H. W. Chang, N. L. Craig, and D. W. Setser, *J. Phys. Chem.*, **76**, 954 (1972).
(23) Reference 9, p 315.
(24) W. Forst, "Theory of Unimolecular Reactions," Academic Press, New York, N.Y., 1973, p 225.
(25) H. vanWeyssenhoff and E. W. Schlag, *J. Chem. Phys.*, **59**, 729 (1973).
(26) A. M. Halpern and W. R. Ware, *J. Chem. Phys.*, **53**, 1969 (1970).
(27) C. J. Sneed and H. H. Harris, *J. Chem. Phys.*, **60**, 1355 (1974).
(28) The small difference arises from the fact that the previous calculation did not quite match the experimental points at D/S = 1, ref 2b.
(29) T. Valencich and D. L. Bunker, *Chem. Phys. Lett.*, **20**, 50 (1973); T. Valencich and D. L. Bunker, *J. Chem. Phys.*, **61**, 21 (1974); T. Valencich, Ph.D. Thesis, University of California, Irvine, Calif., 1974 (University Microfilms, Ann Arbor, Mich.).
(30) L. M. Raff, *J. Chem. Phys.*, **60**, 2220 (1974).
(31) The threshold for T-for-D substitution in CD_4 is also 35 kcal/mol; C. C. Chou and F. S. Rowland, *J. Chem. Phys.*, **50**, 2763 (1969).
(32) P. J. Estrup and R. Wolfgang, *J. Amer. Chem. Soc.*, **82**, 2665 (1960); R. Wolfgang, *J. Chem. Phys.*, **39**, 2983 (1963).
(33) See the trajectory results of ref 29 and 30.
(34) R. N. Porter, *J. Chem. Phys.*, **45**, 2284 (1966); R. N. Porter and Sinan Kunt, *ibid.*, **52**, 3240 (1970).
(35) The experimental results with which we are primarily interested are the values of D/S for c-C_4H_7T and c-C_4D_7T measured for samples simultaneously containing c-C_4H_8 and c-C_4D_8.[4] In these mixtures both molecules are exposed to the same tritium atom flux and the D/S values have been measured for equivalent experimental conditions. However, the D/S values for c-C_4H_7T in pure c-C_4H_8[3] and in c-C_4H_8–c-C_4D_8 mixtures[4] are the same, indicating the T atom flux and the deactivation processes of c-C_4H_7T do not differ appreciably in the two systems.
(36) The distance of the H or D atom from the cyclobutane center of mass is 2 Å.
(37) T. Valencich and D. L. Bunker, ref 29, find at a T-atom energy of 200 kcal/mol Walden inversion substitutions results in the ejected atoms carrying an average fraction of 0.20 of the incident energy with a largest fraction of 0.48. For substitution with retention the fractions are 0.25 and 0.62, respectively. These fractions change very little over a 500 kcal/mol range of T-atom energies; *e.g.*, for retained substitutions the smallest average fraction of energy carried by the ejected atom is at 130 kcal/mol and equals 0.22, with a largest average fraction at 400 kcal/mol equal to 0.36.
(38) P. J. Kuntz, E. M. Nemeth, J. C. Polanyi, and W. H. Wong, *J. Chem. Phys.*, **52**, 4654 (1970); f equals 0.57, 0.26, 0.42, and 0.38 at 46, 92, 138, and 277 kcal/mol, respectively.
(39) E. K. C. Lee and F. S. Rowland, *J. Amer. Chem. Soc.*, **85**, 2907 (1963); E. K. C. Lee, G. Miller, and F. S. Rowland, *ibid.*, **87**, 190 (1965); J. W. Root and F. S. Rowland, *J. Phys. Chem.*, **74**, 451 (1970).

Thermochemistry of Gas-Phase Equilibrium $CF_3CH_3 + I_2 = CF_3CH_2I + HI$. The Carbon–Hydrogen Bond Dissociation Energy in 1,1,1-Trifluoroethane and the Heat of Formation of the 2,2,2-Trifluoroethyl Radical

E-Chung Wu and Alan S. Rodgers*

Thermodynamics Research Center, Department of Chemistry, Texas A & M University, College Station, Texas 77843
(Received April 1, 1974)

The equilibrium constants for the gas-phase reaction $CF_3CH_3 + I_2 = CF_3CH_2I + HI$ have been determined spectroscopically over the temperature range 730–775 K. The entropy of CF_3CH_2I was estimated and combined with known entropies for the other reagents and the experimental equilibrium constants to yield $\Delta H_r°(750) = 16.0 \pm 0.5$ and $\Delta H_r°(298) = 15.3 \pm 0.5$ kcal mol^{-1}. This result yields $DH°_{298}(CF_3CH_2–H) = 106.7 \pm 1.1$ kcal mol^{-1}, indicating a marked strengthening of the C(sp^3)–H bond dissociation energy with β fluorine substitution. This value for the C–H bond dissociation energy was combined with known thermochemistry to yield the heat of formation of the 2,2,2-trifluoroethyl radical, $\Delta H_f°(CF_3\dot{C}H_2, g, 298) = -123.6 \pm 1.2$ kcal mol^{-1}.

Introduction

In a recent analysis of the kinetic data (both thermal and chemically activated) on the unimolecular decomposition of 1,1,1-trifluoroethane to HF and 1,1-difluoroethene[1] the enthalpy of formation of 1,1,1-trifluoroethane was derived as -178.2 ± 1.6 kcal mol^{-1} in excellent agreement with calorimetric data[2] corrected to the most recent values for $\Delta H_f°$(HF, aq, 298).[3] Also, the study of the kinetics of the reaction of 2,2,2-trifluoroethyl iodide with HI[4] has resulted in $DH°_{298}(CF_3CH_2–I) = 56.3 \pm 1$ kcal mol^{-1}. Consequently, this study of the equilibrium

$$CF_3CH_3 + I_2 = CF_3CH_2I + HI \qquad (1)$$

was undertaken to determine not only $\Delta H_f°(CF_3CH_2I, g, 298)$ but also $DH°_{298}(CF_3CH_2–H)$ as well as $\Delta H_f°(CF_3\dot{C}H_2, g, 298)$.

Experimental Section

1,1,1-Trifluoroethane and 2,2,2-trifuoroethyl iodide were obtained from PCR Inc. and hydrogen iodide was obtained from Matheson Co. All of these materials were purified by vacuum distillation. Iodine was purified before use by vacuum sublimation.

The experimental apparatus and procedure were the same as described in our previous work,[4] except that the formation of CF_3CH_2I and HI were followed spectrophotometrically at 2600 Å. Preliminary experiments indicated that the equilibrium was far to the left (reaction 1) so that

TABLE I: Data for Equilibrium Studies of the Reaction $CF_3CH_3 + I_2 = CF_3CH_2I + HI$

Temp, °K	$P°(I_2)$, Torr	$P°$(RH), Torr	P(HI), Torr	ln K_{eq}	$\Delta H°$, kcal/mol	$\Delta t_{1/2}$, sec Calcd	$\Delta t_{1/2}$, sec Obsd
776	24.7	305.3	0.76	—9.48	16.64	13.3	12
	24.4	182.6	0.58	—9.50	16.68	17	15
	24.1	120.4	0.45	—9.56	16.76	21	12
	23.6	396.4	0.83	—9.52	16.70	11.7	13
	19.6	328.4	0.72	—9.43	16.55	12.8	12
	15.5	308.5	0.55	—9.67	16.93	13.2	12
	14.8	348.6	0.68	—9.31	16.37	12.5	12
	10.1	393.4	0.61	—9.29	16.35	11.7	12
752	24.3	419.2	0.83	—9.60	16.27	32	33
	23.9	109.6	0.51	—9.24	15.74	63	60
	19.9	173.6	0.52	—9.44	16.04	50	48
	19.7	354.8	0.62	—9.82	16.61	35	36
	19.5	41.2	0.30	—9.11	15.54	103	120
	10.3	334.7	0.58	—9.24	15.74	36.3	36
732	25.4	251.2	0.68	—9.53	15.72	96	105
	21.2	320.8	0.59	—9.89	16.24	84	84
	20.7	109.3	0.33	—9.94	16.32	144	140
	20.7	127.3	0.50	—9.28	15.36	134	80
	20.7	261.5	0.61	—9.60	15.82	94	90
	20.5	131.5	0.50	—9.31	15.40	132	150
	20.1	119.4	0.39	—9.69	15.96	138.6	190
	10.4	263.1	0.55	—9.11	15.11	93.4	96
	9.9	148.6	0.48	—8.77	14.61	124	144
	5.1	238.4	0:37	—9.10	15.10	98	84
				Av	16.0 ± 0.5		

even with high temperatures and partial pressures of the reactants, the optical density (OD) of the products at 2600 Å was 0.1 OD units or less. Furthermore, 2,2,2-trifluoroethyl iodide decomposed at the high temperatures used, consequently its extinction coefficient was determined at lower temperatures and extrapolated into the experimental temperature range by assuming that the molar extinction coefficient at the maximum (2600 Å) would be temperature independent.

The decomposition of 2,2,2-trifluoroethyl iodide was greatly inhibited in the presence of I_2 so in an experiment at, e.g. 750 K, one would observe an initial, and fairly rapid, increase in OD in the first 5–10 min of reaction, followed by a very much slower, but steady, increase in OD. The former was presumed due to reaction 1 while the latter was attributed to the decomposition of the CF_3CH_2I formed. The data were interpreted as follows. An approximate half-life of the initial OD increase was estimated and five half-lives were marked off. The value of the OD at five half-lives was taken as the equilibrium value for reaction 1 and recorded. Then the half-life of the reaction based on (OD) equilibrium was determined and recorded. Equilibrium partial pressures were calculated from the absorption coefficients and the assumption that the partial pressures of HI and CF_3CH_2I were equal. This, and the initial partial pressures of I_2 and CF_3CH_3, permitted the calculation of the equilibrium constants for reaction 1.

Results

The experimental results obtained for reaction 1 are summarized in Table I. The observed change in OD at equilibrium was of the order of 0.05–0.10 OD units, measured to a precision of ±0.01 OD units. Thus, the partial pressures of HI have a precision of ±10–20% and the equilibrium constants, which depend upon the square of HI partial pressure (since $P_{CF_3CH_2I} = P_{HI}$), have a precision of ±20–40%. Data with such a large variance can still yield free energy changes with a precision of ±1 kcal mol^{-1}, but cannot be used in a Van't Hoff plot to determine both $\Delta S_r°$ and $\Delta H_r°$. Thus, entropy data for reactants and products are needed to yield the desired $\Delta H_r°$. The thermodynamic functions of HI and I_2 are well known[5] and those for CF_3CH_3 have been evaluated using the same procedures as in the recent calculations for chloroethanes.[6] The entropy at 298 K and heat capacity at various temperatures for CF_3CH_2I has been estimated by group additivity methods.[7] The relevant thermodynamic data are summarized in Table II and lead to

$$\Delta S_r°(1, T) = 1.2 + 1.5 \ln (T/300) \quad 300 \leq T \leq 800 \tag{2}$$

Equation 2 may be combined with the experimental values of $\Delta G_r°(1, T)$ to yield $\Delta H_r°(1, T)$, given in the sixth column of Table I. The mean of these results and its standard deviation is $\Delta H_r°(1, 750) = 16.0 \pm 0.5$ kcal mol^{-1}. From Table II, one can calculate $\Delta C_{p_r}° = 1.5 \pm 1$ cal mol^{-1} K^{-1} from 750 to 298 K, so that $\Delta H_r°(1, 298) = 15.3 \pm 0.5$ cal mol^{-1}.

The equilibrium constant for reaction 1 at the mean temperature, 750 K, is given by

$$K_1 = 10^{0.56-16.0/\theta} \quad (\theta = 2.3RT \text{ kcal mol}^{-1}) \tag{3}$$

It is not possible to verify that the system is at equilibrium by a study of the reverse reaction. However, the kinetics of the reverse reaction have been determined[4] so it is possible to check the validity of the equilibrium constant by comparing the observed and calculated times required for HI and CF_3CH_2I to reach 50% of their equilibrium values ($\Delta t_{1/2}$). It is to be noted, that while the experimental equilibrium constants show a barely discernable trend in this temperature range, the values for $\Delta t_{1/2}$ (column 8, Table I) increase by a factor of 10 with increasing temperature.

The mechanism for this reaction has been shown to be[4]

$$I_2 + M \rightleftharpoons 2I + M \quad K_{I_2}$$

$$CF_3CH_3 + I \underset{b}{\overset{a}{\rightleftharpoons}} CF_3\dot{C}H_2 + HI \tag{a, b}$$

$$CF_3\dot{C}H_2 + I_2 \underset{d}{\overset{c}{\rightleftharpoons}} CF_3CH_2I + I \tag{c, d}$$

and

$$K_1 = \frac{k_a k_c}{k_b k_d} = 10^{0.56-16.0/\theta}\langle T\rangle = 750 \text{ K} \tag{3}$$

From previous work[4]

$$k_d = 10^{11.50-19.9/\theta} \ M^{-1} \text{ sec}^{-1} \tag{4}$$

$$k_c/k_b = 10^{0.65+1.0/\theta} \tag{5}$$

so that

$$k_a = 10^{11.4-36.9/\theta} \ M^{-1} \text{ sec}^{-1} \tag{6}$$

From a steady-state treatment of the reaction mechanism, one has

$$\frac{d(HI)}{dt} = k_a K_{I_2}^{1/2} (I_2)_0^{1/2} (CF_3CH_3)_0 \times \left[1 - \frac{(CF_3CH_2I)(HI)}{(CF_3CH_3)(I_2)K_1}\right] \tag{7}$$

Because of the small extent of reaction (see Table I) equilibrium concentrations of CF_3CH_3 and I_2 are essentially equal to their initial concentrations; and, if one lets $X = (HI) = (CF_3CH_2I)$ then eq 7 becomes

TABLE II: Thermodynamic Data for the Reaction $CF_3CH_3 + I_2 = CF_3CH_2I + HI$

Compd	$\Delta H_f°(298)$, kcal mol^{-1}	$S°(298)$, cal K^{-1} mol^{-1}	$C_p°(298)$, cal K^{-1} mol^{-1}	$C_p°(800)$, cal K^{-1} mol^{-1}
CF_3CH_3[a]	−178.2 ± 0.4	68.7	18.8	32.0
I_2[b]	14.9	62.3	8.8	9.0
HI[b]	6.3	49.4	7.0	7.6
CF_3CH_2I[c]		82.8	21.9	35.1

[a] B. J. Zwolinski, private communication, Thermodynamic Research Center, Department of Chemistry, Texas A & M University. [b] Reference 5. [c] Estimated, S. W. Benson, *et al.*, *Chem. Rev.*, **64**, 279 (1969).

$$\frac{dX}{dt} = k_a K_{I_2}^{1/2} (I_2)_0^{1/2} (CF_3CH_3)_0 \left[1 - \frac{X^2}{X_{eq}^2}\right] \quad (8)$$

Equation 8 may be integrated from $X = 0$ at $t = 0$ to $X = 0.5X_{eq}$ at $t = \Delta t_{1/2}$ to yield

$$\Delta t_{1/2} = (X_{eq} \ln 3)/(2k_a K_{I_2}^{1/2} (I_2)_0^{1/2} (CF_3CH_3)_0) \quad (9)$$

Finally, one may substitute

$$X_{eq} \cong (K_1 (I_2)_0 (CF_3CH_3)_0)^{1/2}$$

so that

$$\Delta t_{1/2} = (K_1^{1/2} \ln 3)/(2k_a K_{I_2}^{1/2} (CF_3CH_3)_0^{1/2}) \quad (10)$$

The values of $\Delta t_{1/2}$ were calculated from eq 10 and are given in column 7 of Table I ($K_{I_2}^{1/2}$ was taken from ref 5). The good agreement between the observed and calculated values confirms the fact that the experimental data of Table I do, indeed, correspond to equilibrium conditions for reaction 1.

Discussion

The result, $\Delta H_r°(1, 298) = 15.3 \pm 0.5$ kcal mol^{-1}, can be combined with the data of Table II to yield $\Delta H_f°(CF_3CH_2I, g, 298) = -154.3 \pm 0.7$ kcal mol^{-1}. Also, the enthalpy change for reaction 1 can be expressed as

$$\Delta H_r°(1, 298) = DH°(CF_3CH_2-H) + DH°(I_2) - DH°(CF_3CH_2-I) - DH°(H-I) \quad (11)$$

The values are $DH°_{298}(I_2) = 36.2$,[5] $DH°_{298}(HI) = 71.3$,[5] and $DH°_{298}(CF_3CH_2-I) = 56.3 \pm 1$[4] kcal mol^{-1}, thus $DH°_{298}(CF_3CH_2-H) = 106.7 \pm 1.1$ kcal mol^{-1}. This latter value may be combined with $\Delta H_f°(CF_3CH_3, g, 298)$ of Table II and $\Delta H_f°(H, g, 298) = 52.1$[5] to yield $\Delta H_f°(CF_3\dot{C}H_2, g, 298) = -123.6 \pm 1.2$ kcal mol^{-1}.

The value for the C–H bond dissociation energy (BDE) in 1,1,1-trifluoroethane, $DH°_{298}(CF_3CH_2-H) = 106.7 \pm 1.1$ kcal mol^{-1}, is unexpectedly high. This is, after all, a β substituted ethane and, it may be recalled, β substitution with methyl groups (*e.g.*, neopentane) leaves the C–H BDE nominally unchanged.[8] Quite apparently, this is not the case for β fluorine substituents. This high value for the C–H BDE is, however, in good agreement with data on the bromination of CF_3CH_3 obtained by Coomber and Whittle.[9] Their results for reaction 12, which lead them to propose that $DH°_{298}(CF_3CH_2-H) \leq 110$ kcal mol^{-1} are log $(k_{12}/\text{mol}^{-1}\ \text{sec}^{-1}) = 11.0 - 23.5/\theta$ $\langle T \rangle = 650$ K. Using the results of this work and $\Delta H_f°$(Br) and (HBr) of ref 5 one obtains $\Delta H_r°(12, 298\ K) = 19.2 \pm 1.2$ kcal mol^{-1}. Taking $\Delta C_p°(12) = +1$ cal K^{-1},[7] one calculates $\Delta H_r°(12, 650) = 19.6 \pm 1.2$ kcal mol^{-1} and, therefore, $E_{-12} = E_{12} - \Delta H_r°(12, 650) = 3.8 \pm 1.3$ kcal mol^{-1}. This value is in line with that obtained for $CF_3\dot{C}F_2 + HBr$ ($E_a = 3.1 \pm 1$ kcal mol^{-1})[10] by Whittle and coworkers at similar temperatures.

$$CF_3CH_3 + Br \rightleftharpoons CF_3\dot{C}H_2 + HBr \quad (12)$$

It has already been noted that the C–C BDE in 1,1,1-trifluoroethane was much larger than expected from group additivity considerations and that this added strength was attributed, primarily to attractive dipole–dipole interactions in the 1,1,1-trifluoroethane molecule.[1] It is interesting to speculate along similar lines in attempting to explain the unexpected strength of the C–H bond also.

Certainly, calculations of the charge distribution in 1,1,1-trifluoroethane at the CNDO/2 level of approximation with standard geometry[11] yields the β carbon negative and the hydrogen positive. However, the charge on the hydrogen is small and the electrostatic attraction is approximately 1 kcal mol^{-1}; this is in the right direction, but not nearly large enough. There are, however, other changes taking place in the dissociation reaction 13 which could

$$CF_3CH_3 \longrightarrow CF_3\dot{C}H_2 + H \quad (13)$$

contribute to the strengthening of the C–H bond (*i.e.*, to the enthalpy of reaction 13).

If the carbon atom β to the fluorines becomes less negatively charged in changing from sp^3 hybridization in the reactant to sp^2 in the product, then the dipole–dipole energy (attractive) would be less in CF_3CH_2 than in CF_3CH_3. This energy has been estimated at −6 kcal mol^{-1} in CF_3CH_3[1] so that a significant contribution to the enthalpy change of reaction 13 would be possible. While we hope to be able to quantify these speculations in the near future, we have at least shown that they are in the right direction and, taken together, could be of the correct size.

Acknowledgment. The authors wish to express their appreciation to the Robert A. Welch Foundation for support of this research.

References and Notes

(1) A. S. Rodgers and W. G. F. Ford, *Int. J. Chem. Kinet.*, 5, 965 (1973).
(2) V. P. Kolesov, A. M. Martynov, and S. M. Skuratov, *Russ. J. Phys. Chem.*, **39**, 223 (1965).
(3) G. K. Johnson, P. N. Smith, and W. N. Hubbard, *J. Chem. Thermodyn.*, **5**, 793 (1973).
(4) E-Chung Wu and A. S. Rodgers, *Int. J. Chem. Kinet.*, **5**, 1001 (1973).
(5) D. Stull, Ed., "JANAF Thermochemical Tables," Dow Chemical Co., Midland, Mich.
(6) J. Chao, A. S. Rodgers, R. C. Wilhoit, and B. J. Zwolinski, *J. Phys. Chem. Ref. Data*, in press.
(7) S. W. Benson, "Thermochemical Kinetics," Wiley, New York, N.Y., 1969.
(8) D. M. Golden and S. W. Benson, *Chem. Rev.*, **69**, 125 (1969).
(9) (a) J. W. Coomber and E. Whittle, *Trans. Faraday Soc.*, **62**, 1553 (1966); (b) J. C. Amphlett and E. Whittle, *Trans. Faraday Soc.*, **64**, 2130 (1963).
(10) K. C. Ferguson and E. Whittle, *J. Chem. Soc., Faraday Trans. 1*, **68**, 295 (1972).
(11) J. A. Pople and D. L. Beveridge, "Approximate Molecular Orbital Theory," McGraw-Hill, New York, N.Y., 1970.

Rate Constants for the Reaction of Ozone with Olefins in the Gas Phase

S. M. Japar,* C. H. Wu, and H. Niki

Fuel Sciences Department, Scientific Research Staff, Ford Motor Company, Dearborn, Michigan 48121 *(Received June 7, 1974)*

Publication costs assisted by the Ford Motor Company

Bimolecular rate constants for 17 gas-phase ozone–olefin reactions have been determined by monitoring the ozone decay with the NO–O_3 chemiluminescence technique. The constants derived range from 1.9×10^{-18} cm^3 molecule^{-1} sec^{-1} for ethylene to 1.5×10^{-15} cm^3 molecule^{-1} sec^{-1} for 2,3-dimethyl-2-butene. Evidence is presented which indicates that the reported rate constants probably are the true primary bimolecular rate constants for the ozone–olefin reactions.

Introduction

The ozonolysis of olefins is one of the important driving reactions in the formation of photochemical smog,[1-3] and it is primarily for this reason that numerous kinetic studies of this system have been carried out in recent years.[4-10] Published rate constants for a number of these reactions are presented in Table I.

The most extensive investigation of this system is that of Cvetanović and coworkers.[5,6] Their work was carried out with reactant concentrations near 10,000 ppm (1–5 Torr) and relative rate constants for a large number of olefins were determined by gas chromatographic analysis of products formed during competitive reaction of ozone with mixtures of olefins. Studies have also been carried out under conditions more nearly approximating those in the real atmosphere.[4,7-10] In these cases rate constants were determined by directly measuring the decay of one of the reactants, usually ozone, by any of a number of different methods, including long pathlength infrared spectroscopy,[4] wet chemical analysis,[7-8] and, most recently, O_3–NO chemiluminescence techniques.[9]

Among all of these investigations there is general agreement concerning the relative reactivities of terminal olefins; however, an order of magnitude difference exists in the measured reactivities of internal olefins, as shown in Table I.

The present investigation of the rate constants for the reaction of ozone with a large number of aliphatic olefins was undertaken to expand the amount of kinetic data gathered using NO–O_3 chemiluminescence in order to check for internal consistency of the technique as well as to identify any trends in the kinetic data which might help explain the disparate results summarized in Table I.

Experimental Section

Ozonolysis was carried out in a 45-l. Pyrex bell jar with a Teflon-coated stainless steel base. The reactor could be evacuated to below 1 mTorr with a mechanical pump and a liquid nitrogen trap. The leak rate was less than 1 mTorr min^{-1} upon isolation from the pumping system.

Pure ozone was prepared by condensing ozonized oxygen in a silica gel trap at 195°K and pumping off oxygen. The purity of ozone was checked by decomposing a sample in a Pyrex bulb (~100 cm^3) with a Tesla coil and measuring the pressure change. The observed purity was 98 ± 3%. The research grade olefins (Phillips) were vacuum distilled prior to use. UPC Air (Air Products and Chemicals, dew point = −125°F) was used as received.

Reactant mixtures of ozone and olefin in the ppm concentration range (1 ppm = 2.45×10^{13} molecules cm^{-3} at 760 Torr, 298°K) were prepared by first filling calibrated volumes to the desired pressures. The contents of these were then flushed into the evacuated bell jar with diluent gas to a total pressure of 760 Torr. The individual reactant pressures, up to 20 Torr in the calibrated volumes, were measured by a pressure transducer (Pace Wiancko, CD25) which had been calibrated against an oil manometer. The reactant concentrations in the gas mixtures thus prepared can be reproduced better than ±3%. The temperature of the gas mixture was 26 ± 2° during kinetic measurements.

Ozone was continuously sampled from the reactor using a capillary probe (flow rate ~35 cm^3 min^{-1}) and was analyzed by an NO–O_3 chemiluminescence detector.[11] The overall response time of the instrument is less than 1 sec. The ozone concentration was calibrated by titration with NO of known concentration.[11] Linearity of the signal *vs.* concentration was checked from 10^{-3} to 10^2 ppm using an exponential dilution method. Olefins were analyzed gas chromatographically using a flame ionization detector and a stainless steel column (⅛ in. × 12 ft) packed with DC 200 on Chromosorb W. The reaction mixture was sampled into a 0.2-cm^3 loop and introduced to the column using a Carle minivolume valve. Olefin concentrations were calibrated by preparing known concentrations in the bell jar by the standard pressure–volume technique mentioned above.

Results and Discussion

The experiments were carried out under olefin-rich conditions, with the initial ozone concentration 1–10% of the olefin concentrations. The ozone decay was recorded with respect to time, and was found to exhibit good exponential behavior with a reproducibility of better than 5%. This being the case, the ozone decay could accurately be represented by the pseudo-first-order expression

$$d \ln [O_3]/dt = -k\overline{[HC]} \quad (1)$$

where k is the bimolecular rate constant for the reaction and $\overline{[HC]}$ is the average concentration of the particular olefin being studied. Since olefin consumption is minimal under the experimental conditions employed, $\overline{[HC]}$ can be taken to be the initial olefin concentration, $[HC]_0$.

Equation 1 predicts a linear dependence of the first-

TABLE I: Rate Constants for Gas Phase Ozone–Olefin Reactions

	k, 10^{-18} cm^3 molecule^{-1} sec^{-1}	
	Literature	Present
Ethylene	1.2,[e] 1.3,[b] 1.6,[f] 2.6,[c] 2.7,[d] 3.0[a]	1.9 ± 0.1
Ethylene-d_4		2.3 ± 0.1
Propylene	6.2,[a] 7.5,[e] 8.2,[b] 11.0,[c] 12.5,[f] 13[i]	13.0 ± 0.1
Propylene-d_6		15.1 ± 0.3
1-Butene	9.0,[c] 10.0[d]	12.3 ± 0.4
1-Pentene	5.3,[a] 7.5,[b] 9.0[c]	10.7 ± 0.4
1-Hexene	9.2,[g] 10.0.[a,b] 10.2,[c] 11.0,[d,f,h] 16[i]	11.1 ± 0.3
Dialkylethylenes		
Isobutene	6.2,[b] 8.4,[c] 15,[h] 23[d]	13.6 ± 0.2
cis-2-Butene	28,[e] 50,[b] 140,[i] 340[d]	161 ± 7
trans-2-Butene	35,[c] 166,[h] 260,[i] 275,[f] 430[d]	260 ± 9
Trialklethylenes		
2-Methyl-2-butene	29,[c] 790[i]	493 ± 16
cis-3-Methyl-2-pentene		456 ± 8
trans-3-Methyl-2-pentene		563 ± 17
Tetraalkylethylenes		
2,3-Dimethyl-2-butene	39,[c] 750[d]	1510 ± 80
Others		
Cyclopentene		813 ± 79
Cyclohexene	30,[i] 59[a]	169 ± 15
1,3-Butadiene	8.2,[b] 9.1[i]	8.4 ± 0.2

[a] R. D. Cadle and C. Schadt, *J. Amer. Chem. Soc.*, **74**, 6002 (1952). [b] Reference 4. [c] Reference 6. [d] Reference 8. [e] W. B. DeMore, *Int. J. Chem. Kinet.*, **1**, 209 (1969). [f] Reference 9. [g] Reference 7. [h] E. A. Schuck and G. J. Doyle, Report No. 29, Air Pollution Foundation, San Marino, Calif., 1959. [i] Reference 5. [j] Reference 10.

order decay of ozone on olefin concentration. This was the case for all olefins listed in Table I, and is illustrated for the 2-butenes in Figure 1. The first-order ozone decay was found to be independent of ozone concentration for all olefins studied, also as predicted by eq 1. This is a very good indication that the reactions are first order in each of the reactants. The bimolecular rate constants obtained with eq 1 are summarized in Table I, together with the data of previous workers. The error limits indicated for the present work represent one standard deviation.

Comparison of the data in Table I makes it clear that the relative rate data obtained by Wei and Cvetanović[6] at much higher reactant concentration, while consistent with the present values for terminal olefins, exhibit an order of magnitude discrepancy for the internal olefins. On the other hand, when data obtained under experimental conditions similar to those reported here[4,7–10] are considered, the agreement with the present values is good for all olefins studied.

The source of the disparity between the results obtained at low and high reactant concentrations is not at all clear. It should be pointed out that the relative rate data of Wei and Cvetanović[6] is based on analysis of reaction products obtained from the reaction of ozone with a mixture of olefins. The relation between the reaction product ratio and the relative rates of ozone–olefin reactions is based on a number of assumptions[5,6] which, while appearing quite reasonable, may be unfounded in what is certainly a very complex reaction system. In fact it has recently been shown that product formation in these systems is not simply related to the rate of consumption of reactants, and attempts to derive absolute rate constants from rates of product formation have been unsuccessful.[10]

Although the available rate data obtained under conditions reasonably related to those found in the atmosphere are in reasonable agreement, the question still arises as to the relation of the rate constants listed in Table I to the real bimolecular rate constants for the ozone–olefin reactions. In considering this problem the kinetics and stoichiometry of the ozonolysis of propylene have been investigated in great detail. (This will be the subject of a separate report.) It was found that in the absence of O_2 the reaction rate was considerably faster, and the number of ozone molecules consumed for each primary reaction step increased. This is a strong indication that secondary consumption of ozone by reaction intermediates is occurring in the absence of O_2. However, if the faster rate is corrected for the observed change in stoichiometry, the value obtained is the rate constant measured in air. This provides limited evidence that the values presented in Table I are the true bimolecular rate constants for the reactions.[6]

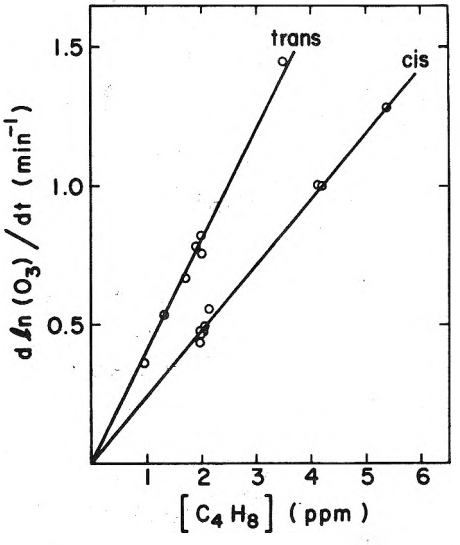

Figure 1. First-order decay rate of ozone as a function of excess *cis*- and *trans*-2-butene concentration at 299° and 760 Torr total pressure.

A further check on the importance of secondary reactions in the decay of ozone was carried out through a num-

ber of experiments conducted with mixtures of olefins, including isobutene + 1-pentene and isobutene + 1-pentene + *trans*-2-butene. Under a variety of conditions (olefin ratios, total olefin content, ozone content) the measured ozone decay rate was strictly an additive function of the individual olefins present, *i.e.*, no synergistic effects exist among the olefins. This agrees with the results of a similar study by Bufalini and Altshuller,[8] and further supports the assumption that consumption of ozone by secondary reactions is relatively unimportant in this system.

A brief discussion of some of the individual rate constants presented in Table I is of interest. With the exception of isobutene, increasing alkyl substitution on the olefinic double bond is responsible for large increases in the reaction rate constant. Thus, there is agreement with the same general trends reported by other investigators.[8]

Other than isobutene, there is only one significant deviation from the overall trend in the rate constants reported, and that is the value reported for cyclopentene. This is a cis olefin which would be expected to behave similarly to *cis*-2-butene and cyclohexene, which do exhibit the same reactivity. However, cyclopentene is five times more reactive toward ozone, and it is likely that the sizable ring strain present in cyclopentene is responsible for this rather marked difference.

Of additional interest is the 15% increase in reactivity on perdeuteration of ethylene and propylene. This is very similar to the effect on propylene reactivity toward hydroxyl radical,[12] and may be taken as another illustration of the electrophilic-like nature of the ozone attack on olefins.[6]

Conclusions

The data in Table I indicate that the NO_3 chemiluminescent technique is capable of generating reaction rate constants with a high degree of precision under conditions representative of those in the atmosphere. In addition, the experimental indications are that these constants correspond closely to the true bimolecular rate constants for the various ozone–olefin systems studied.

References and Notes

(1) P. A. Leighton, "Photochemistry of Air Pollution," Academic Press, New York, N.Y., 1961.
(2) A. P. Altshuller and J. J. Bufalini, *Environ. Sci. Tech.*, **5**, 39 (1971).
(3) H. Niki, E. E. Daby, and B. Weinstock, *Advan. Chem. Ser.*, **No. 113**, 16 (1972).
(4) P. L. Hanst, E. R. Stephens, W. E. Scott, and R. C. Doerr, "Atmospheric Ozone-Olefin Reactions," The Franklin Institute, Philadelphia, Pa., 1958.
(5) T. Vrbaski and R. J. Cvetanović, *Can. J. Chem.*, **38**, 1053, 1063 (1960).
(6) Y. K. Wei and R. J. Cvetanović, *Can. J. Chem.*, **43**, 913 (1963).
(7) B. E. Saltzman and N. Gilbert, *Ind. Eng. Chem.*, **51**, 1415 (1959).
(8) J. J. Bufalini and A. P. Altshuller, *Can. J. Chem.*, **45**, 2243 (1965).
(9) D. H. Stedman, C. H. Wu, and H. Niki, *J. Phys. Chem.*, **77**, 2511 (1973).
(10) R. A. Cox and S. A. Penkett, *J. Chem. Soc., Faraday Trans. 1*, **68**, 1735 (1972).
(11) D. H. Stedman, E. E. Daby, F. Stuhl, and H. Niki, *J. Air Pollut. Contr. Ass.*, **22**, 260 (1972).
(12) E. D. Morris, Jr., and H. Niki, *J. Phys. Chem.*, **75**, 3640 (1971).

Ions in Ammonia Flames[1]

C. Bertrand and P. J. van Tiggelen*

Laboratoire de Physico-chimie de la Combustion, Université Catholique de Louvain, Louvain-la-Neuve, Belgium

(Received January 30, 1973; Revised Manuscript Received July 16, 1974)

Publication costs assisted by the European Office of Aerospace Research

Chemiionization in flames burning with mixture of ammonia–oxygen–nitrogen has been investigated. Besides NH_4^+ and H_3O^+, NO^+ is by far the most abundant ion detected by mass spectrometry. The rate of the ion production, as measured by the saturation current method, is 10 times smaller than the one observed in methane flames at the same temperature. The overall activation energy is about 118 kcal/mol. Arguments are presented to prove that NO^+ is the primary ion. The dependence on pressure of ion production indicates a well-defined second-order rate. Different mechanisms for ion production are discussed and only an elementary process involving oxygen and nitrogen atoms, the nitrogen atoms being in the metastable state (2^2D_J), agrees with all the experimental data. A preexponential factor for the reaction between $O(^3P)$ and $N(^2D)$ atoms would be about 10^{-12} cm^3/molecule sec with an activation energy around 10 kcal/mol. A short discussion of the reactions of secondary ions is also given.

Introduction

Ionization phenomena occurring in combustion processes have been studied extensively over the last 10 years. Most of the research effort[2] has been devoted to the investigation of flames where the measured concentration of ions in the hot gases region are largely above the equilibrium values. This has been noticed particularly with flames burning in mixtures of either hydrocarbon–oxygen or cyanogen–oxygen. However, flames where carbon atoms are completely absent also exhibit a similar behavior, as, for example, ammonia–oxygen flames. Preliminary results[3a] indicate that the rate of ion generation was only a factor 10 smaller than the rate measured in methane–oxygen flames around

2500°K. This could be viewed as an unexpected result at first glance. The well-established mechanism for ion production in hydrocarbon flames,[2] $CH + O \rightarrow CHO^+ + e^-$ ($\Delta H \sim 0$ kcal/mol), does not have a counterpart in ammonia flames.

As a matter of fact, the energy released during the formation of a NO bond is only 150 kcal/mol, as compared with CO bond formation, 256 kcal/mol. Therefore, bimolecular reactions with species in the ground state are too endothermic to explain the measured chemiionization rate in ammonia flames. This suggests that electronically excited species could be involved in the primary chemiionization step as

$$A^* + B \longrightarrow C^+ + e^-$$

To our knowledge, a systematic study of ionization in ammonia flames has not been performed so far, only few preliminary results on the nature of ions were obtained previously.[3b] We have measured first the overall order of the chemiionization rate in order to check if the reaction responsible for the primary ion formation is a bimolecular process as it is for hydrocarbon flames, or if a termolecular reaction is required as it has been suggested for the cyanogen–oxygen system.[4]

The influence of pressure, temperature, and equivalence ratio on chemiionization has also been systematically studied.

Experimental Section

A slightly modified flat flame burner of the Botha–Spalding type[5] was employed. It consists of tube of 0.78 cm i.d. filled with 200 small inconel tubes of 0.4 mm diameter 16 cm long. The gas flows were monitored with sonic nozzle in glass. Commercial grade gases from Air Liquide have been used without further purification: NH_3 (99.5%), O_2 (99.9%), and N_2 (99.9%). Ion formation rates have been measured by the saturation current technique; the burner mouth was the cathode and the anode was a stainless steel disk 4 cm in diameter and 1 cm thick, cooled by electrically insulated water cooling. The burner and the anode are located inside a stainless steel container connected to a vacuum pump allowing flames to burn between 0.1 and 1 atm. Portholes with quartz window have been drilled for emission spectroscopy measurements (Figure 1). Ignition of the gases was obtained with an electric discharge. The chemiionization current was measured with a Keithley microammeter.

Identification and concentration measurements were performed with a mass spectrometer described previously.[6] From the current intensity i_s (amp) at the saturation, the ionic yield can be written as follows

$$\eta_+ = i_s/\epsilon F_B = 13.74(i_s/D_B) \quad (1)$$

where ϵ is the electron charge (coulomb), F_B and D_B are the flows of fuel (NH_3) in molecule/sec and cm^3/min, respectively.

Similarly, the overall reaction rate of ion production (U_+) is

$$U_+ = i_s/\epsilon S e_i \quad (2)$$

where S and e_i represent the flame surface and the thickness of the ionization zone, respectively. This can be taken as the thickness of the reaction zone which is related to the Schlieren thickness.[7]

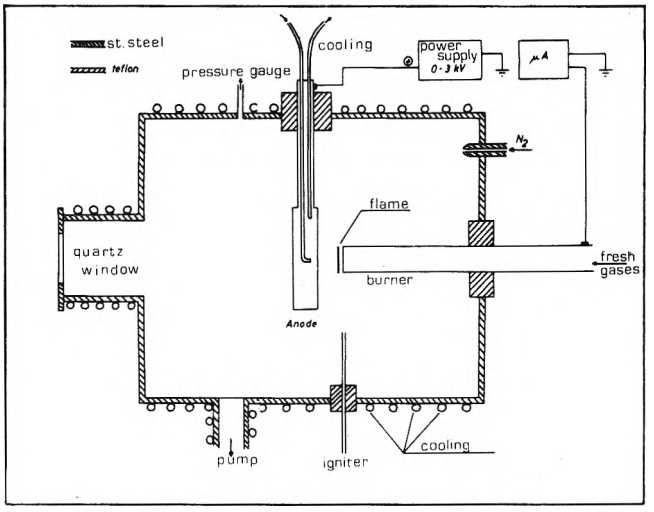

Figure 1. Low pressure equipment used for saturation current measurements.

TABLE I:

Flame	% H_2	% O_2	% CO	% N_2	% NH_3	T_f, °K	V_0, cm/sec
I		50.0			50.0	2695	145
II	32.0	14.1		52.1	1.8	2324	276
III		21.3	41.1	36.6	1.0	2359	37

Results

(1) *Nature of Ions.* The identity of ions for three different ammonia flames burning at atmospheric pressure as specified in Table I have been determined.

The detected ions in these flames are as follows: flame I NO^+, NH_4^+, N_3O^+, mass 31 ($^{15}NO^+$ or HNO^+), mass 32 ($^{18}NO^+$ or O_2^+); flame II NO^+ (80%), H_3O^+ (20%); flame III NO^+.

The ion in highest concentration is always NO^+. The concentrations of individual ionic species for flame I are plotted in Figure 2. These profiles will be discussed in detail later, but the decay of NO^+ is typical of a recombination process. Ions of mass 31 and 32 have not been plotted since their concentrations are very low (10^9 ions/cm^3). A profile of mass 31 similar to NO^+ allows us to assume that mass 31 corresponds to $^{15}NO^+$, it also fits the natural isotopic abundance. Mass 32, near the sensitivity limit of the equipment, is more probably O_2^+. The recombination coefficient k_{rec} of NO^+ can be deduced from the decay curve of this ion in the burned gases region by using a method described previously.[6]

$$k_{rec} = 7.6 \times 10^{-8}\ cm^3/sec\ ion\ at\ T_f = 2700°K$$

(2) *Ionic Yield.* Several flames burning at atmospheric pressure in mixtures of NH_3–O_2–N_2 have been studied systematically. Their composition is characterized by two parameters $r = [NH_3]/[NH_3] + [O_2]$; $\alpha = [N_2]/[N_2] + [NH_3] + [O_2]$. Figure 3 shows the evolution of the ionic yield η_+ as a function of the composition of the fresh gas mixtures. The maximum yield and the flame temperature peak out at the same value of r. Keeping the temperature constant (dashed line), the ionic yield is practically independent of the mixture strength, although a slightly higher value of η_+ on the lean side is noticed.

In Figures 4 and 5 the ionic yield has been plotted *vs.* the

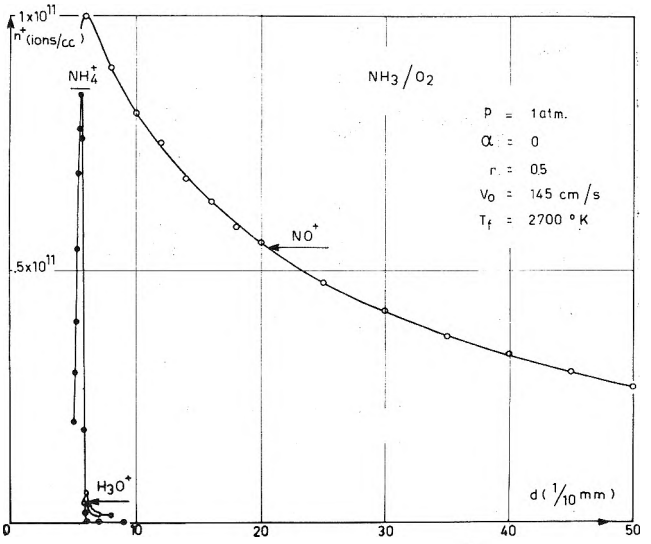

Figure 2. Ions profiles (n_+) in the undiluted equimolar ammonia–oxygen flame.

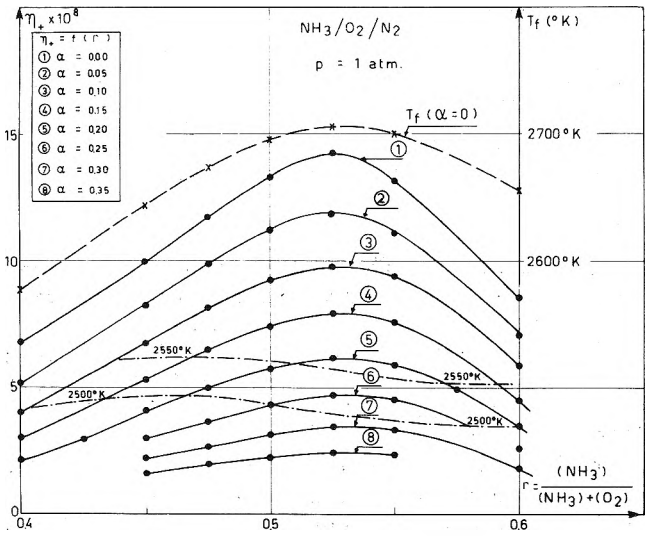

Figure 3. Ionic yield (η_+) as a function of mixture strength (r). The dashed line indicates the final temperature, the dashed-dotted lines represent isothermal mixtures of burnt gases.

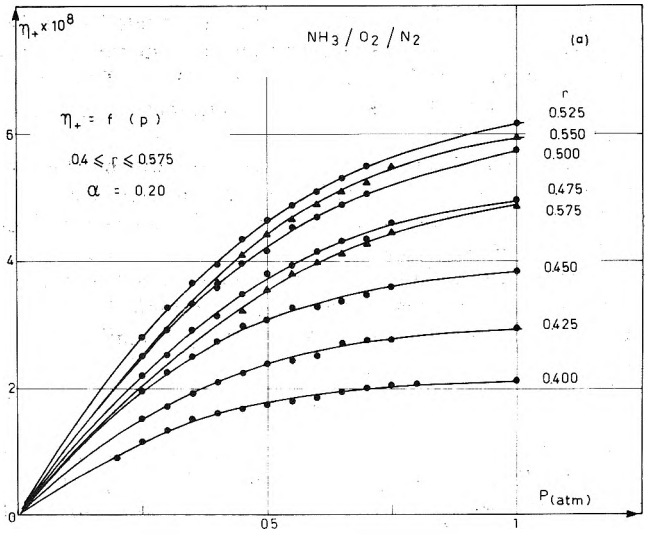

Figure 4. Ionic yield (η_+) as a function of pressure at constant dilution (α) and for different mixture strengths (r).

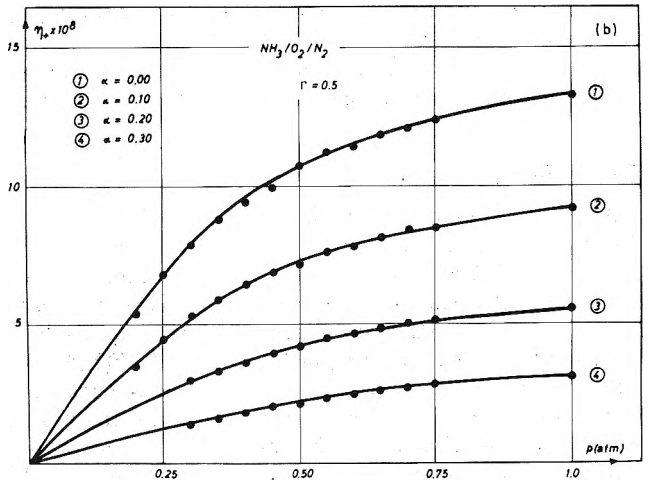

Figure 5. Ionic yield (η_+) as a function of pressure at constant (r) and different dilutions (α).

overall pressure p for different mixture strengths r and for different dilutions α. The result is that the pressure dependence is similar regardless of the way the composition is modified in the range studied.

Data Reduction

In any case, the rate of ion formation in an ammonia–oxygen flame can be written

$$U_+ = k_+ n^{(x+y)} X_{O_2}{}^x X_{NH_3}{}^y \exp(-E_i/RT_m) \quad (3)$$

The preexponential factor and the activation energy of the overall rate constant for ion formation are k_+ and E_i, respectively. R represents the gas constant; the apparent partial orders with respect to oxygen and ammonia are x and y. n is the number of molecules per cm^3 at the mean temperature T_m of the flame front which is related to the fresh and burnt gases temperatures[8] as follows

$$T_m = T_i + 0.74(T_f - T_i) \quad (4)$$

X_{O_2} and X_{NH_3} are the initial mole fractions of the reactant. The formal rate for ion formation can also be written as

$$U_+ = k_+ n^{(x+y)} (X_{O_2}/X_{NH_3})^x X_{NH_3}{}^{(x+y)} \exp(-E_i/RT_m) \quad (5)$$

A similar equation describes the overall burning rate of ammonia

$$U_c = k_c n^{(x'+y')} (X_{O_2}/X_{NH_3})^{x'} X_{NH_3}{}^{(x'+y')} \exp(-E_c/RT_m) \quad (6)$$

The ionic yield η_+ as defined by eq 1 is the number of ions created per molecule of ammonia entering the flame front, it is therefore equivalent to the ratio of the chemiionization rate and the burning rate

$$\eta_+ = U_+/U_c \quad (7)$$

Hence

$$\eta_+ = (k_+/k_c) n^{(x+y-x'-y')} (X_{O_2}/X_{NH_3})^{(x-x')} \times X_{NH_3}{}^{(x+y-x'-y')} \exp(-\Delta E_i/RT_m) \quad (8)$$

with $\Delta E_i = E_i - E_c$. At constant ratio X_{O_2}/X_{NH_3} and con-

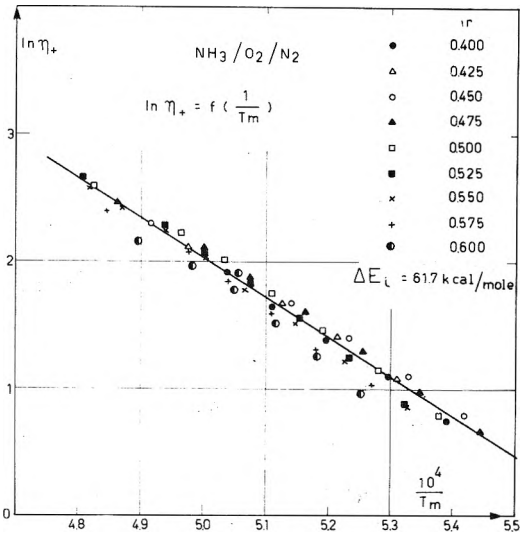

Figure 6. Arrhenius plot of the ionic yield (η_+). The mean temperature (T_m) is deduced from eq 4 and the overall order for ionization is $x + y = 2$.

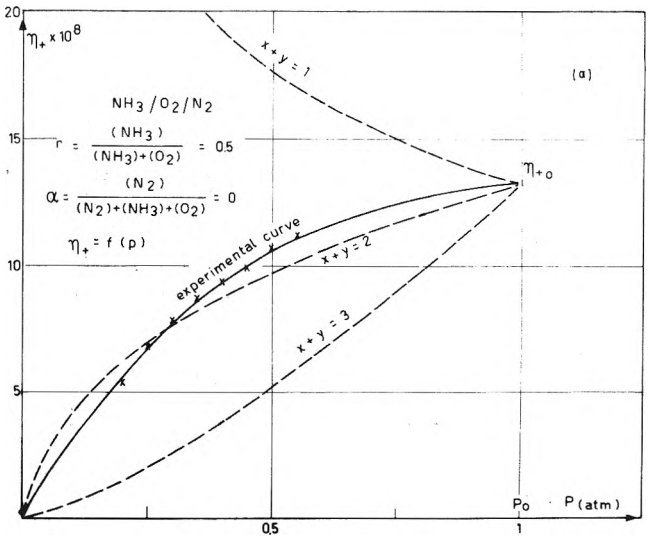

Figure 7. Comparison between experimental and theoretical curves of the ionic yield (η_+) for different pressures for an equimolar undiluted mixture; dashed lines correspond to different hypotheses over the overall order ($x + y$) of the ion production rate.

stant pressure, eq 8 becomes

$$\eta_+ = K(X_{NH_3}/T_m)^{(x+y-x'-y')} \exp(-\Delta E_i/RT_m) \qquad (9)$$

K is independent of the temperature.

Several authors[9,10] have noticed that the overall order of the combustion process ($x' + y'$) for ammonia–oxygen flames is 2.

The difference ΔE_i of activation energies is immediately deduced from the slope of the straight line by plotting [ln $\eta_+(T_m/X_{NH_3})^{(x+y-2)}$] *vs.* $1/T_m$, for a given value of $x + y$. The temperature varies with the dilution in nitrogen at constant mixture strength; one obtains ΔE_i = 74.2 kcal/mol for $x + y = 1$, ΔE_i = 61.7 kcal/mol for $x + y = 2$ (Figure 6), and ΔE_i = 51.5 kcal/mol for $x + y = 3$.

Using these values for ΔE_i and η_+ at atmospheric pressure, the curves of Figure 7 have been drawn. These patterns show the theoretical variation of η_+ as a function of the pressure for different values of the overall order for chemiionization (1, 2, or 3). The temperature of low pressure flames has been computed from the thermodynamic equilibrium and corrected for the discrepancy noticed at atmospheric pressure between the measured temperature and the equilibrium temperature.

Very good agreement between theoretical and experimental curves is observed with an overall second-order dependence for ion formation (Figure 7 and 8). At constant mixture strength the rate U_+ is given by

$$U_+ = Kn^2 X_{NH_3}{}^2 e^{-118,000/RT_m}$$

with the overall activation energy $E_i = E_c + \Delta E_i$ = 56 + 61.7 ≃ 118 kcal/mol.

At a final flame temperature of 2700°K (r = 0.5; α = 0.0), U_+ is 3.3 × 10^{16} ions/cm^3 sec. For the thickness of the flame front, use has been made of the Schlieren thickness as measured by Van Wonterghem.[11]

Intermediate species in the flame front are considered usually to be first-order dependent with respect to the pressure. At flame temperature, indeed, these species are produced and disappear essentially in bimolecular processes. Therefore, we assume that the experimental second-order mechanism corresponds to an elementary bimolecular reaction for chemiionization

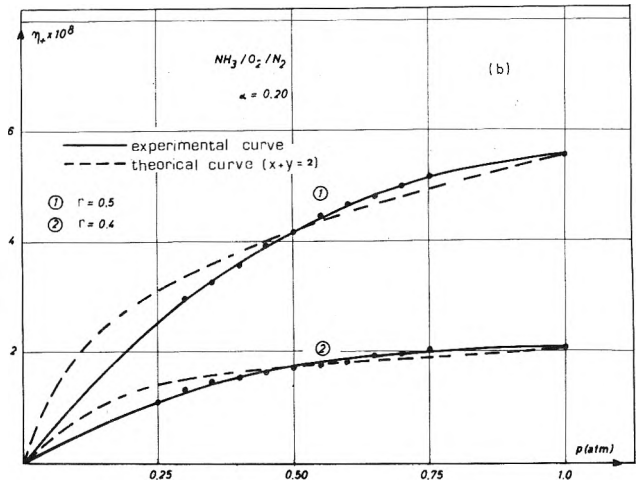

Figure 8. Comparison between experimental and theoretical curves of the ionic yield (η_+) for different pressures for flames with different mixture strengths (r).

$$A + B \longrightarrow C^+ + e^-$$

Besides flames burning in ammonia–oxygen–nitrogen mixtures, some data have been collected from H_2–O_2–N_2 and CO–O_2–N_2 flames where traces of ammonia were added.

Using the same techniques and applying similar equations to analyze the data, one obtains ΔE_i = 22.6 kcal/mol and E_i = 47.6 kcal/mol. The ionic yield at T_m = 1823°K is 8 × 10^{-8} in the CO–O_2–N_2 system and 4 × 10^{-8} in H_2–O_2–N_2. Moreover for both types of flames, the partial order (z) with respect to ammonia equals one as derived from Figure 9.

Discussion of Ion Formation

(*1*) *Primary Ion.* From the three most abundant ions detected by mass spectrometry, only NO^+ could be viewed as the primary ion. The energy released by the formation of H–H_2O and H–NH_3 bonds is, indeed, not large enough to

TABLE II:

No.	Reaction	ΔH_f,[a] kcal/mol
I	$N(^4S) + O(^3P) \rightarrow NO^+(^1\Sigma) + e^-(2s)$	62
II	$NH(^3\Sigma) + HO_2 \rightarrow NO^+(^1\Sigma) + H_2O + e^-(2s)$	82
III	$NH(^3\Pi) + O \rightarrow HNO^+ + e^-(2s)$	25
IV	$NH(^3\Pi) + OH \rightarrow NO^+(^1\Sigma) + H_2 + e^-(2s)$	51
V	$NH(^3\Pi) + HO_2 \rightarrow NO^+(^1\Sigma) + H_2O + e^-(2s)$	−3
VI	$NO(A^2\Sigma) + H \rightarrow HNO^+ + e^-(2s)$	66

[a] All thermochemical values are from JANAF. ΔH_f for HNO^+ has been measured by F. C. Kohout and F. W. Lampe, *J. Chem. Phys.*, **45**, 1074 (1966), and ΔH_f for $NH(^3\Sigma)$ by W. E. Kaskan and M. P. Nadler, *J. Chem. Phys.*, **56**, 2220 (1972).

TABLE III:

No.	k_i, cm³/molecule sec	Concn or concn products
I	$10^{-12} \exp(-65{,}000/5400)$	$[N(^4S)] = 1.2 \times 10^{17}$ [a]
II	$10^{-12} \exp(-82{,}000/5400)$	$[NH(^3\Sigma)][HO_2]\ 1.1 \times 10^{35}$ [b]
III	$10^{-12} \exp(-25{,}000/5400)$	$[NH(^3\Pi)] = 7.9 \times \times 10^{13}$ [c]
IV	$10^{-12} \exp(-51{,}000/5400)$	$[NH(^3\Pi)] = 1.9 \times 10^{15}$ [c]
V	10^{-12}	$[NH(^3\Pi)][HO_2] = 3.3 \times 10^{28}$ [b]
VI	$10^{-12} \exp(-66{,}000/5400)$	$[NO(A^2\Sigma)] = 10^{17}$ [c]

[a] Atoms/cm³. [b] Molecules²/cm⁶. [c] Molecules/cm³.

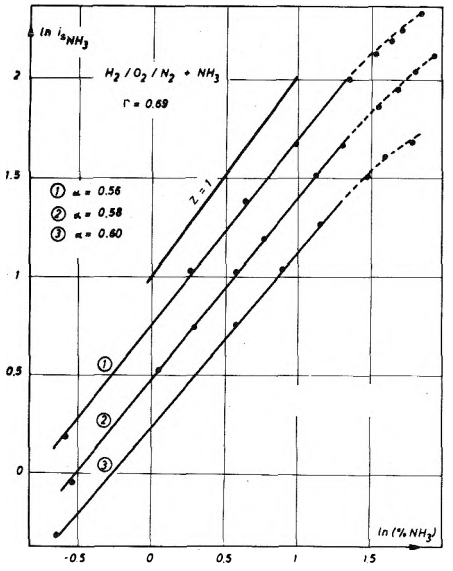

Figure 9. Dependence of the saturation current with respect to the ammonia concentration added to hydrogen–oxygen flames at different dilutions (α).

induce the ionization (*e.g.*, 107 kcal/mol are required to produce NH_4^+ under the most favorable conditions). Furthermore, if H_3O^+ and NH_4^+ are the primary ions, the ionic yield at constant temperature would be larger on the rich side than on the lean one.

However, HNO^+ can also be considered as a primary ion, although its occurrence has not been detected. Its concentration ought to be low, indeed, due to fast proton transfer reactions, hence the $N^{15}O^+$ at mass 31 can mask it.

Different bimolecular reactions, thermodynamically feasible, which lead to NO^+ or HNO^+ formation are listed in Table II.

For reaction I Lin and Teare[12] have measured a rate constant $k_1 = 5 \times 10^{-11}\ T^{-1/2} e^{-65{,}000/RT}$ cm³/molecule sec. For flame I (Table I), the preexponential factor is then 10^{-12} cm³/molecule sec. The rate constant of reactions II–VI are unknown; however, as a first approximation, one can assume for preexponential factors values of the same order of magnitude (*i.e.*, 10^{-12} cm³/molecule sec) and for activation energy, the endothermicities of the reactions. With the measured rate of chemiionization ($U_+ \simeq 3.3 \times 10^{16}$ ions/cm³ sec, around $T_f \sim 2700$°K), one does compute for flame I (a) the N, NH, and NO concentrations required for reactions I, III, IV, or VI to be responsible for chemiionization (O, OH, and H concentrations are the thermodynamically computed values, *i.e.*, 5×10^{16}, 2×10^{17}, and 5×10^{16} particles/cm³, respectively); (b) the $[NH(^3\Sigma)]\ [HO_2]$ and $[NH(^3\Pi)]\ [HO_2]$ concentrations products necessary for process II and V to be the chemiionization reaction.

The results are given in Table III. As the total number of molecules per cm³ at 2700°K is about 3×10^{18}, since the ground states of N, NH, and HO_2 species are by no means chain carriers and the species of $NH(^3\Pi)$ and $NO(^2\Sigma)$ are electronically excited, all the computed concentrations of Table III are much higher than those effectively encountered in the flame front. The absolute $NH(^3\Pi)$ concentration has been measured spectroscopically and amounts to 10^8–10^9 molecules/cm³.[13] In order to decrease the endothermicity of the processes, we are constrained to take into account the role of other excited states of the species involved in the aforementioned reactions.

As is derived from the potential curves of NH[14] and NO,[15] the metastable electronically excited states of those molecules can be ruled out as well. Reactions II–VI, involving $NH(c^1\Pi)$ and $NO(E^2\Sigma)$, have not to be taken into account, since the corresponding emission spectra have not been detected. Moreover, these states are not yet rich enough in energy.

N and O are the only atomic species which could be electronically excited in the flame front. The (2^1S) and (2^1D) states of the atomic oxygen can be excluded; reactions of $N(2^4S)$ with these oxygen states leading to $NO^+(X^1\Sigma)$ are, indeed, spin forbidden. Besides, the reaction III involving the excited states of oxygen does not account for the measured chemiionization rate. Chemiluminescence studies about the same system[13] have indicated, indeed, that the $NH(^3\Pi)$ concentration was around 10^8–10^9 molecules/cm³.

On the contrary, (2^2D) and (2^2P) states of atomic nitrogen can lead to the production of the NO^+ ion in elementary processes similar to reaction I.

$$N(2^2D) + O(^3P) \longrightarrow NO^+(^1\Sigma) + e^-(2s) \quad \Delta H_r = 10 \text{ kcal/mol} \quad (I')$$

$$N(2^2P) + O(^3P) \longrightarrow NO^+(^1\Sigma) + e^-(2s) \quad \Delta H_r = -15 \text{ kcal/mol} \quad (I'')$$

A computation method identical with the one previously used allows the determination that $N(2^2D)$ and $N(2^2P)$ concentrations of 3×10^{12} and 5×10^{11} atoms/cm^3, respectively, are large enough to account for the measured rate of chemiionization in ammonia flames.

To our knowledge, the concentrations of these excited atomic species in the flame front have not been measured so far. However, Husain, *et al.*,[16] have reported rate constants for their collisional removal by O_2, N_2, NO, ... *i.e.*, species occurring in high concentration inside the reaction zone of ammonia–oxygen flames. For example, with NO, the rate constant is around 5×10^{-11} cm^3/molecule sec. So, the mean lifetime of $N(2^2D)$ can be estimated as 10^{-7} sec, if the main process of its disappearance involves a partner with a mole fraction of about 10%. With the steady-state assumption for $N(2^2D)$, its lifetime then corresponds to a rate of formation of about 3×10^{19} atoms/cm^3. Such a rate is possible only if the forerunners are in sufficiently high concentrations. This occurs effectively when $N(2^2D)$ is produced in the weakly endothermic reaction.

$$NH_2 + O \longrightarrow N(2^2D) + H_2O \quad \Delta H_r = 7 \text{ kcal/mol} \quad (VII)$$

As a matter of fact, NH_2 and O radicals can be viewed as chain carriers radicals, *i.e.*, species present in the flame front with mole fractions of about 1%.

Of course, what has been said about the (2^2D) state is also valid for the (2^2P) state. Nevertheless, reaction VII is then 32 kcal/mol endothermic and since reaction I'' is almost as rapid as reaction I', ion formation should be somewhat less favorable.

Fontijn[17] using a fast flow reaction has called attention to the role of excited N_2 molecules in reactions producing ions in nitrogen containing system

$$NO^* + N_2{}^* \longrightarrow NO^+ + e^- + N_2$$

Both molecules were considered to be in unspecified excited states. Such reactions do not agree with our experimental data, particularly with that concerning the partial order of chemiionization with respect to ammonia (first-order dependence), when ammonia traces are added to flames burning in mixtures of either hydrogen–oxygen–nitrogen or in carbon monoxide–oxygen–nitrogen. Moreover, the occurrence of reactions between two excited species ought to be extremely low and cannot account for the relatively high rate of chemiionization.

The mechanism in ammonia flames we favored is therefore for combustion[18]

$$NH_3 + OH \longrightarrow NH_2 + H_2O$$
$$NH_2 + O_2 \longrightarrow HNO + OH$$
$$NH_2 + O \longrightarrow HNO + H$$

for ion production

$$NH_2 + O \longrightarrow N(2^2D) + H_2O \quad (VII)$$
$$N(2^2D) + O \longrightarrow NO^+ + e^- \quad (I')$$

A rate constant for elementary reaction I' can be estimated to amount to $10^{-12} \exp(-10{,}000/RT)$ cm^3/molecule sec.

(2) *Secondary Ions.* The decay of NH_4^+ and H_3O^+ (Figure 2) is much too fast to characterize recombination processes. The removal of ions is therefore essentially due to $NO^+ + e^- \rightarrow N + O$.

Besides the fast reactions studied by Fehsenfeld and Ferguson[19] to produce NH_4^+ and H_3O^+, another reaction path is also feasible: the formation of an intermediate ion HNO^+ according to the reaction

$$NO^+ + H \longrightarrow HNO^+ \quad \Delta H = -27 \text{ kcal/mol} \quad (VIII)$$

Fehsenfeld[20] estimated an upper limit of this rate constant of $k_8 = 10^{-11}$ cm^3/molecule sec at room temperature. Since proton transfer reactions have rate constants of about 10^{-9} cm^3/molecule sec, the steady-state concentration of HNO^+ should be around 10^8 ions/cm^3 which is lower than the detection limit of our mass spectrometer. The proton transfer reactions are

$$HNO^+ + NH_3 \longrightarrow NH_4^+ + NO \quad \Delta H = -79 \text{ kcal/mol} \quad (IX)$$

$$HNO^+ + H_2O \longrightarrow H_3O^+ + NO \quad \Delta H = -35 \text{ kcal/mol} \quad (X)$$

The reaction

$$H_3O^+ + NH_3 \longrightarrow NH_4^+ + H_2O \quad \Delta H = -44 \text{ kcal/mol} \quad (XI)$$

is very close to equilibrium in the flame front. The decay of the NH_4^+ ion is due to the reverse of reaction XI at a position where the ammonia concentration becomes negligible. Process X in the reverse direction allows the production again of HNO^+ ions which disappear and give NO^+ ions in exothermic reactions with all radicals (NO, OH, N, and O) in the burnt gases region.

In conclusion, ionization phenomena in ammonia–oxygen flames appears to lead to the formation of NO^+ ions in an elementary process involving the ground state atomic oxygen and the excited electronic state of atomic nitrogen: either the (2^2P) or more probably the (2^2D) state.

Acknowledgment. This research has been sponsored in part by the Aerospace Research Laboratories through the E.O.A.R., O.A.R., USAF, under Contract No. F 61052-70-C-0016.

We acknowledge also the support received from the Fonds de la Recherche Fondamentale et Collective (Belgium).

One of us (C.B.) express his gratitude to the Institut Français du Pétrole for the allocation of a postgraduate fellowship.

References and Notes

(1) This work has been presented in part at the 164th National Meeting of the American Chemical Society, New York, N.Y., Aug. 1972.
(2) H. F. Calcote, *AGARD Conf. Proc.*, **No. 8**, 1 (1965); J. A. Green and T. M. Sugden, *Symp. (Int.) Combust., [Proc.], 9th, 1962*, 605 (1963); J. Peeters and A. van Tiggelen, *Symp. (Int.) Combust., [Proc.], 12th, 1968*, 437 (1969).
(3) (a) C. Bertrand and P. J. van Tiggelen, Second International Colloquium on Gas Kinetics, Swansea, England, July 1971, (b) S. de Jaegere, J. Deckers, and A. van Tiggelen, *Symp. (Int.) Combust., [Proc.], 8th, 1960*, 155 (1962).
(4) E. M. Bulewicz, *Symp. (Int.) Combust., [Proc.], 12th, 1968*, 957 (1969); A. van Tiggelen, J. Peeters, and C. Vinckier, *Symp. (Int.) Combust., [Proc.], 13th, 1970*, 311 (1971).
(5) J. P. Botha and D. B. Spalding, *Proc. Roy. Soc., Ser. A*, **211**, 445 (1952).
(6) A. van Tiggelen, J. Peeters, and C. Vinckier, *Oxid. Combust. Rev.*, **4**, 93 (1969).
(7) P. J. van Tiggelen and A. Duval, *Bull. Cl. Sci., Acad. Roy. Belg.*, **53**, 326 (1967).
(8) A. van Tiggelen, *Mém. Acad. Roy. Belg., Cl. Sci.*, **27**, 1 (1952).
(9) M. Gilbert, *Symp., (Int.) Combust., [Proc.], 6th, 1956*, 74 (1957).
(10) D. G. R. Andrews and P. Gray, *Combust. Flame*, **8**, No. 2, 113 (1964).
(11) J. F. Van Wonterghem and A. van Tiggelen, *Bull. Soc. Chim. Belg.*, **64**, 99 (1955).
(12) S. C. Lin and J. D. Teare, *Phys. Fluids*, **6**, 355 (1963).

(13) C. Bertrand and P. J. van Tiggelen, to be submitted for publication.
(14) G. Herzberg, "Spectra of Diatomic Molecules," 2nd ed, Van Nostrand, Princeton, N.J., 1950.
(15) F. R. Gilmore, *J. Quant. Spectrosc. Radiat. Transfer*, **5**, 369 (1965).
(16) D. Husain, L. J. Kirsch, and J. R. Wiesenfeld, *Discuss. Faraday Soc.*, **53**, 201 (1972).
(17) A. Fontijn's comment on E. M. Bulewicz's paper, *Symp. (Int.) Combust., [Proc.], 12th, 1968*, 957 (1969).
(18) D. J. Mc Lean and H. Gg. Wagner, *Symp. (Int.) Combust., [Proc.], 11th, 1966*, 871 (1967).
(19) F. C. Fehsenfeld and E. E. Ferguson, *J. Chem. Phys.*, **54**, 439 (1971).
(20) F. C. Fehsenfeld, private communication.

Forst "Fall-Off" Procedures Utilizing Direct Count State Densities

M. Christianson, D. Price,* and R. Whitehead

Department of Chemistry and Applied Chemistry, University of Salford, Salford M5 4WT, Lancastershire, England
(Received May 16, 1974)

The use of direct count state densities has led to unacceptable sensitivity to energy step length in previous attempts to use the Forst procedure. The basis of this sensitivity is examined in general terms and criteria which both avoid it and, in addition, give optimal accuracy are derived. In the case of a constant energy step length calculation, the optimal accuracy is achieved when the step length is equal to the lowest frequency of the molecule. An improved result is obtained when a variable step length is utilized such that one increment in the number of states occurs within the step length. Fall-off calculations using these criteria are given for methyl isocyanide and 3,3,4,4-tetrafluorocyclobutene.

1. Introduction

Forst[1] has developed a scheme for the variation of rate constant with pressure (commonly referred to as the "fall-off") for a unimolecular gas reaction based primarily on the Laplace transform of the appropriate partition function. The utility of the scheme lies in its independence of any proposed activated complex. Frey, Hopkins, and Vinall[2] have attempted to calculate a fall-off for the thermal isomerization of 3,3,4,4-tetrahydrofluorocyclobutene with this scheme utilizing a direct count of the number of energy states. They found that the results were strongly dependent on the energy step employed in the calculation; a less precise method to calculate the number and density of states (steepest descents[3]) was, in fact, used.

In the present paper we give an explanation of this interesting effect and propose a criterion which enables an exact count procedure to be used without difficulties in a Forst treatment. However, it must be stated that this does not in any way improve the assumptions on which the inversion procedure leading to eq 1 is based, but addresses itself to the numerical problems associated with its use. Finally, fall-offs are computed on the Frey system and the model reaction used by Forst, *i.e.*, methyl isocyanide isomerization.

2. Theoretical Discussion

Forst[1] obtains for the specific energy rate constant by means of the Laplace transform inversion the expression (using the notation of ref 1)

$$k(E) = \frac{A_\infty N(E - E_\infty)}{N(E)} \quad \text{for } E > E_\infty$$
$$= 0 \quad \text{for } E < E_\infty \tag{1}$$

where $N(E)$ is the density of vibrational-internal rotational energy states at energy E and E_∞ and A_∞ are the high-pressure Arrhenius factors, centrifugal effects being ignored. Substitution of (1) into the basic RRKM type expression for k_{uni}, the unimolecular rate constant

$$k_{uni} = \frac{1}{Q}\int_0^\infty \frac{k(E)N(E)e^{-E/RT}}{1 + k(E)/\omega}\,dE \tag{2}$$

where Q is the partition function for the active "modes" and ω is the collision frequency, gives

$$k_{uni} = \frac{1}{Q}\int_{E_\infty}^\infty \left[A_\infty N(E - E_\infty)e^{-E/RT}\,dE \Big/ \left\{1 + \frac{A_\infty}{\omega}\frac{N(E - E_\infty)}{N(E)}\right\}\right] \tag{3}$$

Setting $E' = E - E_\infty$ and rearranging we obtain

$$k_{uni} = \frac{\omega e^{-E_\infty/RT}}{Q}\int_0^\infty \left[N(E')e^{-E'/RT}\,dE' \Big/ \left\{\frac{N(E')}{N(E' + E_\infty)} + \frac{\omega}{A_\infty}\right\}\right] \tag{4}$$

which is in the form used by Frey, but unfortunately there is a typographical error in the denominator in his expression.

The form we shall use is

$$k_{uni} = \frac{k_\infty}{Q}\int_0^\infty \left[N(E)e^{-E/RT}\,dE \Big/ \left\{1 + \frac{A_\infty}{\omega}\frac{N(E)}{N(E + E_\infty)}\right\}\right] \tag{5}$$

We shall now investigate the sensitivity of the integral to various methods of expressing the density of states.

Following Forst and Frey we shall assume that a continuous function, *e.g.*, Whitten–Rabinovitch (WR),[4] Haarhoff,[5] etc., is a suitable approximation for $N(E + E_\infty)$. Such approximations are badly in error for $N(E)$ at the lower energies and it may be formally expressed, because of its discrete form, as

$$N(E) = \sum_{i=1}^{n_E} W(E_i)\,\delta(E - E_i) \quad (6)$$

where $W(E_i)$ is the number of vibration-internal rotation states occurring at the quantized energy E_i, $\delta(E - E_i)$ is the Dirac delta function; E_1 is the ground (lowest) energy state, and E_{n_E} ($\leq E$) is the energy state closest to E; $N(E)$, $W(E_i)$, and Q all being defined for the same set of states. That this is a proper and consistent expression for $N(E)$ is easily demonstrated by the following argument.

Now we define the usual multistep function $G(E)$ by

$$G(E) = \int_0^E N(E)\,dE = \int_0^E \sum_{i=1}^{n_E} W(E_i)\,\delta(E - E_i)\,dE \quad (7)$$

and as the integrand is identically zero for $E < E_1$ and $E > E_{n_E}$ then we write the integral in the form

$$G(E) = \int_{-\infty}^{+\infty} \sum_{i=1}^{n_E} W(E_i)\,\delta(E - E_i)\,dE \quad (8)$$

As the integrand is a finite sum, each term of which is also finite (and positive), we can interchange the order of the summation and integration giving

$$G(E) = \sum_{i=1}^{n_E} \int_{-\infty}^{+\infty} W(E_i)\,\delta(E - E_i)\,dE = \sum_{i=1}^{n_E} W(E_i) \int_{-\infty}^{+\infty} \delta(E - E_i)\,dE = \sum_{i=1}^{n_E} W(E_i) \quad (9)$$

i.e., $N(E)$ is a series of appropriately weighted delta functions while $G(E)$ is the corresponding multistep function.

It is convenient to split the integration range, the first part, $E < E_D$, being that range over which a discrete density function must be used *i.e.*

$$k_{uni} = \frac{k_\infty}{Q}\left[\int_0^{E_D}\left[N(E)e^{-E/RT}\,dE \Big/ \left\{1 + \frac{A_\infty}{\omega}\frac{N(E)}{N(E + E_\infty)}\right\}\right] + \int_E^\infty \left[N(E)e^{-E/RT}\,dE \Big/ \left\{1 + \frac{A_\infty}{\omega}\frac{N(E)}{N(E + E_\infty)}\right\}\right]\right] \quad (10)$$

where the Whitten–Rabinovitch or similarly suitable approximation may be used for all densities in the second term.

Substitution of the delta function expression for the state density in the first term leads to

$$\frac{k_\infty}{Q}\int_0^{E_D}\left[\sum_{i=1}^{n_E} W(E_i)\,\delta(E - E_i)e^{-E/RT}\,dE \Big/ \left\{1 + \frac{A_\infty}{\omega}\sum_{i=1}^{n_E}\frac{W(E_i)\,\delta(E - E_i)}{N(E + E_\infty)}\right\}\right] \quad (11)$$

First consider the value of the integrand at any point $E \neq E_i$ (for all i). Due to the property of the Dirac delta function, $N(E)$ represented by $\Sigma_{i=1}^{n_E} W(E_i)\,\delta(E - E_i)$ equals zero and thus the integrand is identically zero. Now consider any representative point $E = E_i$, the density becomes $W(E_i)\,\delta(E_i - E_i) = W(E_i)\,\delta(0)$ which, by virtue of the delta function, is large without limit and all the other terms $W(E_j)\,\delta(E_i - E_j)$ are zero thus the integrand becomes

$$W(E_i)\,\delta(0)e^{-E/RT} \Big/ \left\{\frac{A_\infty}{\omega}\frac{W(E_i)\,\delta(0)}{N(E_i + E_\infty)}\right\} = \frac{\omega}{A_\infty}N(E_i + E_\infty)e^{-E/RT} \quad (12)$$

which has the appropriate finite value. Hence over the range of integration, the integrand is merely a finite collection of such point values, which are themselves always finite, and thus the integral is identically zero.

This, at first sight, somewhat surprising result (the greater the range over which we use a discrete representation of $N(E)$ the poorer our result) arises from the incompatibility of utilizing a discrete representation of $N(E)$ together with a continuous representation of $N(E + E_\infty)$ in the same expression. When such integrals are computed by numerical procedures one must expect sensitivity to the "step length," and increasingly so as the "step" is made small as both Forst and Frey found. This behavior is, of course, completely contrary to that found with integrals representing continuous functions. A consideration of the computation of the partition function utilizing a direct count of states readily shows that the sensitivity to step length is normal to such numerical procedures and, in fact, the value tends to the exact value as the step length becomes small. This problem does not arise in RRKM theory in the discrete region because the integrand contains an expression for the sum of energy states up to the given value of E which, in terms of discrete energy states, is a multistep function and not a series of Dirac delta functions, *i.e.*, the integrand exists (*i.e.*, nonzero) for all E in the energy range.

3. Numerical Investigation of Step-Length Sensitivity

Consider the contribution of the discrete part of the energy range; in particular

$$\Delta k_{uni}{}^D = \frac{k_\infty}{Q}\int_0^{E_D}\left[N(E)e^{-E/RT}\,dE \Big/ \left\{1 + \frac{A_\infty}{\omega}\frac{N(E)}{N(E + E_\infty)}\right\}\right] \quad (13)$$

converting this to a summation with a step ΔE gives

$$\Delta k_{uni}{}^D = \frac{k_\infty}{Q}\sum_{E_K=0}^{E_D}\left[N(E_K)e^{-E/RT}\,\Delta E \Big/ \left\{1 + \frac{A_\infty}{\omega}\frac{N(E_K)}{N(E_K + E_\infty)}\right\}\right] \quad (14)$$

Now since $N(E)\,\Delta E \simeq \Sigma_{\Delta E} W(E_i)$, *i.e.*, the sum of states over the range ΔE

$$\Delta k_{uni}{}^D = \frac{k_\infty}{Q}\sum_{E_K=0}^{E_D}\left[\sum_{\Delta E(K)} W(E_i)e^{-E_K/RT} \Big/ \left\{1 + \frac{A_\infty}{\omega}\frac{\sum_{\Delta E(K)} W(E)}{N(E_K + E_\infty)\Delta E}\right\}\right] \quad (15)$$

where

$$\sum_{\Delta E(K)} W(E_i) = \sum_{E_K}^{E_K + \Delta E} W(E_i) \quad (16)$$

with $E_K \leq E_i \leq E_K + \Delta E$. This final form of the discrete contribution was used in two ways to investigate the effect of step length. A computer program supplied by Robinson[6] was used to obtain $\Sigma W_{\Delta E}(E_i)$ and the Whitten–Rabinovitch[4] approximation was used for $N(E_K + \Delta E/2 + E_\infty)$. (a) Using the same step ΔE in the summation and the exact count a calculation of the discrete contribution (up to 41.8 kJ mol^{-1}) was made in the case of ethane decomposition at 873.2°K and 1 Torr (1 Torr = 133.32 Nm^{-2}) utilizing the data of Lin and Laidler[7] (LL) except that the frequencies were grouped as in Table I. No attempt was

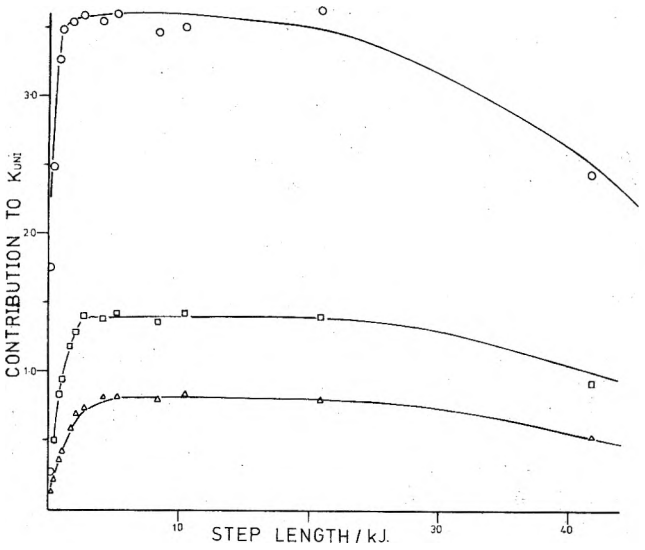

Figure 1. A plot of the contribution to k_{uni} (at 1 Torr) from discrete summation against step length: lowest frequencies in model (O) 100 cm^{-1}; (□) 273 cm^{-1}; (Δ) 500 cm^{-1}.

TABLE I: Molecular Vibration Frequencies of Ethane Used in Calculations for Figures 1 and 2

Frequency, cm^{-1}	Degeneracy	Frequency, cm^{-1}	Degeneracy
2961	6	993	1
1473	4	820	2
1377	2	273	1
1155	2		

made to find the actual rate constant. The results are plotted in Figure 1. Figure 1 also shows the effect of the lowest frequency of the model on the position of the maximum in the discrete range. (b) The second study made used a constant direct count step and a variable summation step length on the same ethane system. The results are plotted in Figure 2.

Figures 1 and 2 clearly demonstrate that the Forst scheme is sensitive to step length in the discrete region and that the summation tends rapidly to zero at smaller step lengths as was shown in section 2. With increasing step length the summation tends first to its correct value, *i.e.*, the maximum of the curve, then begins to fall due to the usual increase of error attendant upon a large step in the numerical integration procedure. Thus a fall-off calculation should optimally use the energy step which corresponds to the maximum discrete contribution.

The criterion of the optimal step length is that it must be as small as possible providing zeros do not occur in $\Sigma_{\Delta E} W(E_i)$. The maximum discrete contribution thus corresponds to a constant step length equal to the discrete quantum energy of the lowest vibrational frequency. It should be noted that if active rotations are considered the optimal step length would necessarily be considerably smaller thus increasing the overall accuracy of the summation.

4. Application to Unimolecular Fall-Off Studies

Calculations using a direct count of energy states in the discrete region, with the above criterion for the step length, have been combined with the WR approximation in the continuous region for the thermal isomerization of methyl isocyanide[1,8] and 3,3,4,4-tetrafluorocyclobutene.[2] The

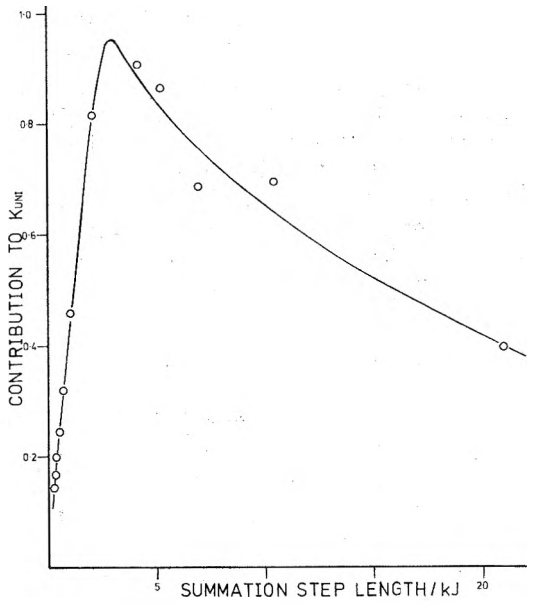

Figure 2. A plot of the contribution to k_{uni} from discrete summation against step length for a summation using a constant direct count of energy states.

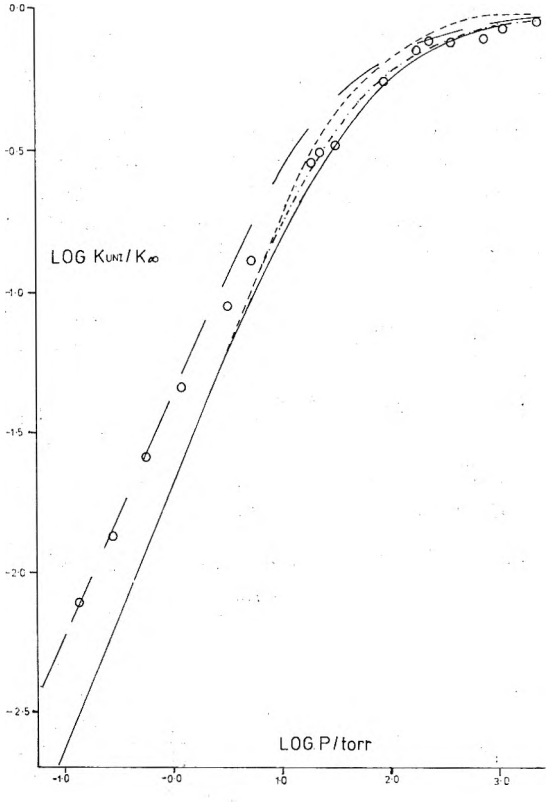

Figure 3. A plot of log k_{uni}/k_∞ against log P (Torr) for methyl isocyanide: (O) experimental results; (– –) RRKM plot (model given in ref 1); (——) Forst procedure (Forst's calculation); (- - -) present calculations (constant lowest frequency step length); (- · · ·) present calculations (variable step length).

curves obtained (Figures 3 and 4) are in very good agreement with those using the steepest descents approximation used by the previous authors.

5. Variable Energy Step Length

The maximum accuracy in a Forst treatment in the discrete region may be obtained by using a variable step

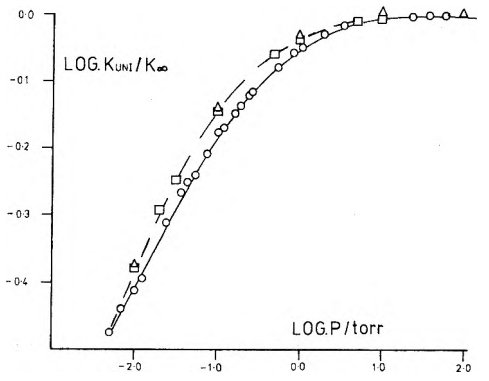

Figure 4. A plot of log k_{uni}/k_∞ against log P (Torr) for 3,3,4,4-tetrafluorocyclobutene: (O) experimental results; (- - -) RRKM plot (model given in ref 2); (□) Forst procedure (Frey's calculation); (Δ) present calculations (constant lowest frequency step length).

length in the summation. This step length is the difference in energy between successive nonzero values of $W(E_i)$. A simple alteration to the computer program has been developed and a calculation has been carried out for methyl isocyanide; the results compare favorably with those obtained using the "smallest frequency" criterion, Table II and Figure 3. The value of the vibrational partition function calculated in this manner is in considerably better agreement with the exact value than is that obtained using the constant step method. This is a useful test of the efficacy of the procedure. However, the remaining discrepancy between the direct count evaluated partition function and the exact value deserves comment. Robinson's[6] procedure was used to obtain the direct count and essentially finds all the states which occur in the step length ΔE, and hence the "weighting" due to the exponential term in the partition function is somewhat in error after the first few steps. This error could be eliminated by either utilizing an appropriately smaller step in the direct count procedure or, more efficiently, using an alternative procedure, such as that of Stein and Rabinovitch[9] which computes the number of states at a given energy, albeit by the use of "rounded-off" frequencies.

TABLE II: Vibrational Partition Functions and Fall-Off Points for the Two Procedures Using the Methyl Isocyanide System

	Constant step length[a]	Variable step length[b]
Vibrational partition function[c]	5.187	4.095
Pressure, Torr	k_{uni}/k_∞	k_{uni}/k_∞
1000	0.938	0.909
100	0.648	0.589
10	0.175	0.165
1	2.127×10^{-2}	2.084×10^{-2}
0.1	2.175×10^{-3}	2.143×10^{-3}
0.01	2.180×10^{-4}	2.149×10^{-4}

[a] Step length = 3.260 kJ mol^{-1}. [b] Step length in direct count procedure = 0.418 kJ mol^{-1}. [c] Vibrational partition function from exact calculation = 4.338. *Note Added in Proof.* Vibrational partition function calculated by Stein and Rabinovitch[9] procedure = 14.335.

Acknowledgments. One of us (M.C.) is indebted to the Science Research Council for an SRC award during the period of this investigation. The authors thank Dr. Robinson for the copy of his computer program.[6]

References and Notes

(1) (a) W. Forst, *J. Phys. Chem.*, **76**, 342 (1972); (b) W. Forst, "Theory of Unimolecular Reactions," Academic Press, New York, N.Y., 1973, pp 123 and 178.
(2) H. M. Frey, R. G. Hopkins, and I. C. Vinall, *J. Chem. Soc., Faraday Trans. 1*, **68**, 1874 (1972).
(3) W. Forst and Z. Prášil, *J. Chem. Phys.*, **51**, 3006 (1969).
(4) C. Z. Whitten and B. S. Rabinovitch, *J. Chem. Phys.*, **38**, 3466 (1963).
(5) P. C. Haarhoff, *Mol. Phys.*, **6**, 337 (1963).
(6) Exact count of vibrational energy levels was performed using a computer program supplied by P. J. Robinson Chemistry Department, UMIST, Manchester, England.
(7) M. C. Lin and K. J. Laidler, *Trans. Faraday Soc.*, **64**, 79 (1968).
(8) F. W. Schneider and B. S. Rabinovitch, *J. Amer. Chem. Soc.*, **84**, 4215 (1962).
(9) S. E. Stein and B. S. Rabinovitch, *J. Chem. Phys.*, **58**, 2438 (1973).

Hydroperoxyl Radical Reactions. III. Pulse-Radiolytic Study of the Reaction of the Hydroperoxyl Radical with Some Metal Ions

D. Meisel, Y. A. Ilan, and G. Czapski*

Department of Physical Chemistry, The Hebrew University of Jerusalem, Jerusalem, Israel *(Received February 22, 1974)*

The reactions of $HO_2\cdot$ with U(VI), Th(IV), and Ce(III) were studied by the pulse radiolysis technique. Optical spectra of the U(VI) and Th(IV) complexes with $HO_2\cdot$ were obtained as well as the rate of their formation and decay. Evidence is presented that Ce(III) is oxidized by $HO_2\cdot$ radicals to give Ce(IV) and this rate was measured.

Introduction

The reaction of $HO_2\cdot$ radicals with metal ions was shown to yield relatively stable radical complexes[1-13] as compared to free $HO_2\cdot$.

$$M^{n+} + HO_2\cdot \rightleftharpoons [M\text{–}HO_2\cdot]^{n+} \quad (1)$$

Most of these studies employed epr spectroscopy for the detection of these radicals. Hardly any optical studies of these complexes have been made. Recent results, obtained by the use of the flow-epr technique, indicate that the rate of formation of $[M\text{–}HO_2\cdot]^{n+}$, for M^{n+} = U(VI) and Th(IV), is very fast, beyond the time resolution of this technique.[13] In view of the current interest in the reaction of $HO_2\cdot$, and their possible role in radiation chemistry and radiation biology,[14] we decided to study the kinetics, stability constants, and optical spectra of some of these complexes.

In this study the pulse-radiolysis technique was employed. The hydroperoxyl radical was generated in acid solutions containing H_2O_2 and oxygen-saturated, *via* the sequence of reactions 2–6. The formation of the complex through reaction 1 was followed spectrophotometrically.

$$H_2O \rightsquigarrow e_{aq}^-, H\cdot, OH\cdot, H_2O_2, H_2 \quad (2)$$

$$e_{aq}^- + H^+ \longrightarrow H\cdot \quad (3)$$

$$e_{aq}^- + H_2O_2 \longrightarrow OH\cdot + OH^- \quad (4)$$

$$H\cdot + O_2 \longrightarrow HO_2\cdot \quad (5)$$

$$OH\cdot + H_2O_2 \longrightarrow HO_2\cdot + H_2O \quad (6)$$

The stability constants, K_1, and decay kinetics of several such complexes were also determined.

Experimental Section

Triply distilled water was used throughout this study. All reagents were of the highest purity available, and were used without further purification. All solutions were 0.1 *M* in $HClO_4$ and 0.1–0.05 *M* in H_2O_2 unless otherwise stated. Fresh solutions were prepared before irradiation and were oxygen saturated, unless otherwise stated, by bubbling ultrapure oxygen through the solutions, using the syringe technique.[15] Metal ions were used as the sulfate salts. The complexation of U(VI) and Th(IV) with the sulfate was negligible in the range of concentrations used[16,17] while the contrary holds for cerium, which was totally complexed.[18,19]

Although M^{n+} may yield complexes with H_2O_2, it was shown to have no effect on the paramagnetic complexes produced in reaction 1.[20]

The Varian 7715 linear accelerator was used in this study. Solutions were subjected to 1.5-μsec pulses with a 200-mA current of 5-MeV electrons. Such a pulse generated a total of about 3×10^{-5} *M* of radicals. No effect was detected (neither on the yield nor on the kinetics of the systems studied) when using up to 20 pulses on a given solution. A Spectrosil irradiation cell, 4 cm long, with an optical path of 12.3 cm, was used. The analyzing light source was a 150-W xenon arc lamp. A 1P28, or solar-blind R166 for λ <300 nm photomultipliers, in conjunction with a Bausch and Lomb 1350 grating monochromator constituted the detection system. Appropriate light filters were used to minimize photochemical and scattered light effects.

Results and Discussion

a. U(VI) + $HO_2\cdot$. The formation of the transient obtained on irradiating a 1 m*M* UO_2^{2+} oxygen-saturated solution, 0.1 *M* in H_2O_2 and 0.1 *M* in $HClO_4$, is shown in the insert of Figure 1. A similar solution with no H_2O_2, and saturated with argon, gave a transient which decayed much faster than the formation of the species observed in Figure 1.

We attribute the species in the O_2-saturated solution to the complex of U(VI) with $HO_2\cdot$, schematically represented as $[U(VI)\text{–}HO_2\cdot]$,[21] formed through reactions 1–6. The spectrum of this complex, peaking at λ_{max} 305 nm, is shown in Figure 1.

The kinetics of the formation of this complex were of pseudo first order, as checked by plotting ln $(OD_{t=\infty} - OD_t)$ *vs.* time, and shown in the insert of Figure 2. No dependence of the observed rate constant on dose was observed on changing the pulse width in the range of 1.5–0.5 μsec. As can be seen in Figure 2a the observed rate constant is linearly dependent on $[UO_2^{2+}]$. Yet this dependence yielded a positive intercept. Assuming that the formation curve represents the achievement of equilibrium 1a, the ob-

$$UO_2^{2+} + HO_2\cdot \rightleftharpoons [U(VI) - HO_2\cdot] \quad (1a)$$

served rate constant, k_{obsd}, equals $k_{1a}[UO_2^{2+}] + k_{-1a}$. From the slope in Figure 2a we obtain $k_{1a} = (1.5 \pm 0.1) \times 10^5\ M^{-1}\ sec^{-1}$ and from its intercept we get $k_{-1a} = (1 \pm 0.2) \times 10^2\ sec^{-1}$. The stability constant is thus $K_{1a} = k_{1a}/k_{-1a} = (1.5 \pm 0.3) \times 10^3\ M^{-1}$. This value is in excellent agreement with the one obtained recently from flow-epr studies.[13] This provides additional evidence for the identification of the species as the paramagnetic complex $[U(VI)\text{–}HO_2\cdot]$.

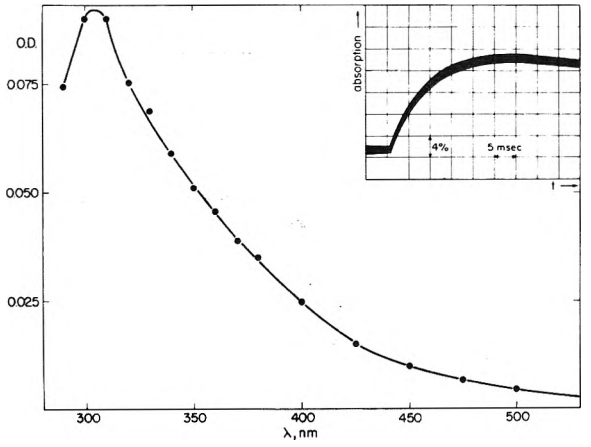

Figure 1. Spectrum of U(VI)–HO_2· obtained on irradiation of 1 m*M* UO_2^{2+} + 0.1 *M* H_2O_2 in 0.1 *M* $HClO_4$ oxygen-saturated solution, 25 msec after the pulse. The insert shows an oscillogram obtained on pulse irradiating the above solution (λ 310 nm).

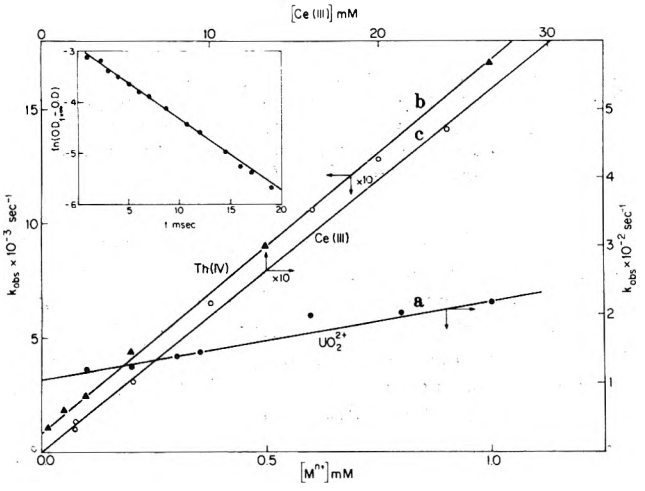

Figure 2. The dependence of the observed first-order-rate constants for the reaction of M^{n+} with HO_2·. (a) Formation of [U(VI)–HO_2·] *vs.* [UO_2^{2+}]. The insert shows the first-order criterion for that formation: [H_2O_2] = [$HClO_4$] = 0.1 *M*, O_2-saturated, measured at λ 320 nm. (b) Formation of [Th(IV)–HO_2·] *vs.* [Th(IV)]: oxygen saturated, 50 m*M* H_2O_2, 0.1 *M* $HClO_4$ solutions. Lower scale should be multiplied by 10. (c) Formation of Ce(IV) *vs.* [Ce(III)]: O_2 saturated, 0.8 *N* H_2SO_4 solutions. Right-hand scale should be multiplied by 10.

The equilibrium constant of the complex, K_{1a}, is given by

$$K_{1a} = \frac{[\text{U(VI)–HO}_2\cdot]}{[UO_2^{2+}]([HO_2\cdot]_0 - [\text{U(VI)–HO}_2\cdot])} \quad (7)$$

We measured the OD of the complex at λ 330 nm, where HO_2· has negligible absorption, as a function of the initial [UO_2^{2+}]. In this case 1/OD should depend linearly on 1/[UO_2^{2+}] according to

$$\frac{1}{OD} = \frac{1}{OD_\infty}\left(1 + \frac{1}{K_{1a}[UO_2^{2+}]}\right) \quad (8)$$

where OD is the absorbance of the complex when equilibrium 1a is achieved, and OD_∞ is that when total scavenging of HO_2· by UO_2^{2+} is achieved. Equation 8 will hold provided that no self-recombination of HO_2· radicals occurs in the time range of the formation of the complex. This is obviously the case under our experimental conditions, since

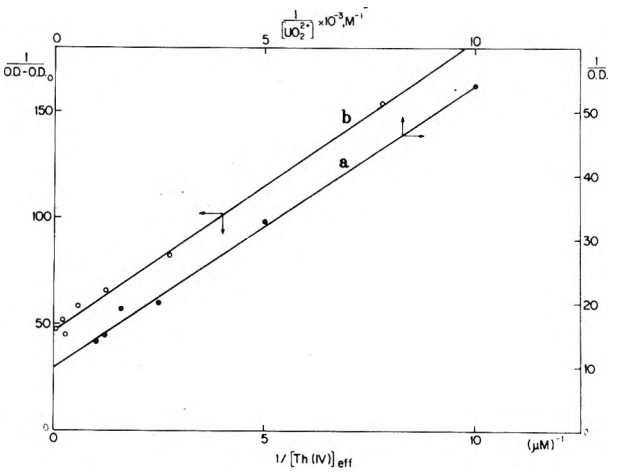

Figure 3. The dependence of the yield of [M^{n+}–HO_2·] on (M^{n+}): (a) 1/OD at λ 320 nm *vs.* 1/[UO_2^{2+}]; (b) 1/(OD − OD_0) *vs.* 1/[Th(IV)]$_{eff}$.

$k_9 = 7.5 \times 10^5\ M^{-1}\ \text{sec}^{-1}$ [22] and [U(VI)–HO_2·] decays even slower.

$$HO_2\cdot + HO_2\cdot \longrightarrow H_2O_2 + O_2 \quad (9)$$

As can be seen in Figure 3a, eq 8 is fairly well obeyed. Since in our experiments, the lowest [UO_2^{2+}] > 0.1 m*M*, no correction in [UO_2^{2+}] was necessary for the amount complexed. The ratio of the intercept to the slope in Figure 3a yields $K_{1a} = (2 \pm 0.2) \times 10^3\ M^{-1}$, not far off from the value we obtained kinetically. Assuming G[U(VI)–HO_2·] = $G(HO_2\cdot) = G_H + G_{e_{aq}^-} + G_{OH}$ = 6.2 molecules/100 eV, we can estimate from OD_∞, ϵ_{305} 725 ± 100 $M^{-1}\ \text{cm}^{-1}$.

The decay kinetics of [U(VI)–HO_2·] were followed at λ 330 nm. In accordance with previous observation[13] the decay rate was inversely proportional to [UO_2^{2+}]. This is attributed to the replacement of the relatively fast self-recombination, reaction 9, by the slower cross recombination, reaction 10, and the self-recombination (reaction 11), of the

$$[M^{n+}\text{–HO}_2\cdot] + HO_2\cdot \longrightarrow M^{n+} + H_2O_2 + O_2 \quad (10)$$

$$[M^{n+}\text{–HO}_2\cdot] + [M^{n+}\text{–HO}_2\cdot] \longrightarrow 2M^{n+} + H_2O_2 + O_2 \quad (11)$$

complex. Since equilibrium 1a is achieved rapidly as compared to the slow decay of [U(VI)–HO_2·], the rate of the disappearance of the complex can be given by

$$-d[\text{U(VI)–HO}_2\cdot]/dt = 2\{k_9/(K_{1a}[UO_2^{2+}])^2 + k_{10}/K_{1a}[UO_2^{2+}] + k_{11}\}\left(1 + \frac{1}{K_{1a}[UO_2^{2+}]}\right)^{-1} \times [\text{U(VI)–HO}_2\cdot]^2 = 2k_d[\text{U(VI)–HO}_2\cdot]^2 \quad (12)$$

The decay rate was measured and was found to be a superposition of pseudo first and second orders. The second-order component of the decay is attributed to reactions 9–11, while the first-order component probably reflects the reaction of [U(VI)–HO_2·] with impurities. For the first 75% of the reaction, where the contribution of the second-order processes is the dominant, the decay rate fitted quite well with the second-order criterion of 1/OD *vs.* time. We thus determined from the initial decay rate the dependence of k_d on [UO_2^{2+}]. Using a non-linear least-mean-squares method,[23] we computed the values of k_{10}, k_{11}, and K_{1a}, assuming $k_9 = 7.5 \times 10^5\ M^{-1}\ \text{sec}^{-1}$.[22] The experimental results, along with the best-fit curve, yielded $k_{10} = 4.1 \times 10^5\ M^{-1}\ \text{sec}^{-1}$, $k_{11} = 7.5 \times 10^4\ M^{-1}\ \text{sec}^{-1}$, and $K_{1a} = 1.4 \times 10^3$

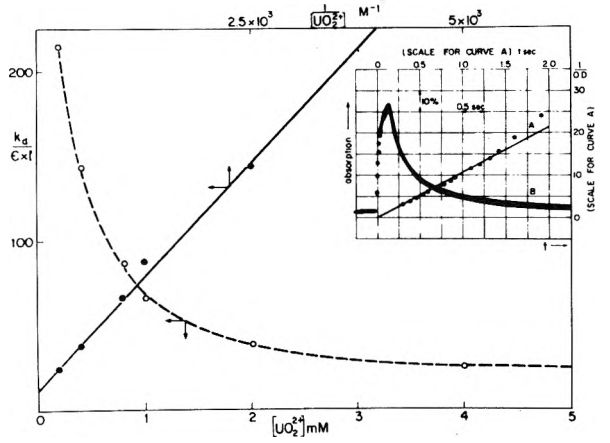

Figure 4. The dependence of the second-order-rate constant, k_d, for the decay of [U(VI)–HO_2·] on [UO_2^{2+}]: dashed line, best fitted line; $\epsilon l = 6.6 \times 10^3\ M^{-1}$. Insert A shows the second-order decay of [Th(IV)–HO_2·] obtained on repetitive pulsing of a 1 mM $Th(SO_4)_2$ + 50 mM H_2O_2 + 0.1 M $HClO_4$ oxygen-saturated solution. Oscillogram B shows the build up and decay of the complex during and after repetitive pulse radiolysis (λ 290 nm).

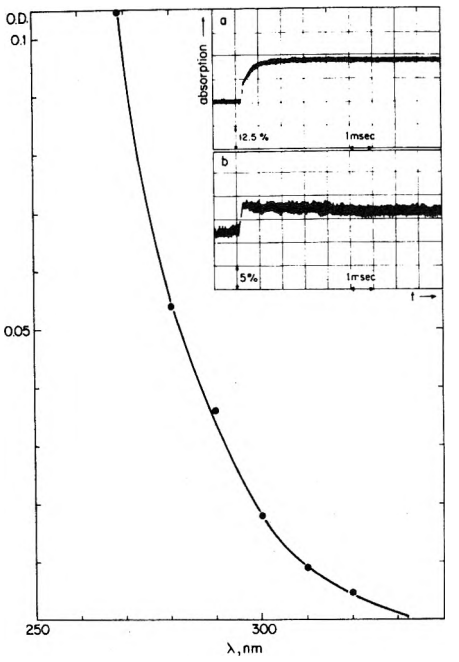

Figure 5. Spectrum of the [Th(IV)–HO_2·] complex obtained on irradiation of a 1 mM $Th(SO_4)_2$ + 0.1 M $HClO_4$ + 50 mM H_2O_2 oxygen-saturated solution. Insert a is an oscillogram obtained on irradiation of the above solution. Insert b is an oscillogram obtained on irradiation of the same solution with no Th(IV) (λ 270 nm).

M^{-1}, as shown in Figure 4. The use of this method can only lead to an indication of the magnitude of the various modes of decay of the complex. A more accurate method is the following: at high enough concentration of UO_2^{2+}, where most of HO_2· is complexed, *i.e.*, when $K_{1a}[UO_2^{2+}] > 1$, and when the contribution of reaction 9 is negligible compared to reactions 10 and 11, k_c reduces to

$$k_d = \frac{k_{10}}{K_{1a}[UO_2^{2+}]} + k_{11} \qquad (13)$$

Thus, k_d should linearly depend on $1/[UO_2^{2+}]$. In Figure 4 it can be seen that eq 13 is obeyed at the higher concentrations of UO_2^{2+}. From the slope in Figure 4 and taking $K_{1a} = 1.5 \times 10^3\ M^{-1}$, we get $k_{10} = (5 \pm 1) \times 10^5\ M^{-1}\ sec^{-1}$, and from the intercept $k_{11} = (8 \pm 2) \times 10^4\ M^{-1}\ sec^{-1}$.

b. Th(IV) + HO_2·. Upon irradiating $Th(SO_4)_2$ oxygen-saturated solutions in 0.1 M $HClO_4$ and 50 mM H_2O_2, a fast formation of a transient could be observed, followed by a slower formation. An oscillogram thus obtained is shown as an example in insert a of Figure 5. In the insert b of Figure 5, is shown an oscillogram obtained upon irradiating the same solution without Th(IV). In both cases there is the same fast formation with nearly the same yield. This fast-formed absorption is attributed to the HO_2· radical, produced through reactions 2–6. In the absence of H_2O_2 and in argon-saturated solution, there was no absorption at this wavelength. The build up of the second species is attributed to the formation of the Th(IV)–HO_2· complex.

$$Th(IV) + HO_2\cdot \rightleftarrows [Th(IV)\text{–}HO_2\cdot] \qquad (1b)$$

The absorption of this complex was examined in the range 260–320 nm and the resulting spectrum is shown in Figure 5. Due to the high concentration of H_2O_2 it was not possible to study the absorption at shorter wavelengths.

The kinetics of the Th(IV)–HO_2· formation followed a pseudo-first-order rate law, independent of dose, and linearly dependent on [Th(IV)]. As can be seen in Figure 2b, the dependence results in a positive intercept, similar to the one observed in the case of U(VI)–HO_2· formation. However, due to the relatively lower value of the intercept, *i.e.*, higher value of K_{1b}, its determination is liable to a larger experimental error which renders it impracticable to measure. The rate constant k_{1b} was found to be $(1.8 \pm 0.2) \times 10^6\ M^{-1}\ sec^{-1}$, which is higher than the lower limit previously estimated.[13] In order to arrive at the value of K_{1b} we studied the dependence of the yield of [Th(IV)–HO_2·] on [Th(IV)]. Since [Th(IV)–HO_2·] absorbs light at the same wavelengths where HO_2· absorbs, eq 14 rather than eq 7,

$$\frac{1}{OD - OD_0} = \frac{1}{OD_\infty - OD_0}\left(1 + \frac{1}{K_{1b}[Th(IV)]_{eff}}\right) \qquad (14)$$

was adopted. The indexes in eq 14 refer to the [Th(IV)] concentrations. Since [Th(IV)] in some of the experiments was rather low, the effective concentration of Th(IV) was calculated by subtracting the amount of [Th(IV)–HO_2·] from the initial [Th(IV)] assuming a 1:1 ratio between Th(IV) and HO_2· in the complex. As can be seen in Figure 3b, $1/(OD - OD_0)$ is linearly dependent on $1/[Th(IV)]_{eff}$ and the value obtained for the stability constant is $K_{1b} = (4 \pm 1) \times 10^4\ M^{-1}$. This value is four times lower than the value estimated from flow-epr studies.[13] This discrepancy might indicate the existence of different complexes of Th(IV) with HO_2· as was found for several other metal ions.[20] However, since the experimental error in both studies is rather large, we hesitate to draw this conclusion for certain.

The decay of [Th(IV)–HO_2·] was followed at λ 290 nm. On increasing [Th(IV)], the lifetime of the complex increased, as was found previously.[13] The slow decay followed an observed first-order rate law, in contrast with the second-order rate law observed for the paramagnetic species in the flow-epr technique. However, there was a substantial difference in the concentrations of radicals between these two experiments, as the concentration of HO_2· was higher in the flow-epr experiments. We were therefore led to sus-

TABLE I: Rate Constants for the Reaction of $HO_2\cdot$ with M^{n+}, Stability Constants of the Complexes Formed, Their Rate of Decay, and Extinction Coefficients

M^{n+}	ϵ, M^{-1} cm^{-1}	λ, nm	k_1, M^{-1} sec^{-1}	k_{-1}, sec^{-1}	K_1, M^{-1}	k_{10}, M^{-1} sec^{-1}	k_{11}, M^{-1} sec^{-1}
U(VI)	725 ± 100	305	(1.5 ± 0.1) × 10^5	(1 ± 0.2) × 10^2	(1.7 ± 0.3) × 10^3 [a]	(5 ± 1) × 10^5	(8 ± 2) × 10^4
Th(IV)	1000 ± 100	270	(1.8 ± 0.2) × 10^6	(4.5 ± 1) × 10^1 [b]	(4 ± 1) × 10^4		
					(1.7 ± 0.4) × 10^5 [c]	(8 ± 2) × 10^5 [c]	(5 ± 2) × 10^2 [c]
Ce(III)	5650 ± 500	320[d]	(2.1 ± 0.2) × 10^5		≤10		

[a] Average value. [b] Estimated from K_1 and k_1. [c] Reference 13. [d] Ce(IV).

pect that the reaction of [Th(IV)–$HO_2\cdot$] with trace amounts of unavoidable impurities is responsible for the observed first-order decay. Evidently, the lower the radical concentration, the greater the contribution of such a reaction is. So as to check this assumption, we repeatedly pulsed the solution with 15 pulses, at a repetition rate of ~100 pulses/sec, *i.e.*, before any appreciable decay of [Th(IV)–$HO_2\cdot$] can occur. The results of such an experiment are shown in the insert of Figure 4. The yield of [Th(IV)–$HO_2\cdot$], as can be seen in the insert of Figure 4, reaches a limiting value after ~15 pulses (probably due to effective competition reactions of the primary radicals with the complex). In any case, as is shown in the insert of Figure 4, the decay in this experiment followed a second-order rate law for about 80% of the reaction. The observed rate constant for this same decay was calculated to be $2k_d = 1.4 \times 10^4\ M^{-1}\ \text{sec}^{-1}$, in close agreement with the value observed previously.[13] Most probably, the main contribution to k_d is the corresponding reaction 10.

c. Ce(III) + $HO_2\cdot$. The reaction of Ce(III) with $HO_2\cdot$ was studied in 0.8 *N* H_2SO_4 oxygen-saturated solutions. Under these conditions, both ceric and cerous ions are fully complexed with the sulfate. A typical oscillogram, obtained on pulse irradiating 10^{-2} *M* $Ce_2(SO_4)_3$ in 0.8 *N* H_2SO_4 oxygen-saturated solution, is shown in Figure 6. The fast process, attributed to the oxidation of Ce(III) by OH· radicals

$$Ce(III) + OH\cdot \longrightarrow Ce(IV) + OH^- \qquad (15)$$

is completed at the end of the pulse. The slower process is attributed to the oxidation of Ce(III) by $HO_2\cdot$ radicals

$$Ce(III) + HO_2\cdot \xrightarrow{H^+} Ce(IV) + H_2O_2 \qquad (16)$$

The spectra obtained at the end of the pulse, and 500 μsec later, are given in Figure 6. Both spectra seem to be identical, with λ_{max} 320 nm, and resemble closely the well-known spectrum of Ce(IV) in 0.8 *N* H_2SO_4.[24] In argon-saturated similar solutions, only the first product could be observed. The ratio of the yields of Ce(IV) in these two processes equals 1.2, *i.e.*, identical with the ratio $(G_H + G_{e_{aq}^-})/G_{OH} = 1.2$. Taking $G_{e_{aq}^-} = G_{OH} = 2.8$ and $G_H = 0.6$, we calculate ϵ_{320} for the first and second products to be 5400 ± 300 and 5650 ± 300 M^{-1} cm^{-1}, respectively, both in excellent agreement with the value of ϵ_{320} 5580 M^{-1} cm^{-1} for $Ce(SO_4)_3^{2-}$.[24] We think therefore that we can safely conclude that Ce(III) reacts with $HO_2\cdot$ radicals to yield Ce(IV). This conclusion confirms the suggestion of Sigler and Masters[25] regarding the mechanism of the reduction of Ce(IV) by H_2O_2, corroborated also by Czapski, *et al.*[9,26] The agreement in ϵ_{320}, on the basis of the above-mentioned G_{OH}, is in accordance with Sworski's, *et al.*,[27] conclusion that G_{ox} = 3.0 molecules/100 eV in similar solutions (where G_{ox} includes the contribution of other oxidizing radicals, other than OH, such as SO_4^- or HSO_4). Any SO_4^- radical, or HSO_4^-, produced under our experimental conditions is expected to react very rapidly with Ce(III). This Ce(III) system might serve as a rather convenient chemical dosimeter.

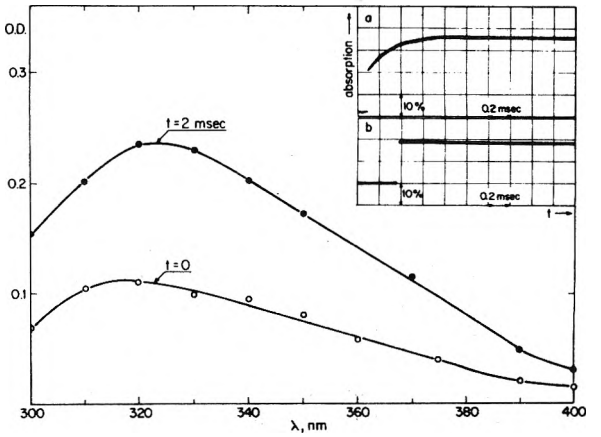

Figure 6. Spectra obtained on pulse irradiating 10^{-2} *M* $Ce_2(SO_4)_3$ in a 0.8 *N* H_2SO_4 oxygen-saturated solution at the end of the pulse and 2 msec later. Insert a is a typical oscillogram of the above solution. Insert b is an oscillogram obtained on irradiating the same solution but with argon saturation (λ 340 nm).

The kinetics of reaction 16 were studied as a function of [Ce(III)]. In all the cases studied, the rate of formation of Ce(IV) followed an observed first-order rate law, linearly depending on [Ce(III)] (*cf.* Figure 2c). The rate constant obtained is $k_{16} = (2.1 \pm 0.2) \times 10^5\ M^{-1}\ \text{sec}^{-1}$.

Regarding the possible formation of the [Ce(III)–$HO_2\cdot$] complex in the mechanism of reaction 16, the following reactions should be considered

$$Ce(III) + HO_2\cdot \rightleftharpoons [Ce(III)\text{–}HO_2\cdot] \qquad (16a)$$

$$Ce(III)\text{–}HO_2\cdot \xrightarrow{H^+} Ce(IV) + H_2O_2 \qquad (16b)$$

assuming the steady-state approximation for [Ce(III)–$HO_2\cdot$] we get for the formation rate of (Ce^{4+})

$$-\frac{d(Ce^{4+})_\infty - (Ce^{4+})]}{dt} = \frac{k_{16b}K_{16a}[Ce^{3+}]}{1 + k_{16b}/k_{-16a} + K_{16a}[Ce^{3+}]}[(Ce^{4+})_\infty - (Ce^{4+})] = k[Ce^{3+}][Ce_\infty^{4+} - (Ce^{4+})]$$

In the absence of the complex, $k = k_{16a} = k_{16}$, and k will be independent of $[Ce^{3+}]$. If the complex exists in solutions of H_2SO_4, which is not indicated by the esr studies,[6,9] k would depend on $[Ce^{3+}]$ at high enough concentrations; such a behavior was not observed by us up to 2.5×10^{-2} *M*

of Ce^{3+}. Therefore $[1 + (k_{16b}/k_{16a})] \geq 10K_{16a}[Ce^{3+}]$ or as $[Ce^{3+}] \leq 2.5 \times 10^{-2}[1 + (k_{16b}/k_{16a})] \geq 0.25K_{16a}$.

There are two extreme cases from which we may get limits for k_{16a} and k_{16b}: (a) $1 > k_{16b}/k_{16a}$, then equilibrium 16a is achieved, $K_{16a} \leq 4\ M^{-1}$ and $k_{16b} \geq 5 \times 10^4$, in this case reaction 16b is the rate-determining step; (b) $1 < k_{16b}/k_{16a}$, equilibrium is never achieved and we get $k_{16b}/k_{-16a} \geq 10K_{16a}[Ce^{3+}] = 10(k_{16a}/k_{-16a})[Ce^{3+}]$ which results in the relation $k_{16b}/k_{16a} \geq 0.25$ and $k_{16a} \sim 2 \times 10^5\ M^{-1}\ sec^{-1}$, and again $k_{16b} \geq 5 \times 10^4\ sec^{-1}\ M^{-1}$, in this case reaction 16a is the rate-determining step.

Both these assumptions predict a very low concentration of $[Ce(III)–HO_2\cdot]$ in H_2SO_4 which could agree with the failure to observe it in this work and earlier ones.[6,9] Of course, there is also the possibility that the complex is not formed at all and the reaction proceeds directly through reaction 16.

Conclusions

The reaction of the $HO_2\cdot$ radical with several metal ions was studied. The hydroperoxide radical may form complexes with some metal ions, or may act as oxidizing agent with others. The rates of the reactions of some metal ions with $HO_2\cdot$, stability constants of the complexes formed, their decay rates, and optical spectra were studied and are summarized in Table I.

Acknowledgment. The financial assistance of the U. S. Atomic Energy Commission, under Contract No. AT(11-1)-3221, is gratefully acknowledged.

References and Notes

(1) W. T. Dixon and R. O. C. Norman, *Nature (London)*, **196**, 891 (1962).
(2) V. H. Fischer, *Ber. Bunsenges. Phys. Chem.*, **71**, 685 (1967).
(3) M. S. Bains, J. C. Arthur, and O. Hinojosa, *Ber. Bunsenges. Phys. Chem.*, **72**, 2250 (1968).
(4) V. F. Shuvalov and M. Bazhin, *Zh. Strukt. Khim.*, **10**, 548 (1969).
(5) M. S. Bains, J. C. Arthur, and O. Hinojosa, *J. Amer. Chem. Soc.*, **91**, 4673 (1969).
(6) G. Czapski, H. Levanon, and A. Samuni, *Isr. J. Chem.*, **7**, 375 (1969).
(7) A. Samuni and G. Czapski, *Isr. J. Chem.*, **8**, 563 (1970).
(8) A. Samuni and G. Czapski, *J. Phys. Chem.*, **74**, 4592 (1970).
(9) A. Samuni and G. Czapski, *Isr. J. Chem.*, **8**, 551 (1970).
(10) G. Czapski and A. Samuni, *Isr. J. Chem.*, **7**, 361 (1969).
(11) Y. Shimizo, T. Shiga, and K. Kuwata, *J. Phys. Chem.*, **74**, 2929 (1970).
(12) A. P. Mezkulov, N. M. Bazhin, and V. M. Berdnikov, *Zh. Strukt. Khim.*, **11**, 1121 (1970).
(13) G. Czapski, D. Mesel, and A. Samuni, *J. Amer. Chem. Soc.*, **95**, 4148 (1973).
(14) J. Rabani, D. Klug, and I. Fridovich, *Isr. J. Chem.*, **10**, 1095 (1972).
(15) J. K. Thomas, S. Gordon, and E. J. Hart, *J. Phys. Chem.*, **68**, 1524 (1964).
(16) K. A. Allen, *J. Amer. Chem. Soc.*, **80**, 4133 (1958).
(17) E. L. Zebroskie, H. W. Alter, and F. K. Heamann, *J. Amer. Chem. Soc.*, **73**, 5646 (1951).
(18) S. Fronaeus, *Sov. Kem. Tidsskr.*, **64**, 317 (1952)
(19) T. J. Hardwick and E. Robertson, *Can. J. Chem.*, **29**, 828 (1951).
(20) A. Samuni, *J. Phys. Chem.*, **76**, 2207 (1972).
(21) The noncommitant notation $M(X)–HO_2\cdot$ was adopted throughout this study, stressing the undetermined state of complexation or oxidation of the metal in the complex. The oxidation state shown in parentheses refers only to the oxidation state of the parent metal ion.
(22) D. Behar, G. Czapski, J. Rabani, L. M. Dorfman, and H. A. Schwartz, *J. Phys. Chem.*, **74**, 3209 (1970).
(23) J. L. Dye and V. A. Nicely, *J. Chem. Educ.*, **48**, 443 (1971).
(24) A. I. Medalia and B. J. Byrne, *Anal. Chem.*, **38**, 453 (1951).
(25) P. B. Sigler and B. J. Masters, *J. Amer. Chem. Soc.*, **79**, 6353 (1957).
(26) G. Czapski, B. H. J. Bielski, and N. Sutin, *J. Phys. Chem.*, **67**, 201 (1963).
(27) R. W. Matthews, H. A. Mahlman, and T. J. Sworski, *J. Phys. Chem.*, **76**, 1265 (1972).

Oxidation of Hydroxycyclohexadienyl Radical by Metal Ions[1]

Kishan Bhatia and Robert H. Schuler*

Radiation Research Laooratories, Center for Special Studies and Department of Chemistry, Mellon Institute of Science, Carnegie-Mellon University, Pittsburgh, Pennsylvania 15213 *(Received May 6, 1974)*

Publication costs assisted by the U. S. Atomic Energy Commission and Carnegie-Mellon University

The radiation chemical yield for the production of phenol in the radiolysis of N_2O saturated aqueous solutions of benzene containing 10^{-4} to 10^{-3} *M* ferricyanide has been found to be 6.0. This result implies that the hydroxycyclohexadienyl radical produced by the addition of OH to benzene is quantitatively oxidized to phenol by the ferricyanide and that there is negligible interference from side reactions including those resulting from the buildup of ferrocyanide. Other metal oxidants examined (Cu^{2+}, Ag^+, Fe^{3+}, Cr^{3+}) gave lower radiation chemical yields and complications are apparent. For 10^{-4} to 10^{-3} *M* cupric ion the initial yield appears to be ~6 but the actual yields observed at doses $>10^{17}$ eV/g are lower and markedly dependent on the cupric concentration. The pronounced curvature in the phenol production curves which occurs when >10% of the Cu^{2+} ion has reacted can be explained if the hydroxycyclohexadienyl radical is reduced by cuprous ion ~5 times more rapidly than it is oxidized by cupric. Permanganate interferes by oxidizing the phenol produced further and silver ion does not effectively compete with the other radical termination processes. Hydroxylation of bromobenzene in the presence of ferricyanide accounts for a yield of only 3.9. Bromide produced by OH attack at the Br position accounts for an additional yield of 0.8 for a total yield of 4.7. In this case the oxidation of the intermediate hydroxycyclohexadienyl radicals by the ferricyanide is somewhat less than quantitative.

The recent development of high-speed liquid chromatography has made it practical to analyze the products from the radiolysis of aqueous solutions of organic solutes at low doses, particularly in the case of aromatic substances where many of the products absorb sufficiently strongly at 254 nm that they can be readily measured at concentrations of the order of micromolar or less.[2] In many of these studies one is interested in the yields of individual radicals produced by attack of H and OH on the substrate. Conclusions are frequently based on analysis of the products formed as the result of combination and disproportionation reactions but such conclusions are subject to the interpretation of the mechanistic aspects of the overall reaction. One can approach the situation somewhat better by converting the radicals directly to measurable products by oxidation or reduction reactions so that an independent measurement of the yields of the initial radicals is available to provide insight into the overall mechanism. Thus Holian and Garrison[3] have examined the radiolysis of pyrimidine bases using Cu^{2+} ion to oxidize the intermediate radicals and their studies have been recently extended by the work of Haysom, Phillips, and Scholes[4] on the oxidation of the radicals produced by the attack of OH on dihydrouracil. Volkert and Schulte-Frohlinde[5] have studied the isomeric distribution in the radiation-induced hydroxylation of benzoic acid using ferricyanide as the oxidizing agent to convert the resultant radicals to the corresponding hydroxybenzoic acids and Behar, Samuni, and Fessenden[6] have examined e_{aq}^- attack on CH_3Cl by using Ti^{3+} to reduce the CH_3 radicals to CH_4. Because of analytical limitations most of these previous studies have been only of a semiquantitative nature. In the present study we have used liquid chromatographic methods to explore in more detail the quantitative aspects of this type of approach in a survey of the oxidation of hydroxycyclohexadienyl radical produced in radiolysis of aqueous solutions of benzene by various metal ions. Christensen and Gustafsson[7] have already shown that the conversion of this radical to phenol is markedly enhanced by the presence of ferric ion. Radiolysis is a particularly convenient way to introduce an accurately known number of OH radicals into the reaction system and since their addition appears to be the only important reaction in the case of benzene the initial yield of hydroxycyclohexadienyl radicals is presumably known quite accurately. As a result complications introduced by secondary reactions can be examined quite readily. Metal ions are, of course, commonly used as oxidants in organic reactions, many of which are now known to take place *via* free-radical mechanisms.[8] The present work is closely related to studies such as those of Walling and Kato[9] who have generated radicals from the alcohols with Fenton's reagent and have examined their subsequent oxidation by Cu^{2+} ion.

Of the radical oxidants examined here ferricyanide seems to be the least complicated. It is shown that ferricyanide concentrations of ~10^{-4} *M* are sufficient to quantitatively convert the intermediate radical to phenol as the measurable product. Results with other oxidizing systems are reported and in particular it is shown that cupric ion is a suitable oxidant but only at very low concentrations and conversions. A brief study of the production of the isomeric bromophenols in the hydroxylation of bromobenzene is also reported.

Experimental Section

Benzene (5 μl) (Phillips Research Grade) or 2 μl of bromobenzene (Eastman) was added to 5 ml of solution previously purged of oxygen and saturated with N_2O at atmospheric pressure. Benzene and bromobenzene concentrations were 0.010 and 0.0040 *M*, respectively, and in both cases below the saturation limit. Irradiations were carried in ^{60}Co sources at dose rates of either 5.25×10^{16} or 7.3×10^{17} eV g^{-1} min^{-1}. Doses were mainly in the range of

TABLE I: Aqueous Liquid Chromatographic Retention Data and Detection Limits of a Spectrophotometric Detector

Compound[a]	t_r b	t_r c	t_r d	Peak width at half-height, min	Rel sensitivities and detection limit,[e] μM
Phenol	[1.00]	[1.00]	[1.00]	1.4;[b] 1.2;[c] 0.8[d]	0.8;[b] 1.7;[c] 1.0[d]
Benzene	2.2	2.00		3.5;[b] 4.2[c]	
o-Bromophenol			1.10	0.9	0.43
m-Bromophenol			1.57	2.2	1.15
p-Bromophenol			1.90	2.9	0.74
Bromobenzene			5.20	1.60	

[a] All retention tmes (t_r) are relative to that of phenol. Phenol eluted in 15.5, 13.8, and 1.50 min under conditions b–d, respectively. Columns are described in the text. Column, column temperature, eluent and flow rates were as described in footnotes *b*, *c*, and *d*. [b] 4 m long, 35°, 2 m*M* $NH_2H_2PO_4$, pH 5.5, ~0.8 ml/min.[2] [c] 3 m long, 43°, 20 m*M* $NH_4H_2PO_4$, pH ~5.0, ~0.6 m/min. [d] 5 m long, 43°, 3 m*M* Na_2B_4O , pH ~9.0, ~0.6 ml/min. [e] Detection limits of the Laboratory Data Control 1205 uv monitor (254 nm) are for a signal-to-noise ratio >2 under the elution conditions used.

10^{17}–10^{18} eV/g. All inorganic materials used were of standard reagent grade.

The aqueous liquid chromatographic (alc) apparatus and methods used in the study are described elsewhere.[2,10] The uv detector (Laboratory Data Control Model 1205) operating at 254 nm was used to measure phenol but because the extinction coefficient for phenol is only ~520 M^{-1} cm^{-1} at this wavelength the sensitivity was only moderate (~10^{-6} *M* for S/N = 2). At the doses used phenol was produced at concentrations of 3–30 × 10^{-5} *M*. The benzene solutions were examined immediately after irradiation by alc methods using a column (2.3 mm i.d. × 4 m long) the first half of which was packed with polyamide-coated silicious material (Reeve Angel) and the second half with octadecylsilyl-bonded silicious material (Waters) or a column (2.3 mm i.d. × 3 m long) packed with phenylalkylsilyl-bonded silicious material (Waters). The columns were operated isothermally at 35 or 43° using 2–20 m*M* ammonium phosphate as eluent (isocratic conditions). The irradiated bromobenzene solutions were examined by alc using a column (2.3 mm i.d. × 5 m long) the first two-fifths of which was packed with polyamide-coated material and the second three-fifths with phenylalkylsilyl-bonded material. This column was operated at 43° using 3 m*M* borate buffer to separate phenol, *o*-, *m*- and *p*-bromophenol, and bromobenzene. The chromatographic sensitivity was determined separately for each of the individual substrates. Pertinent chromatographic data of interest in the present studies are summarized in Table I.

The bromide ion produced in the reaction of hydroxyl radical with bromobenzene was determined using ion selective electrode methods as previously described.[11]

Results and Discussion

The radiation chemistry of aqueous solutions of benzene has been the subject of a large number of investigations.[12] The qualitative formation of hydroxycyclohexadienyl radical (I) by addition of OH to benzene

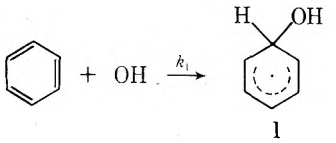

(1)

I

has been conclusively established by pulse radiolysis[13] and steady-state esr[14] studies. Whereas it is generally assumed that OH radicals react with benzene solely *via* reaction 1, the yield of phenol in the radiolysis of aqueous solutions of benzene is known to be low. In the absence of added solutes

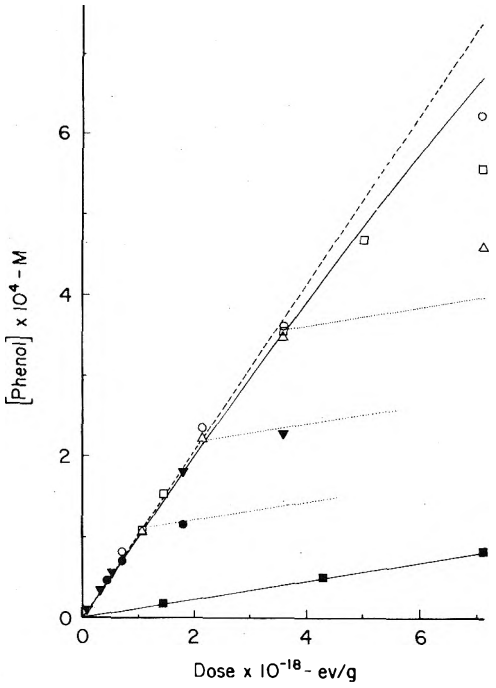

Figure 1. Production of phenol in the radiolysis of N_2O-saturated aqueous solutions of benzene at pH 7.5. Solutions contained (■) 0, (●) 1.1 × 10^{-4}, (▼) 2.2 × 10^{-4}, (△) 3.6 × 10^{-4}, (□) 4.8 × 10^{-4}, and (○) 1.1 × 10^{-3} *M* potassium ferricyanide. The solid curve is that calculated for an initial yield of 6.0 (dashed line) taking into account the reaction of OH with the ferrocyanide. The dotted lines superimpose the slope for no added ferricyanide at the point where the phenol produced is equal to the ferricyanide added.

the yield accounts for ~10% of the OH (see the lowest curve in Figure 1) and is subject to post-irradiation effects and to interferences by other hydroxylated products.[12] This phenol obviously accounts for only a small fraction of the OH chemistry and it is clear that hydroxycyclohexadienyl radicals are removed from the system mainly by processes other than disproportionation. Christensen[7] and Gustafsson have shown that addition of 10^{-3} *M* ferric ion increases the phenol yield by an order of magnitude and it is obvious from their work that with appropriate oxidants a significant fraction of the hydroxycyclohexadienyl radicals are converted to phenol, *e.g.*

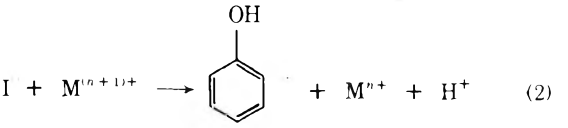

(2)

A yield of only 4.0 (or ~60% of the OH) is, however, reported for 10^{-3} M Fe^{3+} solutions saturated with N_2O.

The studies reported in Figure 1 on N_2O saturated solutions show that at pH 7.5 reaction 2 is essentially quantitative in the presence of 10^{-4} M ferricyanide or greater. In these studies very nearly all (>99%) of the e_{aq}^- reacts with the N_2O ($k(e_{aq}^- + N_2O) = 5.6 \times 10^9$ M^{-1} sec^{-1})[15] as long as the ferricyanide concentration is less than 4×10^{-4} M ($k(e_{aq}^- + Fe(CN)_6^{3-}) = 4 \times 10^9$ M^{-1} sec^{-1}).[15] Also there is essentially no interference from reaction of e_{aq}^- with benzene ($k(e_{aq}^- + C_6H_6) = 1.4 \times 10^7$ M^{-1} sec^{-1}) or from the phenol ($k(e_{aq}^- + C_6H_5OH) < 4 \times 10^6$ M^{-1} sec^{-1}) or ferrocyanide (k $(e_{aq}^- + Fe(CN)_6^{4-}) < 10^5$ M^{-1} sec^{-1}) produced in the radiolysis. In this system the yields of H and OH are, respectively, 0.6 and 6.0.[16] Because the rate constants for addition of both to benzene are very high (10^8 and 3×10^9)[15,17] it is reasonable that addition will be quantitative and that the yields of cyclohexadienyl and hydroxycyclohexadienyl will also be 0.6 and 6.0. It is seen in Figure 1 that in the region below 10^{13} eV/g the phenol builds up with a yield of 6.0 as long as at least 10^{-4} M ferricyanide was originally added to the sample. In this case it is clear that the alternate oxidation product, dihydroxycyclohexadiene, which could be found by the reaction of the intermediate carbonium ion with water

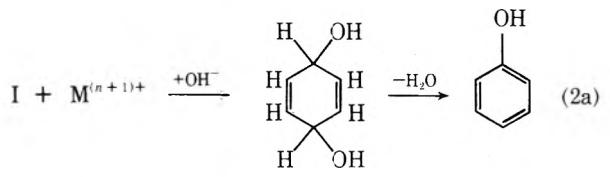

(2a)

is sufficiently less stable that it is an unimportant product. In the case of the hydro- and hydroxyuracil radicals the analogous oxidation products have, however, been observed to be the major products in acidic solutions.[3,4]

In Figure 1 it is seen that breaks in the curve occur approximately where all of the ferricyanide has been consumed. Extrapolation of the results on the solutions containing 1.1 and 2.2×10^{-4} M ferricyanide according to the slope for phenol production in the absence of added metal ion indicates break points when phenol reached concentration of 1.05 and 2.1×10^{-4} M, respectively, so that it is clear that very little ferricyanide is needed for the oxidation. As ferrocyanide builds up, a small decrease in the rate for production of phenol is expected as a result of reaction of OH with the ferrocyanide (which has a rate constant of 1.0×10^{10} M^{-1} sec^{-1} as compared with 5×10^9 M^{-1} sec^{-1} for reaction of OH with benzene).[15,18] The solid curve of Figure 1 gives the expected dose dependence taking this competition into account. The solutions containing 3.6 and 4.8×10^{-4} M ferricyanide irradiated to a dose of 7×10^{18} eV/g show slightly more phenol than expected based on the oxidizing power of the ferricyanide initially added (by $\sim 5 \times 10^{-5}$ M) so that a small amount of spurious oxidation does seem to take place. It seems likely that some additional oxidation may result either directly from the buildup of peroxide ($\sim 8 \times 10^{-5}$ M at this dose) or as a result of the intermediate oxidation of the metal ion by the peroxide. There is no evidence in the data that there is any significant reduction of the hydroxycyclohexadienyl radical as the result of its reaction with the $Fe(CN)_6^{4-}$ produced in the reaction.

Studies of the oxidation of hydroxycyclohexadienyl radical by cupric ion similar to those of Figure 1 (N_2O saturated solutions at pH ~5) showed that at doses ~10^{18} eV/g the phenol yields were considerably lower than those obtained with ferricyanide. A small decrease is expected since e_{aq}^- reacts rapidly with Cu^{2+} ($k \sim 3 \times 10^{10}$)[15] so that in the millimolar region significant interference with scavenging by the N_2O occurs. From the rate constants the OH yields are calculated to be 5.9, 5.7, and 5.5, respectively, at Cu^{2+} concentrations of 1, 4, and 8×10^{-4} M.[16] Studies at low doses, reported in Figure 2, show that the initial yields are about as expected from these OH yields but that the yield decreases rapidly as product builds up. The yield drops off by ~10% when only 2% of the cupric ion has been consumed. It is obvious that oxidation by cupric ion is far more complicated than that by ferricyanide.

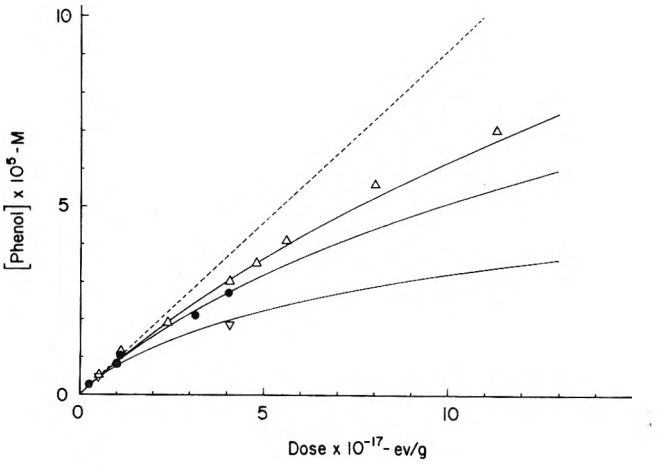

Figure 2. Production of phenol in the presence of (▽) 1.4×10^{-4}, (●) 4×10^{-4}, and (△) 8×10^{-4} M cupric ion. Curves are calculated by integration of eq 3 as described in the text. The initial slope used in the calculation at 8×10^{-4} M (G(OH) = 5.5) is indicated by the dashed line.

It is clear that some product of the reaction rapidly removes hydroxycyclohexadienyl from the system and it seems likely that reduction by the cuprous ion produced in reaction 2 may be involved. If so the results will be further complicated by the chemical instability of the cuprous ion. If we assume that Cu^+ lives until it can reduce the intermediate radical (with a rate constant k_3) then the rate of phenol production should be given by

$$\frac{d[PhOH]}{dt} = \frac{10GD}{N}\left[1\Big/\left(1 + \frac{k_3[Cu^+]}{k_2[Cu^{2+}]}\right)\right] \qquad (3)$$

(G is the yield of hydroxycyclohexadienyl radicals, D the dose in eV/g, and N Avogadro's number.) The data of Figure 2 can be reproduced quite well by integrating eq 3 with k_3/k_2 taken as ~5 if it is assumed that as the reaction progresses the cuprous concentration is equal to that of the phenol produced corrected for the amount that has been reoxidized. Curves calculated by numerical integration of eq 3 (taking $[Cu^+] = f(2[PhOH] - 10GDt/N)$ and $[Cu^{2+}] = [Cu^{2+}]_0 - [Cu^+]$ with $f = 1.1$ to account for the cyclohexadienyl radicals produced by H addition to benzene) are given in Figure 2 for the three experimental concentrations. These calculations effectively give a minimum required relative rate for the processes interfering with reaction 2. One would like to add more cupric ion to the system but the high rate constant for direct reduction by e_{aq}^- prevents this.

Other potential oxidants examined during this study were $KMnO_4$, $KCr(SO_4)_2$, $K_3Cr(CN)_6$, Ag_2SO_4, $FeNH_4(SO_4)_2$, EDTA–Fe^{3+} complex, and $Co(NH_3)_6Cl_3$.

With $KMnO_4$, the chromic salts, and EDTA–Fe^{3+} complex no phenol at all was observed. The phenol yield with 6×10^{-4} M $K_3Mn(CN)_6$ at a pH of ~9.3 and a dose of 3×10^{17} eV g^{-1} was only ~3.0 and in the presence of the other salts was only marginally higher than in the absence of oxidant ($G < 1.5$). Silver ion did not increase the yield significantly (by only 0.2). It must be concluded either that the phenol is never formed because of reduction of the hydroxycyclohexadienyl radical by competing processes or that it is further oxidized. The latter is unquestionably the case with permanganate since phenol rapidly disappeared when 3×10^{-4} M $KMnO_4$ was added to a 10^{-4} M phenol solution. Phenol was found to be stable in the presence of the Cr^{3+} so that it is perhaps surprising that one does not observe an appreciable phenol yield in this case.

One can, of course, regard reaction 2 as taking place *via* the transfer of an electron from the hydroxycyclohexadienyl radical to the metal ion and should be able to get at least a qualitative idea of the efficiency of the different metal ions from considerations of their standard reduction potentials. Values for the various ions surveyed here (*vs.* nhe) vary from −0.41 V for Cr^{3+} to + 0.80 V for Ag^+ while those for $Fe(CN)_6^{3-}$ and Cu^{2+} are 0.36 and 0.16 V, respectively. While the reduction potential of the hydroxycyclohexadienyl radical has been measured to be −0.26 V *vs.* sce[19] (−0.01 V *vs.* nhe) its oxidation potential is unknown. From the fact that both Cu^{2+} and $Fe(CN)_6^{3-}$ appear to oxidize the radical a value >0.1 V seems reasonable. The reduction potential for Cr^{3+} is apparently too negative to permit electron transfer. Metal ions with reduction potentials greater than ~0.1 V should be capable of oxidizing the radical. Silver ion, which has a considerably higher reduction potential than does ferricyanide, has little effect on the yield presumably because it is kinetically slow (the mean lifetime of the radicals is ~30 msec in these ^{60}Co experiments). Clearly the detailed nature of the electron transfer complex is very much involved in these radical oxidations.

As a more general example of the applicability of metal oxidants to the determination of individual radical yields we have examined the product bromophenols produced by OH attack on bromobenzene. The yields measured for N_2O saturated solutes in the presence of 5×10^{-4} M $Fe(CN)_6^{3-}$ at doses of 0.7 and 2.1×10^{18} eV/g were 1.9 for *o*-bromophenol, 0.9 for *m*-bromophenol, and 1.1 for *p*-bromophenol. Bromide ion was produced with a yield of 0.95 but ~0.2 of this is ascribable to attack of e_{aq}^- directly on the bromobenzene ($k(e_{aq}^- + PhBr) = 4 \times 10^9$).[15] The total yield is, therefore, 4.7 or only 81% of the expected yield of 5.8. It is noted that the yields of the ortho and para isomers are about as expected from random attack of OH on the ring (G = ~1 at each position) but that both the relative and absolute yields of the meta isomer are low by a factor of 2. It does not seem likely that Br will have this large a directing effect on the OH addition so that it would appear that the substitution affects the reactivity of the resultant radicals in the oxidation step. One obviously must use extreme caution in interpreting results of studies such as those illustrated here in terms of the yields of the initial radicals.

References and Notes

(1) Supported in part by the U. S. Atomic Energy Commission.
(2) K. Bhatia and R. H. Schuler, *J. Phys. Chem.*, **77**, 1356 (1973).
(3) J. Holian and W. M. Garrison, *Nature (London)*, **212**, 394 (1966).
(4) H. R. Haysom, J. M. Phillips, and G. Scholes, *J. Chem. Soc., Chem. Commun.*, 1082 (1972).
(5) O. Volkert and D. Schulte-Frohlinde, *Tetrahedron Lett.*, **17**, 2151 (1968).
(6) D. Behar, A. Samuni, and R. W. Fessenden, *J. Phys. Chem.*, **77**, 2055 (1973).
(7) H. C. Christensen and R. Gustafsson, *Nukleonik*, **12**, 49 (1969).
(8) W. A. Waters, Report of the 23rd International Congress of Pure and Applied Chemistry, Vol. IV, Butterworths, London, 1971, p 307.
(9) C. Walling and S. Kato, *J. Amer. Chem. Soc.*, **93**, 4275 (1971).
(10) K. Bhatia, *Anal. Chem.*, **45**, 1344 (1973).
(11) K. M. Bansal, L. K. Patterson, and R. H. Schuler, *J. Phys. Chem.*, **76**, 2386 (1972).
(12) For a summary of work on this subject, see K. Bhatia, *Radiat. Res.*, **59**, 537 (1974).
(13) L. M. Dorfman, I. A. Taub, and R. E. Bühler, *J. Chem. Phys.*, **36**, 3051 (1962).
(14) K. Eiben and R. W. Fessenden, *J. Phys. Chem.*, **75**, 1186 (1971).
(15) M. Anbar and P. Neta, *Int. J. Appl. Radiat. Isotopes*, **18**, 493 (1967).
(16) The yield of OH produced directly from the water is 2.8 and an additional yield of 3.2 is produced by reaction of e_{aq}^- with the N_2O; see T. I. Balkas, J. H. Fendler, and R. H. Schuler, *J. Phys. Chem.*, **74**, 4497 (1970). If reaction between the reduced form of the metal ion and peroxide is important at the concentrations produced in these radiolyses (~10^{-5} to 10^{-4} M) the OH yield could be higher by as much as the molecular peroxide yield (~0.7).
(17) P. Neta and R. H. Schuler, *J. Amer. Chem. Soc.*, **94**, 1056 (1972).
(18) L. M. Dorfman and G. E. Adams, *Nat. Stand. Ref. Data Ser., Nat. Bur. Stand.*, **No. 46** (1973).
(19) M. Grätzel, A. Henglein, J. Lilie, and M. Scheffler, *Ber. Bunsenges. Phys. Chem.*, **76**, 67 (1972).

Proton Exchange of Carboxylic Acids in 1-Octanol[1]

Stefan Highsmith and Ernest Grunwald*

Chemistry Department, Brandeis University, Waltham, Massachusetts 02154 *(Received April 18, 1974)*

Publication costs assisted by the Petroleum Research Fund

First-order rate constants (nk_1/sec^{-1}) for proton exchange in 1-octanol at 25.1° are 1.7×10^5 for octanoic acid, 3.3×10^5 for hydrocinnamic acid, and 5.2×10^5 for *N*-acetyl-D-phenylalanine, and thus tend to increase with acid strength. For octanoic acid, the mean number (n) of solvent molecules reacting with one acid molecule is 2.5 ± 0.4. Values of nk_1 are similar in magnitude to corresponding values for carboxylic acids of comparable strength in methanol and ethanol, showing that solvent dielectric constant and viscosity are unimportant. This is surprising for a reaction which otherwise conforms to prediction for a rate-determining acid-ionization step.

First-order rate constants for proton exchange between carboxylic acid and solvent molecules in water, methanol, and ethanol are orders of magnitude greater than rate constants for acid dissociation.[2,3] Because the rate constants for proton exchange tend to increase with the acid strength of the carboxylic acid RCO_2H,[4,5] a reaction mechanism involving a rate-determining ionization to an ion pair has been proposed. Measurements in methanol have shown that carboxyl exchange involves *ca.* two solvent molecules (SOH), and a cyclic structure has been proposed for the reaction intermediate (eq 1).[2,6]

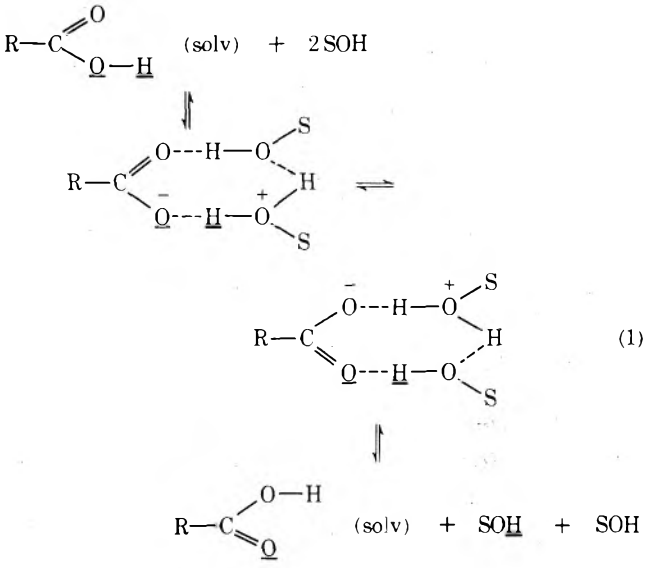

(1)

One of the problems concerning the proposed ion-pair intermediate (1) is that if we make plausible estimates of the equilibrium constant for its formation, we are forced to conclude that its lifetime is extremely short, less than 10^{-12} sec.[7] A lifetime of such a short duration would be consistent with proton tunneling, but would not allow solvent realignment to form an intermediate according to classical concepts.

In connection with work on proton transfer between amino acids to form ion pairs[8] we have measured rates of exchange between CO_2H and solvent OH protons in 1-octanol, which we wish to report presently. These exchange rates were measured by nuclear magnetic resonance (nmr) techniques analogous to those used previously.[2] Because of the special properties of 1-octanol, the new results enhance our picture of the reaction mechanism.

The relevant properties of 1-octanol are compared with those of other solvents in Table I. Compared to methanol and ethanol, 1-octanol has a low dielectric constant (ϵ), high viscosity (η), and long dielectric relaxation time (τ_D); yet its hydrogen-bonded structure and basicity are comparable to those of methanol and ethanol, as indicated by Kirkwood g factors and relative basicities. The relative basicity, b, is defined in eq 2. The values listed for b in Table I were measured in the alcohol solvents.[9]

$$b = [H_2O][ROH_2^+]/[H_3O^+][ROH] \qquad (2)$$

Our results for proton exchange of carboxylic acids in 1-octanol are listed and compared with data for other solvents in Table II. k_1 is the first-order rate constant for the exchange of the solute CO_2H protons; nk_1 is the corresponding first-order rate constant for the exchange of the solvent OH protons. That is, $-d[CO_2H]/dt = k_1[RCO_2H]$; $-d[OH]/dt = nk_1[RCO_2H]$; and n is the average number of 1-octanol molecules reacting per carboxylic acid molecule.

All measurements were made on buffered solutions at acid/sodium salt ratios ranging from 10 to 1000. Most measurements were made at high dilutions ($<10^{-3}$ M acid) where the rate law was nicely first order. However, for octa-

TABLE I: Solvent Properties

Solvent	$g_{Kirkwood}$[a]	η, cP[b]	ϵ[b]	$10^{10}\tau_D$, sec[c,d]	b[e]
H_2O	2.91	0.894	78.30	0.083	1.00
MeOH	3.16	0.545	32.70	0.50	0.0093
EtOH	3.23	1.078	24.55	1.56	0.0035
1-OctOH	3.00	7.6	9.88	17.8	0.0031[f]

[a] Calculated using a dipole moment of 1.82 D for water and 1.69 D for all alcohols in the gas phase. In applying these values to the pure liquids, the Onsager correction for the reaction field was used. The values of g are consistently larger than those obtained by Oster and Kirkwood (*J. Chem. Phys.*, **11**, 175 (1943).) [b] J. A. Riddick and W. B. Bunger, "Organic Solvents," 3rd ed, Wiley-Interscience, New York, N.Y., 1970. [c] S. K. Garg and C. P. Smyth, *J. Phys. Chem.*, **69**, 1294 (1965). [d] J. B. Hasted and G. W. Roderick, *J. Chem. Phys.*, **29**, 17 (1958). [e] The relative basicity b is defined in eq 2. Data from L. S. Guss and I. M. Kolthoff, *J. Amer. Chem. Soc.*, **62**, 1494 (1940). [f] *n*-Butyl alcohol.

TABLE II: First-Order Rate Constants for Proton Exchange of Carboxylic Acids in Hydroxylic Solvents

Acid	10^5K_a (H_2O)	$10^{-5}nk_1$, sec^{-1}	$10^{-5}k_1$, sec^{-1}	$10^{-5}nk_1/b$	Ref
		H_2O			
CH_3CO_2H	1.75	950		950	3
		MeOH			
$C_6H_5CO_2H$	6.3	1.3(24.8°)	0.71(24.8°)		2
		0.00216(−81.6°)	0.00100(−81.6°)		
CH_3CO_2H	1.75	(1.0)[a](24.8°)		110	10
		0.00170(−81.6°)	0.00075		
		EtOH			
HCO_2H	17.7	10 ± 2(20°)			4
CH_3CO_2H	1.75	0.5 ± 0.3(20°)		140	4
		1-OctOH			
n-$C_7H_{15}CO_2H$	1.27	1.7(25.1°)	0.68(25.1°)	550	
$C_6H_5CH_2CH_2CO_2H$	2.19	3.3(25.1°)			
D-$C_6H_5CH_2 \cdot CHCO_2H$	32	5.2(25.1°)			
$CH_3CO \cdot NH$					

[a] Estimated from data at −81.6°, assuming the same activation energy as for benzoic acid.

noic acid–sodium octanoate buffers some measurements were made at higher concentrations where a second-order reaction, with solvent participation, between octanoic acid and its conjugate base became significant. The second-order rate constant was found to be 4.7×10^7 sec^{-1} M^{-1} at 25.1°.

Although both nk_1 and k_1 were measured in 1-octanol only for octanoic acid, the fact that the ratio, $n = 2.5 \pm 0.4$, is similar to that for benzoic acid in methanol (1.9 ± 0.2 at 24.8° and 2.2 ± 0.2 at −81.6°)[2] and for acetic acid in methanol (2.3 ± 0.3 at −81.6°)[10] makes us feel that the reaction mechanisms are similar, probably for all processes listed in Table II. However, the theory that n may be identified with the stoichiometric integer 2 (as in eq 1) is now less tenable, and it becomes more reasonable to regard n as a nonintegral average for a range of processes involving participation by one, two, three, ... solvent molecules. In support of this view, for the formally analogous proton exchange of neopentyl alcohol with acetic acid (in which acetic acid is the *solvent*), $n = 1$ exactly, yet the pseudo-first-order rate constant is 6.7×10^5 at 25°,[11] comparable to rate constants listed in Table II, showing that processes involving one alcohol molecule can be quite fast. At the same time, model building indicates that cyclic structures with one or two solvent molecules cannot be formed without considerable bending of the hydrogen bonds, while a structure with three solvent molecules may be formed without hydrogen-bond strain.

The data in Table II suggest that values of nk_1 for acids of comparable strength are quite similar in the three alcohols, showing that neither the dielectric constant nor the viscosity is an important factor. The relatively high rate constant in water might be due to the difference in hydrogen-bonded solvent structure of water relative to the alcohols, or, more likely, to the relatively high basicity of water. As shown in Table II values of k_1/b vary less, by *two orders of magnitude*, than those of k_1. This fairly good correlation with solvent basicity, in addition to the clear tendency of nk_1 to increase with the strength of the carboxylic acid, are of course consistent with an ionization mechanism.

The apparent paradox of a reaction which involves ionization yet whose rate constant is not markedly affected by the dielectric constant of the solvent is all the more puzzling in view of recent kinetic studies for proton transfer of the same charge type in aprotic solvents.[12] Here it is clear, from measurements of deuterium kinetic isotope effects for the process $B + HA \rightarrow BH^+A^-$, and from an analysis in terms of proton tunneling, that the potential barrier which separates the un-ionized and ionized states along the reaction coordinate varies appreciably with the solvent as the latter is changed from toluene to CH_2Cl_2 or CH_3CN.[12]

Experimental Section

N-Acetyl-D-phenylalanine and hydrocinnamic acid were recrystallized three times from chloroform and dried *in vacuo*. Octanoic acid and octanol were distilled twice at reduced pressure, taking center fractions. Sodium salts of the acids were prepared by neutralization with NaOH followed by repeated crystallization from methanol–ether. All solutions were prepared by weight. The nmr measurements and kinetic analysis were analogous to those described in ref 2, except that the OH proton resonance in the absence of exchange is a triplet. Theoretical spectra for comparison with experimental spectra and calculation of reaction rates have been given by Loewenstein and Meiboom.[13] The following nmr parameters were used: spin–spin coupling of OH and α-CH_2 protons in 1-octanol, $J = 5.0$ Hz; for octanoic acid in 1-octanol, chemical shift of CO_2H protons relative to solvent OH protons, 5.87 ppm (downfield).

References and Notes

(1) Acknowledgment is made to the donors of the Petroleum Research Fund, Administered by the American Chemical Society, for support of the research.
(2) E. Grunwald, C. F. Jumper, and S. Meiboom, *J. Amer. Chem. Soc.*, **85**, 522 (1963).
(3) Z. Luz and S. Meiboom, *J. Amer. Chem. Soc.*, **85**, 3923 (1963).
(4) H. Feldbauer and A. Weller, *Z. Phys. Chem. (Frankfurt am Main)*, **33**, 263 (1962).
(5) E. Grunwald and S. Meiboom, *J. Amer. Chem. Soc.*, **85**, 2047 (1963).
(6) J. Hine, *J. Amer. Chem. Soc.*, **94**, 5766 (1972).
(7) E. Grunwald, *Progr. Phys. Org. Chem.*, **3**, 317 (1965).
(8) S. Highsmith, *Biophys. Biochem. Acta.*, submitted for publication.
(9) The basicity of the alcohols as solutes in water as the solvent continues to be a topic for controversy. For noteworthy recent work on ethanol in water and a review of the previous literature, see D. G. Lee and R. Cameron, *J. Amer. Chem. Soc.*, **93**, 4724 (1971).
(10) E. Grunwald and C. F. Jumper, unpublished results.
(11) M. Cocivera and E. Grunwald, *J. Amer. Chem. Soc.*, **87**, 2551 (1965).
(12) E. F. Caldin and S. Mateo, *Chem. Commun.*, 854 (1973).
(13) A. Loewenstein and S. Meiboom, *J. Chem. Phys.*, **27**, 1067 (1957); for further details see "Tables of Exchange Broadened Nmr Multiplets," Technical Note No. 2, Contract No. AF 61(052)-03, The Weizman Institute of Science, Rehovot, Israel, 1957.

Chemical Relaxation as a Mechanistic Probe of Hydrogen Bonding. Thermodynamics and Kinetics of Lactam Isoassociation in Nonpolar Solvents[1]

Rudolf F. W. Hopmann

Department of Biophysical Chemistry, Biocenter of the University of Basel, CH-4056 Basel, Klingelbergstrasse 70, Switzerland
(Received April 9, 1974)

Lactam isoassociation was investigated with ir spectroscopy and a special dielectric relaxation technique. Synoptic analysis of the results suggests that the associative behavior should be described in terms of a trimerization model which is more marked in cyclohexane than in tetrachloromethane, but not recognizable in benzene. The primary bimolecular rate constants decrease in that order of the solvents with values from 7 to 5×10^9 M^{-1} sec^{-1}. Interpretation of the amplitudes of the kinetic reaction signals leads to the conclusion that the second possible hydrogen bond of the associated complex may not be formed in benzene (offering an explanation of the rather low association constant $K_2 = 28$ M^{-1}) but in cyclohexane ($K_2 = 550$ M^{-1}). Tetrachloromethane seems to represent an intermediate case ($K_2 = 200$ M^{-1}). The enthalpy of about 9 kcal/mol as determined from the temperature dependence of the ir spectra is considered to be the sum of two formed hydrogen bonds. The monomer dipole moments of ϵ-caprolactam and γ-butyrolactam as derived from the chemical field effect measurements are 4.30 and 4.10 D, respectively, within ±5%.

Introduction

One of the fastest primary rate processes (nanoseconds), studied by ultrasound[2] and dielectric[3-5] absorption techniques, is the formation of hydrogen bonds. Bivalently hydrogen-bonded complexes, *e.g.*, the self-associates of lactams and the purine–pyrimidine base pairs, are of particular interest as models of important biological reactions. The interpretation of the concentration dependent variation of the relaxation times has shown that these reactions in dilute solutions are diffusion controlled ($2 < 10^{-9} k_R$ M^{-1} $sec^{-1} < 8$, see ref 1 for a collection of data). Moreover, the relaxation times can be used as a probe for the association mechanism. For instance, a 1:1 stoichiometric isoassociation should yield a linear dependence of the squared reciprocal relaxation times on the analytical weight concentration. Apart from several examples in the literature[6,7] which do not fulfill this condition we shall discuss in this paper deviations of the above prediction for the lactam isoassociation in nonpolar solvents. It is assumed widely that lactams dimerize in nonpolar solvents. Tsuboi[8,9] was the first to make an ir spectroscopic investigation of the hydrogen bonded self-association of δ-valerolactam (2-piperidone) in tetrachloromethane. Pimentel and coworkers[10] noticed that the strength of lactam association varies with the solvent. They observed significant spectral changes even with seemingly similar solvents. Notably the ir measurements by Lord and Porro[11] brought a first assessment of the stoichiometry and the thermodynamics of the self-association of ϵ-caprolactam (I, 1,2,3,4,5,6,7-hexahydro-2-azepinone) in tetrachloromethane. They concluded from their results that I dimerizes in this solvent. More recently several research groups studied lactam self-association by means of ir[12-14] and nmr techniques.[15-17] With regard to the mechanism of association and to the evaluation of the data, many authors have made reference to the interpretation by Lord and Porro. Differences of the associative strength due to the ring size of the lactams are well accepted. This was shown by Luck[13] and by Walz and Huisgen.[18] The latter authors measured dielectric polarization of benzene solutions of a series of low membered lactams and explained their data by the formation of dimers throughout.

First reports of kinetic data for I in tetrachloromethane and benzene have been given by Bergmann, Eigen, and De Maeyer.[3] These data were obtained from dielectric absorption measurements on the basis of chemical relaxation by observing the frequency-, field-, and concentration-dependent variation of dielectric absorption in the rf range. A static electric field superimposed on the rf voltage is used to disturb the equilibrium. The static field must be very strong to achieve a measurable displacement of the equilibrium of the reaction. The dielectric absorption measurements suffered most from technical difficulties which have now been overcome. For example, in a recent chemical relaxation study of uracil–uracil and uracil–adenine association we have demonstrated the fundamental possibility of deriving from the data an interpretation of the molar moment of reaction in terms of the structures of the hydrogen bonded associates. This is possible because the essential contribution of interest to the molar moment of reaction is

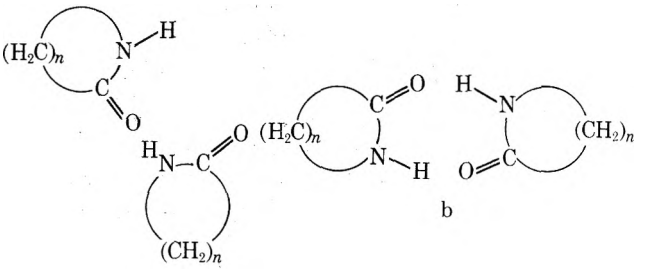

a b

I, $n = 5$
II, $n = 4$
III, $n = 3$

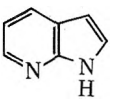

IV

the difference of the squared dipole moments of the reactants and the products. We use an improved version of the apparatus described earlier[4,19] to yield reliable kinetic data. These cast some doubt on the generality of the dimerization scheme for lactams and suggest that, especially at high concentrations, an oligomerization takes place which can scarcely be noticed by spectroscopic techniques.

The synopsis of thermodynamic and kinetic data, including the evaluation of the relaxation amplitudes, reveals some features of the associative behavior of lactams. Although this study is concerned mainly with the isoassociation of I and of γ-butyrolactam (II, 2-pyrrolidinone) in tetrachloromethane, cyclohexane, and benzene, we believe that some generalizations can be drawn from the results.

Experimental Section

Materials and Methods. Except compound I which was synthesized[20] all compounds and solvents of AR grade were obtained from commercial sources and conformed to standard literature data[21] after proper purification. Cyclohexane and benzene were cycled over Na–K alloy (10:1) or Dri-Na (Baker Reagent) in an apparatus similar to the one described by Schupp and Mecke.[22] Tetrachloromethane was shaken in quantities of 500 ml with freshly heated potassium carbonate in the original bottle for several hours, and cycled over phosphorpentoxide. The quality of the dried solvents was repeatedly checked by ir and uv spectroscopy. The absence of any appreciable conductivity and any "solvent effect" during measurements with the strong dc field showed them to be essentially moisture free. Solutions were made by weighing the solute in a 25-ml cylindrical flask with a NS 14 ground glass joint. Two short capillary sidearms with flat stopcocks (Brand, Wertheim), to which NS 5 capillary glass joints were attached by 2-mm fitted PTFE tubes, allowed us to transfer the solvents and solutions in an atmosphere of dried nitrogen.

The solutions for the spectrophotometric measurements were prepared in the previously mentioned special flask and introduced under dry nitrogen into an all-glass buret apparatus which allowed the dilution of quantities of the stock solution with solvent without exposure to the air. Flexible connections between store bulbs, burets, mixing chamber, and the cuvets to be filled were provided by glass joints and fitted Teflon tubes. The apparatus was heated prior to use, and flushed with dried nitrogen both on cooling, and during the experiments. Dilution experiments with II were also carried out by adding appropriate amounts of the liquid to the solvent in the thermostatted cuvet with the help of an AGLA-micrometer all-glass syringe (Burrough, Welcome and Co.). The temperature was kept constant within 0.1° by means of thermostatted brass cuvet holders of our design connected to a circulating water bath. Dilution experiments were carried out in QI cuvets of different path length (Hellma, Müllheim) at 22°. Thermodynamic measurements were carried out by heating solutions of specified concentrations. The temperature was monitored within the cuvet with a thermistor and was compared to a calibrated thermometer. Ir measurements with tetrachloromethane as solvent were made with a Perkin-Elmer 237 ir grating instrument to which a transmission-extinction converter with zero-suppression facility was connected. The spectra were recorded on a Mosely 7035 strip chart recorder (Hewlett-Packard). Provision was made to ensure appropriate calibration. The data were processed according to well-known procedures[11] and were corrected,

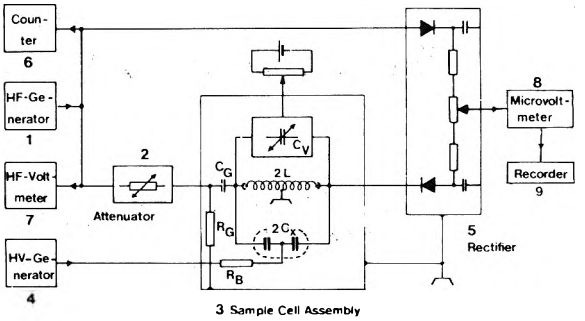

Figure 1. Block diagram of the differential circuit. The sample cell assembly (3) comprises the parallel resonance circuit with the two sample capacitors C_X in series, an interchangeable inductance with the two symmetric halves L, and an electronically variable capacitance C_V. The resonant voltage and the HF-generator voltage are compared by means of two opposed diodes and a precision potentiometer of the rectifier (5) to which a high impecance microvoltmeter (8) with a recorder (9) is connected. The field effect is brought about by the application of a strong dc field generated by (4) *via* R_B to the sample capacitors. The generator signal is checked by a frequency counter (6) and high-frequency volt meter (7).

when necessary, for volume expansion. A proper baseline to account for the absorption of overlapping bands was drawn and substracted. Because of the high background absorption of cyclohexane in the frequency region of interest, *viz.* 3500 to 3000 cm^{-1}, measurements with this solvent were made in the near ir on a Cary 14 recording spectrophotometer (Varian) in the reverse operating condition. Because of the possible photolysis by the high uv light influx of the tungsten lamp, WG-2 cut-off filters (Schott GEN., Mains) were placed between the light source and the sample. The first overtone of the NH stretching mode was used to follow the change in extinction on diluting the lactam solution. The absolute overall experimental error is estimated not to exceed ±3%, the relative accuracy is much better.

Kinetic data have been acquired by means of the chemical dipole field effect. The instrumentation described earlier[4,19] was further developed[23] in collaboration with De Maeyer and Rabl. The sample cell circuit was modified, and an electronically variable capacitance (Varactor circuit) was added to facilitate measurements at fixed frequencies. Further improvements concerned mainly the shielding. The circuit configuration is shown in Figure 1. Consideration of the circuitry along the lines discussed by De Maeyer[24] leads to the equation

$$(\Delta \tan \delta)^{ch} = -(f_U\gamma/kQ_R)(\Delta U/U_R) \qquad (1)$$

where the first parentheses contains the calibration factors, U_R is the resonant voltage of the tuned bridge, and ΔU is the voltage change which can be observed at the terminals of the bridge when the chemical system contained in the capacitors C_X of the parallel resonant circuit is subjected to a high static field.

Q_R was determined for each solution at each frequency and was calculated according to $Q_R = f_R/(f_1 - f_2)$ where f_R is the resonant frequency. If the resonant voltage of the balanced bridge is attenuated by 3 dB ($\equiv U_R/\sqrt{2}$) the bandwidth Δf is easily determined as the frequency difference of two new balancing points f_1 and f_2 by tuning with the rf generator. Q_R is of the order of 400 over most of the frequency range and accurate to within ±0.3%. The γ factor is derived from measurements of the resonant frequencies of a given inductance coil with samples of different permittivities ϵ_1 and ϵ_2. In practice, the resonant frequency associated with ϵ_2 is determined for the cell flushed with

dried nitrogen ($\epsilon_2 = 1.000$), and is denoted f_0. By taking into account that $C_X = \epsilon_i C_0$, and by defining the resonant conditions for the different permittivities, one obtains

$$\gamma = (\epsilon_i - 1)/\epsilon_i[1 - (f_i/f_0)^2]$$

The values for γ are about 1.35 at low frequencies decreasing to about 1.20 at high frequency, and are accurate to within 1%. Estimates of k are in the range of 0.86.[25] The factor f_U has been introduced into eq 1 to account for the relationship between small variations of the resonant voltage and the voltage changes appearing at the terminal of the bridge. If the attenuator is set at different positions α_1 and α_2 where $\Delta\alpha = 0.1$ dB, the two terminal voltages U_1 and U_2 fit the calculated relation $(U_1 - U_2)/U_1 = -f_U^{-1} \cdot \Delta\alpha/\alpha_1$. The factor f_U is nonlinearly dependent on the generator voltage. It increases from 0.73 at 0.5 V approaching asymptotically about 0.84 at 5 V with an intermediate value of 0.83 for the present measurements where $U_G = 3$ V throughout.

Results of the Measurements

Due to the van't Hoff equation written for studies with the electric field E as the intensive variable

$$\mathrm{d} \ln K/\mathrm{d}E = \Delta M/RT \qquad (2)$$

(K is equilibrium constant, ΔM the molar moment of reaction, R the gas constant, and T the temperature) the equilibrium state of chemical systems will be shifted if the dielectric moments of reactants and products are different. The increased polarizability causes an increased dielectric loss which is measured as the chemical increment of the loss tangent $(\Delta \tan \delta)^{ch}$

$$(\Delta \tan \delta)^{ch} = (\Delta \tan \delta)_{max}{}^{ch} \varphi''(\omega) \qquad (3)$$

where $\varphi''(\omega)$ is the Debye absorption term $\omega\tau/(1 + \omega^2\tau^2)$ ($\omega = 2\pi f$, ω is the angular frequency, τ the relaxation time = $1/\omega_{max}$).

Figure 2a–d shows typical field effect measurements where the chemical loss increments measured at a series of frequencies have been plotted *vs.* the frequency on a double logarithmic scale. The curves in the Figure 2a–d have been drawn with a template representing $\varphi''(\omega)$ to give the best visual fit to the points. The points fit well to the curves indicating that only one relaxation process occurs in the accessible frequency range.

If we assume that I dimerizes in benzene

$$2\mathrm{M} \rightleftharpoons \mathrm{D} \qquad (4)$$

(M is the monomer, D the dimer) the stability constant will be defined by

$$K^0 = \bar{c}_2/\bar{c}_1^2 = k_R/k_D \qquad (5)$$

and the mass conservation law will be

$$\bar{c}^0 = \bar{c}_1 + 2\bar{c}_2 \qquad (6)$$

where c^0 is the analytical weight concentration, and $\bar{c}_1$ and $\bar{c}_2$ are the equilibrium concentrations of the monomers and the dimers, respectively. The relaxation time is then given by[26]

$$1/\tau = 4k_R\bar{c}_1 + k_D = (4K^0\bar{c}_1 + 1)k_D \qquad (7)$$

where k_R and k_D are the phenomenological rate constants of association and dissociation without considering any detail of the association mechanism. Using eq 5 and 6, eq 7 can be formulated alternatively

$$(1/\tau)^2 = k_D{}^2(1 + 8K^0c^0) = k_D{}^2 + 8k_Rk_Dc^0 \qquad (8)$$

Thus, a plot of the squared reciprocal relaxation time *vs.* c^0 should be linear. The plot is shown in Figure 3 where a least-squares regression line has been drawn through the

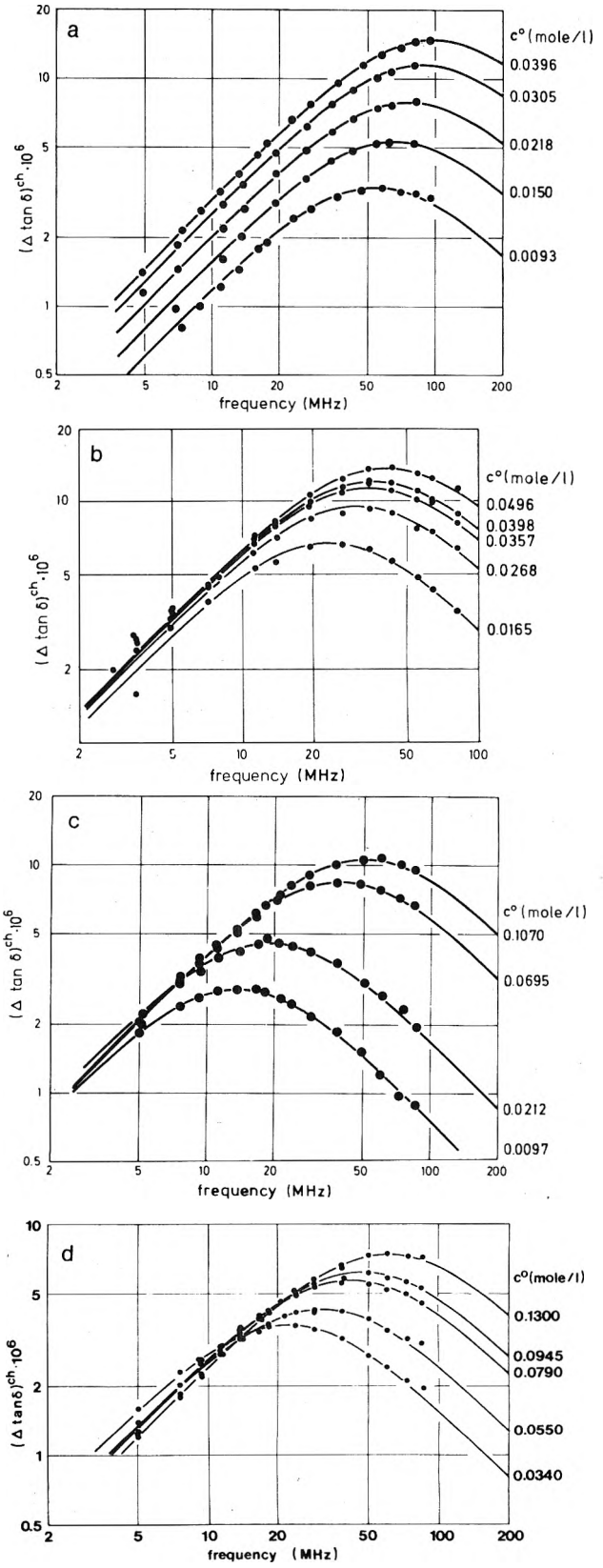

Figure 2. Some typical dielectric absorption curves: (a) I in benzene; (b) I in tetrachloromethane; (c) I in cyclohexane; (d) II in cyclohexane. Solid curves show the theoretical Debye absorption as represented by $\varphi''(\omega)$. The concentrations are indicated on the graphs: temperature 22°, E = 200 kV/cm.

TABLE I: Equilibrium, Kinetic, and Amplitude Parameters for the Isoassociation of I in (a) Benzene and (b) Tetraehloromethane[a]

	$10^{-9}k_R$, M^{-1} sec^{-1}	$10^{-7}k_D$, sec^{-1}	K^0, M^{-1}	ln $(\Delta\mu^2)^2$	Slope	σ^c	$\Delta\mu^2$, D^2	μ_M,[d] D	$K^{0,e}$ M^{-1}
a	5.0 ± 0.1	22 ± 1	24[b] ± 1	6.77	1.002	0.0399	±29.6	3.85	30
b[f]	5.7 ± 0.1	2.9 ± 0.1	200[e]	7.24	1.004	0.0133	±37.4	4.33	210

[a] 22°. [b] From the kinetic data. [c] The standard error σ refers to the evaluation of the amplitude data. The overall accuracy is estimated to be about ±10%. [d] Calculated assuming $\mu_D \simeq 0$ D. [e] From the amplitude evaluation. [f] Derived from the points $c^0 < 0.07$ M.

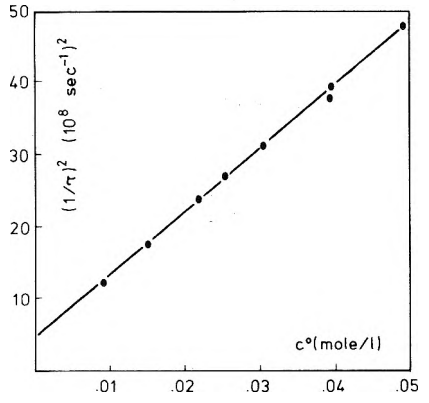

Figure 3. Plot of the squared reciprocal relaxation time *vs.* c^0 for I in benzene.

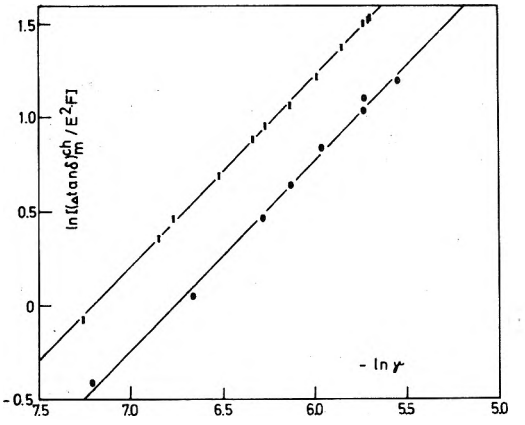

Figure 4. Double logarithmic plot of the normalized amplitude data $(\Delta \tan \delta)^{ch}/E^2F$ *vs.* the γ factor: filled circles, I in benzene; squares, I in tetrachloromethane.

points. The resulting rate and equilibrium constants are listed in Table I.

The equation describing the amplitude factor $(\Delta \tan \delta)_{max}^{ch}$ belonging to ω_{max} was derived by Bergmann, Eigen, and De Maeyer,[3] and can be found elsewhere[4,5]

$$(\Delta \tan \delta)_{max}^{ch} = \gamma \Delta M^2 / 2\epsilon_0 \epsilon_r VRT \qquad (9)$$

(ϵ_0 is the permittivity *in vacuo*,[27] ϵ_r the relative permittivity of the medium (the solution), V the volume factor = 10^3) where γ accounts for the equilibrium condition and stoichiometry of the reaction. It is generally defined by[26]

$$\gamma^{-1} = \sum_n \nu_n^2 / c_n \qquad (10)$$

(ν_n is the stoichiometric coefficient of the nth species) but can be expressed conveniently in the case of dimerization in terms of c^0 and K^0

$$\gamma = [(1 + 4K^0c^0)/(1 + 8K^0c^0)^{1/2} - 1]/8K^0 \qquad (11)$$

The molar moment of reaction ΔM is connected to the dipole moments μ_1 and μ_2 of the monomers and dimers, respectively, by

$$\Delta M = [\epsilon_r^2/(n^2 + 2)^2/(2\epsilon_r^2 + n^4)] \times [N_A(\mu_2^2 - 2\mu_1^2)E/9kT] \qquad (12)$$

(n is the refractive index and K Boltzmann's constant). Thus, eq 9 may be rewritten in a logarithmic form convenient for evaluating the amplitudes

$$\ln [(\Delta \tan \delta)_{max}^{ch}/E^2F] = \ln \gamma + \ln (\mu_2^2 - 2\mu_1^2)^2 \qquad (13)$$

This equation predicts a straight line with unit slope if the logarithm of the amplitude factor normalized with respect to the electric field strength is plotted *vs.* ln γ (F contains all constant factors occurring in eq 9). Thus, for a given set of data, K^0 may be varied in the expression 11 for γ until a least-squares treatment yields the desired result. The plot for I in benzene is found in Figure 4. The resulting value of K^0 is in agreement with the value derived from the rate constants and some ir spectroscopic measurements (K^0 = 25 M^{-1}; a_m = 80 M^{-1} cm^{-1}). The resulting $\Delta\mu^2 = \mu_2^2 - 2\mu_1^2 = \pm 29.6$ D^2 will be discussed below.

The plot of the squared reciprocal relaxation times for I in tetrachloromethane is not linear over the entire concentration range (Figure 6). Even omitting points which deviate visually from the straight line which can be drawn through the concentrations $c^0 < 0.07$ M, a least-squares treatment yields a negative intercept clearly outside the standard error. Because this result could be due to experimental errors we turn first to the evaluation of the amplitudes according to the procedure outlined above (see Figure 4 and Table I for the results). If the resulting value of K^0 is used to construct a plot according to eq 8 (Figure 5) we can calculate k_D from the slope, and then the association rate constant (Table I). The value of K^0 is higher than reported hitherto in the literature (varying from about 70[14] to 110 M^{-1} [11]) and is contrasted by our own spectroscopic determination (K^0 = 70 M^{-1}) discussed below. The tendency of the relaxation times, for $c^0 > 0.07$ M, to increase proportionally faster than the concentrations would allow suggests the occurrence of an additional relaxation process. This is more obvious for I and II in cyclohexane as solvent; the respective plots according to eq 8 are not linear (Figure 6). We have made some ir spectroscopic measurements to see whether the model of dimerization should be extended to include oligomerization.

On the basis of the dimeric self-association described by eq 4, the concentration dependence of the absorption of the free ν_{NH} band in the fundamental stretching region can be expressed by[11]

$$A = (a_m'/2K^0)(c^0/A) - a_m'/2K^0 \qquad a_m' = a_m l \qquad (14)$$

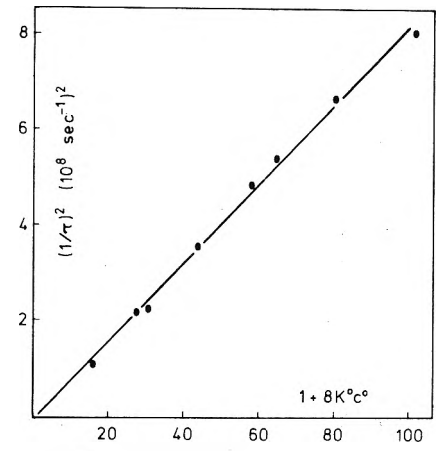

Figure 5. Plot of τ^{-2} *vs.* $(1 + 8K^0c^0)$ according to eq 14 for the concentrations $c^0 > 0.7$ *M* of I in tetrachloromethane.

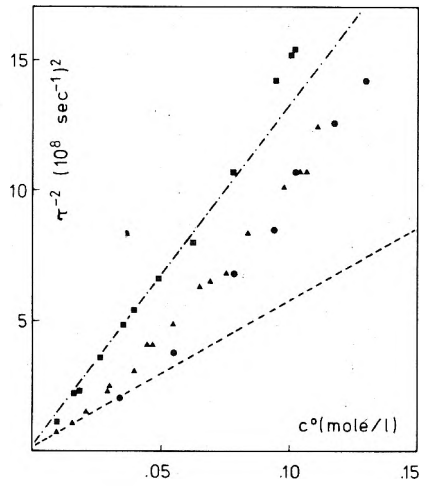

Figure 6. Plot of τ^{-1} *vs.* c^0 for I (triangles), II (filled circles), both in cyclohexane, and I (filled squares) in tetrachloromethane. The dashed line corresponds to $k_R = 5 \times 10^9$ M^{-1} sec^{-1} and $K^0 = 500$ M^{-1} the point-dash line to the constants listed in Table I for compound I in tetrachloromethane.

(A is the absorbance, a_m the monomeric absorptivity of the ν_{NH} band around 3450 cm^{-1}; l the pathlength). Because of the high solvent absorption of cyclohexane in this frequency region, these measurements had to be carried out at 6760 cm^{-1} (1.48 μm) where the first overtone of the NH-stretching band occurs. We have assumed that eq 14 holds equally well for the absorption changes of the overtone band as was assumed[11] for the fundamental stretching band. Typical results plotted according to eq 14 are shown in Figure 7 for I (63 points, 10 different stock solutions prepared from different samples of dried solvent and solute) and II (24 points from 4 stock solutions) in cyclohexane. The measurements can be described well by a straight line. The same is true for similar measurements of the lactams in tetrachloromethane in the fundamental stretching region with the exception of compound I for which we noticed some deviations to smaller absorbances at very high concentrations.

The straight line behavior of these dilution experiments is in agreement with the conventional dimerization model. For this interpretation it is presumed that only the free NH group of the monomers contribute to the absorption used in eq 14 (the overlapping of neighboring bands was

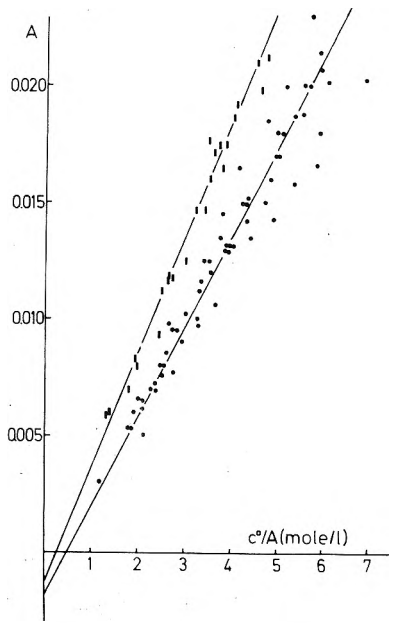

Figure 7. Plot of absorbancies *vs.* c^0/A for I (filled circles) and II (filled rectangles) in cyclohexane according to eq 20. The results are listed in Table II.

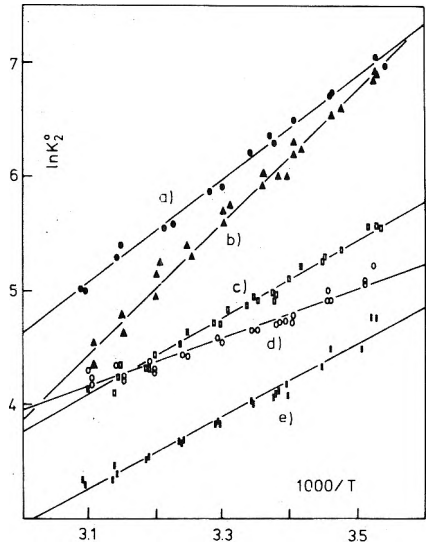

Figure 8. Van't Hoff plots of the temperature dependence of ln K_2^0; (a) I in cyclohexane, (b) IV, (c) II, (d) III, and (e) I, all in tetrachloromethane. With the exception of a, the plots are derived from three different concentrations according to the procedure outlined in the Experimental Section.

corrected for). It has already been disclosed earlier[11] that the dilution experiments on their own cannot distinguish between the open-chained (acyclic) and the ring-closed (cyclic) dimer (structures a and b, respectively). Formation of b was then postulated on the basis of the thermodynamic data.[11] In Figure 8, some of our thermodynamic measurements are shown. The ln K_2^0 values plotted *vs.* the reciprocal temperature have been calculated under the dimerization model by means of eq 14 rearranged for this special purpose. The resulting thermodynamic data calculated from the least-squares regression lines according to van't Hoff's and Gibbs' equations are listed in Table II. Altogether, the results are not as conclusive as we had hoped. No substantial result emerged which would contradict the

TABLE II: Spectroscopic and Thermodynamic Data of the Self-Association of Lactams (n = 3, 4, 5) and of 7-Azaindole in Different Solvents[a]

	a_m,[b] M^{-1} cm^{-1}	K^0,[b] M^{-1}	$-\Delta G$, cal/mol	$-\Delta H$, cal/mol	$-\Delta S$, eu	σ[c]	ϕ[d]
I[e]	2.0 ± 0.2	550 ± 60	3750	8980	17.7	0.116	15
II[e]	3.8 ± 0.5	1600 ± 200	4320	8940	15.0		
I[f]	80 ± 10	20 ± 5	1900				
I[g]	115 ± 7	60 ± 10	2450	6280	13	0.140	25
III[g]	130 ± 10	115 ± 15	2790	4260	5	0.132	24
II[g]	145 ± 13	160 ± 20	2980	6640	12.4	0.128	26
IV[g]	50 ± 2	400 ± 10[h]	3594	11400	26.8	0.200	24

[a] Referred to 25°. [b] From dilution experiments. [c] Standard error. [d] Degree of freedom. [e] Cyclohexane. [f] Benzene. [g] Tetrachloromethane. [h] 180 M^{-1}.[32]

dimerization scheme as borne out by the following considerations. Extending the dimerization model to include an oligomerization, we should have used instead of eq 14

$$A = (a_m'^2/2K_2^0)(c^0/A) - a_m'/2K_2^0 - (n/2)K_n^0K_2^{0(n-3)}a_m'^{-(n-2)}A^{(n-1)} \quad (15)$$

where the last term accounts for the oligomerization (n = 3 represents trimerization, n = 4 tetramerization). It can be seen that a contribution from this term may be expected only if K_n^0, the oligomerization constant, is sufficiently large and/or, together with a high concentration level, if a_m is low. These conditions are partially fulfilled by the lactams in cyclohexane. Close inspection of the dilution experiments (Figure 7) reveals indeed a faint statistical scatter of the points in the correct direction; model calculations have demonstrated a striking increase of the curvature in this kind of plots with increasing values of K_n^0. They suggest that, in cyclohexane and even more so in the other solvents, $K_2^0 > K_n^0$. The ratio K_n^0/K_2^0 must exceed 0.1 to yield significant deviations from a straight line. For the evaluation of the thermodynamics the respective equation for trimerization reads

$$\ln K_2^0 = \ln [(c^0 - A/a_m')/2(A/a_m')^2] - \ln [1 + 3(A/a_m')K_3^0] \quad (16)$$

or, in the case of tetramerization

$$\ln K_2^0 = \ln [(1 + 4(c^0 - A/a_m')K_4^0)^{1/2} - 1] - \ln 4(A/a_m')^2K_4^0 \quad (17)$$

(note both equations converge to that describing the dimerization model if $3(A/a_m')K_3^0$ or $4(c^0 - A/a_m')K_4^0 < 1$). The calculations showed that the terms accounting for the oligomerization are merely minor corrections to the dominant dimerization process inasmuch as the calculated enthalpy and entropy values remain almost the same if it is accepted that K_n^0 is much smaller than K_2^0 as suggested by the dilution experiments.

The qualification of taking into account an oligomerization was substantiated when the measured reciprocal relaxation times were plotted *vs.* the initial concentrations. Compound II in cyclohexane yielded a plot linear over the entire concentration range studied, for I in cyclohexane and tetrachloromethane, a major portion of these plots were linear. We derived apparent equilibrium constants 46, 20 and 18 M^{-1}, respectively, and, within 10%, an apparent bimolecular rate constant 2.4 × 10^9 M^{-1} sec^{-1}. These results indicate that a further association process must be envisaged. The analysis of the amplitudes of I in cyclohexane under the dimerization model (K_2^0 = 550 M^{-1}, eq 13) resulted in $\Delta\mu^2$ values decreasing with increasing concentrations. An extrapolation to zero concentration yielded ±36.2 D^2. The analysis under an overall oligomerization model yielded no meaningful result. Surprisingly, both models yielded a good description of the amplitudes of II with $\Delta\mu^2$ = ±32.4 (dimerization) and ±46.0 D^2 (trimerization). This result is readily understood because eq 10 becomes $\gamma = c_1/\nu^2$ with $\nu^2c_n > c_1$ in the limiting case of a stronger association. Thus, the right-hand side of eq 13 can be rewritten $\ln c_1 + \ln (\Delta\mu^2/\nu^2)$. Consequently, the monomer concentration controls the γ factor, whereas the coefficient of stoichiometry is included in the second term so that the ratio of the two $\Delta\mu^2$ values reflects mainly that of the two stoichiometric coefficients. These findings corroborate the view than an additional relaxation process must be taken into consideration. It is natural to seek an explanation of the particular behavior of these systems with an oligomerization scheme, most probably with a trimerization.[28]

Thus the mechanism of isoassociation of lactams in nonpolar solvents may be visualized as

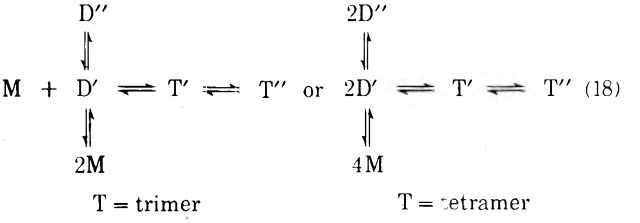

(18)

where the prime and double prime are introduced to discriminate the acyclic and the cyclic associates. This reaction sequence would require that the dielectric absorption curves be described in terms of four coupled relaxation processes. The successful description of the measurements by one Debye term without significant indications of an additional relaxation process at lower or higher frequencies does not deny the occurrence of two or more relaxation processes which may have, for example, much smaller amplitudes, or could be spaced very closely on the time axis. In any event, the coupling of the various relaxation processes leads to an unique concentration-dependent behavior of the measured relaxation times as it was found actually. Attempting to compute the dielectric curves it seemed futile to us to take more than two relaxation processes into consideration because every additional process requires the introduction of three additional variables (any two of the rate and equilibrium constants, and the moment of reaction) thus leading to an unwanted degree of computational freedom. Therefore, we based our calculations on the following two reaction equations with reference to the trimerization model

$$\begin{matrix} 2M \rightleftharpoons D \\ M + D \rightleftharpoons T \end{matrix} \quad (19)$$

where the acyclic dimer and trimer are considered to be in a steady state (an acceptable simplification). In the calculations, D and T represent formally the total concentrations of dimers and trimers, respectively. By virtue of $K_n'' = c_n''/c_n'$, the ratio of the cyclic to the acyclic structures is included in the rate constants contained in the resultant two differential equations which were treated according to the known procedures[26] and as outlined previously.[5] (The secular equation is solved for the two eigenvalues which are the negative reciprocal relaxation times, and the normal γ factors were obtained by means of a congruence transformation[29] of the thermodynamic matrix, whereby the transformation matrix contained the eigenvectors belonging to each eigenvalue.) The final equation sums the individual (normal) contributions with i and j counting the two relaxation processes uncoupled by the transformation

$$(\Delta \tan \delta)^{ch} = FE^2 \sum_{i}^{j} \gamma_i (\Delta\mu^2)_i^2 \varphi''(\omega)_i \qquad (20)$$

Note that $(\Delta\mu^2)_i$ is a linear combination of $\Delta\mu_1^2$ and $\Delta\mu_2^2$, the subscripts 1 and 2 referring to the two reaction steps in eq 19. The calculated $(\Delta \tan \delta)^{ch}$ has been plotted *vs.* the frequency on a double logarithmic scale with the help of the plotter of a desk calculator and has been compared visually to the actual measurements. The calculations were started with values for the various rate and equilibrium constants, and $\Delta\mu_1^2$, which were close to, or identical with, the values discussed above. The solely free parameter $\Delta\mu_2^2$ was chosen such that the total moment of reaction would correspond approximately to the compensation of three monomeric dipole moments of about 4 D. The initial values needed only minor corrections by trial and error to yield a faithful reproduction of the measurements (see Table III). Two important results emerged from these calculations. First, the calculated absorption curves were slightly broader than single Debye absorption terms. The accuracy of our measurements did not allow us to establish that the measured curves are composed of more than one relaxational contribution. Second, although other models have been considered equally, *e.g.*, a chain association or the tetramerization,[30] no description approximately as good could be obtained. For the sake of completeness we mention that the calculated curves were some 10% lower than the measured curves. This could be due to the omission of any further relaxation process or, more probably, it should be attributed to the inaccuracy of the calibration data and to some imperfections of the machine not dealt with.

It was claimed in the literature[31] that 7-azaindole (IV) dimerizes through hydrogen bonding. No thermodynamic data are found in the literature. We determined it for its isoassociation in tetrachloromethane; the results are included in Table II. Both the enthalpy and the entropy are about twice as large as for the lactams. While the enthalpy may be due to a favored steric situation and to the type of hydrogen bond (NH · · · N), the entropy indicates the magnitude of translational and rotational loss when a rigid dimer is formed. (There is no experimental result whatsoever throwing doubt upon a dimer formation.) Unfortunately, this compound gave no measurable field effect probably because of the compensation of the partial dipole moments associated with the pyridine and pyrrazole rings.

Discussion

In view of the thermodynamic data one would argue that lactams in the various solvents dimerize. The kinetic data, especially the chemical relaxation measurements where the reaction signals are observed in a unique manner, open time as an additional dimension. Comprehensive analyses urge the extension of the reaction model of lactam self-association to include a trimerization step. Even for the purpose of assessing the stoichiometry of these associations, thermodynamic data of one compound in different solvents cannot be compared with ease. The stereochemical situation, dipole and multipole interaction energies, dispersion, and other forces, each one on its own not very determinative, merge to yield the delicate balance of solute–solute and solute–solvent interactions which dictates the strength and stoichiometry of the association. Therefore, the ratio of the enthalpy and the entropy values for I in tetrachloromethane and cyclohexane are not necessarily an indication that trimers are formed in cyclohexane. Because dimerization is apparently the thermodynamically dominant process, and trimerization is not registered properly by the spectral changes as discussed above, we interpret the enthalpy of I in cyclohexane as the sum of the enthalpic energy of two formed hydrogen bonds. The enthalpies for lactam isoassociation in tetrachloromethane reported in three recent studies by different techniques (nmr,[17] ir,[33] and calorimetry[34]) are in the range of 8–9 kcal/mol and would strengthen this conclusion, although these values are opposed to those of this and previous studies. The discrepancy is difficult to rationalize. We found that even small quantities of moisture in the solutions can easily falsify the results. This could explain in part, too, the differences among the various a_m values of one compound reported here and in the literature. It is interesting also to note that most van't Hoff plots of lactam association, which we reconstructed from data reported in the literature, show a faint curvature similar to that shown (*e.g.* in Figure 8) by our measurements (compare *e.g.* Figure 2, ref 14).

TABLE III: List of Data Used to Fit the Measured Dielectric Loss Increments of I and II in Cyclohexane (Figure 2c and 2d) under the Trimerization Model

	K_1, M^{-1}	k_{+1}, 10^9 M^{-1} sec^{-1}	$\Delta\mu_1^2$	K_2, M^{-1}	k_f, 10^9 M^{-1} sec^{-1}	$\Delta\mu_2^2$
I	550	8	−36.5	20	3.0	−18
II	1600	8	−32	40	3.5	−17

One key to the understanding of the isoassociation lies with the $\Delta\mu^2$ values. Clearly outside the experimental error, the $\Delta\mu^2$ for I in benzene is smaller than for the other solvents. Therefore, we discuss this value first. If a closed dimer (structure b) with two hydrogen bonds is formed, and since it is not unreasonable to assume that such a cyclic dimer has no, or at least a very small, dipole moment because of its symmetry, $\Delta\mu^2$ will yield a monomer dipole moment of about 3.9 D, in close agreement with the value reported by Huisgen and Walz.[18] However these authors report also a dipole moment of about 2.6 D for the dimer. This finding can be interpreted in two different ways. Either their monomer dipole moment is correct in accordance with our above interpretation of $\Delta\mu^2$, and the dimer dipole moment is due to some error made during those authors' measurements or analyses of the data; or the monomer dipole moment as given is incorrect which could be due to the necessary extrapolation of the molar polarization to infinite dilution (a common source of error in this kind of work). Then we calculate $\mu_M = 4.26$ D from $\Delta\mu^2$ with the knowledge of that μ_D, and the monomers enclose an angle θ of

some 35°. The formation of an extended acyclic dimer with $\theta > 90°$ can be precluded because of the decrease of the molar polarization with increasing concentration. It seems to us that the latter explanation is more reasonable because this monomer dipole moment is well related to the respective values we calculate from $\Delta\mu^2$ for I in cyclohexane extrapolated to infinite dilution, and in tetrachloromethane. The solvent dependency should be of no greater importance. Thus, we conclude that the monomer dipole moment of I in nonpolar solvents is 4.30 D, and that of II is about 4.10 D. Considering all possible sources of error, the accuracy is estimated to be about ±5%. The only indication of the magnitude of $\Delta\mu^2$ of the trimerization step comes from the calculations. Nevertheless, the values indicate the disappearance of one monomer.

If the formation of a dimer with only one hydrogen bond in benzene is the correct interpretation of the amplitude data, the respective association rate constant will represent the diffusion-controlled formation of this single hydrogen bond. Because the other dimerization rate constants are only slightly higher (as one would expect by virtue of the physical properties of these solvents) one must attribute to them the same implication. This is borne out by expressing k_R in terms of the rate constants k_{12} and k_{23} of the two steps leading from the monomers *via* the acyclic to the cyclic dimer (vertical pathways in the schemes of eq 18). Depending on whether ring closure is more rapid or slower than the dissociation into the two monomers, $k_R = k_{12}$ or $k_R = K_2'k_{23}$, respectively ($K_2' = c_2'/c_1^2$). It is safe to assume that K_2' should cause a larger variation of k_R than actually observed. This confirms the earlier view[3] that the bimolecular association is slower than the intramolecular interconversion. Note that the second step leading from D′ to D″ should be accompanied by a finite moment of reaction, *i.e.*, a relaxation process with finite amplitude at higher frequencies. As mentioned above, no indication of such a relaxation process was detected. If θ of the acyclic dimer is small, as indicated by the benzene measurements ($\Delta\mu^2$ for the ring closure < 10), the amplitude would be less than a tenth of the measured relaxation processes.

If the trimer formation is also diffusion controlled, the association rate constants will be similar to those of the dimer formation. The fact that they are lower suggests a preequilibrium, *viz*, between the open and the closed structures. This is implied by a straightforward calculation based on the reaction schemes proposed above. By taking into account that ring closure for the trimer is faster than dissociation similarly to the dimers, we obtain $k_f = k_{+2}/K_2''$, with $K_2'' = c_2''/c_2'$, and k_{+2} the bimolecular rate constant for the formation of T′. If k_{+2} has approximately the same value as k_{+1} ($\equiv k_R$), K_2'' will be roughly 3 to 4. This means, that the cyclic dimer is slightly favored over the acyclic dimer. Then it becomes understandable that no cyclic dimer may be formed in benzene on the grounds of particular solvent properties. The associative behavior of the lactams in tetrachloromethane is then intermediate to that in benzene and cyclohexane. The less polar the solvent the more leads the presence of acyclic dimers to the formation of trimers.

Acknowledgments. Most measurements were carried out while the author stayed at the MPI for Physical Chemistry (Göttingen). I am gratefully indebted to Professor M. Eigen for his encouragements, to Professors L. de Maeyer and C. R. Rabl for many stimulating discussions, and to Mrs. G. Tofahrn who assisted in most of the spectrophotometric work.

References and Notes

(1) Part II on bivalently hydrogen bonded complexes. For part I see ref 5.
(2) (a) L. De Maeyer, *Isr. J. Chem.*, **9**, 351 (1971); (b) J. Rassing, *Dan. Tidesk. Farm.*, **45**, 149 (1971).
(3) K. Bergmann, M. Eigen, and L. De Maeyer, *Ber. Bunsenges. Phys. Chem.*, **67**, 819 (1963).
(4) L. De Maeyer, M. Eigen, and J. Suarez, *J. Amer. Chem. Soc.*, **90**, 3157 (1968).
(5) R. Hopmann, *Ber. Bunsenges. Phys. Chem.*, **77**, 52 (1973).
(6) G. G. Hammes, and H. O. Spivey, *J. Amer. Chem. Soc.*, **88**, 1621 (1966).
(7) G. G. Hammes and A. C. Park, *J. Amer. Chem. Soc.*, **91**, 956 (1969).
(8) M. Tsuboi, *Bull. Chem. Soc. Jap.*, **22**, 215 (1949).
(9) M. Tsuboi, *Bull. Chem. Soc. Jap.*, **24**, 75 (1951).
(10) W. Klemperer, M. Cronyn, A. Maki, and G. C. Pimentel, *J. Amer. Chem. Soc.*, **76**, 5846 (1954).
(11) R. C. Lord and Th. J. Porro, *Z. Elektrochem.*, **64**, 672 (1960).
(12) J. S. Franzen and B. C. Franzen, *J. Phys. Chem.*, **68**, 3898 (1964).
(13) W. Luck, *Naturwissenschaften*, **52**, 25 (1965).
(14) C. Y. S. Chen and Ch. A. Swenson, *J. Phys. Chem.*, **73**, 1363 (1969).
(15) A. Veillard, *J. Chim. Phys.*, **59**, 1956 (1962).
(16) J. L. Mateos, E. Diaz, and R. Cetina, *Bol. Inst. Quim. Univ. Nacl. Anton. Mex.*, **14**, 61 (1962).
(17) W. Krüger, Thesis, Braunschweig, 1970.
(18) R. Huisgen and H. Walz, *Chem. Ber.*, **89**, 2616 (1956).
(19) K. Bergmann, *Ber. Bunsenges. Phys. Chem.*, **67**, 826 (1963).
(20) L. Gattermann and H. Wieland, "Die Praxis des organischen Chemikers," De Gruyter, Berlin, 1956, p 304.
(21) Ch.D. Hodgman, R. C. Weast, R. C. Shankland, Ed., "Handbook of Chemistry and Physics," 43rd ed., The Chemical Rubber Publishing Co., Cleveland, Ohio, 1962.
(22) R. L. Schupp and R. Mecke, *Z. Elektrochem.*, **52**, 49 (1943).
(23) R. Hopmann, submitted for publication.
(24) L. De Maeyer, "Electric Field Methods, in Fast Reactions," Vol. XVI of "Methods in Enzymology," K. Kustin Ed., Academic Press, New York, N.Y., 1969, p 101.
(25) R. Rabl, private communication.
(26) M. Eigen and L. De Maeyer, "Relaxation Methods" in "Techniques of Organic Chemistry," Vol. 8, Part II, S. L. Friess and A. Weissberger, Ed., Interscience, New York, N.Y., 1961, p 895.
(27) Using the rational system, $\epsilon_0 = 8.854 \times 10^{-14}$ A sec V^{-1} cm^{-1}. k (Boltzmann's constant) = 1.38×10^{-23} A sec V deg^{-1}; μ (D) = 3.33×10^{-28} A sec cm.
(28) Osmotic vapor pressure data of I in cyclohexane were interpreted in terms of a trimerization by Th. Funck (private communication).
(29) P. Schimmel, *J. Chem. Phys.*, **54**, 4136 (1971).
(30) The partially possible reconciliation of some of our results by the tetramerization had led us previously[31] to assume that this variant is correct.
(31) R. Hopmann, *Ber. Bunsenges. Phys. Chem.*, **74**, 935 (1970).
(32) K. C. Ingham, M. Abu-Elgheit, and M. Ashraf El-Bayoumi, *J. Amer. Chem. Soc.*, **93**, 5023 (1971).
(33) M. V. Schablygin and N. V. Mikhailov, *Vysokomol. Soedin., Ser. B*, **11**, 454 (1969); *Chem. Abstr.*, **71**, 81825 (1969).
(34) M. Lazniewski and T. Jankowsky, *Rocz. Chem.*, **46**, 1115 (1972).

Mechanism of Photosubstitution Reactions of Square-Planar Platinum(II) Complexes. II. Effect of the Leaving Ligand on the Photosubstitution Mechanism of Diethylenetriamineplatinum(II) Complexes[1]

Carlo Bartocci, Franco Scandola,* and Vittorio Carassiti

Istituto Chimico dell'Università, Centro di Studio sulla Fotochimica e Reattività degli Stati Eccitati dei Composti di Coordinazione del C.N.R., Ferrara, Italy *(Received November 5, 1973; Revised Manuscript Received June 3, 1974)*

Publication costs assisted by Consiglio Nazionale delle Ricerche, Italy

The photosubstitution reactions of $Pt(dien)I^+$ and $Pt(dien)py^{2+}$ have been investigated in aqueous solutions containing various concentrations of Br^- and OH^- ions. The irradiation with 313-nm light of $Pt(dien)I^+$ in aqueous solutions containing 1.5×10^{-2} to 2×10^{-3} *M* Br^- caused the formation of $Pt(dien)Br^+$, with quantum yields in the range 0.02–0.08 increasing with increasing Br^- concentration. When the irradiation of $Pt(dien)I^+$ was carried out in alkaline (pH 12) solutions $Pt(dien)OH^+$ only was formed (Φ = 0.10), regardless of the presence of Br^- in the irradiated solution. These results are interpreted in terms of a mechanism previously formulated for the analogous photoreactions of $Pt(dien)Br^+$, which involves the dissociative formation of a geminate pair intermediate of the $Pt(dien)(H_2O)_2^{2+} \cdot I^-$ type. Such an intermediate is 100% scavengeable by OH^- and it can undergo an efficient geminate recombination process in competition with substitution by other ligands. The irradiation with 254-nm light of $Pt(dien)py^{2+}$ in aqueous solution caused the formation of $Pt(dien)H_2O^{2+}$, $Pt(dien)OH^+$, or $Pt(dien)Br^+$ depending on the pH and on the presence of Br^- in the irradiated solutions. The quantum yield of pyridine released was 0.018 independent of pH (in the range 4–12) and of Br^- concentration (up to 2×10^{-2} *M*). These results indicate the absence of geminate recombination in the photosubstitution of $Pt(dien)py^{2+}$ and are interpreted assuming $Pt(dien)H_2O^{2+}$ as the primary photochemical intermediate. The difference in behavior between $Pt(dien)X^+$ (X = Br, I) complexes and $Pt(dien)py^{2+}$ is considered to be indicative of the electrostatic (ion pair) nature of the residual bonding in the photochemical intermediate which is responsible for geminate recombination.

In recent development of the photochemistry of coordination compounds,[2,3] little attention has been devoted to the problem of the intimate chemical mechanism of the ligand photosubstitution reactions which are obtained by ligand field excitation. The thermal substitution reactions of coordination compounds proceed by a variety of mechanisms, with dissociative activation being generally favored for octahedral complexes and associative activation being preferred by square-planar compounds.[4,5] As compared to the ground state, ligand field excited states of coordination compounds show a decreased electron density in essentially nonbonding π orbitals and an increased electron population in strongly antibonding σ^* orbitals. Although the mechanistic importance of the decreased electron density in nonbonding d orbitals has been stressed in some cases,[6,7] it seems likely that the main effect of ligand field excitation lies in the considerable weakening of the metal–ligand bonds which accompanies the increase in electron density in σ^* antibonding orbitals. Since this bond weakening should clearly favor the dissociation of the leaving ligand in a substitution process, it is to be concluded that dissociative mechanisms are generally more likely to occur in photochemical substitution reactions than in the corresponding thermal processes.

In the case of octahedral Co(III) and Cr(III) complexes, whose thermal substitution reactions involve dissociative activation, it is easy to predict dissociative photosubstitution mechanisms. Direct experimental evidence for this prediction has been obtained by Adamson, *et al.*,[8] and Wrighton, *et al.*,[9] in the study of some $Co(CN)_5X^{3-}$ complexes. In the case of square-planar d^8 metal complexes, however, the effect of the excited state metal–ligand bond weakening is not easily predictable, since these complexes react thermally by associative mechanisms. In the previous paper of this series,[1] a study of the photosubstitution mechanism of the $Pt(dien)Br^+$ complex ion was performed using NO_2^- as the entering ligand and working in the presence of various concentrations of Br^- and OH^-. It was shown that the photosubstitution reaction

$$Pt(dien)Br^+ + NO_2^- \xrightarrow{h\nu} Pt(dien)NO_2^+ + Br^- \quad (1)$$

proceeded through the formation of a primary photochemical intermediate which could be quantitatively scavenged by OH^-. This behavior contrasted strikingly with the thermal one and was taken as evidence of a dissociative mechanism for photosubstitution reaction 1. Quite interestingly, competition experiments clearly showed that the coproducts of the primary photochemical process had a high probability of undergoing a geminate recombination process before diffusing apart. Thus, the primary photochemical intermediate had still to contain the labilized ligand. In view of its ability to be scavenged by OH^- and to undergo geminate recombination, the intermediate was tentatively formulated as $Pt(dien)^{2+} \cdot Br^-$ or, alternatively, $Pt(dien)H_2O^{2+} \cdot Br^-$.

The detection of this efficient geminate recombination process in the photosubstitution reactions of $Pt(dien)Br^+$ could be of some general interest in the photochemistry of other Pt(II) complexes and perhaps of other metal complexes too. In fact, most of the photosubstitution studies

carried out until now are actually photoaquation studies performed in the absence of entering ligands other than water.[2,3] In these photoreactions it is obviously very difficult to distinguish an efficient geminate recombination from an efficient radiationless deactivation of the excited reagent complex, so that geminate recombination could be a more common process than presently believed. We thought it was interesting to obtain further insight into the nature of the primary intermediates and into the factors which determine the efficiency of the geminate recombination process in the photosubstitution reactions of Pt(II) complexes. We report here the results of a comparative study of the photosubstitution mechanisms of two other complexes of the $Pt(dien)X^{n+}$ family, namely, $Pt(dien)I^+$ and $Pt(dien)py^{2+}$.

Experimental Section

Materials. [Pt(dien)Br]Br was prepared according to Mann[10] and twice recrystallized from water. [Pt(dien)I]I was precipitated from aqueous solutions of [Pt(dien)Br]Br by the addition of excess NaI and was twice recrystallized from water. $[Pt(dien)I](ClO_4)$ was prepared by adding a stoichiometric amount of $AgNO_3$ to an aqueous solution of [Pt(dien)I]I, filtering off the precipitated AgI, and crystallizing the product in the presence of excess $NaClO_4$. The perchlorate salt was twice recrystallized from water; its aqueous solutions were found to contain less than 0.1% free I^-. $[Pt(dien)py](ClO_4)_2$ was prepared as follows. $AgNO_3$ (2 equiv) was added to an aqueous solution of [Pt(dien)Br]Br, and the resulting AgBr was eliminated by filtration. Then, a stoichiometric amount of pyridine was added to the solution. Crystallization in the presence of excess $NaClO_4$ yielded white crystals of the perchlorate salt. The salt was twice recrystallized from water. Aqueous solutions of $Pt(dien)H_2O^{2+}$ were prepared by adding 2 equiv of $AgNO_3$ to an aqueous solution of [Pt(dien)Br]Br and by filtering off the precipitated AgBr. All the chemicals used were of reagent grade.

Apparatus. The light sources and general equipment used to obtain 254- and 313-nm radiations were the same as previously described.[1,11] The reaction cells were standard 1-cm spectrophotometric cells which could be thermostated in suitable metal cell holders. Spectrophotometric measurements were performed with Optica CF4 NI (double beam) and Shimadzu QV 50 (single beam) spectrophotometers. pH measurements were carried out with a Knick KpH 350 and a Radiometer PHM digital pH meter. The electrodes were Ingold glass–reference combined microelectrodes.

Procedures. In order to allow for thermal substitution reactions simultaneous to the photochemical ones, the photochemical kinetic runs were always performed in a differential mode, using as the reference blank a dark solution identical with the irradiated one. During irradiation, the solutions were always stirred by a continuous stream of pure nitrogen from a glass capillary. Spectrophotometric kinetic measurements were carried out by periodically taking the irradiated and dark reaction cells to the spectrophotometer for measure. Kinetic pH measurements, on the contrary, could be performed continuously during the irradiation with the microelectrodes directly placed in the reaction cells (that in the irradiated cell being screened from the exciting light).

The initial concentration of the reagent complexes was always selected to ensure the maximum light absorption at the wavelength of excitation compatible with the type of measurement to be performed. In the kinetic measurements, the time of irradiation was limited so as to decompose a few per cent units of the initial complex concentration. Under these conditions, experimental zero-order kinetics was always obeyed, and the calculation of the quantum yield values was straightforward. The quantum yield calculation was always based on two actinometric measurements[12] performed in the reaction cell before and after each photochemical run.

Results

Pt(dien)I⁺. The spectra of $Pt(dien)I^+$, $Pt(dien)Br^+$, $Pt(dien)H_2O^{2+}$, and $Pt(dien)OH^+$ in aqueous solution are shown in Figure 1.

When $[Pt(dien)I](ClO_4)$ was dissolved in aqueous solution at 25°, no appreciable hydrolysis was observed to occur. This behavior is consistent with the known values of the rate constants for the forward[13] and reverse[15] reactions of the hydrolysis equilibrium

$$Pt(dien)I^+ + H_2O \rightleftharpoons Pt(dien)H_2O^{2+} + I^- \qquad (2)$$

which is expected to be completely displaced toward the left. When Br^- ions were added to $Pt(dien)I^+$ solutions at 25°, spectral variations indicated the occurrence of the thermal substitution reaction

$$Pt(dien)I^+ + Br^- \longrightarrow Pt(dien)Br^+ + I^- \qquad (3)$$

with observed rate constant values in agreement with those reported by Gray.[14] If the solutions containing $Pt(dien)I^+$ and Br^- were thermostated at 2°, reaction 3 was slowed considerably, giving an observed pseudo-first-order rate constant of 5.9×10^{-6} sec^{-1} at $[Br^-] = 10^{-2}$.

When solutions containing 2×10^{-3} *M* $[Pt(dien)I](ClO_4)$ and 2×10^{-3} to 1.5×10^{-2} *M* Br^- were irradiated with 313-nm light, the observed spectral variations were qualitatively the same as those obtained in the dark, but the rate of absorbance change was greatly accelerated. Differential spectrophotometric measurements performed on irradiated and dark solutions at 2° allowed us to measure the kinetics of the photochemical reaction

$$Pt(dien)I^+ + Br^- \xrightarrow{h\nu 313} Pt(dien)Br^+ + I^- \qquad (4)$$

If the extent of photoreaction was limited to less than 5% the kinetics of reaction 4 always obeyed a good zero-order behavior, indicating that in the experimental conditions used (a) light absorption by the reactant complex remained appreciably constant during the irradiation and (b) any bimolecular process involving the released I^- was unimportant. The quantum yield values for reaction 4 obtained at different Br^- concentrations from the slopes of the zero-order plots are reported in Table I.

When the irradiation of $Pt(dien)I^+$ was carried out in basic (pH 12) solutions, the observed spectral variations clearly indicated that the only photoreaction occurring was

$$Pt(dien)I^+ + OH^- \longrightarrow Pt(dien)OH^+ + I^- \qquad (5)$$

regardless of the presence or absence of Br^- in the irradiated solutions. Quantum yield values for reaction 5 were easily obtained by differential spectrophotometric measurements and are reported in Table I.

Pt(dien)py²⁺. The spectra of $Pt(dien)py^{2+}$ and pyridine in aqueous (pH 8) solutions are shown in Figure 2.

The thermal hydrolysis of aqueous solutions of $[Pt(dien)py](ClO_4)_2$ at 25° was absolutely negligible in the time scale of our photochemical experiments. When Br^- was

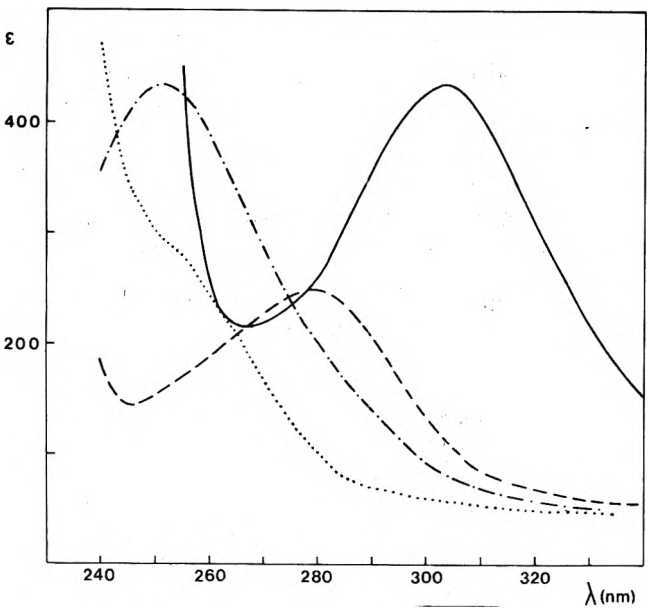

Figure 1. Absorption spectra of $Pt(dien)I^+$ (—), $Pt(dien)Br^+$ (- - - -), $Pt(dien)H_2O^{2+}$ (- · - · -), and $Pt(dien)OH^+$ (· · · · ·) in aqueous solutions.

added to aqueous solutions of $[Pt(dien)py](ClO_4)_2$, a slow thermal substitution reaction

$$Pt(dien)py^{2+} + Br^- \longrightarrow Pt(dien)Br^+ + py \qquad (6)$$

was observed to occur.

When aqueous solutions of $[Pt(dien)py](ClO_4)_2$ were irradiated with 254-nm radiation, the growth of an intense absorption band was observed, with maximum wavelength depending on the initial pH of the irradiated solution. These spectral variations, as well as their pH dependence, were essentially the same as those observed by Joussot-Dubien and Houdard Pereyre[16] in the photolysis of pyridine in aqueous solutions to give glutaconic aldehyde. In order to establish whether the decomposition of pyridine observed on irradiation of $Pt(dien)py^{2+}$ was a primary or a secondary photoprocess, the kinetics of formation of the pyridine decomposition products was measured. It was found that the rate of product formation increased with time of irradiation and was higher the lower was the initial complex concentration. Both these results demonstrated that the photolysis of pyridine was actually a secondary photoprocess occurring by light absorption by the free pyridine released in a primary photochemical reaction.

The spectral variations, even when recorded for the very initial irradiation periods, did not allow the identification of the primary pyridine releasing photoprocess. In fact, the spectrum of $Pt(dien)py^{2+}$, which is dominated by the pyridine absorption (see Discussion), is too intense with respect to the spectra of all the possible Pt-containing photoproducts. However, other types of evidence could be used to characterize the primary photoreaction. The addition of I^- ions to irradiated aqueous solutions of $Pt(dien)py^{2+}$ caused the formation of the characteristic 300-nm absorption of $Pt(dien)I^+$. Moreover the following pH variations were obtained upon irradiation of aqueous solutions of $Pt(dien)py^{2+}$ of various initial pH values: the pH of acid (pH 4) solutions increased, that of slightly basic (pH 8) solutions decreased, while that of pH ~6 solutions remained appreciably constant under irradiation. These results indicate that the primary photoreaction obtained upon irradiation

TABLE I: Photosubstitution Quantum Yields of $Pt(dien)I^+$

pH	$[Br^-]$	Φ^c
6[a]	2×10^{-3}	0.021
6[a]	8×10^{-3}	0.057
6[a]	1.5×10^{-2}	0.081
12[b]	0	0.10
12[b]	1.5×10^{-2}	0.10

[a] Natural pH. [b] 10^{-2} *M* NaOH. [c] Estimated error, ±5%.

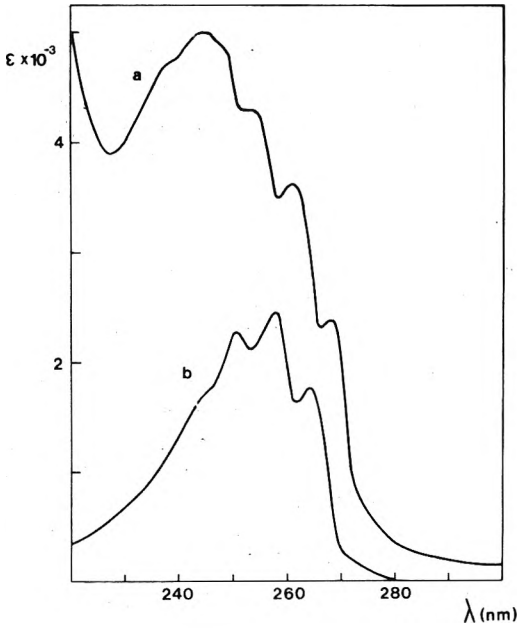

Figure 2. Absorption spectra of $Pt(dien)py^{2+}$ (a) and pyridine (b) in aqueous solutions (pH 8).

of aqueous solutions of $Pt(dien)py^{2+}$ was the photoaquation reaction

$$Pt(dien)py^{2+} + H_2O \xrightarrow{h\nu 254} Pt(dien)H_2O^{2+} + py \qquad (7)$$

In fact, $Pt(dien)H_2O^{2+}$ is known to undergo fast substitution by I^-.[15] On the other hand, while the basic properties of pyridine ($K_b = 1.8 \times 10^{-9}$) are well known, the acid character of $Pt(dien)H_2O^{2+}$ was suggested to account for the exceedingly high reactivity of OH^- toward this complex.[14] A titration of aqueous solutions of $Pt(dien)H_2O^{2+}$ against standard NaOH gave indeed $K_a = 7.6 \times 10^{-7}$ for the equilibrium

$$Pt(dien)H_2O^{2+} \overset{K_a}{\rightleftharpoons} Pt(dien)OH^+ + H^+ \qquad (8)$$

Quantum yield values for reaction 7 were determined in two ways. In moderately acid solutions (pH 4), the release of pyridine could be conveniently followed by pH measurements. When pH variations were converted into pyridine concentration by the use of suitably measured calibration plots, good zero-order kinetics was obtained,[17] allowing a straightforward calculation of the quantum yield values. On the other hand, spectrophotometric measurements carried out for initial irradiation periods in the wavelength range 220–240 nm, where the absorbance of free pyridine is low with respect to that of the complex, allowed calculation of quantum yield values of reaction 7 in both acid and basic solution.[18] The agreement between the quantum yield values obtained by pH measurements and by spectrophoto-

TABLE II: Photosubstitution Quantum Yields of Pt(dien)py^{2+}

pH	[Br$^-$]	Φ^d
4[a]	0	0.018
4[a]	2×10^{-2}	0.017
5.8[b]	0	0.019
5.8[b]	2×10^{-2}	0.018
12[c]	0	0.017
12[c]	2×10^{-2}	0.018

[a] 10^{-4} *M* $HClO_4$. [b] Natural pH. [c] 10^{-2} *M* NaOH. [d] Estimated error, ±5%.

metric methods was excellent. The quantum yields of photoreaction 7 are reported in Table II.

When solutions of Pt(dien)py^{2+} containing Br$^-$ ions were irradiated at 254 nm, no appreciable difference in spectral variations was observed with respect to simple aqueous solutions of the complex. As already pointed out, this fact does not allow identifying the photoreaction as reaction 7, since all possible products (except pyridine) are very weakly absorbing species with respect to the original complex. Most probably, however, the overall photoreaction occurring in the presence of Br$^-$ in acid solution is

$$\text{Pt(dien)py}^{2+} + \text{Br}^- \xrightarrow{h\nu 254} \text{Pt(dien)Br}^+ + \text{py} \qquad (9)$$

This photoreaction is to be expected on the basis of the known high substitution rate of Br$^-$ on Pt(dien)H_2O^{2+} and also by analogy to the behavior exhibited by Pt(dien)I$^+$ and Pt(dien)Br$^+$.[1] Similarly, when basic solutions containing Pt(dien)py^{2+} and Br$^-$ were irradiated at 254, the only photoreaction occurring was most probably

$$\text{Pt(dien)py}^{2+} + \text{OH}^- \xrightarrow{h\nu 254} \text{Pt(dien)OH}^+ + \text{py} \qquad (10)$$

The quantum yields of reactions 9 and 10 were determined as usual by pH and spectrophotometric[19] measurements. The values are reported in Table II.

Discussion

Types of Excitation and Photoreaction. The electronic spectra of most Pt(dien)X^{n+} complexes are characterized by the presence of a medium intensity band (molar absorptivities in the 200–2000 range) in the ultraviolet region.[1,20] This band has been assigned to spin allowed ligand field transitions (of the $d_{xy} \rightarrow d_{x^2-y^2}$ type) with some degree of ligand-to-metal charge transfer (LMCT) character.[20] In the case of Pt(dien)I$^+$, as in the previously examined case of Pt(dien)Br$^+$,[1] the excitation was performed in this band. The type of photoreaction obtained, namely, photosubstitution, is just that expected on the basis of the reactivity of a ligand field excited state.[2] On the other hand, it should be pointed out that, aside from one noticeable exception,[21] Pt(II) complexes have not been found to exhibit redox photochemical behavior even by excitation in LMCT bands.[2,3] Thus, it is not surprising at all that the partial LMCT character of the transitions excited in Pt(dien)I$^+$ and Pt(dien)Br$^+$ is not sufficient to bring about any redox photochemical consequence.

The interpretation of the spectrum of Pt(dien)py^{2+} is less straightforward than that of the typical spectra discussed above. It consists of two different though partially overlapping absorption zones. By comparison with the spectrum of free pyridine (Figure 2), the structured absorption at wavelengths longer than 240 nm can be confidently assigned to the π–π^* transitions of the pyridine ligand, only slightly displaced relative to free pyridine due to coordination. The intense absorption below 240 nm, which is absent in free pyridine as well as in other Pt(dien)X^{n+} complexes, can be likely assigned to a d–π^* MLCT transition similar to that shown by several other pyridine-containing transition metal complexes.[22] In this complex, the ligand field bands are evidently hidden by these much more intense absorptions.

The wavelength of excitation used in the case of Pt(dien)py^{2+} corresponds to the absorption band of the coordinated pyridine ligand. The fact that this excitation gives rise to ligand photosubstitution rather than to pyridine decomposition implies that the π–π^* excited states of the coordinated pyridine deactivate to lower lying ligand field excited states before reacting. In this regard, it should be noted that the mechanism proposed for the photoreaction of pyridine in water[16] involves abstraction of hydrogen from water by the pyridine nitrogen atom. Since in the complex the lone pair of the nitrogen atom is engaged in bonding to the metal, a marked decrease in the reactivity of the intraligand excited states relative to those of free pyridine is to be expected.

Photosubstitution Mechanism. The results obtained with Pt(dien)I$^+$ are rather similar to those previously observed for Pt(dien)Br$^+$ [1] and point toward a common mechanism for the photosubstitution reactions of these two complexes. These results may be summarized as follows: (i) even in the presence of equivalent amounts of Br$^-$ ions, OH$^-$ is 100% efficient in capturing the primary photoreaction intermediate; (ii) the quantum yield of reaction 4 increases markedly with increasing Br$^-$ concentration, in the absence of any competing bimolecular substitution process; (iii) the quantum yields of reaction 4 are always lower than that of reaction 5 occurring in basic solution.

Point i clearly shows that the primary photoreaction intermediate cannot be an electronically excited state of Pt(dien)I$^+$ undergoing bimolecular substitution reactions with the same mechanism as the ground state. The primary photoreaction intermediate must rather be the product of a dissociative process involving the labilization of I$^-$. Point ii indicates that the reaction of Br$^-$ with the primary intermediate, which is certainly fast and should not be by itself rate determining, competes with a reactive pathway of the intermediate converting it back to Pt(dien)I$^+$.[23] Point iii indicates that the Br$^-$ photosubstitution quantum yields are always lower than the primary quantum yields of intermediate formation, thus confirming the existence of such a competition. The conclusions which follow from these results are thus similar to those reached from the study of Pt(dien)Br$^+$.[1,24] In particular, it is to be concluded that the primary product in the photosubstitution reactions of Pt(dien)I$^+$ is a dissociated intermediate which is completely scavengeable by OH$^-$ and *is capable of undergoing an efficient geminate recombination process* in competition with substitution by other ligands. If this reaction intermediate is indicated by A (for a discussion of the nature of A, see below), the mechanism of the photosubstitution reactions 4 and 5 may thus be schematized as follows

$$\text{Pt(dien)I}^+ \xrightarrow{h\nu} {}^*\text{Pt(dien)I}^+ \qquad (11)$$

$${}^*\text{Pt(dien)I}^+ \longrightarrow \text{Pt(dien)I}^{+\cdot} \qquad (12)$$

$${}^*\text{Pt(dien)I}^+ \longrightarrow \text{A} \qquad (13)$$

$$\text{A} \longrightarrow \text{Pt(dien)I}^+ \qquad (14)$$

$$\text{A} + \text{OH}^- \longrightarrow \text{Pt(dien)OH}^+ + \text{I}^{\cdot} \qquad (15)$$

$$\text{A} + \text{Br}^- \longrightarrow \text{Pt(dien)Br}^+ + \text{I}^- \qquad (16)$$

According to this mechanism, the quantum yield of reaction 4 in acid solution (where process 15 is negligible) is given by

$$\frac{1}{\phi} = \frac{1}{\phi'}\left(1 + \frac{k_{14}}{k_{16}}\frac{1}{[Br^-]}\right) \qquad (17)$$

where $\phi' = k_{13}/(k_{12} + k_{13})$ is the primary quantum yield of intermediate formation. A plot of the quantum yield data of Table I according to eq 17 is shown in Figure 3. The data satisfactorily fit the observed Br^- concentration dependence, and the primary quantum yield obtained from the intercept of the plot compares well with that directly measured in basic solution (where processes 14 and 16 are negligible with respect to 15).

A comparison between the quantum yield data of Tables I and II clearly indicates a fundamental difference in the photosubstitution mechanisms of Pt(dien)I^+ and Pt(dien)py^{2+}. As a matter of fact, the prominent features of the Pt(dien)py^{2+} behavior (Table II) are as follows: (i) the quantum yield of reaction 9 occurring in acid solution is independent of the entering ligand concentration; (ii) the quantum yields of reactions 7 and 9 in acid solution are the same as that of reaction 10 in basic solution. These results imply that *the primary intermediate in the photosubstitution reactions of Pt(dien)py^{2+} does not undergo any appreciable geminate recombination process.* It could be argued that protonation of pyridine could be a possible reason for the lack of geminate recombination in acid, pH 4, solutions. However, this argument does not hold for pH 5.8 solutions, in which pyridine is about 80% in its basic form. Therefore, the lack of geminate recombination in these conditions points toward a sharp difference in the nature of the intermediates which are formed in the photosubstitution reactions of Pt(dien)py^{2+} and Pt(dien)X^+ (X = Br,I). In this case, the most plausible mechanism is a rather straightforward one, involving the aquo complex as the primary photoreaction intermediate.

$$Pt(dien)py^{2+} \xrightarrow{h\nu} {}^*Pt(dien)py^{2+} \qquad (18)$$

$${}^*Pt(dien)py^{2+} \longrightarrow Pt(dien)py^{2+} \qquad (19)$$

$${}^*Pt(dien)py^{2+} + H_2O \longrightarrow Pt(dien)H_2O^{2+} + py \qquad (20)$$

$$Pt(dien)H_2O^{2+} + OH^- \longrightarrow Pt(dien)OH^+ + H_2O \qquad (21)$$

$$Pt(dien)H_2O^{2+} + Br^- \longrightarrow Pt(dien)Br^+ + H_2O \qquad (22)$$

As usual, processes 21 and 22 are fast, so that the constant quantum yield value obtained in all the experimental conditions used corresponds to the primary photoaquation quantum yield.

The results obtained in this work give some insight into the mechanism of the photosubstitution reactions of Pt(II) complexes. In this regard, the most interesting result is the sharp difference in behavior observed between Pt(dien)py^{2+} and Pt(dien)X^+ (X = Br,I) complexes. The last complexes exhibit an efficient geminate recombination process following the photodissociation of the X ligand, while the former one seems to undergo photosubstitution without any appreciable recombination process.

The concept of geminate recombination has usually been associated with that of the cage effect.[25] In this effect, the action of the solvent in preventing the immediate separation of a pair of species in close contact in solution is considered. The two species may find themselves in the solvent cage either following a bimolecular collision or as the coproducts of a unimolecular (perhaps photochemical) bond dissociation. In either case, in the absence of specific interactions between the two component species, the lifetime of the caged pair (often called the "encounter" lifetime) is controlled by diffusion. In order to show sizeable recombination during such a very short time lag, the caged species must have a very high inherent reactivity. Thus, the cage effect has usually been studied for homolytic reactions, and the geminate recombination process is usually considered to be a radical recombination. In the field of the photochemistry of coordination compounds, radical cage recombination has recently been shown to occur in the redox decomposition of Co(III) complexes.[26,27] In the Pt(II) photosubstitution reactions studied in this work, the photochemical bond splitting is a heterolytic one and the primary produced species do not have any radical character. However, the presence of a vacant coordination site on the Pt atom is likely to make the recoordination process a very fast one, possibly as fast as to compete with diffusion.

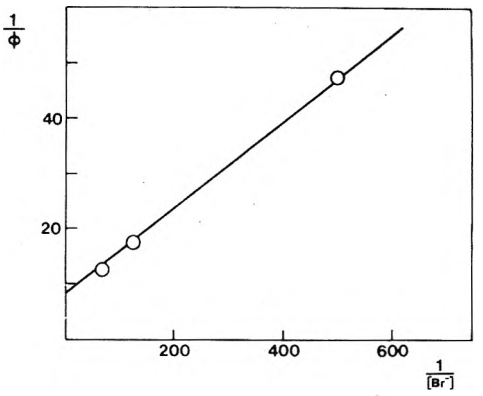

Figure 3. Dependence of the quantum yield of reaction 4 on the Br^- concentration.

Actually, the fact that no geminate recombination has been detected for Pt(dien)py^{2+} seems to indicate that the solvent cage effect alone cannot account for the occurrence of geminate recombination in the other complexes of this series. Instead, some kind of residual bonding between the Pt-containing moiety and the released ligand seems to be required in order to increase the lifetime of the caged species so as to allow recombination before diffusion apart of the coproducts. In this regard, both weak covalent (*e.g.*, axial coordination) and electrostatic (ion pair) interactions between the released ligand and the complex moiety could be envisioned. The fact that recombination is observed with the negatively charged Br^- and I^- leaving ligand and not with the neutral pyridine ligand points toward a substantial contribution of electrostatic (ion pair) bonding to the leaving ligand in the formation of the photoreaction intermediate (A in eq 11–16) which is capable of geminate recombination in the photosubstitution reactions of these Pt(II) complexes.

As far as the detailed structure of the geminate intermediate is concerned, the basic model assumed is thus that of a Pt(dien)$^{2+}$ moiety being weakly bonded with the released X^- ligand in a solvent caged ion-pair structure. As an additional feature, it is very likely to envision that two water molecules are very weakly coordinated in the axial positions of the Pt(dien)$^{2+}$ moiety. This type of axial solvation is often considered in the chemistry of four coordinated square-planar complexes, and the strength of the axial bonds could be substantially increased by the dissociation of one in-plane ligand. Moreover, the presence of axial

water molecules in the intermediate could help to account for the high efficiency exhibited by OH^- in capturing the geminate intermediate. The proposed structure of the geminate intermediate can be schematized as follows

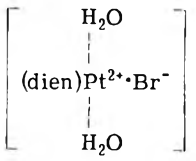

solvent cage

It might be noted that this structure is rather similar to the standard picture[15] of the tetragonal transition state for the minor dissociative path of the thermal substitution reactions of Pt(II) complexes.

References and Notes

(1) Part I: C. Bartocci, F. Scandola, and V. Balzani, *J. Amer. Chem. Soc.*, **91,** 6948 (1969).
(2) V. Balzani and V. Carassiti, "Photochemistry of Coordination Compounds," Academic Press, New York, N.Y., 1970.
(3) P. D. Fleischauer, A. W. Adamson, and G. Sartori in "Inorganic Reaction Mechanism," J. O. Edwards, Ed., New York, N.Y., 1972, p 1.
(4) F. Basolo and R. G. Pearson, "Mechanisms of Inorganic Reactions," 2nd ed, Wiley, New York, N.Y., 1967.
(5) C. H. Langford and H. B. Gray, "Ligand Substitution Processes," W. A. Benjamin, New York, N.Y., 1966.
(6) R. A. Plane and J. P. Hunt, *J. Amer. Chem. Soc.*, **79,** 3343 (1957).
(7) F. Scandola, O. Traverso, and V. Carassiti, *Mol. Photochem.*, **1,** 11 (1969).
(8) A. W. Adamson, A. Chiang, and E. Zinato, *J. Amer. Chem. Soc.*, **91,** 5467 (1969).
(9) M. Wrighton, G. S. Hammond, and H. B. Gray, *J. Amer. Chem. Soc.*, **93,** 5254 (1971).
(10) F. G. Mann, *J. Chem. Soc.*, 466 (1934).
(11) V. Balzani, V. Carassiti, L. Moggi, and F. Scandola, *Inorg. Chem.*, **4,** 1243 (1965).
(12) C. G. Hatchard and C. A. Parker, *Proc. Roy. Soc., Ser A,* **253,** 518 (1956).
(13) The rate constant for the forward hydrolysis reaction corresponds to that of the first-order path (k_1) given by Gray[14] for several substitution reactions of Pt(dien)I^+.
(14) H. B. Gray, *J. Amer. Chem. Soc.*, **84,** 1548 (1962).
(15) H. B. Gray and R. J. Olcott, *Inorg. Chem.*, **1,** 481 (1962).
(16) J. Joussot-Dubien and J. Houdard Pereyre, *Bull. Soc. Chim. Fr.*, **8,** 2619 (1969).
(17) The photolysis product of pyridine (glutaconic aldehyde) has about the same basic dissociation constant as pyridine itself. Thus, no appreciable pH change accompanied the photolysis of an aqueous solution of pyridine. For this reason, the pH variations observed in the photolysis of Pt(dien)py^{2+} were free of any effect from secondary photolysis of pyridine.
(18) The quantum yields were calculated in the spectrophotometric method by using the extinction coefficients of the following Pt-containing products: pH 4, Pt(dien)H_2O^{2+}; pH 5.8, Pt(dien)H_2O^{2+} and Pt(dien)OH^+ in a 2/1 ratio; pH 10, Pt(dien)OH^+. It should be noted, however, that the extinction coefficients of all these complexes in the 220–240-nm range are almost negligible (less than 5%) with respect to the absorbancy of Pt(dien)py^{2+}.
(19) In the spectrophotometric method, the extinction coefficients of the following Pt-containing products were used: pH 4 and 5.8, Pt(dien)Br^+; pH 10, Pt(dien)OH^+. Here again the choice of these product spectra only has a 5% effect on the final quantum yield values.
(20) W. H. Baddley, F. Basolo, H. B. Gray, C. Nölting, and A. J. Poë, *Inorg. Chem.*, **2,** 921 (1963).
(21) C. Bartocci and F. Scandola, *Chem. Commun.*, 531 (1970).
(22) E. König and H. L. Schläfer, *Z. Phys. Chem.*, **26,** 371 (1960).
(23) It should be stressed that result ii cannot be an experimental artifact caused by the competition between Br^- and the released I^- on a primary Pt(dien)H_2O^{2+} intermediate. In fact this trivial explanation is inconsistent with the following experimental results: (a) strictly zero-order plots of different slope were obtained at different Br^- concentrations (see Results), while a set of curves with a common initial slope and different curvatures would be required by this explanation; (b) the concentration of released I^- (thermal + photochemical) was always less than 1.6×10^{-4} *M* (measured concentration at the end of the photochemical run with the highest Br^- concentration), while a "mean" I^- concentration of about 2×10^{-3} *M* should be required to explain the observed differences in photosubstitution rates following this mechanism, in view of the published relative reactivity of Br^- and I^- toward Pt(dien)H_2O^{2+}.[15]
(24) It should be noted that the interpretation of results ii and iii in this case is free of some quantitative complications which were present in the previous study of Pt(dien)Br^+.[1] In that study, it proved impossible to carry out the irradiation of Pt(dien)Br^+ in the absence of external Br^-. In principle, therefore, the presence of free leaving ligand in the irradiated solutions could have been taken as a reason for results such as ii and iii. In the case of Pt(dien)Br^+, this possibility was discarded on quantitative grounds. In the present case, no appreciable concentration of I^- was initially present in the irradiated solutions, and the qualitative evidence for these effects is quite clear-cut.
(25) J. P. Lorand in "Inorganic Reaction Mechanism," J. O. Edwards, Ed., Interscience, New York, N.Y., 1972, p 207.
(26) F. Scandola, C. Bartocci, and M. A. Scandola, *J. Amer. Chem. Soc.*, **95,** 7899 (1973).
(27) J. F. Endicott, private communication.

Photophysical Effects of Stereoisomers in Thiacarbocyanine Dyes

J. Thomas Knudtson and Edward M. Eyring*

Department of Chemistry, University of Utah, Salt Lake City, Utah 84112 *(Received June 10, 1974)*

Publication costs assisted by the Air Force Office of Scientific Research, Chemical Directorate, and by the Office of Naval Research

Fluorescence, exitation, and transient absorptions were used to characterize two stereoisomers in 3,3′-dimethylthiacarbocyanine and 3,3′-dimethyl-9-ethylthiacarbocyanine. The trans isomer fluoresces at room temperature with increasing intensity at lower temperatures. The cis isomer fluoresces in alcoholic glasses at −196°. Substitution of an ethyl group for a proton in the 9 position greatly increases the cis concentration but has little effect on the absorption spectra of the stereoisomers. The rate of ground electronic state cis–trans isomerization was measured as a function of temperature, and a new fluorescence peak was observed at high laser powers that is attributed to excimer formation.

Introduction

Cyanine dyes have proven to be very successful long wavelength photographic sensitizers in silver halide emulsions. They have also served to mode-lock several lasers (ruby, neodymium, and dye lasers). As mode lockers these dyes are responsible for the very short laser pulses, in the picosecond range, which extend the time scale of chemical investigation down close to the period of a molecular vibration. Consequently, the photophysical properties of these dyes are of interest in several areas of investigation.

We have used several techniques, laser-induced fluorescence, laser-induced transient absorption, and the more common quantum yield measurements and absorption spectroscopy, to investigate photoinduced cis–trans isomerization of the stereoisomers in two cyanine dyes: 3,3′-dimethylthiacarbocyanine iodide (dye I) and 3,3′-dimethyl-9-ethylthiacarbocyanine iodide (dye II). Rate measurements of the ground electronic state isomerization were made as a function of temperature, and Arrhenius parameters were determined. The fluorescence properties of these dyes revealed that one stereoisomer is responsible for the room temperature fluorescence. Also the fluorescence of these dye solutions displays a strong temperature dependence. At high laser powers (11×10^6 W cm^2) used for excitation a new fluorescence peak appears which may result from excimer formation in alcoholic solvents.

West and coworkers have done extensive work with thiacarbocyanines. These dyes dimerize readily in aqueous solution (but not in alcoholic solvents) and the extent and nature of the dimerization has been reported.[1] The existence of two stereoisomers in equilibrium in the 9-ethyl dye (dye II) and their identification by low-temperature absorption spectroscopy in alcoholic solvents was subsequently studied.[2] Photoinduced cis–trans isomerization was first reported by McCartin[3] and used by West[2] to help characterize the stereoisomers. The low-temperature absorption, fluorescence, and phosphorescence spectra of several thiacarbocyanines which were forced by additional cyclic groups to have only one stereo configuration were reported.[4,5] Sufficiently high concentrations were used to investigate the dimers and higher aggregates of these dyes. It is interesting to note that fluorescence from cyanine dimers has not been observed.

Cooper has used the external heavy atom effect to investigate the influence of the triplet state in the photoisomerism of thiacarbocyanines.[6] The reported increase in trans to cis photoisomerization rate is indicative of triplet state involvement. Several reports of delayed fluorescence in cyanine dyes have been shown to be due to impurities.[7]

The nature of the stereoisomers revealed by West is best shown in Figure 1, the low-temperature (alcoholic solvent) absorption spectra of dyes I and II. Dye I has a typical cyanine spectrum with its peak at 560 nm and a shoulder on the short wavelength side attributable to a second vibronic transition (~1200 cm^{-1} from the 0–0 transition). Dye II however shows the effect of the 9-ethyl substitution. The large peak at 542 nm (Figure 1) is the result of a new stereoisomer which exists in equilibrium with the first stereoisomer, observable as a shoulder at 560 nm. Thus, dye II has two observable stereoisomers in solution in equilibrium.

The stereoisomer which predominates in dye I and has its absorption peak at 558 nm is the all trans configuration shown in Figure 2a. Substitution of the ethyl group in the 9 position (dye II) increases steric repulsions, probably between the ethyl group and the sulfur atoms in the heterocycle and allows another stereoisomer to compete energetically with the all trans isomer. This is probably the mono-cis isomer shown in Figure 2b with dye II (absorption peak at 542 nm). These assignments have been made by West and coworkers.[2]

Experimental Section

The laser apparatus used for the fluorescence and transient absorption experiments is shown in Figure 3. The Nd glass laser produces a 1.2 J pulse at 1.06 μm. Using a 2×10^{-8} sec pulse width and a 0.78-cm aperture, the calculated power density is 140×10^6 W/cm^2. Frequency doubling with KD*P is about 8% efficient resulting in a power density of 11×10^6 W/cm^2 at 530 nm.

The monochromator (¼-m Bausch and Lomb) and photomultiplier (Dumont KM2433) response were corrected to read photons/second using a tungsten–iodine lamp (General Electric 6.6A|T4|1C1) and lamp data from ref 8. The spectral resolution in all experiments unless otherwise noted was 1.65 nm.

Fluorescence spectra were taken point by point for each wavelength, typically every 5 nm. These data were multiplied by correction factors at each wavelength obtained for the monochromator–photomultiplier combination as de-

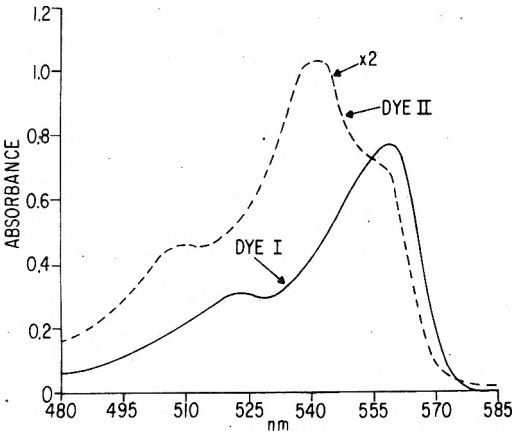

Figure 1. Low-temperature absorption spectra: 4×10^{-6} *M* alcoholic solvent.

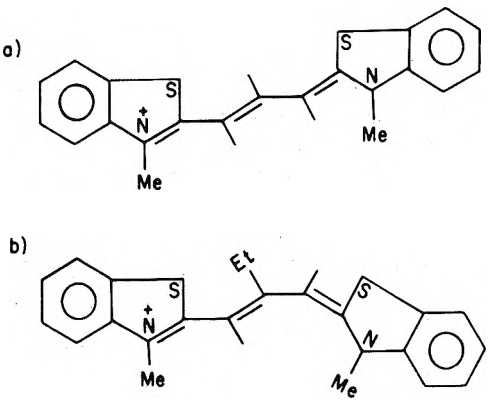

Figure 2. (a) 3,3′-Dimethylthiacarbocyanine (dye I) in the all-trans stereo configuration. (b) 3,3′-Dimethyl-9-ethylthiacarbocyanine (dye II) in mono-cis stereo configuration.

scribed above. For absolute quantum yields the laser power was reduced by high power neutral density filters to prevent saturation of the absorption.

To obtain transient absorption spectra a tungsten–iodine lamp was placed opposite the monochromator slit (Figure 3). The image of the lamp filament was focused in the 1-cm sample cell. The transient absorption spectra were also taken point by point at each wavelength.

The laser power dependence of fluorescence and transient absorption were determined to avoid saturation effects and to detect possible two photon processes. The laser power was variably attenuated with a pair of Polaroid film polarizers. The first polarizer could be rotated and the second was fixed. This maintained the polarization of the laser pulse independently of the power. The attenuated power was monitored by an ITT F4000 biplanar photodiode.

For kinetic measurements the photomultiplier was loaded to 10^4 Ω. All measurements were made dc coupled for good low-frequency response.

Low-temperature studies were done in a Pyrex dewar which was cooled by cold gaseous nitrogen. Temperature was measured by a copper–constantan thermocouple placed in the dye solution, in the optical path. The alcoholic glasses used in these experiments were broken by the first laser pulses at liquid nitrogen temperatures.

All absorption spectra were taken with a Cary 17 spectrometer.

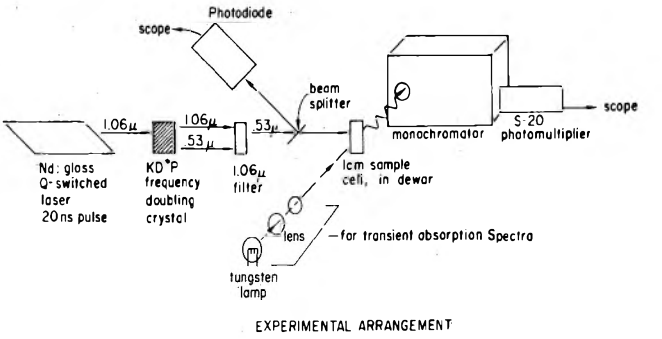

Figure 3. Laser fluorescence and transient absorption experimental apparatus.

Results

Absorption. The two particular cyanine dyes, dye I and dye II, were chosen for this study because their absorption spectra overlap the 530-nm frequency doubled output of the Nd glass laser used in these experiments. Initially it was thought that the laser would excite only one of the two stereoisomers in equilibrium in solution. However, the absorption spectrum of a single isomer is skewed to the short wavelength side and the absorption of a mixture of the two stereoisomers at 530 nm has contributions from both species.

Both dyes (purchased from K and K Laboratories, Inc.) were examined by thin layer chromatography and found free of contamination. The dye solutions decompose at differing rates with half-lives ranging from many months to a few hours. The stability of the solutions decreased in the order alcoholic > H_2O > EPA > *p*-dioxane (alcoholic = ethanol:methanol, 1:1, EPA = ethanol:diethyl ether:isopentane 2:5:5). To avoid interference from the products of decomposition fresh solutions were used throughout these experiments unless otherwise noted. All solvents used were spectroquality.

The results of a room temperature absorption study of solvent effects on these two dyes are shown in Table I. The *p*-dioxane solutions were made by diluting 1 ml of alcoholic 10^{-4} *M* solution to 10^{-6} *M* with *p*-dioxane. The spectral band width reported here, $\Delta\nu_{0.67}$, increases for both dyes with increasing dielectric constant of the solvent:[9] ϵ_{H_2O} = 80.4, $\epsilon_{(MeOH)}$ = 32.6, $\epsilon_{(EtOH)}$ = 24.3, $\epsilon_{(p\text{-dioxane})}$ = 2.2. Similarly, the wavelength of the absorption maximum shifts to shorter wavelengths with increasing dielectric constant of the solvent. It appears from these results that the equilibrium distribution of stereoisomers depends on the nature of the solvent. The isomer absorbing at the longer wavelength (peak at ~560 nm in both dyes), which has been shown to be the all trans form,[2] is favored by the lower dielectric constant solvent. Thus, in going from *p*-dioxane, to alcoholic, to aqueous solutions the equilibrium concentration of the mono-cis isomer is increased relative to the all trans and the absorption maxima and spectral band widths are shifted and increased accordingly. Similar observations have been made by Cooper.[6]

The mono-cis stereoisomer is a more twisted structure, and the electrically charged atoms in the heterocyclic nucleus are brought closer together than in the all trans configuration (Figure 1). The high dielectric constants of alcoholic and aqueous solvents diminish the electrostatic repulsions in the cis isomer and allow it to be energetically competitive with the trans.

It should be noted that solvent dielectric constants in-

TABLE I: Absorption Characteristics as a Function of Solvent

Dye[a]	Solvent: Dioxane $\Delta\nu_{0.67}$,[b] cm^{-1}	Dioxane Absorption max, nm	Alcoholic[c] $\Delta\nu_{0.67}$,[b] cm^{-1}	Alcoholic Absorption max, nm	Aqueous $\Delta\nu_{0.67}$,[b] cm^{-1}	Aqueous Absorption max, nm
3,3′-Dimethyl-thiacarbocyanine	735 ± 40	567	820 ± 40	556	1120 ± 38	551
3,3′-Dimethyl-9-ethyl-thiacarbocyanine	695 ± 34	564	1200 ± 39	542	1350 ± 39	536

[a] 10^{-6} *M* concentration. [b] Full-width at 0.67 maximum; estimated uncertainty in reading ±0.4 nm. [c] 1:1 ethanol: methanol.

crease rapidly with decreasing temperature. (For example, for ethanol ϵ = 24.3 at 25°, ϵ = 41.0 at −60°.[9]) Thus, the cis–trans equilibrium constant may not obey the expected $1/T$ temperature dependence.

Fluorescence. The fluorescence spectra of the dyes were taken under many conditions of concentration, solvent, and temperature in an attempt to observe the effect of differing isomer concentration on the spectra and fluorescence quantum yield.

The spectra obtained with the laser fluorimeter, which permits 2 nm or better spectral resolution with weakly fluorescing materials, are shown in Figure 4. Both dyes were in alcoholic solvent. The most interesting feature is their almost identical shape in spite of the significant differences in absorption spectra (Figure 2 and Table I).

Fluorescence quantum yields were determined only in the alcoholic solvents. The dioxane solutions decompose too rapidly for accurate measurements, and dimer formation in aqueous solutions interferes with the measurement of the optical density at 530 nm.

The integrated fluorescence spectra (using laser excitation) were compared to that of a known compound, Rhodamine 6G, to determine the fluorescence quantum yields, ϕ_F, using the method of Parker.[10] Rhodamine 6G fluoresces over almost the same frequency range as the two cyanine dyes. The fluorescence quantum yields relative to Rhodamine 6G were $0.07\phi_F^{R6G}$ for dye I and $0.002\phi_F^{R6G}$ for dye II. Dye II has an excitation wavelength dependent ϕ_F as will be discussed below. The absolute fluorescence quantum yield for rhodamine has been reported as 0.97[11] and 1.0.[12] The ϕ_F value for dye I is in reasonably good agreement with the result reported for 3,3′-diethylthiacarbocyanine, ϕ_F = 0.048.[13]

Care was taken to prevent errors due to the effects of saturation by the high power laser. Dilute solutions (dye I = 2×10^{-7} *M*, dye II = 1×10^{-6} *M*, and Rhodamine 6G = 2×10^{-7} *M*) were used to eliminate errors due to self-absorption.

Excitation spectra were taken for both dyes in alcoholic solution using a conventional (Aminco) spectrofluorimeter with a xenon lamp and S-20 photomultiplier. Since the lamp intensity varies less than 10% over the 500–575-nm range no correction for lamp intensity was made. The excitation and absorption spectra of dye I are nearly identical as expected (Figure 5a). However, the excitation spectrum of dye II does not parallel its absorption spectrum but is shifted to longer wavelengths (Figure 5b). The two excitation spectra are in fact nearly identical with one another and with the absorption spectrum of dye I.

The above data should be considered in light of the two stereoisomers known to exist in solution. Dye I consists almost entirely of the trans isomer based upon its low-temperature absorption spectrum and its absorption band

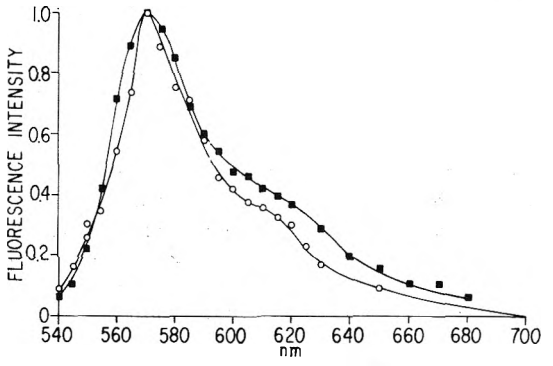

Figure 4. Fluorescence spectra, 22°, 1×10^{-6} *M* alcoholic solvent, normalized to maximum = 1.0: dye I, O; dye II, □.

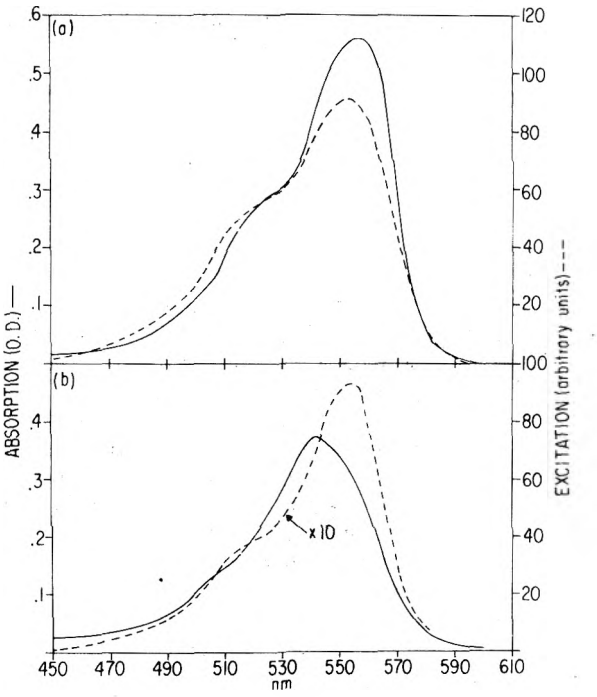

Figure 5. Excitation (- - -) and absorption spectra, alcoholic solvent, 4×10^{-6} *M*: (a) dye I; (b) dye II.

width (Table I). Therefore the excitation spectrum of dye I can be considered to be the excitation spectrum of the trans stereoisomer, and indeed its excitation and absorption spectra are identical.

Dye II, however, is made up of nearly equal optical amounts of two stereoisomers based on its low-temperature absorption spectrum (Figure 2) and its absorption band width (Table I). Its fluorescence and excitation spectra are identical with that of dye I which is the all trans isomer.

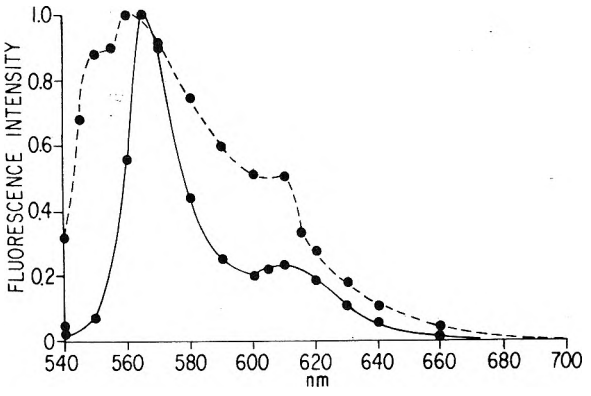

Figure 6. Fluorescence spectra, −196°, alcoholic solvent, normalized to maximum = 1.0: (——) dye I (2×10^{-7} *M*); (- - - -) dye II (1×10^{-6} *M*).

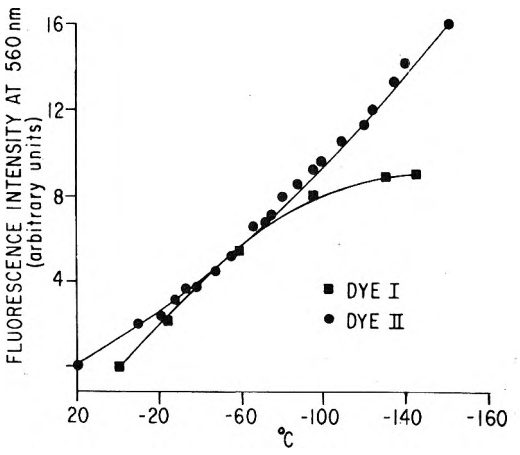

Figure 7. Fluorescence intensity as a function of temperature, alcoholic solvent, 1×10^{-6} *M*.

We conclude that the cis isomer in dye II does not have any observable fluorescence and the trans isomers in dyes I and II have identical excitation and fluorescence spectra.

It is important to note that alcoholic solutions of dye II should display wavelength dependent quantum yields based on the above discussion. Excitation of short wavelengths will produce lower quantum yields than excitation at longer wavelengths. Also the quantum yields for both dyes should appear to be solvent dependent based on the absorption data in Table I. The absorption spectra of the two isomers are almost completely overlapping preventing absolute ϕ_F measurements for individual stereoisomers in dye II.

The mono-cis isomer has a very rapid nonradiative decay mechanism that competes effectively with the radiative decay. Suspecting that this process might be a cis → trans isomerization in the excited state, fluorescence spectra were taken in an alcoholic glass matrix at −196°. The viscosity of the matrix is very large (6×10^{12} P at −158°)[14] and should make isomerization very unlikely. Without the possibility of isomerization the cis isomer should fluoresce.

The fluorescence spectra of dyes I and II, taken in the glass matrix, are shown in Figure 6. It is immediately obvious that the spectrum of dye II is much broader than that of dye I. Closer inspection reveals a shoulder at 550 nm and a peak at 565 nm that represent fluorescence from the two different stereoisomers. The shoulder and the peak are separated by 500 cm^{-1} in the fluorescence spectrum which is in good agreement with the separation observed in the low-temperature absorption spectrum of 550 cm^{-1}.

The cis stereoisomer does fluoresce in a low-temperature high-viscosity matrix. In order to separate the effects of temperature and viscosity a room-temperature high-viscosity matrix was desired. Attempts to observe fluorescence from a poly(methyl)methacrylate matrix failed because the dye inhibited polymerization or was destroyed in the process of polymerization. Fluorescence spectra taken down to about −100° show no cis fluorescence.

It was noted that the low-temperature fluorescence was much more intense than at room temperature. Figure 7 shows the increase in fluorescence intensity for both dyes in alcoholic solvent with decreasing temperature. Below −150° dimerization becomes important and affects the optical density at 530 nm (the laser wavelength) making interpretation unreliable.

The fluorescence intensities in Figure 7 are normalized to that of room temperature for dye II and 0° for dye I. The substantial increase in intensity is indicative of a temperature-dependent nonradiative process that competes with the fluorescence. The radiative lifetimes of these dyes were calculated, using the integrated absorption spectra, to be dye I = 3.0×10^{-9} sec, dye II = 3.3×10^{-9} sec.

An unexpected fluorescence feature appeared at high laser power densities first in the fluoresence spectrum of dye II in alcoholic solvents. The 10^{-6} *M* spectrum was, as expected, a mirror image of the absorption spectrum. However, at 10^{-5} *M* a small peak appeared at about 610 nm and the 10^{-4} *M* spectrum was completely dominated by this red-shifted peak (see Figure 8). Some self-absorption in the 10^{-4} *M* sample accentuates this effect. Dye I displayed the same behavior, but the red-shifted peak (centered at about 625 nm) appeared at much lower dye concentrations. It is quite visible at 2×10^{-7} *M* and is equal to the normal dye fluorescence in intensity at 10^{-6} *M* (see Figure 9).

The new peak does not appear in fluorescence spectra taken with a conventional (Aminco) apparatus. If the laser power is reduced enough, the normal mirror image spectrum is reproduced. Therefore, dependence of the fluorescence intensity on laser power was examined.

Figure 10 shows a log–log plot of the fluorescence intensity of dye I as a function of laser power over a range of about 10^3-fold. The laser power at maximum intensity is about 11 MW/cm^2. This experiment was done with three emission wavelengths none of which can be said to be pure dye I fluorescence or pure red peak emission. However, they were chosen to emphasize one of the two. At 700 nm there is no fluorescence at low laser power levels. Hence, this wavelength should represent the power dependence of the red-shifted peak reasonably well. The two other wavelengths, at 580 (dye fluorescence maximum) and 625 nm (red peak fluorscence maximum), probably represent a weighted mixture of both emissions.

Clearly, Figure 10 excludes any two-photon processes which would have a slope of two on a log–log plot. The red peak has about the same power dependence in the low power region (slope = 1) as the fluorescence at 580 and 700 nm, corresponding to the expected one-photon process. However, at higher power levels the dye transition is saturated and the fluorescence increases with a slope of about 0.3 over the range of laser power measured. The fluorescence at 625 nm saturates at the same power but increases with a slope of about 0.5. Therefore, at high laser powers the red peak gains in intensity compared to the normal dye fluorescence.

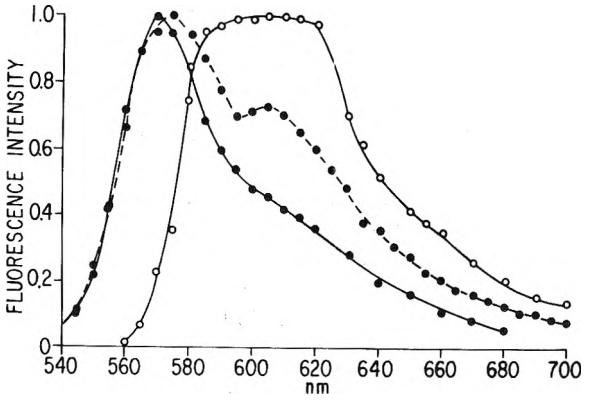

Figure 8. Dye II fluorescence spectrum at high laser powers, normalized to maximum = 1.0: (——) 1×10^{-6} *M*; (- - -) 1×10^{-5} *M*; (- O -) 1×10^{-4} *M*.

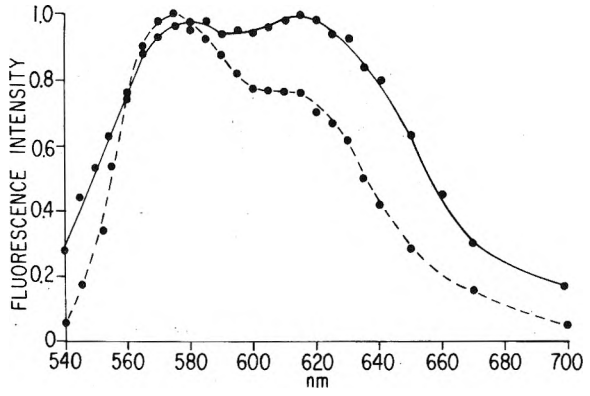

Figure 9. Dye I fluorescence spectrum at high laser power normalized to maximum = 1.0: (——) 1×10^{-6} *M*; (- - -) 2×10^{-7} *M*.

A number of possible explanations have been considered and tested. The possibility of a solvent exciplex was eliminated by fluorescence measurements in two other solvents, *p*-dioxane ≫ alcoholic > H_2O. The same peak appears in all three solvents but with differing intensities. The order of red-shifted peak intensity for both dyes was *p*-dioxane ≫ H_2O at 10^{-6} *M*. Another possibility considered was a dye–iodide complex. Addition of NaI (to yield 10^{-4} *M*) caused no change in the fluorescence spectrum. Dye I was changed to the chloride form using a 10^6-fold excess of chloride anion exchange resin, and the high power laser fluorescence spectrum was virtually unchanged.

The possibility of emission related to dye decomposition was tested repeatedly. Fresh dye solutions were made and their fluorescence spectra determined. Then the solutions were left in room light long enough for ⅓ to ¼ of the dye to decompose. In other experiments a portion of a solution that had completely decomposed was added to the fresh sample. The fluorescence spectrum remained unchanged by any of these effects.

The phosphorescence spectra were observed from an alcoholic glass (−196°) and like the low-temperature fluorescence, the spectrum of dye II was much broader than that of dye I (full-width at half-height; dye I = 800 cm^{-1}, dye II = 1400 cm^{-1}). The phosphorescence maxima occurred at 730 (dye I)[15] and 690 nm (dye II) in agreement with previous reports. The emission decay obeyed first-order kinetics and the measured rate constants were 3.2×10^1 (dye I) and 4.5×10^1 sec^{-1} (dye II).

Transient Absorption. The change in absorption of a dye solution following a laser pulse is typically a decrease in the optical density (bleaching) at and around the wavelength of the laser light.[16] Subsequently, the optical density should return to its value prior to the laser pulse, in the time required for the excited dye molecules to relax. Typically, this time would be several nanoseconds or less.

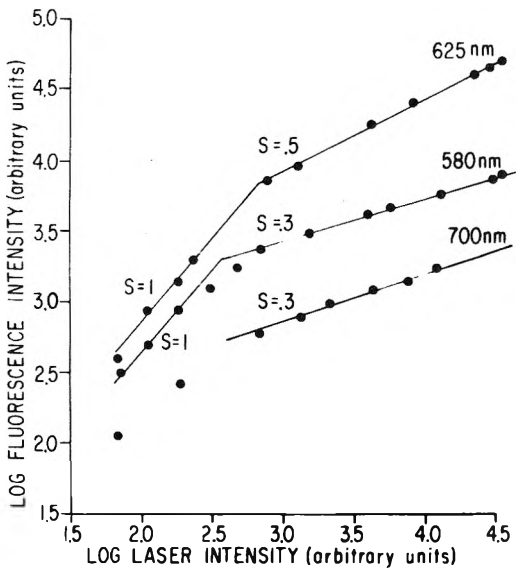

Figure 10. Fluorescence intensity as a function of laser power at 625, 580, and 780 nm (dye I, 1×10^{-6} *M*). The data have been displaced vertically for clearer presentation (s = slope).

The absorption changes following a laser pulse in dyes I and II were observable on a very much longer time scale. This is a result of the light-induced cis–trans isomerization reported by West[2] and Cooper.[6]

At any wavelength λ, the absorbance before the laser pulse, *A*, has contributions from both stereoisomers of concentration C_1 and C_2 with extinction coefficients ϵ_1 and ϵ_2.

$$A = C_1\epsilon_1 + C_2\epsilon_2 \quad (1)$$

After the laser pulse the concentration of one stereoisomer has been increased by ΔC and the other decreased by ΔC.

$$A' = (C_1 + \Delta C)\epsilon_1 + (C_2 - \Delta C)\epsilon_2 \quad (2)$$

The change in absorbance is ΔA.

$$\Delta A = \Delta C(\epsilon_1 - \epsilon_2)$$

The transient absorption spectrum, ΔA, as a function of wavelength is the difference between absorption spectra of the two stereoisomers.

The changes in absorption of the dye solutions were observed with a lamp–monochromator–photomultiplier combination arranged perpendicular to the optical path of the laser (Figure 3). At each wavelength the intensity of light transmitted by the sample, *I*, and the change in intensity of transmitted light, ΔI, were recorded following the laser pulse. It should be noted that changes in transmittance decay on a very slow time scale, microseconds at room temperature, and are consequently easy to observe.

The change in absorbance ΔA is related to *I* and ΔI by

$$\Delta A = -\log\left[1 + (\Delta I/I)\right] \quad (3)$$

The plot of ΔA *vs.* wavelength is shown for both dyes, each at two temperatures, in Figure 11a,b.

The negative direction on the ΔA axis corresponds to an increase in optical transmission and consequently a decrease in concentration of the absorbing species. Taking

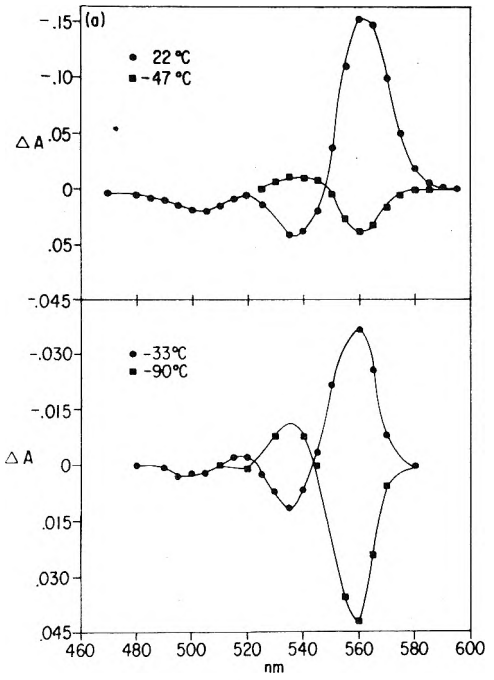

Figure 11. Transient absorption spectra of (a) dye I and (b) dye II.

the transient absorption of dye I at 22° and dye II at −33°, we observe that they are quite similar. There is a large decrease in the stereoisomer absorbing at 560 nm (trans) and an increase in stereoisomer absorbing at 535 nm (cis). This is an unusual situation in which there is an increase in absorption at the laser wavelength (530 nm) following laser excitation. When overlayed the two transient absorption spectra are almost identical except that the 560-nm peak is about 20% larger in dye I. The absolute amplitudes of the transient absorption spectra are a function of temperature, but their relative features change only slightly with temperature.

The most interesting feature of the transient absorption is that it changes sign as the sample temperature is lowered. That is, the amplitude of the transient absorption signal decreases until at −52 ± 4° for dye I and −62 ± 4° for dye II it is zero. Then as the temperature is decreased further, the signal reappears but with opposite sign. What was a decrease in optical density becomes an increase in optical density and *vice versa*. The transient absorption spectra above and below the inversion temperature are identical but opposite in the sign of ΔA.

The inversion temperature was the same when the solvent was changed to EPA. Although both solvents are quite similar in many respects, their macroscopic viscosities as a function of temperature are quite different.[14] Also the inversion occurs at much higher temperatures than any reported phase transitions in these solvents.

The dependence of the transient absorption amplitude on the laser power was examined. In all cases the amplitude increased linearly with laser power.

The rate of return to equilibrium was measured as a function of time, most often using the transient absorption change at 560 nm. The rate was found to be independent of concentration and laser power. The changes in isomer concentration were kept small so that changes in transmission followed linearly the changes in concentration. Semilog plots of change in transmission *vs.* time gave straight lines.

The kinetic scheme for the relaxation process following the perturbation of the laser pulse is simply

$$A \underset{k_2}{\overset{k_1}{\rightleftharpoons}} B$$

where A and B are the two isomers. The laser pulse creates a nonequilibrium increase in concentration of A or B (depending on the temperature of the sample) and the system relaxes back at the rate[17] $k_1 + k_2$.

The temperature dependence of $(k_1 + k_2)$ can be used to separate the activation energies of the two rate processes, if they are significantly different.

$$k_1 + k_2 = A_1 \exp(-E_1/RT) + A_2 \exp(-E_2/RT)$$

The quantity ln $(k_1 + k_2)$ *vs.* $1/T$ would produce two straight lines in the case of $E_1 \gg E_2$. At low temperatures the smaller activation energy, E_2, can be determined because it dominates the rate process. Knowing E_2 and A_2, the kinetic data at higher temperatures can be used to determine A_1 and E_1.

At first glance, Figure 12a,b, which is a plot ln $(k_1 + k_2)$ *vs.* $1/T$, shows two straight lines which could represent the activation energies of the two processes. However, the data in the low-temperature range result in an improbably low preexponential factor of about 10^4. It is much more likely that another mechanism is coming into play at these low temperatures. Low-temperature data are definitely not an artifact of the experiment, and a similar result has been observed by Dorr[18] in alcoholic solvents.

The rate data were fitted to the Arrhenius equation by a least-squares method. Subtraction of the extrapolated low-temperature rates makes no substantial change in the Arrhenius parameters. The rate data are summarized in Table II.

Discussion

The results of absorption data for both dyes in three solvents show increasing cis stereoisomer concentration with increasing solvent dielectric constant. Dye II has approximately equal optical amounts of each isomer in alcoholic solvent as seen in the low-temperature absorption spectrum. Dye I under the same conditions contains only the trans isomer in observable quantity.

The fluorescence, fluorescence excitation, and transient absorption spectra demonstrate that the stereoisomers in dye I have the same absorption and fluorescence (trans isomer only) spectra as those in dye II. The optical similarity of the stereoisomers in dyes I and II is somewhat surprising. The substitution of the 9-ethyl group in dye II is thought to twist the conjugated π electron system out of planarity due to steric repulsions. This would be expected to affect the absorption spectrum of the trans isomer in dye II. All the experimental evidence strongly supports the conclusion that the trans isomers in dyes I and II are optically identical.

The cis isomer in alcoholic solution of dye II does not have observable fluorescence at room temperature. At −196° in a high viscosity glass matrix the cis isomer does have readily observable fluorescence. There is no sign of cis fluorescence except at temperatures close to −196°.

A very fast nonradiative relaxation mechanism must be responsible for the lack of cis fluorescence. This mechanism has no observable temperature dependence down to −100°, but is effectively slowed in the temperature range corresponding to high solvent viscosity.[14]

The laser-induced photoisomerism was used to measure

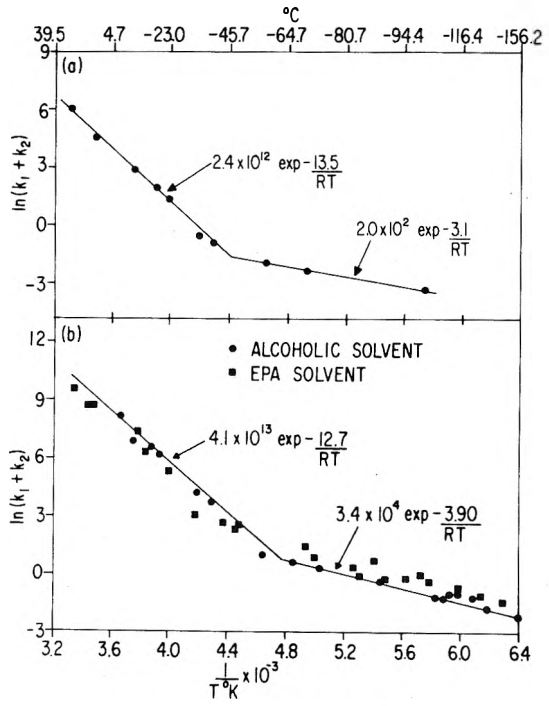

Figure 12. Rate of ground electronic state isomerization *vs.* $1/T$ for (a) dye I and (b) dye II.

TABLE II: Arrhenius Equations for the Rate of Ground-State Isomerization

	High-temp range	Low-temp range
Dye I, alcoholic solvent	$k = 2.4 \times 10^{12} \times \exp(-13.5/RT)$	$k = 2.0 \times 10^{2} \times \exp(-3.1/RT)$
Dye II, alcoholic solvent	$k = 4.1 \times 10^{13} \times \exp(-12.7/RT)$	$k = 3.4 \times 10^{4} \times \exp(-3.90/RT)$
Dye II, EPA solvent	$k = 1.3 \times 10^{13} \times \exp(-12.3/RT)$	$k = 4.4 \times 10^{4} \times \exp(-3.81/RT)$

the rate of cis–trans isomerism in the ground state. The temperature dependence of these rates shows two regions of Arrhenius equation behavior and the Arrhenius parameters are given in Table II.

The bend in the ln k *vs.* $1/T$ plot (Figure 12) at low temperatures is relevant to experiments in which low temperatures have been used to stop the ground-state equilibration following photoisomerism.[6] Using the Arrhenius parameters determined not far from room temperature, a temperature of −120° would be expected to slow the ground-state isomerization rate to several hours. However, as can be seen in Figure 12 the observed equilibration took place in only a few seconds.

The inversion of the transient absorption results from excitation of both isomers by the laser pulse at 530 nm. Following the laser pulse, a net trans–cis (t → c) conversion results and at low temperatures a net cis to trans (c → t) dominates.

The quantity of trans converted to cis, [t → c], is the product of the number of trans molecules excited [t*], and the probability of isomerization, $\phi_{t\to c}$.

$$[t \rightarrow c] = [t^*]\phi_{t\to c}$$

$$[c \rightarrow t] = [c^*]\phi_{c\to t}$$

The transient absorption signal is proportional to the net conversion, [t → c] − [c → t], and at the inversion temperature these two quantities are equal.

The absorption spectra of the dyes in alcoholic solution show only a few per cent change at 530 nm over the 20 to −120° temperature range. Therefore, the temperature dependence of the transient absorption must lie in the probability of isomerization. The macroscopic viscosity does not affect the inversion temperature based upon experiments in alcoholic and EPA solvents. Quantitative rates of excited state isomerism were not possible with the present experimental methods since the spectra of the two isomers overlap completely.

Dye I in alcoholic solution has only a small quantity of cis stereoisomer, consequently, much more [trans*] is produced by the laser. Yet a net cis to trans conversion takes place below −52°. The probability of the trans to cis isomerization must therefore have a strong temperature dependence compared to the cis to trans. Cooper[6] has measured the temperature dependence of the photoisomerism rate for 3,3′-diethyl-9-methylthiacarbocyanine and based on these Arrhenius parameters the quantity $\phi_{t\to c}$ decreases by a factor of 300 going from 20 to −52°. The fluorescence intensity of both dyes increases with decreasing temperature (Figure 8). It may well be that the temperature-dependent process competing with fluorescence is the trans to cis isomerization.

Cooper has reported[6] an enhancement of the trans to cis photoisomerization rate by the heavy atom effect implicating the triplet state in the isomerism pathway. Addition of 2.5 M ethyl iodide to dye II alcoholic solution increased the amplitude of the trans to cis transient absorption signal by a factor of 2.3 in agreement with the results of Cooper. However, in the temperature region of net cis to trans conversion (−83°), the amplitude was essentially unaffected (reduced by 10%) in the presence of the heavy atom. Therefore, the cis to trans isomerism path does not appear to include the triplet state.

A thorough search was made for the origin of the red-shifted fluorescence peak seen at high laser powers (Figures 8 and 9). The following possibilities were experimentally excluded: impurities resulting from decomposition, exciplexes of I^- and solvent, and resonant Raman scattering (no second harmonic peak). The processes of ionization and recombination were considered, but single-photon ionization of the dye cation is not energetically reasonable. The power dependence of the fluorescence shows no evidence of any two-photon processes (Figure 10). The fluorescence at 560 nm (dye peak) and red-shifted peak (620 nm) decayed faster than the 5-nsec response time of the detection system (at room temperature).

The most interesting characteristic of the new fluorescence is the strong intensity dependence on the solvent dielectric constant (or polarity). The intensity of the red-shifted peak decreases in the order p-dioxane > alcoholic > H_2O. In alcoholic solvent the red-shifted fluorescence increases in intensity with decreasing temperature faster than the dye fluorescence. At −196°, a 10^{-6} M solution of dye II has approximately equal intensities of the two fluorescence components.

Initially it was thought that the fluorescence was due to a dimer which absorbed at the laser wavelength. Two facts exclude this possibility. First, dimer concentration increases dramatically in going from alcoholic to aqueous solvents. The new fluorescence intensity decreases dramati-

cally in going from alcoholic to aqueous solvents. Secondly, the alcoholic absorption spectrum of dye II shows no sign whatsoever of dimer formation in the 10^{-4} to 10^{-6} M range while the red-shifted peak increases rapidly in the same concentration range (Figure 8).

The possibility of excimer fluorescence from thiacarbocyanines has been predicted by West[2] and is a possible explanation, although not without its drawbacks. An excimer is essentially a dimer consisting of an excited and a ground-state molecule. The intermolecular potential is such that the excimer is stable only in the excited state and unstable when both members are in the ground state.

A quantitative theory exists which can be used to calculate the energy levels of a dimer or excimer.[19] The interaction of the two dipoles causes the first excited singlet to be split into two levels (Figure 13). The higher of the two is coupled to the ground state by a dipole-allowed transition while the lower one is not allowed. Dimer absorption is therefore on the short wavelength side of the monomer absorption.

The two split levels of the dimer or excimer excited state are sufficiently close together that there is rapid internal conversion from the upper to the lower. If the aggregate is to fluoresce it will therefore be from the lower level. This fluorescence will appear on the long wavelength side of the main dye absorption.

The ground electronic state of the dimer is lower in energy than the ground state of an isolated molecule due to the attractive intermolecular potential. Similarly for the excimer, the ground electronic state is higher in energy, due to the repulsive intermolecular potential for two dye molecules. The ground electronic state for both excimer and dimer are shown in Figure 13 to be isoenergetic with that of an isolated molecule. Because a dye pair is not stable at room temperature (in alcoholic solvent) but is stable (dimerizes) at low temperatures, the enthalpy of dimerization is probably small ($\sim kT$) compared to the energy of the electronic transitions.

The red-shifted fluorescence peak and dimer absorption are displaced symmetrically (by about 1650 cm^{-1}) on either side of the trans stereoisomer absorption peak. In the case of dye II, there are two monomer absorption peaks (cis and trans) to choose from and only the trans yields a symmetrical displacement for dimer absorption and excimer fluorescence. This suggests that the excimer fluorescence is a result of trans dye molecules. From Table I the concentration of trans isomer increases in the order p-dioxane > alcoholic > H_2O. This is also the order of increasing "excimer" fluorescence intensity.

However, the bimolecular self-diffusion time at the 10^{-4} to 10^{-6} M concentrations used is of the order of 10^{-3} to 10^{-4} sec. The lifetime of excited dye molecules is 10^{-9} sec at best. It seems very unlikely that excimers would have time to form at these concentrations. It becomes necessary to postulate like-charged ion pairing prior to the laser pulse to explain the existence of excimers. This has been suggested by some experimental work and by calculations.[20]

The concentration dependence of the monomer and excimer fluorescence is typically used to demonstrate the existence of an excimer.[12] The overlap of the two fluorescence peaks precludes this experiment. Cooper[21] has reported excimer fluorescence from several cyanine dyes in EPA solvent at −196° using a conventional fluorescence apparatus. The excimer fluorescence results from excitation at the dimer absorption wavelengths (508 nm for thiacarbocyanines). A dye concentration study was in agreement with expected excimer dependence.

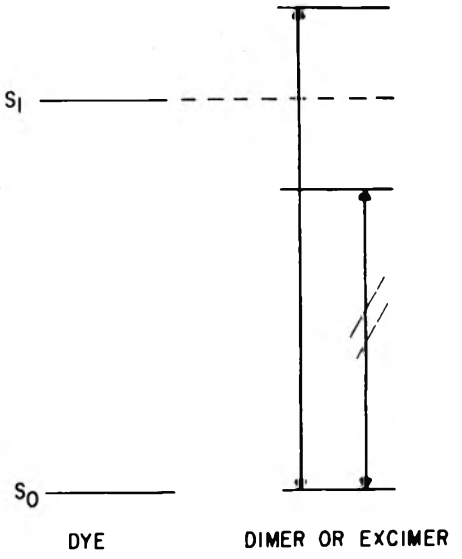

Figure 13. Effect of dimerization on excited singlet state, showing allowed and nonallowed transitions.

Dyes I and II show several interesting and potentially useful photophysical properties. An increase or decrease in absorption at 530 nm following the laser pulse can be determined by temperature control, due to either a net trans to cis or net cis to trans conversion. The lifetime of the excited state depends strongly on the temperature. Possibly the pulse widths of mode-locked lasers may be decreased by increasing the temperature of the cyanine mode-locking dye.

Acknowledgments. This work was sponsored by Grant No. AFOSR 75-2444 from the Directorate of Chemical Sciences, Air Force Office of Scientific Research, and by a contract from the Office of Naval Research. The laser was refurbished under a contract from the Aerospace Research Laboratories, Wright-Patterson Air Force Base. The technical assistance of W. Herrmann, Jr., and of S. L. Olsen as well as helpful discussions with Professors H. Eyring and J. Michl are also gratefully acknowledged.

References and Notes

(1) W. West and S. Pearce, *J. Phys. Chem.*, **69**, 1894 (1965).
(2) W. West, S. Pearce, and F. Brum, *J. Phys. Chem.*, **71**, 1316 (1967).
(3) P. J. McCartin, *J. Chem. Phys.*, **42**, 2980 (1965).
(4) W. West, S. P. Lovell, and W. Cooper, *Photogr. Sci. Eng.*, **14**, 52 (1970).
(5) W. Cooper, S. P. Lovell, and W. West, *Photogr. Sci. Eng.*, **14**, 184 (1970).
(6) W. Cooper and K. A. Rome, *J. Phys. Chem.*, **78**, 16 (1974).
(7) A. A. Muenter and W. Cooper, *Chem. Phys. Lett.*, **22**, 212 (1973).
(8) R. Stair, W. E. Schneider, and J. K. Jackson, *Appl. Opt.*, **2**, 1153 (1963).
(9) "Handbook of Chemistry and Physics," 52nd ed, Chemical Rubber Publishing Co., Cleveland, Ohio, 1971–1972, p E-43.
(10) C. A. Parker, "Photoluminescence of Solutions," Elsevier, New York, N.Y., 1968 p 262.
(11) I. B. Berlman, "Handbook of Fluorescence Spectra of Aromatic Molecules," Academic Press, New York, N.Y., 1971.
(12) J. B. Birks, "Photophysics of Aromatic Molecules," Wiley-Interscience, New York, N.Y., 1970.
(13) A. C. Craig and N. J. L. Roth, *J. Phys. Chem.*, **78**, 1154 (1974).
(14) H. Greenspan and E. Fischer, *J. Phys. Chem.*, **69**, 2466 (1965).
(15) H. Sauvenier, "Scientific Photography," Pergamon Press, New York, N.Y., 1962, p 558.
(16) K. R. Nagvi, D. K. Sharma, and G. J. Hoytink, *Chem. Phys. Lett.*, **22**, 5 (1973).
(17) S. L. Friess, E. S. Lewis, and A. Weissberger, "Investigation of Rates and Mechanisms of Reactions," Interscience, New York, N.Y., 1963, p 903.

(18) V. F. Dorr, S. Kotschy, and H. Kausen, *Ber. Bunsenges. Phys. Chem.*, **69**, 11 (1965).
(19) W. T. Simpson and D. L. Peterson, *J. Chem. Phys.*, **26**, 588 (1957).
(20) P. Hemmes, *J. Amer. Chem. Soc.*, **94**, 75 (1972).
(21) W. Cooper and N. B. Liebert, *Photogr. Sci. Eng.*, **16**, 25 (1972). (We thank a referee for providing us with this reference.)

Thermodynamics of Transfer of Molecules and Groups from Nonpolar to Aqueous Environments. I. Method. *n*-Butyric Acid at 25°

Kenneth J. Breslauer, Bruce Terrin, and Julian M. Sturtevant*

Department of Chemistry, Yale University, New Haven, Connecticut 06520 *(Received April 8, 1974)*

Publication costs assisted by the National Institutes of Health and the National Science Foundation

A method involving flow microcalorimetry is described for determination of the enthalpy of transfer of acidic or basic molecules from water-immiscible organic solvents to water. In this first paper the method is illustrated by application to the transfer of *n*-butyric acid from toluene to water at 25°. Distribution experiments were performed to permit evaluation of the free energy of transfer. Detailed consideration was given to the enthalpy and free-energy contributions arising from dimerization of the solute in the organic solvent. The thermodynamic parameters for the process involving monomeric solute n-C_3H_7COOH (toluene) = n-C_3H_7COOH (H_2O) are $\Delta G°_{298}$ = (−1220 ± 50) cal mol^{-1}, ΔH_{298} = (−3520 ± 150) cal mol^{-1}, and $\Delta S°_{298}$ = (−7.7 ± 0.5) cal deg^{-1} mol^{-1}.

Introduction

In recent years there have been many publications reporting thermochemical measurements on complex biochemical systems. It has generally proven to be impossible to present a satisfactory explanation of the thermochemical data in terms of currently recognized molecular interactions. There is, however, much evidence which indicates that important contributions to the energetics of many biochemical processes arise from the transfer of groups from nonpolar to aqueous environments, or the reverse, and considerable free-energy data for such transfers in model systems have been derived from distribution experiments, solubility determinations, or spectral observations. However, there are very few pertinent enthalpy values. This paper reports the development of a new calorimetric procedure to supply enthalpy and heat capacity data for the transfer of a wide variety of model compounds to water from water-immiscible organic solvents, and the application of the method to the transfer of *n*-butyric acid from toluene to water. It is hoped that data obtained by this method will eventually aid in the recognition of at least the hydrophobic contributions to the enthalpy changes in biochemical reactions.

Experimental Section

n-Butyric acid, obtained from Fisher Scientific Co., was redistilled. Titration with standard alkali gave a purity of 98.6%. It was assumed that the impurity was water. Toluene (Chromatoquality) was purchased from Matheson Coleman and Bell.

The calorimeter utilized was a flow microcalorimeter developed[1-3] in collaboration with Beckman Instruments, Palo Alto, Calif. The calorimeter was calibrated chemically using the neutralization of 0.001 *M* HCl by 0.002 *M* NaOH with both solutions flowing at the same rate. The heat of formation of water was taken to be −13.34 kcal mol^{-1} at 25°.[4] A typical set of 10 calibration experiments at 25° gave a mean value for the calibration constant of 1160 expressed in the arbitrary units of "integrator units" per millicalorie, with a standard error of the mean of 0.14%.

In the transfer experiments, one liquid delivered to the calorimeter was a solution of *n*-butyric acid in toluene and the other was 0.1 *N* NaOH. The organic liquid was delivered at a flow rate of 0.02 ml min^{-1} and the aqueous alkali at a flow rate 4 to 8 times higher. It was ascertained by varying the flow rates that extraction of the solute from the organic phase was complete within the residence time in the calorimeter. In order to minimize the heat of mixing the two solvents, which can be quite large despite the "immiscibility," the toluene and water were mutually presaturated by being vigorously shaken together in a separatory funnel and allowed to stand in contact at 25°. The remaining small heat of mixing of the presaturated solvents was determined and applied as a correction to all the transfer data. This correction also included the heat resulting from viscous flow in the calorimeter.

The quantity of interest is the enthalpy of transfer of the un-ionized monomeric solute from organic solvent to water. It was therefore necessary to determine the enthalpy of ionization of the solute in water and also to deduct the heat of formation of water. The ionization enthalpy of butyric acid was determined by mixing in the flow calorimeter a solution of sodium butyrate (pH 7) with excess HCl. Suitable corrections for dilution heats and heats of viscous flow were applied. It was assumed that the presence of toluene in the aqueous phase had no effect on the enthalpy of ionization.

It was also necessary to correct the overall enthalpy of

transfer for the existence of dimers in the organic phase and the enthalpy of their dissociation. The extent of dimerization was inferred from the variation of the apparent distribution coefficient (see below) with solute concentration, and the enthalpy of dissociation of dimers from heats of dilution of butyric acid solutions in toluene.

Details of the calculation of the transfer enthalpy will be given below. It may be remarked here that much the largest contribution to the observed transfer heat is the heat of formation of water, and that the accuracy of the final result is severely limited by the fact that it is obtained as the small difference between two relatively large numbers.

It may be asked why we have restricted our attention to systems involving immiscible solvents. The answer is that we were unable to find a suitable miscible solvent system, with one solvent being water, where the heats of solvent mixing were not so large as to introduce unacceptable uncertainties in the derived transfer enthalpies.

Free-energy changes for the transfer process were evaluated from distribution coefficients. A known quantity of the solute was distributed between known equal volumes of water and toluene by vigorous stirring over a period of 10 hr. After complete separation of the phases, an aliquot of the aqueous phase was removed and titrated using a micrometer syringe and a Radiometer pH meter to establish the end point. The concentration in the organic phase was calculated from material balance.

Distribution coefficients were determined in a room thermostatted at 25 ± 0.5°. The small heat of transfer makes it clear that small temperature variations have no significant effect; temperature variations of ±1° introduce errors of only ±0.01 kcal mol^{-1} in $\Delta G°$.

Throughout this paper the approximation is made of setting activities equal to molarities.

Results

The enthalpy of ionization of *n*-butyric acid was determined to be −0.64 and −1.08 kcal mol^{-1} at 25 and 40°, respectively. These values compare well with those reported by Christensen, *et al.*,[5] −0.64 and −1.12 kcal mol^{-1}, and give a value of −29 cal deg^{-1} mol^{-1} for the heat capacity of ionization.

If it is assumed that butyric acid forms dimers in toluene but is entirely in monomeric form at low concentrations in water, then the apparent distribution constant K_{app} is given by the expression[6]

$$K_{app} = \frac{c_s}{c_w(1-\alpha)} = K_1 + 2\frac{K_1^2}{K_d}[c_w(1-\alpha)] \quad (1)$$

In this expression, c_s and c_w are the total concentrations of solute in toluene and water, respectively, α is the degree of ionization of butyric acid in water, K_1 is the true distribution coefficient, and K_d is the dissociation constant of the butyric acid dimers in toluene. Values of α were calculated using an ionization constant of 1.55×10^{-5} *M*.

Figure 1 gives a plot of K_{app} *vs.* $c_w(1-\alpha)$. The least-squares straight line leads to the values $K_1 = 0.127 \pm 0.009$ and $K_d = (0.0036 \pm 0.0002)$ *M*. The corresponding changes in free energy are $\Delta G°_1 = (-1220 \pm 50)$ cal mol^{-1} and $\Delta G°_d = (-3330 \pm 50)$ cal mol^{-1}.

The enthalpy of dissociation of the butyric acid dimers in toluene was evaluated from dilution experiments run in the flow calorimeter. Since in the distribution experiments the organic phase was toluene saturated with water, the same solvent was used in the dilution experiments. It was assumed that the solubility of water in toluene is not significantly affected by the presence of as much as 0.13 *M* butyric acid, the highest concentration encountered in the distribution experiments. Four series of experiments with stock solutions ranging in concentration from 0.008 to 0.085 *M* were employed. In each series the stock solution and diluting solvent were mixed in eight or more different ratios, covering dilution ratios up to 1:24.

Calorimetric dilution data can in principle be used to obtain dissociation constants as well as heats of dilution.[7] However, if reliable equilibrium constants can be obtained from noncalorimetric experiments, it is usually preferable to use the calorimetric data only for the evaluation of heats of dilution.[8,9] In the present case, the distribution experiments lead to a more accurate value for K_d than can be obtained from the dilution data, and this value was used in evaluating the dimer dissociation heat.

If butyric acid at a total concentration of $c = c_m + 2c_d$, where c_m and c_d are respectively the concentrations of mo-

TABLE I: Enthalpy of Dissociation of Dimers of *n*-Butyric Acid in Toluene at 25°[a]

C_i, *M*	No. of dilution ratios	c_f, *M* Minimum	c_f, *M* Maximum	ΔH_d, kcal (mol dimer)$^{-1}$
0.0850	14	0.0036	0.068	6.04 ± 0.10
0.0584	9	0.0034	0.029	6.20 ± 0.12
0.0184	8	0.00079	0.0092	6.44 ± 0.16
0.00804	8	0.00034	0.0040	6.76 ± 0.08
			Weighted mean	6.31 ± 0.16

[a] See text for definitions of symbols. The uncertainty limits given for ΔH_d are standard errors of the mean values calculated using eq 2.

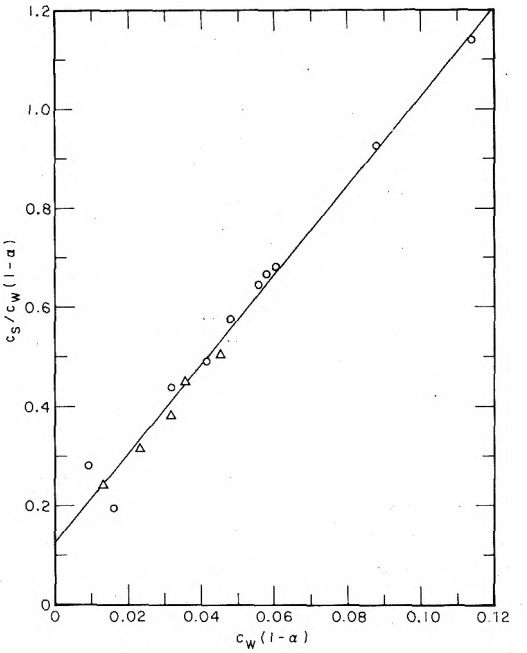

Figure 1. The distribution of *n*-butyric acid between toluene and water at 25°. The apparent distribution constant, $c_s/c_w(1-\alpha)$, is plotted against the concentration of un-ionized acid in the aqueous phase, $c_w(1-\alpha)$. c_s is the concentration of acid (monomers plus dimers) in the organic phase: O, series 1; Δ, series 2. The line was obtained by an unweighted least-squares calculation.

TABLE II: Enthalpy of Transfer of *n*-Butyric Acid from Toluene to Water at 25°[a]

Concn of acid in toluene, *M*	No. of determinations	ΔQ_{obsd}, kcal mol^{-1}	ΔQ_d, kcal mol^{-1}	ΔH_{trans}, kcal mol^{-1}
0.0638	7	−15.21 ± 0.06	2.67	−3.90 ± 0.11
0.0558	11	−15.36 ± 0.11	2.64	−4.02 ± 0.14
0.0393	12	−15.35 ± 0.10	2.55	−3.92 ± 0.13
0.0305	8	−14.85 ± 0.10	2.48	−3.35 ± 0.13
0.0178	47	−15.03 ± 0.07	2.30	−3.35 ± 0.11
0.00299	15	−15.78 ± 0.21	1.45	−3.25 ± 0.22
			Weighted mean	−3.52 ± 0.15

[a] See text for meaning of symbols.

nomeric and dimeric solute, is present in toluene, the fraction of the total solute present which is in monomeric form is given by

$$x = \frac{c_m}{c} = -\frac{a}{4} + \frac{1}{2}\left(\frac{a^2}{4} + 2a\right)^{1/2} \quad (2)$$

where $a = K_d/c$. If Δx is the change in x resulting from the dilution, the enthalpy of dissociation, expressed in kilocalories per mole of dimer, is obtained from the expressions $\Delta Q = \Delta q/c_i$, where Δq is the enthalpy change in kilocalories per liter of stock solution and c_i is the stock concentration, and $\Delta H_d = 2\Delta Q/\Delta x$. It is assumed that there is no significant volume change on mixing.

The results of the dilution experiments are given in Table I. The concentrations of the stock solutions are given in column 1, and the number of different dilution ratios used in column 2. In most cases several determinations were performed at each dilution ratio. The range of dilution ratios employed can be inferred from the final concentrations given in columns 3 and 4. The mean calculated enthalpies of dissociation are listed in column 5 together with the standard errors of the mean.

The values for ΔH_d in Table I appear to increase significantly with decreasing initial concentration. However, we have ignored this apparent dependence on concentration since no such trends appear in the individual series of dilution experiments, and no indications of nonideality can be seen in the distribution data. The mean value, $\Delta H_d = 6.31 \pm 0.16$ kcal (mol of dimer)$^{-1}$, calculated weighting the individual values in proportion to the number of dilution ratios used, was used in evaluating enthalpies of transfer as outlined below.

Stock solutions for transfer experiments were prepared by equilibrating a known amount of *n*-butyric acid with known amounts of water and toluene. The concentration of butyric acid in the organic phase was evaluated, as in the distribution experiments, by titration of aliquots of the aqueous phase with standard alkali. Appropriate corrections to the transfer heats were based on blank experiments in which water-saturated toluene was flowed against an NaOH solution. Six stock solutions were employed ranging in concentration from 0.003 to 0.064 *M*.

The results of the transfer experiments are listed in Table II. The concentrations of the stock solutions in toluene are listed in column 1, the number of transfer experiments run in column 2, and the corrected observed heat effect in column 3.

Several processes are involved in each transfer experiment, as shown in eq 3–6.

$$x\mathrm{HA(org)} + \frac{1-x}{2}(\mathrm{HA})_2(\mathrm{org}) + \mathrm{OH^-(aq)} = \mathrm{A^-(aq)} + \mathrm{H_2O} \quad \Delta Q_{obsd} \quad (3)$$

$$(1-x)\mathrm{HA(org)} = \frac{1-x}{2}(\mathrm{HA})_2(\mathrm{org}) \quad -\Delta Q_d \quad (4)$$

$$\mathrm{H^+(aq)} + \mathrm{A^-(aq)} = \mathrm{HA(aq)} \quad -\Delta H_i \quad (5)$$

$$\mathrm{H_2O} = \mathrm{H^+(aq)} + \mathrm{OH^-(aq)} \quad -\Delta H_w \quad (6)$$

Summing these equations gives

$$\mathrm{HA(org)} = \mathrm{HA(aq)} \quad \Delta H_{trans} = \Delta Q_{obsd} - \Delta Q_d - \Delta H_i - \Delta H_w \quad (7)$$

where the enthalpy of transfer is ΔH_{trans}. The quantity x in eq 3 and 4 is calculated from the equilibrium constant K_d and the stock concentration by means of eq 2; $\Delta Q_d = [(1-x)/2]\Delta H_d$; ΔH_i is the molar heat of ionization of butyric acid; and ΔH_w is the heat of formation of water.

The fourth column in Table II gives the calculated corrections, ΔQ_d, based on the dissociation heat in Table I, and the fifth column the final heats of transfer, ΔH_{trans}, calculated according to eq 7. The uncertainty limits are based on the standard errors of the means for ΔQ_{obsd} and ΔH_d, and uncertainties of ±0.05 kcal mol^{-1} in ΔH_i and ±0.01 kcal mol^{-1} in ΔH_w. It appears that within experimental uncertainty ΔH_{trans} is independent of concentration as expected. The mean of the values in the table, $\Delta H_{trans} = -3.52$ kcal mol^{-1} with a standard error of the mean of ±0.15 kcal mol^{-1} (±4%), was calculated assigning weights to the individual values equal to the numbers in column 2.

Discussion

Goodman[10] studied the distribution of straight-chain fatty acids between heptane and water, and his data were reinterpreted by Smith and Tanford.[11] Extrapolation of the values for the free energy of transfer of octanoic and higher acids to butyric acid gives −1.0 kcal mol^{-1}, as compared with our value of −1.2 kcal mol^{-1} for transfer between toluene and water.

Literature values for the free energies of dissociation of acetic and butyric acid dimers are given in Table III. It appears that there is little or no change in going from acetic to butyric acid in either the aliphatic or the aromatic solvents, and that our value in toluene is thus intermediate between that of Pohl, *et al.*,[12] and the value Davies, *et al.*,[7] would probably have found for butyric acid in benzene if they had studied that system. In making intercomparisons of the values in Table III, it should be noted that the data of Pohl, *et al.*, are for anhydrous solvents while all the other data are for water-saturated solvents. The influence of dissolved water on the dimerization of the fatty acid is unknown.

The enthalpy of dissociation of the dimeric form of *n*-butyric acid, 6.3 kcal mol^{-1}, corresponds to a hydrogen bond energy of 3.2 kcal mol^{-1}.

TABLE III: Free Energies of Dissociation of Fatty Acid Dimers in Organic Solvents at Approximately 25°

Substance	$\Delta G°_d$, kcal mol^{-1} In hexane or heptane	In benzene or toluene	Ref
Acetic acid	−4.8		*a*
	−3.9	−2.8	*b*
	−5.9	−3.6	*c*
n-Butyric acid	−4.9		*a*
		−3.3	*d*
		−3.6	*c*

[a] Goodman.[10] Obtained by linear extrapolation of values for octanoic through myristic acids derived from measurements of the distribution between heptane and water at 23°. [b] Davies, *et al.*[6] Derived from measurements of distribution between hexane and water and between benzene and water at 25°. [c] Pohl, *et al.*[12] Derived from measurements of dielectric polarization of solutes in anhydrous heptane or benzene at 30°. [d] This paper.

TABLE IV: Thermodynamic Parameters for Transfer of Related Compounds from Nonpolar to Aqueous Medium

	$\Delta G°$, kcal mol^{-1}	$\Delta H°$, kcal mol^{-1}	$\Delta S°$, cal mol^{-1} deg^{-1}
n-Butane[a]	+6060	−800	−23
1-Butanol[b]	+2400	−2250	−15.6
n-Butyric acid[c]	−1220	−3520	−7.7

[a] Data for transfer from the pure organic liquid at 20°; Tanford.[15] [b] Data for transfer from the pure organic liquid at 25°; Tanford.[15] [c] Data for transfer from toluene at 25°; this paper.

We find for the transfer of *n*-butyric acid from toluene to water at 25° the thermodynamic parameters $\Delta G°$ = (1220 ± 50) cal mol^{-1}, ΔH = (−3520 ± 150) cal mol^{-1}, and $\Delta S°$ = (−7.7 ± 0.5) cal deg^{-1} mol^{-1}. It is usually considered that the transfer of nonpolar groups from organic to aqueous medium is accompanied by little if any enthalpy change and a decrease in entropy resulting from the ordering of water molecules around the nonpolar groups.[13] The substantial decrease in enthalpy observed in the case of *n*-butyric acid is undoubtedly largely due to the interaction of the polar carboxyl group with water. Further indication of this is indicated by the comparison,[14] given in Table IV, of data for the transfer of *n*-butane and 1-butanol from the respective pure liquids to water with the data for the transfer of *n*-butyric acid from toluene to water. It appears that immersing a carboxyl group in water is about 3 kcal mol^{-1} more exothermic than immersing a methyl group, and that the entropy change is also much more favorable in the case of the carboxyl group. It may be conjectured that the enthalpy difference arises from more energetic hydrogen bonding between carboxyl groups and water molecules than between water molecules, and that the entropy difference reflects less structuring of water molecules around a carboxyl group than around a methyl group.

Acknowledgments. The authors thank Mr. Roy Wiener for his expert assistance. This research was aided by grants from the U. S. Public Health Service, No. GM-04725, and from the National Science Foundation, No. GB 36346X.

References and Notes

(1) J. M. Sturtevant, *Fractions*, **No. 1** (1969).
(2) J. M. Sturtevant and P. A. Lyons, *J. Chem. Thermodyn.*, **1**, 201 (1969).
(3) J. M. Sturtevant, "Methods in Enzymology," Vol. 26, C. H. W. Hirs and S. N. Timasheff, Ed., Academic Press, New York, N.Y., Chapter 11, 1972.
(4) I. Grenthe, H. Ots, and O. Ginstrup, *Acta Chem. Scand.*, **24**, 1067 (1970).
(5) J. J. Christensen, J. L. Oscarson, and R. M. Izatt, *J. Amer. Chem. Soc.*, **90**, 5949 (1968).
(6) M. Davies, P. Jones, D. Patnaik, and E. A. Moelwyn-Hughes, *J. Chem. Soc.*, 1249 (1951).
(7) R. Stoesser and S. J. Gill, *J. Phys. Chem.*, **71**, 564 (1967).
(8) S. J. Gill, M. Downing, and G. F. Sheats, *Biochemistry*, 6, 272 (1967).
(9) S. Cabani and P. Gianni, *Anal. Chem.*, **44**, 253 (1972).
(10) D. S. Goodman, *J. Amer. Chem. Soc.*, **80**, 3887 (1958).
(11) R. Smith and C. Tanford, *Proc. Nat. Acad. Sci. U.S.*, **70**, 289 (1973).
(12) H. A. Pohl, M. E. Hobbs, and P. M. Gross, *J. Chem. Phys.*, **9**, 408 (1941).
(13) W. Kauzmann, *Advan. Protein Chem.*, **14**, 1 (1959).
(14) This comparison was brought to our attention by one of the reviewers of this paper.
(15) C. Tanford, "The Hydrophobic Effect," Wiley, New York, N.Y., 1973, pp 18, 20.

Relation between Molal Volumes and Molal Compressibilities from the Viewpoint of the Scaled-Particle Theory. Prediction of the Apparent Molal Compressibilities of Transfer

N. Desrosiers

Département de Chimie, Université de Sherbrooke, Province of Quebec, J1K 2R1 Canada

and M. Lucas*

Département de Génie Radioactif, Commissariat à l'Energie Atomique, 92260 Fontenay-aux-Roses, France *(Received February 15, 1974)*

Publication costs assisted by the Commissariat à l'Energie Atomique

By means of the scaled-particle theory, the compressibility of transfer from H_2O to 3 *m* urea and to D_2O can be calculated for various salts provided one knows the compressibility in water and the molal volume of salt in 3 *m* urea or in D_2O. The fit between experimental and calculated values is good.

The partial molal volumes and partial molal compressibilities of solutes in water and aqueous solutions are considered important thermodynamic quantities, whose knowledge hopefully gives information about the structural influence of the solute upon water structure.[1] They are usually considered as independent quantities. However, the scaled-particle theory gives a relation between these two quantities and the solute hard-sphere diameter. In this paper, the relation is given and it is shown that the compressibility of transfer from H_2O to 3 *m* urea and from H_2O to D_2O can be calculated for various salts and, in many cases, within the experimental error.

Theory

The coefficient of isothermal compressibility β of a mixture of hard spheres of different diameters is given by eq 16 of ref 2

$$\frac{1}{\beta} = \frac{6kT}{\pi(1-z)^4}[S(1-z)^2 + 6XY(1-z) + 9X^3 + z^2X^3 - 4X^3z] \quad (1)$$

In the case of a mixture of water, urea, and salt, we give the definition

$$\frac{\pi N}{6}\left[\frac{55.51a^p + mu^p + m(b^p + c^p)}{55.51\bar{v}^0_{H_2O} + n\phi_{V_u} + m\phi_{V_S}}\right] = z,\ X,\ Y,\ \text{or}\ S \quad (2)$$

where $p = 3$ for z, $p = 2$ for X, $p = 1$ for Y, and, finally, $p = 0$ for S.

In these equations, a, u, b, and c are respectively the hard-sphere diameters of water, urea, and anion and cation of the salt, n and m are respectively the urea and salt molalities, $\bar{V}^0_{H_2O}$ is the pure water molal volume, ϕ_{V_u} is the apparent molal volume of urea in water, and ϕ_{V_s} is the apparent molal volume of salt in water ($n = 0$) or of salt in aqueous urea solution ($n \neq 0$).

In their eq 16 Tiepel and Gubbins[2] included terms dealing with interaction forces. Those terms, approximate in nature, when added to complete eq 1 lead to a hard-sphere diameter of 2.98 Å for water (ref 2, Table III). On the other hand, when those interaction terms are neglected, then eq 1 yields a hard-sphere diameter of water of 2.74 Å. A good fit of the calculated second virial coefficients to the experimental values has been achieved by Stockmayer,[3] who has found a value of 2.76 Å. Rowlinson[4] has found 2.73 Å. Pierotti[5] has found, by different methods, a water hard-sphere diameter of 2.75 Å, which is close to the oxygen–oxygen intermolecular distance in ice (2.76 Å).[5] Usually, in studies dealing with aqueous solutions, a hard-sphere diameter of 2.76 Å for water is used.[6] Therefore we prefer to use the scaled-particle theory in its simplest form that is by using only the hard-sphere part and neglecting the interaction terms.

Also, the possibility exists that the interaction forces are somewhat taken into account in the case of the compressibilities by the fact that we introduce in the equations the experimental volume of the solutes in the studied solvent.

The concentration dependence of the coefficient of isothermal compressibility can be expressed as[7]

$$\beta = \beta_0 + Am + Bm^{3/2} \quad (3)$$

where $1000A = \phi^0_K - \beta_0\phi^0_V$ and $1000B = S_K - \beta_0 S_V$. Then

$$\frac{\partial\beta}{\partial m} = A + \frac{3}{2}Bm^{1/2} \quad (4)$$

At infinite dilution, we have

$$\left(\frac{\partial\beta}{\partial m}\right)_{m\to 0} = A \quad (5)$$

and then

$$\left(\frac{1}{\beta}\frac{\partial\beta}{\partial m}\right)_{m\to 0} = \frac{1}{1000\beta_0}(\phi^0_K - \beta_0\phi^0_V) \quad (6)$$

Also, taking into account that

$$\left(\frac{1}{z}\frac{\partial z}{\partial m}\right)_{m\to 0} = \frac{\bar{V}^0_{H_2O}d^0}{1000}A_3 \quad (7)$$

$$\left(\frac{1}{X}\frac{\partial X}{\partial m}\right)_{m\to 0} = \frac{\bar{V}^0_{H_2O}d^0}{1000}A_2, \text{ etc.} \quad (8)$$

where

$$A_p = \frac{b^p + c^p}{a^p + 0.018018mu^p} - \frac{\phi^0_{V_S}}{\bar{V}^0_{H_2O} + 0.018018n\phi_{V_u}} \quad (9)$$

and d^0 is the pure water density, it is then possible to derive, from eq 1, that

$$\left(-\frac{1}{\beta}\frac{\partial\beta}{\partial m}\right)_{n\neq 0,\, m\to 0} = \frac{\bar{V}^0{}_{H_2O}d^0}{1000}\left\{A_0\frac{S}{(1-z)^2} + A_1\frac{6XY}{(1-z)^3} + A_2\left[\frac{6XY}{(1-z)^3} + \frac{27X^3}{(1-z)^4} + \frac{3z^2X^3}{(1-z)^4} - \frac{12X^3z}{(1-z)^4}\right] + A_3\left[\frac{2Sz}{(1-z)^3} + \frac{2X^3z^2 + 18XYz - 4X^3z}{(1-z)^4} + \frac{4z^3X^3 - 16z^2X^3 + 36X^3z}{(1-z)^5}\right]\right\}\left[\frac{S}{(1-z)^2} + \frac{6XY}{(1-z)^3} + \frac{9X^3 + z^2X^3 - 4zX^3}{(1-z)^4}\right]^{-1} \quad (10)$$

When there is no urea ($n = 0$)

$$X = \frac{z}{a} \qquad Y = \frac{z}{a^2} \qquad S = \frac{z}{a^3} \quad (11)$$

and

$$z = N\pi a^3/6\bar{V}^0{}_{H_2O}$$

Then eq 10 reduces to

$$\left(-\frac{1}{\beta}\frac{\partial\beta}{\partial m}\right)_{(m\to 0)} = \frac{\bar{V}^0{}_{H_2O}d^0}{1000}\left\{\frac{A_0z}{a^3(1-z)^2} + \frac{6A_1z^2}{a^3(1-z)^3} + A_2\left[\frac{6z^2}{a^3(1-z)^3} + \frac{27z^3}{a^3(1-z)^4} + \frac{3z^5}{a^3(1-z)^4} - \frac{12z^4}{a^3(1-z)^4}\right] + A_3\left[\frac{2z^2}{a^3(1-z)^3} + \frac{2z^5}{a^3(1-z)^4} + \frac{18z^3}{a^3(1-z)^4} - \frac{4z^4}{a^3(1-z)^4} + \frac{4z^6}{a^3(1-z)^5} - \frac{16z^5}{a^3(1-z)^5} + \frac{36z^4}{a^3(1-z)^5}\right]\right\} \times \left[\frac{z}{a^3(1-z)^2} + \frac{6z^2}{a^3(1-z)^3} + \frac{9z^3}{a^3(1-z)^4} + \frac{z^5}{a^3(1-z)^4} - \frac{4z^4}{a^3(1-z)^4}\right]^{-1} \quad (12)$$

And finally, since all a^3 vanish

$$\left(-\frac{1}{\beta}\frac{\partial\beta}{\partial m}\right)_{m\to 0} = \frac{\bar{V}^0{}_{H_2O}d^0}{1000(1-z)[(1+2z)^2 - 4z^3 + z^4]}[A_0(1-z)^3 + 6A_1z(1-z)^2 + 3A_2z(1-z)(2+7z-4z^2+z^3) + A_3(2z + 14z^2 + 16z^3 - 10z^4 + 2z^5)] \quad (13)$$

The apparent molal isothermal compressibility ϕ_K of a salt is given by the relation

$$\phi_K = \beta\phi_{V_S} + W_{55.51}(\beta - \beta^0)/m'd^0 \quad (14)$$

taken from ref 8.

β is the coefficient of isothermal compressibility of the salt solution at aquamolality m'; β^0 and d^0 are respectively the coefficient of isothermal compressibility and density of the solvent (either pure water or aqueous urea). $W_{55.51}$ is the weight of 55.51 mol of solvent or mixed solvent; *i.e.*

$$W_{55.51} = \frac{55.51M_w + nM_u}{(55.51 + n)/55.51} \quad (15)$$

where M_w and M_u are respectively water and urea molecular weights. In the limit of infinite dilution

$$\beta^0\left(\frac{1}{\beta^0}\frac{\partial\beta}{\partial m}\right)_{m\to 0} \approx \frac{\beta - \beta^0}{m} \quad (16)$$

Finally

$$(\phi_K)_{m\to 0} = \beta^0\phi^0{}_{V_S} + \beta^0\left(\frac{1}{\beta}\frac{\partial\beta}{\partial m}\right)_{m\to 0}\left(\frac{\partial m}{\partial m'}\right)\frac{W_{55.51}}{d^0} \quad (17)$$

with $m = m'(55.51 + n)/55.51$.

The knowledge of $\phi^0{}_{V_s}$ and $\phi^0{}_K$ for a given salt in pure water make it possible to compute b and c for a salt provided that a for water is known. This parameter is calculated from the experimental compressibility of pure water of the equation

$$\frac{1}{\beta^0} = \frac{RT}{\bar{V}^0{}_{H_2O}}\frac{(1+2z)^2 - 4z^3 + z^4}{(1-z)^4} \quad (18)$$

taken from ref 9. In this, $z = \pi Na^3/6V^0{}_{H_2O}$ at 25°, $\beta^0{}_{H_2O} = 45.25 \times 10^{-6}$ bar^{-1} and $\bar{V}^0{}_{H_2O} = 18.057$ cm^3 mol^{-1}.[10] Then, a is found to be equal to 2.74 Å, which is not much different from the value 2.76 Å computed by Pierotti with another method. For urea in water at infinite dilution, $\phi^0{}_K = 0.90 \times 10^{-4}$ bar^{-1} cm^3 mol^{-1} and $\phi^0{}_{V_u} = 44.20$ cm^3 mol^{-1}.[8] Then, from eq 5, with

$$A_p = \frac{u^p}{a^p} - \frac{\phi^0{}_{V_u}}{\bar{V}^0{}_{H_2O}}$$

u is found to be equal to 4.408 Å.

Discussion

The hard-sphere diameters of monovalent ions are given in Table I. They have been computed from the experimental ϕ_K of salts in water at 0.1 m,[8] and experimental $\phi^0{}_{V_s}$ of salts given in ref 11 ($\phi^0{}_K$ should have been taken instead of ϕ_K at a finite salt molality, but the rule of extrapolation to zero salt concentration is not known for the ϕ_K). In Table I are also given crystallographic ionic diameters for the same ions. The comparison between the two sets of values shows that, except for F^-, the sets of ionic diameters are very similar. This implies that the ionic response to a variation of pressure is the same as if the water of hydration could be considered as separate particles.

Once a, b, c, and u are known, the $\phi^0{}_K$ for salts in 3 m urea can be computed, if $\phi^0{}_{V_s}$ for salts in urea are known. In fact only ϕ_{V_s} at salt aquamolality 0.1 m was available. Hence $\phi^0{}_{V_s}$ in 3 m urea has been computed from ϕ_{V_s} at 0.1 m in 3 m urea and ϕ_{V_s} for the same salt in pure water assuming that the $\Delta\phi_{V_{tr}}(H_2O \to 3\ m$ urea) is salt concentration independent. However it has been shown that $\Delta\phi_{V_{tr}}(H_2O \to 3\ m$ urea) shows only small salt concentration dependence, given by the equation[8]

$$\Delta\phi_{V_S}{}_{tr}(H_2O \longrightarrow 3\ m \text{ urea}) = 2.14 - 0.39\ m$$

where m is the salt aquamolality. Thus $\phi_{V_s}(m = 0.1)$ must be very nearly equal to $\phi^0{}_{V_s}$. [$\Delta\phi_{K_{tr}}(H_2O \to 3\ m$ urea)

TABLE I: Ionic Diameters of Monovalent Ions (Ångströms)

	Li^+	Na^+	K^+	Cs^+	F^-	Cl^-	Br^-	I^-
Computed	1.37[a]	1.836	2.658	3.329	3.266	3.792	3.948	4.222
Crystallographic[b]	1.37	1.94	2.66	3.34	2.66	3.62	3.92	4.32

[a] Assumed arbitrarily in the initial calculation. [b] "Handbook of Chemistry and Physics," 45th ed, Chemical Rubber Publishing Co., Cleveland, Ohio, 1964–1965.

TABLE II: Comparison of Experimental and Calculated Apparent Molal Isothermal Compressibilities, $\phi_K \times 10^4$ (bar^{-1} cm^3 mol^{-1}), and Transfer Functions $\Delta\phi_K(H_2O \rightarrow 3\ m$ urea or $D_2O) \times 10^4$ (bar^{-1} cm^3 mol^{-1}) at 25°

	Salt						
Solvent	LiCl	NaCl	KCl	CsCl	NaI	NaBr	NaF
H_2O[a] exptl	−38	−45.4	−38.7	−31.3	−25.7	−37.2	−67.6
3 m urea[a] exptl	−26.7	−33.0	−26.7	−21.7	−14.7	−25.9	−54.4
3 m urea[b] computed	−28.8	−35.2	−28.6	−21.4	−16.3	−27.8	−56.9
$\Delta\phi_K(H_2O \rightarrow 3\ m$ urea)[a] exptl	11.3	12.4	12.0	9.6	11.0	11.3	13.2
$\Delta\phi_K(H_2O \rightarrow 3\ m$ urea)[b] computed	9.2	10.2	10.1	9.9	9.4	9.4	10.7
$\Delta\phi_{Ks}(H_2O \rightarrow D_2O)$[c] exptl		−4.4	−2.8	−1.7			−5.5
$\Delta\phi_K(H_2O \rightarrow D_2O)$[b,d] computed		−3.2	−3.0	−1.1			−4.7

[a] Values from ref 8. [b] Values from present work. [c] Adiabatic values from J. G. Mathieson and B. E. Conway, *J. Chem. Soc., Faraday Trans. I*, in press. [d] The necessary $\Delta\phi^0_V$ have been taken from ref 11.

also shows a small concentration dependence which is given by $\Delta\phi_{K_{tr}} = 13.30 - 2.6m$.[8]]

Table II shows the calculated ϕ_K in aqueous 3 m urea. Experimental ϕ_K values of salts 0.1 m in 3 m urea are also given. The agreement with calculated values of ϕ_K is good, the difference in many cases being smaller than 6%. The computed and experimental $\Delta\phi_{K_{tr}}(H_2O \rightarrow 3\ m$ urea) values are also given (experimental values are considered exact within 1×10^{-4} bar^{-1} cm^{-3} mol^{-1}). Table II also includes the calculated $\Delta\phi_{K_{tr}}(H_2O \rightarrow D_2O)$ values. They are compared to experimental $\Delta\phi_K$ values. Although this comparison is weakened by the fact that the calculated $\Delta\phi_K$ values are isothermal, whereas in the case $H_2O \rightarrow D_2O$ the experimental ones are adiabatic, the sign and order of magnitude are probably correct. [$\beta_0(D_2O)$ and $V^0(D_2O)$ are from ref 10.]

Since experimental volumes of the salts are taken, structural information on the influence of the salts upon water and 3 m urea structure are implicitly present in the calculated ϕ_K. One may also guess that the success of the scaled-particle theory in this particular case comes from the fact that the repulsive potential between particles in a solution plays a major role in the determination of the ϕ_K (and the scaled-particle theory takes it into account), whereas sufficient account of attractive potential between particles is taken, if experimental volumes are included in the equation.

Acknowledgments. Helpful suggestions from Professor J. E. Desnoyers are gratefully acknowledged. N. D. is also grateful to the National Research Council of Canada and to the Cooperation Franco-Québécoise for the award of a scholarship. Helpful comments from Dr. Jean-Pierre Morel have been appreciated.

References and Notes

(1) J. E. Desnoyers and P. R. Philip, *Can. J. Chem.*, **50**, 1094 (1972).
(2) E. W. Tiepel and K. E. Gubbins, *J. Phys. Chem.*, **76**, 3047 (1972).
(3) W. H. Stockmayer, *J. Chem. Phys.*, **9**, 398 (1941).
(4) J. S. Rowlinson, *Trans. Faraday Soc.*, **47**, 120 (1949).
(5) R. A. Pierotti, *J. Phys. Chem.*, **69**, 281 (1965).
(6) H. L. Friedman in "Water, a Comprehensive Treatise," Vol. 3, F. Franks, Ed., Plenum Press, New York, N. Y., 1973, p 49.
(7) H. S. Harned and B. B. Owen, "The Physical Chemistry of Electrolyte Solutions," Reinhold, New York, N. Y., 1958, Chapter 8.
(8) N. Desrosiers, G. Perron, J. G. Mathieson, B. E. Conway, and J. E. Desnoyers, *J. Solution Chem.*, in press.
(9) T. Boublik, *J. Chem. Phys.*, **53**, 471 (1970).
(10) G. S. Kell in "Water, a Comprehensive Treatise," Vol. 1, F. Franks, Ed., Plenum Press, New York, N. Y., 1972, p 384.
(11) J.-L. Fortier, P. R. Philip, and J. E. Desnoyers, *J. Solution Chem.*, in press.

Electrical Liquid Membrane Potential. Biionic Isothermal Potential

C. Fabiani,* P. R. Danesi, G. Scibona, and B. Scuppa

Industrial Chemistry Laboratory, C.N.E.N., CSN-Casaccia, Rome, Italy *(Received February 1, 1974; Revised Manuscript Received June 3, 1974)*

Publication costs assisted by the Industrial Chemistry Laboratory

Biionic (Cl^-,NO_3^-) membrane potentials have been measured for liquid membranes formed by dissolving a tetraheptylammonium salt in chlorobenzene, o-dichlorobenzene, and nitrobenzene. The values of the physicochemical parameters required by the theoretical equations which describe the liquid ion-exchange membrane potential have been experimentally obtained by means of conductometric and ion distribution experiments. By using these parameters a rather good agreement between theoretical and experimental membrane potential values has been obtained for all the liquid membranes except nitrobenzene. In fact for this solvent, due to the partial dissociation of the site–counterion ion pairs, a test of the theory was not possible.

Introduction

Liquid ion-exchange membranes are formed by solutions of suitable organic salts or acids (*e.g.*, long-chain alkylammonium salts; bis(2-ethylhexyl)phosphoric acid or salts) in low dielectric constant solvents. When these solutions are interposed between two aqueous electrolyte solutions of suitable composition an electrical potential is generated. As far as the chemistry of these liquid membranes is concerned it has to be noted that the organic salt or acid can form free ions and associated species in the organic solution.

Theoretical equations for the electrical potential of these liquid membranes have been derived under isothermal conditions by coupling ion distribution and ion diffusion processes.[1-3] The same equations have been obtained from an irreversible thermodynamic treatment of the transport processes across a liquid membrane and extended to both the isothermal and nonisothermal conditions.[4] In the case of practical insolubility of the site in the aqueous solutions and coions exclusion, the theoretical treatment suggests the following: (i) the monoionic membrane potential values depend only on the aqueous activity of the counterion and are not affected by any change of the membrane charged site mobility (in other words the membrane is highly permselective); (ii) the biionic membrane potential values depend on the aqueous activity of the counterions, on the mobilities of the species present in the membrane phase, and on the ion-exchange constant, ion distribution constant, and ion pair formation constants. An experimental test of the theoretical predictions has been already performed in the case of liquid cation exchange membranes.[3] This paper is instead devoted to the experimental analysis of the biionic liquid anion exchange membranes. To this purpose we have studied the biionic (chloride, nitrate couple) electrical membrane potential of liquid anion exchange membranes formed by tetraheptylammonium nitrate salt in chlorobenzene (dielectric constant $\epsilon = 5.62$), o-dichlorobenzene ($\epsilon = 9.93$), and nitrobenzene ($\epsilon = 34$). Further all the physicochemical parameters required by the theoretical equations have been experimentally determined.

Equations Describing the Liquid Membrane Potential

We will summarize here the membrane potential equations derived in ref 2 and 4 for the case of two counterions (biionic potentials). The total membrane potential, V_0, is given by

$$(Fz_i/RT)V_0 = -\ln \frac{\sum_{i=1}^{2} u_i k_i a_i''}{\sum_{i=1}^{2} u_i k_i a_i'} - \int_1 \qquad (1)$$

where u_i are the membrane mobilities of the counterions, k_i the single ion distribution constants, a_i the aqueous activities of the counterions, and $\int_1$ accounts for the influence of the associated species.

In the case of complete electrolyte dissociation in the membrane phase eq 1 becomes

$$(Fz_i/RT)V_0 = -\ln \frac{a_1'' + P_{21}a_2''}{a_1' + P_{21}a_2'} \qquad (2)$$

In the case of strong association, *i.e*, when $(u_s c_s/\Sigma_{i=1}^{2} u_{is}c_{is}) \ll 1$ (c_s and c_{is} are the membrane phase concentrations of site s and of ion pairs is) the integral form of eq 1 becomes

$$(Fz_i/RT)V_0 = (1 - \tau) \ln \frac{a_1' + \bar{P}_{21}a_2'}{a_1'' + \bar{P}_{21}a_2''} + \tau \ln \frac{a_1' + \bar{K}_{21}a_2'}{a_1'' + \bar{K}_{21}a_2''} \qquad (3)$$

with

$$\tau = \frac{u_s(u_{2s}/K_{2s} - u_{1s}/K_{1s})}{(u_1 + u_s)u_{2s}/K_{2S} - (u_2 + u_s)u_{1s}/K_{1s}} \qquad (4)$$

K_{1s} and K_{2s} the ion pairs dissociation constants ($\overline{1S} \rightleftharpoons \overline{1^-} + \overline{S^+}$) and K_{21} the ion-exchange constant ($2^- + \overline{1S} \rightleftharpoons \overline{2S} + 1^-$)

$$P_{21} = (u_2/u_1)(K_{1s}/K_{2s})K_{21} \quad (5)$$

$$\bar{P}_{21} = (u_2 + u_s)/(u_1 + u_s)(K_{1s}/K_{2s})K_{21} \quad (6)$$

$$\bar{K}_{21} = (u_{2s}/u_{1s})K_{21} \quad (7)$$

$$u_{is} = 2u_iu_s/(u_i + u_s) \quad (8)$$

When u_1, u_2, u_s, K_{1s}, K_{2s}, and K_{21} are all experimentally measured it is possible to verify the adequacy of eq 2 and 3 to describe experimental $V_0(a_1',a_1'',a_2',a_2'')$ data.

Experimental Section

Reagents and Solutions. KCl, KNO_3, chlorobenzene, *o*-dichlorobenzene, and nitrobenzene were Carlo Erba analytical grade reagents. Tetraheptylammonium nitrate and chloride($THANO_3$, THACl) were prepared as reported in ref 5. Tetrabutylammonium tetraphenylborate (TBATPB) was prepared by mixing an aqueous solution (2%) of TPBNa (Fluka) with a solution (2%) of TBABr (Carlo Erba) in 1/1 molar ratio. The white precipitate was filtered, washed several times with water, and recrystallized twice from a 1/3 water–acetone mixture. Tetraheptylammonium tetraphenylborate (THATPB) was prepared by adding equimolar solutions of TPBNa in water and THAI (Fluka) in methyl alcohol. The white precipitate was filtered, washed several times with a water–acetone mixture, and recrystallized twice from acetone (hot then cold).

Conductometric Measurements. The measurements have been performed by adding the electrolyte solution of known concentration to a given volume of pure solvent previously equilibrated with water. At least two runs were carried out for each salt and the results reported in Tables I–III represent mean values. From these measurements, by using the Shedlovsky procedure[6] (plots of $1/S(z)\Lambda$ *vs.* $c\Lambda f^2S(z)$), Λ_0 and K_{is} were calculated. In all cases the data

TABLE I: Conductometric Measurements in Chlorobenzene Used for Shedlovsky Plots at 25 ± 0.01°

$C \times 10^4$, *M*	Λ, Ω^{-1} cm² mol^{-1}	$C \times 10^4$, *M*	Λ, Ω^{-1} cm² mol^{-1}
TBATPB			
0.016	12.60	0.154	5.79
0.031	10.60	0.230	4.93
0.055	7.30	0.305	4.35
0.085	7.40	0.379	3.95
0.124	6.32		
THATPB			
0.031	10.75	0.232	5.21
0.063	8.15	0.307	4.16
0.094	6.71	0.382	3.83
0.125	6.10	0.456	3.52
0.156	5.57		
$THANO_3$			
0.003	5.58	0.020	3.65
0.005	5.24	0.024	3.36
0.008	4.46	0.025	3.14
0.010	4.74	0.027	2.95
0.013	4.33	0.030	2.80
0.015	4.09	0.032	2.66
0.018	3.86		
THACl			
0.003	3.57	0.036	1.46
0.006	2.68	0.042	1.32
0.011	2.37	0.050	1.29
0.014	2.33	0.057	1.27
0.018	2.16	0.068	1.16
0.023	1.94	0.077	1.13
0.029	1.72		

TABLE II: Conductometric Measurements in *o*-Dichlorobenzene Used for Shedlovsky Plots at 25 ± 0.01°

$C \times 10^4$, *M*	Λ, Ω^{-1} cm² mol^{-1}	$C \times 10^4$, *M*	Λ, Ω^{-1} cm² mol^{-1}
TBATPB			
0.037	26.00	0.476	20.15
0.059	25.20	0.537	20.08
0.077	23.10	0.598	19.43
0.144	22.80	0.656	19.18
0.214	22.20	0.770	18.78
0.282	21.08	0.986	17.73
0.348	20.63	1.085	17.43
0.412	19.70	1.181	17.15
THATPB			
0.034	26.60	0.805	17.95
0.085	24.80	0.956	18.10
0.136	24.38	1.090	17.53
0.169	24.60	1.245	17.15
0.334	22.67	1.385	16.85
0.495	20.13	1.520	16.48
0.652	19.38	1.785	15.80
$THANO_3$			
0.423	12.30	3.070	5.75
0.841	9.50	4.050	5.14
1.050	8.80	5.000	4.72
1.575	7.44	5.970	4.43
2.065	6.73	8.950	3.45
2.565	6.24	14.00	3.04
THACl			
0.055	17.90	1.359	5.25
0.110	12.95	1.840	4.85
0.274	9.60	2.680	3.94
0.546	7.62	3.335	3.54
1.090	5.72	3.975	3.35

TABLE III: Conductometric Measurements in Nitrobenzene Used for Shedlovsky Plots at 25 ± 0.01°

$C \times 10^4$, *M*	Λ, Ω^{-1} cm² mol^{-1}	$C \times 10^4$, *M*	Λ, Ω^{-1} cm² mol^{-1}
TBATPB			
0.744	22.59	6.200	20.10
0.990	23.70	17.43	20.34
1.120	24.59	28.75	20.00
1.840	21.80	50.52	18.80
2.440	21.91	61.16	18.41
3.030	21.51	71.40	18.39
4.760	21.35	91.38	17.81
THATPB			
4.720	18.94	50.50	16.65
7.060	18.56	61.10	16.48
9.450	18.42	71.40	16.08
12.25	18.29	81.50	15.88
17.45	18.04	91.40	15.64
28.95	17.25	101.0	15.37
39.70	17.06	110.5	15.28
$THANO_3$			
4.770	30.63	39.80	26.83
8.220	29.90	50.70	26.23
10.55	30.35	61.00	25.38
12.85	30.20	71.60	25.00
17.50	30.75	81.80	24.45
28.80	27.58		
THACl			
7.720	41.42	47.14	35.11
11.51	39.41	53.80	34.76
18.97	38.46	60.32	33.87
26.25	37.41	66.70	33.44
33.37	36.31	72.95	33.38
40.33	35.81		

fall on straight lines showing that interactions higher than ion pairs can be excluded. In the calculations the viscosity, density and dielectric constants of the pure solvent were used. The limiting equivalent conductivities of the ions (Cl^-, NO_3^-, THA^+) λ_i^0 were obtained by assuming the TBATPB as a reference electrolyte with $\lambda_{TBA}^0 = \lambda_{TPB}^0$. It is in fact known from the literature[7] that in this electrolyte both the anion and the cation have almost the same dimensions. Once $\lambda_{TBA}^0 = \lambda_{TPB}^0$ was known, λ_{Cl}^0, $\lambda_{NO_3}^0$, and λ_{THA}^0 were easily calculated from Λ_0(THATPB), Λ_0(THACl), and Λ_0($THANO_3$) values (Λ_0 equivalent conductance of the electrolyte). In eq 1-8 the mobilities appear as ratios. Therefore they have been substituted with the limiting ionic equivalent conductivities, λ_i^0.

The measurements were performed at 25 ± 0.01° with a WTW, Model LBR/B, conductivity bridge at the frequency of 50 Hz.

Membrane Biionic Potentials. The biionic potential measurements have been performed with stirred (organic and aqueous phases) cells of the type

$$\begin{aligned} &Ag, AgCl\,|\,M_{Cl}'(KCl), M_{NO_3}'(KNO_3); (M_{Cl}' + M_{NO_3}' = \\ &0.1\ M; M_{Cl}'\,|\,M_{NO_3}' = \text{constant})\,|\,THANO_3\,0.05\ M \\ &\text{(in organic solvent)}\,|\,M_{Cl}''(KCl), M_{NO_3}''(KNO_3) \\ &(M_{Cl}'' + M_{NO_3}'' = 0.1\ M; M_{Cl}''\,|\,M_{NO_3}'' = \\ &\text{variable})/AgCl, Ag \qquad (9) \end{aligned}$$

as reported in ref 8 and 9. The emf of the cell 9 is then given by

$$E = V_0 - (RT/F) \ln a_{Cl}'/a_{Cl}''$$

Since a constant aqueous medium was employed we have used concentrations in place of activities.

Ion-Exchange Equilibrium Constant. In order to obtain the ion-exchange equilibrium constants, K_{21}, an organic solution of known concentration (1×10^{-3} *M*) of THACl was shaken at 25° for several hours with an equal volume of an aqueous solution of KNO_3 (1×10^{-3} *M*). After equilibrium was reached the chloride concentration in both phases was measured argentometrically. The concentration ratio $K_{21} = [\overline{THANO_3}][Cl^-]/[\overline{THACl}][NO_3^-]$ was obtained through mass-balance calculations.

TABLE IV: Conductometric Measurements in Chlorobenzene

	Λ_0 (Ω^{-1} cm^2 mol^{-1}) or λ_0 (Ω^{-1} cm^2 equiv^{-1})	K_{1s}(dissociation constant)
TBATPB	26.6	1.00×10^{-6}
THATPB	22.2	1.13×10^{-6}
$THANO_3$	10.1	3.3×10^{-7}
THACl	10.0	1.1×10^{-7}
TBA^+TPB^-	13.3	
THA^+	8.9	
NO_3^-	1.2	
Cl^-	1.1	

Selectivity Factors[a]

$K_{21} = \frac{k_2}{k_1}\frac{K_{1s}}{K_{2s}} = 47 \pm 4$ $\qquad \frac{k_2}{k_1} = 148$ $\qquad \bar{K}_{21} = \frac{u_{2s}}{u_{1s}} K_{21} = 44$

$\tau = 0.88$

$P_{21}^* = 40 \pm 5$ $\qquad P_{21} = \frac{u_2}{u_1}\frac{k_2}{k_1} = 161$ $\qquad \bar{P}_{21} = \frac{u_2^+ u_s}{u_2^+ u_s}\frac{k_2}{k_1} = 150$

[a] The subscripts 1 and 2 refers respectively to Cl^- and NO_3^-. The temperature was 25 ± 0.01°. The Λ_0 values should be accurate to better than 10% and the K_{1s} values to better than 50%.

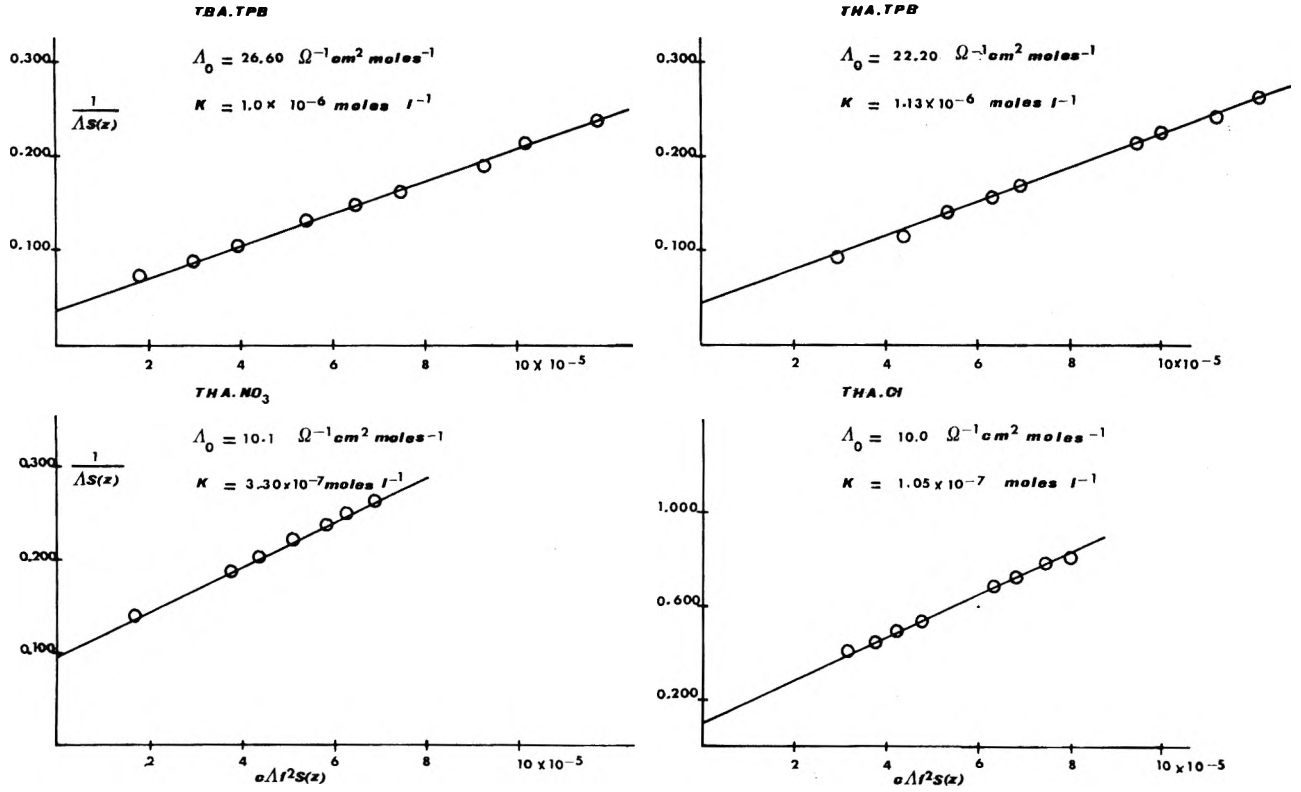

Figure 1. Shedlovsky plots of conductivity measurements in chlorobenzene at 25°: Λ_0, limiting equivalent conductivity; *K*, ion pair dissociation constant.

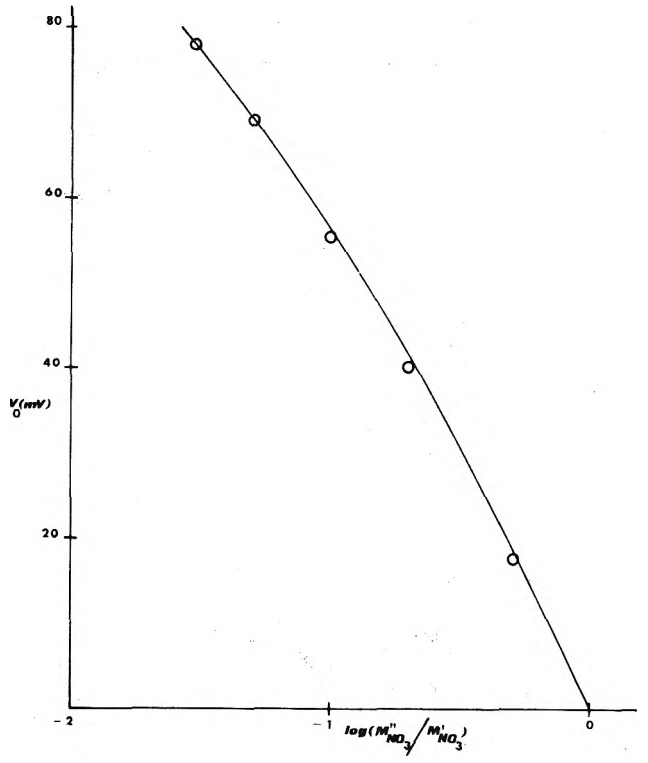

Figure 2. Open circles are experimental liquid membrane biionic potentials (V_0) *vs.* logarithm of nitrate ion concentration ratios in cell 9 with chlorobenzene as solvent. The solid line has been calculated with eq 3 inserting the parameters reported in Table IV.

TABLE V: Conductometric Measurements in *o*-Dichlorobenzene

	Λ_0 (Ω^{-1} cm^2 mol^{-1}) or λ_0 (Ω^{-1} cm^2 equiv^{-1})	K_{1s}(dissociation constant)
TBATPB	27.0	1.1×10^{-4}
THATPB	23.0	2.1×10^{-4}
$THANO_3$	25.0	1.5×10^{-6}
THACl	45.5	1.6×10^{-6}
TBA^+TPB^-	13.5	
THA^+	9.5	
NO_3^-	15.5	
Cl^-	36.0	

Selectivity Factors[a]

$K_{21} = \frac{k_2}{k_1}\frac{K_{1s}}{K_{2s}} = 14 \pm 2$ $\quad \frac{k_2}{k_1} = 130$ $\quad \bar{K}_{21} = \frac{u_{2s}}{u_{1s}}K_{21} = 15$

$\tau = 0.42$

$P_{21}^* = 40 \pm 5$ $\quad P_{21} = \frac{u_2}{u_1}\frac{k_2}{k_1} = 52$ $\quad \bar{P}_{21} = \frac{u_2 + u_s\frac{k_2}{k_1}}{u_1 + u_s\frac{k_2}{k_1}} = 72$

[a] See footnote a, Table IV.

Results and Discussion

Chlorobenzene. The conductivity measurements for the four electrolytes TBATPB, THATPB, $THANO_3$, and THACl in chlorobenzene are reported in Table I. Table IV summarizes the Λ_0, K_{1s}, and K_{2s} values (obtained by means of the Shedlovsky plots, Figure 1) as well as the λ^0, $\bar{P}_{21}$, $\bar{P}_{21}$, $\bar{K}_{21}$, and τ values. It has to be noted that the $THANO_3$ and THACl ion pairs have the same mobility (λ^0 = 10.1 and 10.0). Therefore we can assume $u_{1s} = u_{2s}$. From these values it follows that it is $\tau = 0.88$ and $K_{21} \cong$

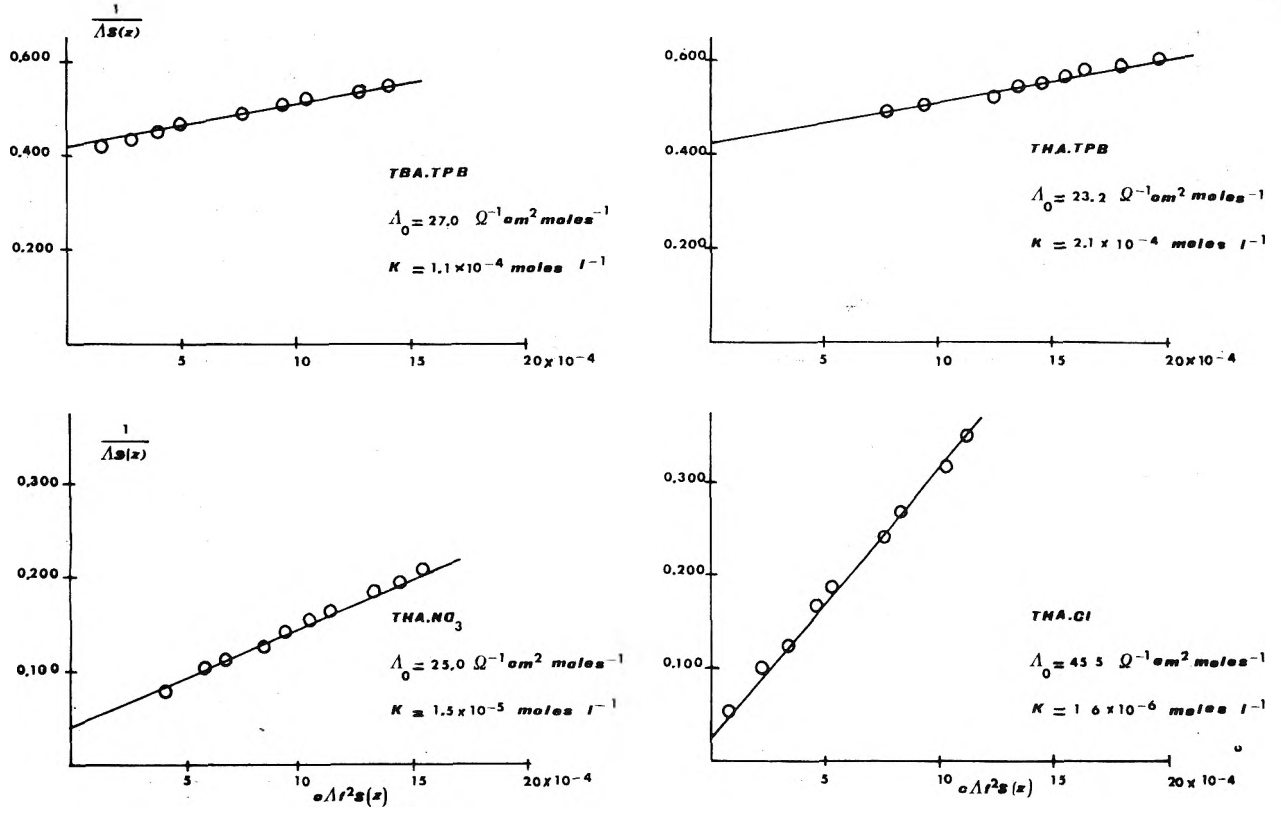

Figure 3. Shedlovsky plots of conductivity measurements in o-dichlorobenzene at 25°: Λ_0, limiting equivalent conductivity; *K*, ion pair dissociation constant.

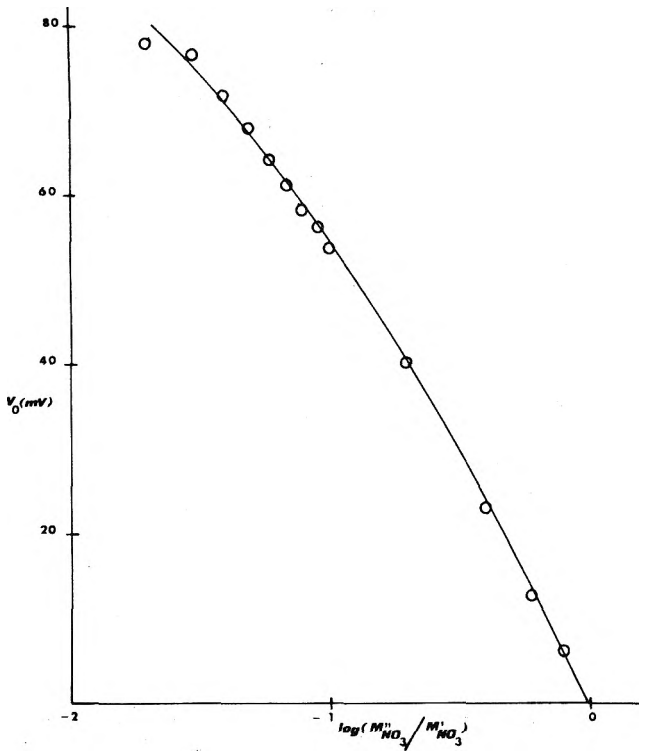

Figure 4. Open circles are experimental liquid membrane biionic potentials (V_0) *vs.* logarithm of nitrate ion concentration ratios in cell 9 with *o*-dichlorobenzene as solvent. The solid line has been calculated with eq 3 inserting the parameters reported in Table V.

TABLE VI: Conductometric Measurements in Nitrobenzene

	Λ_0 (Ω^{-1} cm^2 mol^{-1}) or λ_0 (Ω^{-1} cm^2 equiv^{-1})	K_{1s}(dissociation constant)
TBATPB	22.60	0.077
THATPB	20.50	0.099
$THANO_3$	34.40	0.019
THACl	44.80	0.018
TBA^+TPB^-	11.30	
THA^+	9.20	
NO_3^-	25.20	
Cl^{-3}	35.60	

Selectivity Factors[a]

$$K_{21} = \frac{k_2}{k_1}\frac{K_{1s}}{K_{2s}} = 4.0 \pm 0.5 \qquad \frac{k_2}{k^1} = 4.3 \qquad \bar{K}_{21} = \frac{u_{2s}}{u_{1s}} K_{21} = 4$$

$$P_{21}^* = 53 \pm 5 \qquad P_{21} = \frac{u_2 k_2}{u_1 k_1} = 3.1 \qquad \bar{P}_{21} = \frac{u_2 + u_s k_2}{u_1 + u_s k_1} = 3.2$$

[a] See footnote a, Table IV.

$\bar{K}_{21}$. Since the dissociation constants for $THANO_3$ and THACl (Table IV) are of the order of 10^{-7} we may consider the system strongly associated. The condition $(u_s c_s/\Sigma_i u_{is} \cdot c_{is}) \ll 1$ is then satisfied. In this case it is therefore possible to use eq 3 to analyze the experimental data. In Figure 2 the continuous line represents a V_0 *vs.* log (M_{NO_3}''/M_{NO_3}') curve calculated from eq 3 by using the parameters of Table IV. The same figure shows that the experimental data (black points) are rather well fitted by the theoretical equation. It has to be noted that, as a consequence of the high value of τ, the major contribution to the calculated membrane potential comes from the second term of eq 3. In

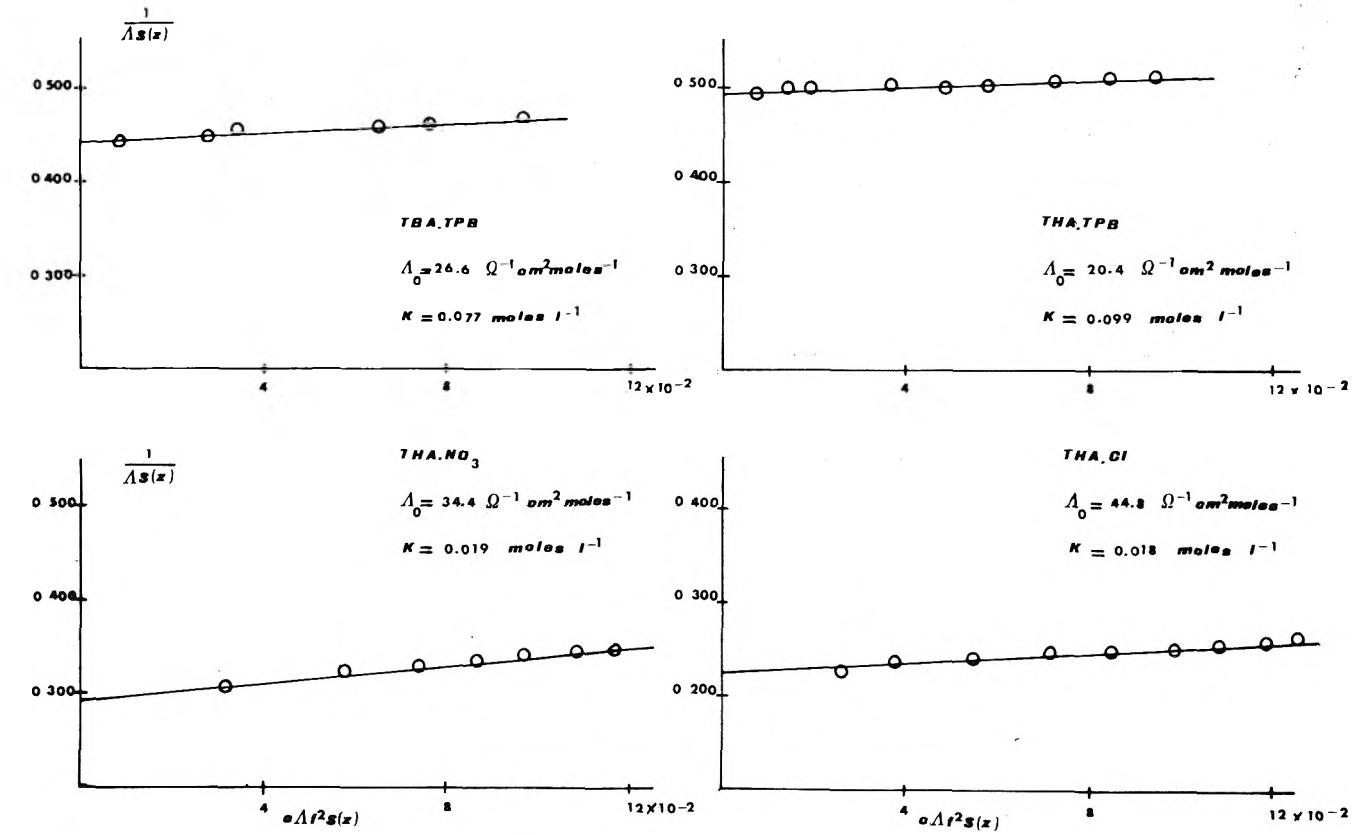

Figure 5. Shedlovsky plots of conductivity measurements in nitrobenzene at 25°: Λ_0, limiting equivalent conductivity; *K*, ion pair dissociation constant.

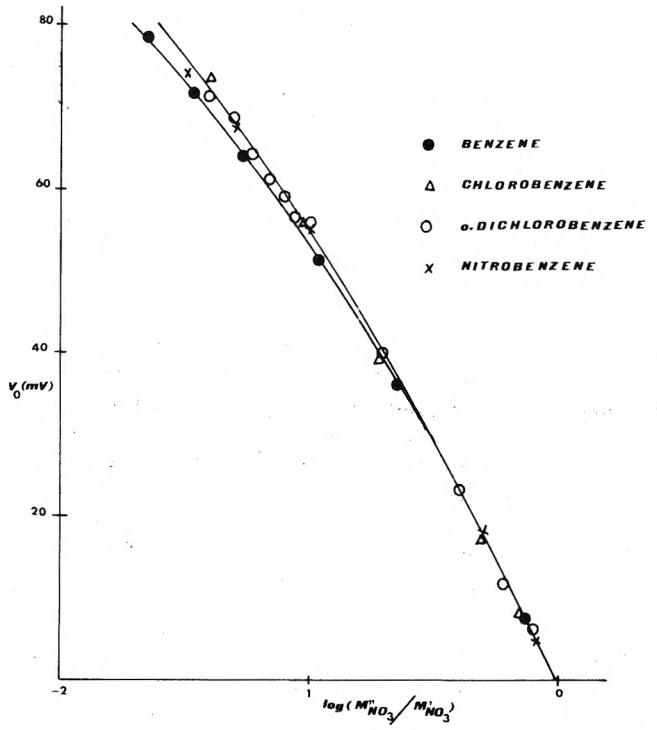

Figure 6. O, Δ, and × show experimental liquid membrane biionic potentials (V_0) *vs.* logarithm of nitrate ion concentration ratios in cell 9. ● show data from ref 9. The solid lines have been calculated with eq 10 with $P_{21}^* = 50$ (upper curve) and $P_{21}^* = 40$ (lower curve).

other words the contribution of the term due to the ion pairs predominates.

o-Dichlorobenzene. Conductometric measurements, Shedlovsky plots, and the values of the P_{21}, $\bar{P}_{21}$, $\bar{K}_{21}$, K_{1s} K_{2s}, λ^0, and τ parameters are reported in Table II, Figure 3, and Table V, respectively.

The order of magnitude of the ion pairs dissociation constants show that we are still dealing with a strongly associated system. The membrane potential will then be expressed again by eq 3. Figure 4 shows the good agreement between the calculated V_0 *vs.* log (M_{NO_3}''/M_{NO_3}') curve (obtained by inserting the parameters of Table V into eq 3) and the experimental data. As a consequence of the τ value ($\tau = 0.42$) both terms on right side of eq 3 contribute to the V_0 values. In agreement with the theoretical predictions the contribution of the ion pairs becomes less important as long as the dielectric constant of the diluent increases (in our case from 5.62 to 9.93).

Nitrobenzene. Conductometric measurements, Shedlovsky plots, and the values of the P_{21}, $\bar{P}_{21}$, $\bar{K}_{21}$, K_{1s}, K_{2s}, and λ^0 parameters are reported in Table III, Figure 5, and Table VI, respectively. The dissociation constants of the ion pairs show that we are dealing with a partially associated system. Therefore the condition $(u_s c_s/\Sigma_i u_{is} c_{is}) \ll 1$ is no more valid and eq 3 cannot be used.

Conclusions

Experimental evidence has been obtained which shows that the contribution of the mobility of the charged site and of the associated species to the electrical membrane potential are both significant. In the case of chlorobenzene the contribution of the associated species (the ion pairs) is quite predominant. These results confirm the validity of the theoretical approach followed in ref 2 (coupling of the ion distribution and of the ion diffusion processes) to obtain eq 3. This equation has also been obtained from a more general thermodynamic approach which includes the nonisothermal case.[4] Of course in the case of nitrobenzene eq 3 cannot be used as the condition of strong association is not verified. It is noteworthy that all the experimental potential data (see Figure 6) can be fitted by the empirical equation

$$(Fz_i/RT)V_0 = \ln \frac{a_1' + P_{21}^* a_2'}{a_1'' + P_{21}^* a_2''} \qquad (10)$$

with P_{21}^* (empirical selectivity factor) = 40–50. Therefore while K_{21} (chemical selectivity factor) varies from 47(chlorobenzene) to 4(nitrobenzene), there is no drastic solvent dependence of P_{21}^*. It is then possible to conclude that in our case the electrical selectivity of the liquid ion-exchange membrane is apparently solvent independent at least for benzene (see ref 9), chlorobenzene, *o*-dichlorobenzene, and nitrobenzene. The theory shows that this independence is produced (for chlorobenzene and *o*-dichlorobenzene) by a compensative effect of the various physicochemical parameters (mobilities and equilibrium constants) which contribute to the liquid membrane potential.

References and Notes

(1) F. Conti and G. Eisenman, *Biophys. J.*, **6**, 227 (1966).
(2) J. Sandblom, G. Eisenman and J. L. Walker, Jr., *J. Phys. Chem.*, **71**, 3862 (1967); **71**, 3871 (1967).
(3) G. Eisenman, *Anal. Chem.*, **40**, 310 (1968).
(4) G. Scibona, P. R. Danesi, and C. Fabiani, *J. Phys. Chem.* submitted for publication.
(5) P. R. Danesi, M. Magini, and G. Scibona, "Solvent Extraction Research," A. S. Kertes and Y. Marcus, Ed., Wiley, New York, N.Y., 1965, p 185.
(6) T. Shedlovsky, *J. Franklin Inst.*, **225**, 739 (1938).
(7) R. M. Fuoss and E. Hirsch, *J. Amer. Chem. Soc.*, **82**, 1013 (1960).
(8) P. R. Danesi, F. Salvemini, G. Scibona, and B. Scuppa, *J. Phys. Chem.*, **75**, 554 (1971).
(9) P. R. Danesi, G. Scibona, and B. Scuppa, *Anal. Chem.*, **43**, 1892 (1971).

Infrared and Ultraviolet Spectra of Adsorbed Diazines. Their Use in Acidity Determinations

Pierre Pichat

Institut de Recherches sur la Catalyse—C.N.R.S., 69626 Villeurbanne, France *(Received January 24, 1974)*

Publication costs assisted by Centre National de la Recherche Scientifique

The ir and uv spectra of three diazines adsorbed on silica, alumina, and silica–alumina samples have been examined. The ir spectra of 1,2-diazine (pyridazine) and 1,4-diazine (pyrazine) are not as informative as those of pyridine, but that of 1,3-diazine (pyrimidine) allows semiquantitative measurements of Lewis and Brönsted acid sites. The shifts of the $n \rightarrow \pi^*$ electronic transition bands support the ir results by showing the protonic acidity of silica–alumina but enable only a rough distinction between the solid samples. Finally, from the comparison of the adsorption of the three diazines one may conclude that the strength of the bonds formed between a basic molecule and an acid surface cannot be readily predicted from the pK_a and the first ionization potential of the base even if differences in molecular sizes are taken into account.

Introduction

Determination of the nature, strength, and number of acid sites on solids is important since in various reactions the catalytic properties of these solids depend on these sites and on their properties.[1] This determination raises the problem of the choice of the method and base employed. Ir studies of ammonia,[2] pyridine,[3] piperidine,[4] and methylpyridines[5] have been carried out, pyridine being the most widely used base. From the ir spectra of adsorbed pyridine the nature of the acid sites is readily deduced. Semiquantitative measurements of their numbers can also be made, essentially to compare different solid samples. The acid strength can be inferred from the frequencies of certain bands and mainly from the stability of the pyridine bands on heating and evacuation.

The present work was concerned with the ir spectra of the adsorbed diazines to determine whether any of these basic molecules may be used instead of pyridine in order to diversify the acidity measurements. On the other hand, it was of interest to determine whether the adsorption bond strength is related to the basic strength of the adsorbate, since the comparison between the diazines is not perturbed by steric factors. As the electronic transition $n \rightarrow \pi^*$ of the dissolved diazines is affected by the nature of the solvents,[6-11] the uv spectra of the adsorbed molecules were also investigated. Previously studied[12-14] silica, alumina, and silica–alumina samples whose surfaces present one or several types of adsorption sites for the diazines (OH groups and Lewis and Brönsted acid sites) were used.

Experimental Section

The silica, alumina, and silica–alumina samples were commercial materials (Aerosil Degussa, Aluminiumoxyd P Degussa, and Ketjen containing 14% alumina). Miscellaneous data on the properties of these materials may be found in ref 12–17.

1,2-Diazine (pyridazine) and 1,3-diazine (pyrimidine) from the Fluka Co. (purum grade) were distilled under vacuum into small bulbs. The contents of each bulb and the vapors of 1,4-diazine (pyrazine, Merck for synthesis) were thoroughly dried over Linde 5A molecular sieve before use.

For uv measurements, the powders were compressed by hand against the quartz window of a cell allowing treatment under various atmospheres or vacuum. The spectra were recorded by the reflectance technique using an Optica CF_4DR spectrophotometer provided with a Pulfrich integrating sphere. MgO was used as a reflectance standard.

For ir measurements, 10–30 mg of powder were compressed at 6000 kgf cm^{-2}. The resulting disks (18 mm diameter) were inserted in a quartz sample holder which was introduced into an ir cell as previously described.[18a] Spectra were recorded on a Perkin-Elmer Model 125 grating spectrophotometer flushed with H_2O and CO_2 free air. The reference beam was attenuated for silica–alumina samples.

Prior to adsorption of diazines, the samples, evacuated at room temperature, were heated in 160 Torr of O_2 for 4–5 hr at 400° and then evacuated overnight at 430 (silica, silica–alumina) or 800° (alumina). The uv and ir spectra were scanned after cooling the samples at room temperature.

Results

Uv Spectra.[18b] Figure 1 shows some of the spectra observed. Rough information on the type of bonding of the diazines adsorbed on different samples and hence on the nature of the adsorption sites may be drawn from the position of the $n \rightarrow \pi^*$ transition band. A band at a frequency close to that of a hydrocarbon solution corresponds to physical adsorption. Adsorption on surface hydroxyl groups or on Lewis acid sites results in spectra similar to those of aqueous or alcoholic solutions, since the frequency of the $n \rightarrow \pi^*$ band does not enable one to distinguish between hydrogen-bonded and coordinated diazines. The strong protonic acidity of the silica–alumina sample[13,14] is reflected by the quasidisappearance of the $n \rightarrow \pi^*$ band as in the case of diazine dissolved in a solution acidified with a protonic acid.

Ir Spectra. The spectra of adsorbed 1,3-diazine will be considered in detail first. Then, as they only give qualitative information, the spectra of the two other adsorbed diazines will be only briefly depicted (see miniprinted material).[18b]

For the vibrational modes 19a and 19b of 1,3-diazine the assignments are those of ref 20–22. These modes are expected in the 1400–1550-cm^{-1} region.

RESULTS JPC-8-1

430°C-pretreated silica and silica-alumina samples have surface OH groups, whereas 800°C-pretreated alumina samples are completely dehydroxylated. Infrared spectra of adsorbed pyridine have shown that Lewis acid sites occur on the alumina samples pretreated at high temperature and on the 430°C-pretreated silica-alumina samples (14). These latter samples also contain a maximum of Brönsted acid sites (14). In the following paragraphs the influence of these three types of adsorption sites (OH groups, Lewis and Brönsted acid sites) on the U.V. and I.R. spectra of the diazines will be examined.

U.V. spectra

The interaction of the n electrons of pyridine with a surface affects the $n \rightarrow \Pi^*$ electronic transition of this molecule. However the frequency of this transition is very close to that of the $\Pi \rightarrow \Pi^*$ transition so that its shift, though visible, is difficult to measure.

By contrast, it was expected that the sufficiently large separation between the $n \rightarrow \Pi^*$ and $\Pi \rightarrow \Pi^*$ transition bands in the spectra of diazines might be useful to characterize the acidity of catalysts by means of U.V. spectroscopy.

The wavelengths of the electronic transition $n \rightarrow \Pi^*$ of the three dissolved or adsorbed diazines are listed in table I. The position of the $\Pi \rightarrow \Pi^*$ band of the diazines is almost insensitive to the solvent and is equally scarcely affected by adsorption. Figure 1 presents spectra of adsorbed 1,3-diazine.

The $n \rightarrow \Pi^*$ transition band is significantly shifted by bonding of the diazines with alcohol or water molecules and even is submerged under the $\Pi \rightarrow \Pi^*$ transition band in the case of an acid solution. Similarly it depends on the adsorbent as well as on the quantity remaining adsorbed. The spectra of samples saturated with a diazine show a $n \rightarrow \Pi^*$ band at a frequency intermediate between those of the same diazine dissolved in a hydrocarbon and in alcohol. Desorption causes a shift to the wavelengths corresponding to the diazine dissolved in aqueous or alcoholic solutions. For silica-alumina, the original $n \rightarrow \Pi^*$ band becomes a shoulder and eventually disappears on desorption as in the case of an acid solution. Spectra similar to those observed on desorption can be obtained by progressive adsorption of small amounts of diazine (fig. 1). In the case of silica-alumina the first quantities adsorbed cause the appearance of the $\Pi \rightarrow \Pi^*$ band whereas the $n \rightarrow \Pi^*$ band constitutes only a suspicion of a shoulder. On the two other samples these bands occur concomitantly.

I.R. spectra - Band assignments : JPC-8-2

Silica and silica-alumina samples become completely opaque around 1250 cm^{-1}, whereas alumina samples remain transparent down to ca. 1000 cm^{-1}. Consequently only the bands corresponding to the modes ν (CH), 8a, 8b, 19a, 19b of the adsorbed diazines can be observed for the two first materials. In addition some other vibrational modes were detected in the case of alumina. The ν (CH) bands are not very intense, particularly for silica and silica-alumina, and generally their frequency shifts do not give meaningful information on the type of bonding between the diazine and the solid surface. Therefore the following paragraphs will be mainly restricted to the 8a, 8b, 19a and 19b ring modes.

1,2-diazine :

In the case of the adsorption on silica or alumina, all the bands considered in table III are only slightly shifted from their positions in the liquid state. In contrast the relative intensities of the 19a and 19b bands are considerably perturbed. In the region of the 8a and 8b vibrations, slightly apart from one another in the liquid, only one band occurs for 1,2-diazine adsorbed on silica (table III). This band may correspond to the superimposition of the vibrations 8a and 8b unequally shifted by adsorption ; alternatively it is possible that one of the vibration modes has such a weak intensity that it is not visible. On the contrary 1,2-diazine adsorbed on alumina shows a doublet (table III). Since the ratio of the optical densities of the components of this doublet is inverted as a result of the adsorption, the high frequency component is likely due to coordinated 1,2-diazine.

The spectrum of 1,2-diazine adsorbed on silica-alumina is a little more complex. The intensity and the behaviour of the 1445 cm^{-1} band may be explained if this band is assigned to the superimposition of the vibration modes due to weakly adsorbed, coordinately adsorbed 1,2-diazine and to 1,2-diazinium ions. This assignment is corroborated by the increase in intensity of the considered band as a result of the admission of a small amount of water vapor at room temperature onto a sample from which the 1,2-diazine has been removed at 150°C. Similarly the bands at 1574 and 1585 cm^{-1} are assigned as indicated in table III. Finally, the shift from 1636 to 1618 cm^{-1} of the broad band due to the vibration of the Si-O lattice on adsorption of 1,2-diazine may be ascribed to the presence of a band resulting from the formation of 1,2-diazinium ions.

1,3-diazine : JPC-8-3

Because of the symmetry of the molecule, the vibrational modes 8a and 8b are infrared inactive in the liquid (27) and solid (28) states. They equally do not occur in the adsorbed state.

The modes 19a and 19b are not significantly displaced from their position in the liquid (table IV). In the case of silica and alumina the ratio of the optical density of the 19b mode to that of the 19a mode is considerably increased. This result is not unexpected since the 19a mode has a weak intensity for the solid and is equally not always observed in complexes of 1,4-diazine (29,31). The increased intensity and the behaviour of the 1485 cm^{-1} band of 1,4-diazine adsorbed on silica-alumina show that this band is partly due to the 19b mode and/or 19a mode of 1,4-diazinium ions, since the corresponding chloride adsorbs at 1460 and 1481 cm^{-1} (32). The 8b mode of 1,4-diazinium ions, expected around 1590 cm^{-1} (32), gives rise to only a very weak band ; however this may be caused by the possible decrease in the intensity of this vibration mode in the adsorbed state. Moreover, the formation of 1,4-diazinium ions on silica-alumina is confirmed by the observation of a ν (CH) band at ca. 3120 cm^{-1} as in 1,4-diazinium chloride (32).

For alumina the spectrum contains a weak band around 1230 cm^{-1}. This band also occurs in metallic complexes (27,29) and has been ascribed to the 9a mode infrared inactive in the liquid state. Its observation tends to indicate that the D_{2h} symmetry is partly perturbed for 1,4-diazine coordinately bonded on alumina.

Changes in OH groups :

Adsorption of the diazines on silica and silica-alumina causes a decrease in the OH band at ca. 3745 cm^{-1} and a new ν (OH...N) band, very intense and broad, occurs around 3225 - 3250 cm^{-1}, which supports the existence of hydrogen-bonded diazines.

Adsorption bond strength :

In table V are indicated the upper limit temperatures at which the 3 solids are capable of holding diazine molecules. In the case of 1,3-diazine, the I.R. bands of the protonated molecules disappear on evacuation at approximately 250°C (fig. 3d).

JPC-8-5

TABLE I: Wavelengths (in nm) of the electronic transition $n \rightarrow \Pi^*$ of dissolved or adsorbed diazines.

Diazine	Solvent				Adsorbent		
	Hydrocarbon (11)	Alcohol (11)	H_2O (11)	Acid (8)	Silica	Alumina	Silica-Alumina
1,2	340	311	300	(19)	325-305	325-305	325-285 and (19)
1,3	298,5	280	271	(19)	290-270	290-270	290-270 and (19)
1,4	328	310	305	(19)	316-302	316-302	320-300 and (19)

TABLE II: Frequencies (in cm^{-1}) of 1,2-diazine (pyridazine).

Modes (26)	Liquid	On Silica	On Alumina	On Silica-Alumina	Presumed adsorption sites
9a-14-15	1061,5		1060		L (25)
3-14	1281		1286		L
19 b	1412,5	1416	1416	1415	OH and/or L
19 a	1443,5	1445	1444	1445	OH and/or L, H^+
				1550	H^+
8 b	1563,5	1573	1573	1574	OH and/or L
8 a	1571		1585	1585	L and/or H^+
				(1618)	H^+

TABLE IV: Frequencies (in cm^{-1}) of 1,4-diazine (pyrazine) JPC-8-4

Modes (27)	Liquid	Solid	On Silica	On Alumina	On Silica-Alumina	Presumed adsorption Sites
13a	1130	1130		1130		L (25)
combination	1149	1152		1150		L
9a				1230		L
19b	1411	1418	1420	1420	1420	OH and/or L
19a	1483	1498	~1485	1485	1485	OH and/or L, H^+

TABLE V: Approximate upper limit temperatures (θ_u) at which the 3 solids are capable of holding diazine molecules after evacuation for 15 h.

Diazine	Silica	Alumina	Silica-Alumina
1,2	35	150	200
1,3	125	250	350
1,4	50	200	300

The 19a mode gives rise to only one band around 1405–1415 cm^{-1} (Figures 2 and 3 and Table II) in the case of hydrogen-bonded 1,3-diazine (on silica and partly on silica–alumina) as well as in the case of coordinately bonded 1,3-diazine (on alumina and partly on silica–alumina). This band has a slightly higher frequency than the corresponding band of 1,3-diazine in CCl_4 (1399.5 cm^{-1}). The correspondence between the frequencies of hydrogen and coordinately bonded 1,3-diazine is not unexpected. For example, the frequency of 1,3-diazine in aqueous solution (1406 cm^{-1})[23] is very close to that of the complexes $Hg(C_4H_4N_2)X_2$ (1410 cm^{-1} for X = Cl, 1405 cm^{-1} for X = Br).[24] In contrast the protonation of the 1,3-diazine causes a substantial shift of vibration 19a (1457 cm^{-1} for the 1,3-diazinium chloride).[24] Therefore the band at 1456 cm^{-1} in the case of silica–alumina (Figure 3) may be assigned to the formation of 1,3-diazinium species.

The 19b mode produces a band around 1470–1476 cm^{-1}. Other features of the spectra show that this band is due to hydrogen bonded (on silica and silica–alumina) or to coordinately bonded 1,3-diazine (on alumina and silica–alumina). Its frequency is close to that of 1,3-diazine in aqueous solution (1469 cm^{-1})[23] and higher than that of the liquid (1466 cm^{-1}) or of 1,3-diazine complexed with Hg^{2+} ions (1458–1462 cm^{-1}).[24] The spectrum of protonated 1,3-diazine contains a band of middle intensity between 1517 and 1537 cm^{-1}.[24] Therefore the 1532-cm^{-1} band of 1,3-diazine adsorbed on silica–alumina (Figure 3) may be attributed to the formation of diazinium ions. However, this band has a weaker intensity that the one at 1456 cm^{-1} and almost vanishes on evacuation at 150° (Figure 3).

Assignment of modes 8a and 8b in the region 1650–1550 cm^{-1} is more tentative. The bands corresponding to these two modes overlap in the spectrum of 1,3-diazine dissolved in CCl_4.[21] The 8b mode is less sensitive to variations in charges on the nitrogen atom than the 8a mode. Consequently the lower frequency bands in this region probably correspond to the 8b mode. For silica only one band is found at 1590 cm^{-1}, however, this band is broadened toward the low frequencies with a shoulder at 1567 cm^{-1} (Figure 2). Hence it seems that the intensity of vibration 8b for hydrogen-bonded 1,3-diazine is very weak and that the band around 1565 cm^{-1} observed for alumina and silica–alumina (Figures 2 and 3) is mainly due to the 8b mode of the coordinated diazine. The 8b vibration of the 1,3-diazinium ion occurs between 1580 and 1605 cm^{-1}.[24] In the case of silica–alumina, no band resistant to evacuation at 150° is observed in this region. However, it is possible that the band at 1608 cm^{-1} may be partly due to 1,3-diazinium ions.

The 1590-cm^{-1} band of 1,3-diazine adsorbed on silica is assigned to vibration 8a of hydrogen-bonded diazine, as well as the 1584-cm^{-1} band for silica–alumina (Figures 2 and 3). The absorption at 1595–1600 cm^{-1} for alumina is assigned to coordinately bonded 1,3-diazine, and the corre-

TABLE II: Frequencies (in cm^{-1}) of 1,3-Diazine (Pyrimidine)

Modes[a]	Liquid or in CCl_4[c]	On silica	On alumina	On silica–alumina	Presumed adsorption sites
15	1158.5		1165		L[b]
3	1226		1228		L
19a	1399.5*	1415	1408	1414	OH and/or L
				1456	H^-
19b	1466	1470	1470	1476	OH and/or L
				1532	H^+
		1567 sh	1565	1564	OH and/or L
8a, 8b	1567.5*				
		1590		1584	OH
			1600	1608	L and/or H^+
				1626	H^+

[a] Reference 21. [b] Reference 25. [c] The frequencies marked with in asterisk were measured in CCl_4.

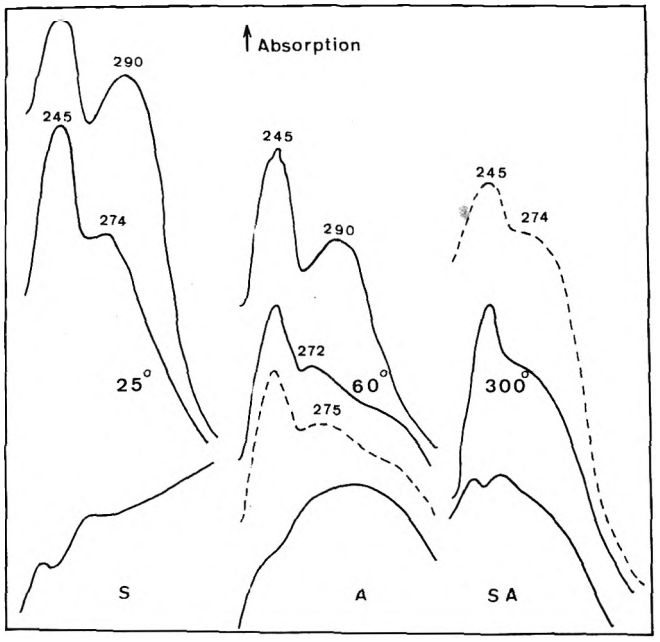

Figure 1. Uv spectra of 1,3-diazine adsorbed on silica (S), alumina (A), and silica–alumina (SA): lower spectra, bare samples; upper continuous spectra, after adsorption (vapor pressure) at room temperature; intermediate spectra, after subsequent evacuation at indicated temperatures for 1 hr; dashed spectra, adsorption of a small amount of 1,3-diazine at room temperature. Wavelengths in nm. In the figures of this paper, spectra are displaced for purpose of display.

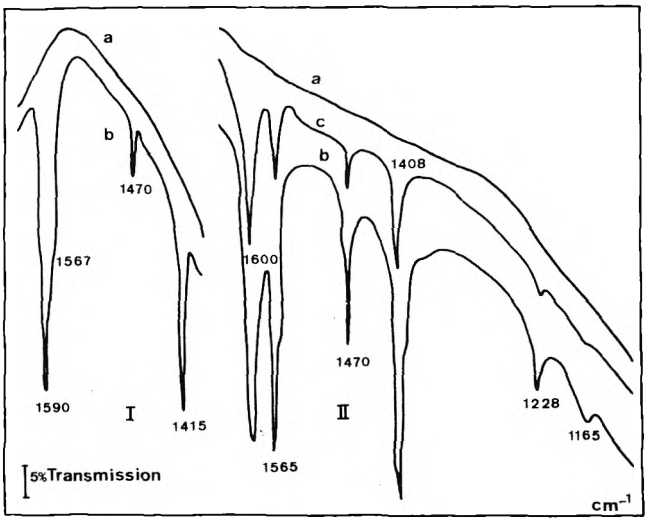

Figure 2. Ir spectra of adsorbed 1,3-diazine: spectrum Ia, 800° treated silica; Ib, after adsorption of 1,3-diazine at 25° for 1 hr, then desorption at 25° for 10 min; IIa 800°-treated alumina IIb, after adsorption of 1,3-diazine at 25° for 2 hr; IIc ther after desorption at 150° for 3 hr.

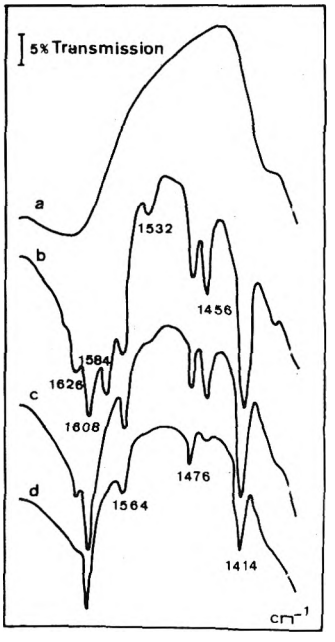

Figure 3. Ir spectra of 1,3-diazine adsorbed on silica–alumina: (a) 430° treated sample; (b) after adsorption of 1,3-diazine at 25° for 1 hr, then desorption at 25° for 3 hr; (c) at 150° for 2 hr; (d) at 250° for 1 hr.

sponding band for silica–alumina is at 1608–1610 cm^{-1}. Like mode 19a, mode 8a of coordinately adsorbed 1,3-diazine has a higher frequency (+10 to +20 cm^{-1}) than coordinated 1,3-diazine in solid complexes.[24] However, this shift does not seem to cast a doubt on the assignment. 1,3-Diazinium ions absorb in the 1620–1630-cm^{-1} range. The spectrum of adsorbed 1,3-diazine adsorbed on silica–alumina presents a band at 1626 cm^{-1} which may be due to 1,3-diazinium ions. This band disappears on evacuation at 200°.

The transparency of alumina also permits the observation of bands at 1228 and 1165 cm^{-1} which correspond to bands at slightly lower frequencies in the spectrum of liquid 1,3-diazine (Table II).

Discussion and Conclusion

The uv spectra of the diazines adsorbed on silica–alumina confirm the strong protonic acidity of this catalyst. On the other hand, no marked differences are observed be-

TABLE VI: Comparison between the Absorption Bond Strength, the pK_a, and the First Ionization Potential of Pyridine and the Three Diazines

Adsorption bond strength	Pyridine > 1,3-diazine > 1,4-diazine > 1,2-diazine
pK_a[a]	Pyridine (5.25) > 1,2-diazine (2.3) > 1,3-diazine (1.3) > 1,4-diazine (0.6)
First ionization potential, eV[a]	Pyridine (9.8) > 1,2-diazine (9.83) > 1,3-diazine (9.9) > 1,4-diazine (10.1)

[a] Reference 33.

tween the uv spectra of the diazines adsorbed on alumina or silica, probably because the electron transfers are similar for adsorption on Lewis acid sites or on OH groups. However, the stronger adsorption on alumina than on silica is reflected by the upper limit temperature at which the uv bands of adsorbed diazines subsist. In this respect it is noteworthy that the uv bands are even a more sensitive means of detecting adsorbed diazines than the ir bands.

In summary the uv spectra of adsorbed diazines provide an interesting confirmation of the acidity of adsorbents but permit only a rough distinction between different adsorbents.

From the ir spectra of adsorbed 1,4-diazine the existence of protonic sites (3120-cm^{-1} band, ratio of the intensities of the 1485- and 1420-cm^{-1} bands) and of Lewis acid sites (1230-cm^{-1} band) can be inferred. However, quantitative measurements of the two types of acid sites are not possible.

The ir spectra of adsorbed 1,2-diazine supply valuable qualitative information. Nevertheless, despite a greater number of bands than in the case of 1,4-diazine, they cannot be used for quantitative measurements either (see miniprinted material).[18b]

By contrast, key bands of adsorbed 1,3-diazine may be utilized for semiquantitative measurements analogous to those made with pyridine, provided hydrogen-bonded molecules have been evacuated. This may be a useful tool to facilitate correlations between acidity and catalytic activity in various reactions in so far as the results obtained by using a sole basic molecule, corresponding to a given range of acidity strength, may be insufficient to interpret the catalytic phenomenon.

The order of bond strength between the three diazines and the three adsorbents is that given in the first line of Table VI. A previous study[14] has shown that pyridine is more strongly held than the diazines by the adsorbents considered here. The question is raised whether the bond strength between the basic molecules and the solid surfaces may be related to the pK_a of these bases in aqueous solutions. From the comparison of the first and second lines of Table VI it may be inferred that if the pK_a of pyridine may explain the strong adsorption of this molecule, the pK_a of the diazines do not enable one to predict the adsorption strength of these molecules.

Similarly the order of the first ionization potentials of the diazines, which might express the capability of these bases to release the electron transferred (partially or not) to the surface electrophilic site, does not correspond to the order of adsorption bond strength (first and third lines of Table VI). It might be useful to consider the second ionization potentials of the diazines. Unfortunately, to our knowledge, these potentials have not been determined.

Steric hindrance has been suggested to explain discrepancies between the order of adsorption bond strength and the order of pK_a.[5] In the present case the molecular sizes of the three diazines are very similar, so this reason cannot be invoked. On the other hand, the relative location of the nitrogen atoms in the heterocycles will most likely play a part in the bond stabilities and this may explain the unexpected behavior of 1,2-diazine. These data point out that the adsorption bond strength of basic molecules cannot be readily predicted from the molecular constants (such as, pK_a and first ionization potentials) even if differences in molecular sizes are taken into account. Presumably, these molecular constants do not reflect sufficiently the electronic structure of the basic molecules in order to be used without precaution in the case of the interaction of these molecules with a solid surface.

Acknowledgment. The author thanks Drs. M. V. Mathieu and B. Imelik for encouragement and Mrs. M. C. Bertrand for excellent help in the experimental work.

Miniprint Material Available. Full-sized photocopies of the miniprinted material from this paper only or microfiche (105 × 148 mm, 24× reduction, negatives) containing all of the miniprinted and supplementary material for the papers in this issue may be obtained from the Journals Department, American Chemical Society, 1155 16th St., N.W., Washington, D. C. 20036. Remit check or money order for $3.00 for photocopy or $2.00 for microfiche, referring to code number JPC-74-2376

References and Notes

(1) K. Tanabe, "Solid Acids and Bases, Their Catalytic Properties," Kodansha, Tokyo, New York, N.Y., 1970.
(2) W. A. Pliskin and R. P. Eischens, *J. Phys. Chem.*, **59**, 1156 (1955); *Advan. Catal.*, **10**, 1 (1958).
(3) E. P. Parry, *J. Catal.*, **2**, 371 (1963).
(4) T. R. Hughes and H. M. White, *J. Phys. Chem.*, **71**, 2192 (1967).
(5) H. Knozinger and H. Stolz, *Ber. Bunsenges. Phys. Chem.*, **75**, 1055 (1971).
(6) F. Halverson and R. C. Hirt, *J. Chem. Phys.*, **17**, 1165 (1949); **19**, 711 (1951).
(7) G. J. Brealey and H. Kasha, *J. Amer. Chem. Soc.*, **77**, 4462 (1955).
(8) S. F. Mason, *J. Chem. Soc.*, 1240 (1959); 1247 (1959).
(9) V. G. Krishna and L. Goodman, *J. Chem. Phys.*, **33**, 381 (1960); *J. Amer. Chem. Soc.*, **83**, 2042 (1961).
(10) H. Linnell, F. Raab, and R. Clifford, *J. Phys. Chem.*, **68**, 1999 (1964).
(11) M. A. Kovner and S. K. Potapov, *Russ. Chem. Rev.*, **36**, 620 (1967), and references therein.
(12) P. Pichat, J. Kermarec, J. Fraissard, and M. V. Mathieu, *Bull. Soc. Chim. Fr.*, 3652 (1966).
(13) P. Pichat, M. V. Mathieu, and B. Imelik, *J. Chim. Phys.*, **66**, 845 (1969).
(14) P. Pichat, M. V. Mathieu, and B. Imelik, *Bull. Soc. Chim. Fr.*, 2611 (1969).
(15) J. Bandiera and C. Naccache, *Bull. Soc. Chim. Fr.*, 2637 (1969).
(16) F. Figueras, A. Nohl, L. de Mourgues, and Y. Trambouze, *Trans. Faraday Soc.*, **67**, 1155 (1971).
(17) D. Ballivet, D. Barthomeuf, and P. Pichat, *J. Chem. Soc., Faraday Trans. 1*, **68**, 1712 (1972).
(18) (a) M. V. Mathieu and P. Pichat in "La Catalyse au Laboratoire et dans l'Industrie," B. Claudel, Ed., Masson and Cie, Paris, 1967, p 319. (b) See paragraph at end of text regarding miniprint material.
(19) The $n \rightarrow \pi^*$ transition is masked by the $\pi \rightarrow \pi^*$ transition.
(20) G. Sbrana, G. Adembri and S. Califano, *Spectrochim. Acta*, **22**, 1831 (1966).
(21) R. Foglizzo and A. Novak *J. Chim. Phys.*, **64**, 1484 (1967).
(22) A. Jacques Lafaix and J. M. Lebas, *Spectrochim. Acta, Sect. A*, **26**, 1243 (1970).
(23) H. Takahashi, K. Mamola, and E. K. Plyler, *J. Mol. Spectrosc.*, **21**, 217 (1966).
(24) R. Foglizzo and A. Novak, *Spectrochim. Acta, Sect. A*, **26**, 2281 (1970).
(25) Lewis acid sites.
(26) Assignment of the modes is disputed. See the following articles: R. C. Lord, A. L. Marston, and F. A. Miller, *Spectrochim. Acta*, **9**, 113 (1957);

V. I. Berezin, *Opt. Spectrosc.*, **18**, 71 (1965); H. D. Stidham and J. V. Tucci, *Spectrochim. Acta, Sect. A*, **23**, 2233 (1967); K. K. Innes, J. P. Byrne, and I. G. Ross, *J. Mol. Spectrosc.*, **22**, 125 (1967); L. Sebagh and J. Zarembowitch, *J. Chim. Phys.*, **69**, 249 (1972); ref 11 and 23.
(27) L. Sebagh and J. Zarembowitch, *J. Chim. Phys.*, **66**, 1974 (1969), and references therein.
(28) S. Califano, G. Adembri, and G. Sbrana, *Spectrochim. Acta*, **20**, 385 (1964).
(29) A. B. P. Lever, J. Lewis, and R. S. Nyholm, *J. Chem. Soc.*, 1235 (1962); 3156 (1963); 5042 (1963).
(30) H. D. Stidham and J. A. Chandler, *J. Inorg. Nucl. Chem.*, 27, 397 (1965).
(31) J. R. Ferraro, C. Cristallini, and G. Roch, *Ric. Sci.*, **37**, 435 (1967); J. R. Ferraro, J. Zipper, and W. Wozniak, *Appl. Spectrosc.*, **23**, 160 (1969).
(32) R. Foglizzo and A. Novak, *Appl. Spectrosc.*, **24**, 601 (1970).
(33) G. Briebleb, "Elektronen-Donator-Acceptor-Komplexe," Springer-Verlag, Berlin, 1961, p 156.

On the Thermochemical State of Gaseous Electron Diffraction Samples

K. L. Gallaher and S. H. Bauer*

Department of Chemistry, Cornell University, Ithaca, New York 14850 *(Received May 17, 1974)*

The mean internuclear distances derived from gas-phase electron diffraction patterns are a function of the sample temperature. However, for uniconformational molecules which do not undergo large amplitude motions this dependence is slight, so that the assumption that the sample temperature is equal to the nozzle temperature generally introduces errors which are less than those from other sources inherent in the experiment. When the amplitudes of vibration are large, or when conformational changes occur with low activation energies, the measured root mean square amplitudes and the relative proportions of conformers are sensitive to the sample temperature, which clearly is less than that of the nozzle. Generalized contour maps (in dimensionless parameters) have been computed for the density and temperature distributions in free jets, such as are normally used in electron diffraction experiments, covering a range of heat capacity ratios. Even though the computer programs were written for ideal gases (constant C_p and γ) and thus do not strictly conform to the situation in electron diffraction jets, the results do permit an analysis of the kinetic and thermochemical states for typical cases of current interest. We conclude that for unsymmetrical molecules with more than five atoms vibrational relaxation occurs in the jet, but only partial chemical relaxation takes place to an extent determined by the internal contour of the nozzle, even for activation barriers as low as 2 kcal/mol. The critical experimental parameters which have not been adequately controlled in most electron diffraction units are the size of the electron beam as the jet, the displacement of its axis above the nozzle lip, and the internal contour of the nozzle exit section.

Introduction

For the determination of molecular structures by gas-phase electron diffraction the sample is injected as a free jet through a small hole (0.2–0.7 mm) from a source pressure of 1–30 Torr, into an evacuated diffraction chamber, generally operated at 10^{-6} Torr. The probing electron beam, approximately 200 μm in diameter at the nozzle, skims the tip at a distance approximately equal to the nozzle aperture. The jet-crossed-beam technique for sampling has proved to be the simplest yet devised, and the most free of perturbing effects, even though during the past 4 decades a variety of enclosures were tested. To the nonpractitioner this is surprising because of the obvious drawbacks characteristic of a free jet. (a) The unavoidable spreading of the sample reduces the sharpness of the diffraction pattern. Concurrently, the increase of ambient pressure in the diffraction unit may lead to multiple scattering which has a complex angular dependence, thus considerably changing the background level.[1,2] Nozzles have been designed to channel the gas flow, and diffraction chambers are constructed so as to contain the ejected gas by means of tubes, and liquid nitrogen cooled surfaces placed close to the region of diffraction.[3] However, experience shows that the measured interatomic distances are little affected by the finite sample spread, whereas analysis indicates that such spreading should increase the measured root mean square amplitudes of vibration by $\Delta l_{ij} \approx \epsilon/l_{ij}$, where $\epsilon \propto r_{ij}^2\delta^2/L^2$ (δ is a measure of the width of sample distribution and L is the nozzle-to-plate distance). Fortunately, Δl is relatively insensitive to the exact shape of the distribution function, as long as the jet expands *symmetrically* about the nozzle axis.[2,4,5] (b) Since the gas sample expands rapidly upon entering the evacuated diffraction chamber its temperature and density decrease, as it passes from a fluid flow regime to a free molecule regime. The measurement and computation of temperature, density, and composition profiles of such jets have been the subject of many studies by those interested in supersonic molecular beams.[6-12] During the past 5 years electron diffraction analyses of crystallites generated in condensed supersonic molecular beams have been made for Ar and Xe;[13] similar work on the structure of water polymers is in progress.[14] CO_2 dimer formation in free jets was detected mass spectrometrically.[15] An interesting recent demonstration of the consequences of cooling in supersonic jets was presented by Klemperer, *et al.*[16] They found that from an effusive source at 25°, a molecular beam of 2,3-dichloro-1,3-butadi-

ene has a polar component, indicative of a less stable isomer, 3 kcal/mol above the nonpolar form. However, there were no polar isomers in a beam from a supersonic jet, because the higher energy species relaxed to the more stable conformation.

Although those concerned with the determination of the dynamic structures of small molecules have raised the question as to what are the effective temperature and the condition of the sample at the point of diffraction,[17-21] in no case in which the authors compared their calculated and measured l_{ij}'s was the difference in temperature between the gas sample and the nozzle taken into account, not in the structure determination nor in the discussion of errors. Within current estimated error limits on both theory and practice, the measured root mean square amplitudes of vibration for many molecules apparently check those computed,[22] but it is not entirely clear that a cancellation of errors had not occurred. When the measured l_{ij}'s are reduced by 3–8% to allow for sample spread and other systematic error which reduce contrast *internal* inconsistencies sometimes appear. For selected molecules the measured l_{ij}'s agree with those calculated for some atom pairs, but are sometimes less than and sometimes greater than those calculated for other atom pairs. Qualitatively, one may argue that for small rigid molecules the vibration–translation relaxation process requires hundreds of collisions; hence to an adequate approximation one may assume that the population distribution of vibrational states in the diffracting sample corresponds to the nozzle temperature. However, when the molecules under consideration have large amplitudes of vibration,[19,21,23-26] or when they participate in association–dissociation equilibria[20,27-29] or conformational transformations,[21,30-33] such that as few as ten collisions may alter the population distribution, one should consider relaxation of the system during its passage through the nozzle, and on to the point of diffraction, where the sample temperature is clearly lower. There is an additional difficulty when a rapid dissociation–association reaction occurs, the possibility of mass separation due to the differential spreading in the jet → beam of species of different molecular weights; this occurs because they have different molecular velocity distributions for the same stream velocity.[34]

We undertook the following analysis to ascertain whether the multitudinous gas-dynamic literature on free jets and nozzle flow provides computational techniques which can be utilized for the solution of the electron diffraction sampling problem. Programs are available which generate the flow fields for free jets of fluids with constant heat capacity ratios (γ); also, programs have been written for convergent and supersonic divergent nozzle flow with reacting fluids in thermochemical equilibrium, and approximate solutions were developed for nonequilibrium nozzle flow. However, the case of a variable γ fluid in free flow has not been treated except by an approximation which replaces the unknown axial distribution in the jet by an equivalent axial distribution in a divergent nozzle. In this report we present a set of dimensionless plots of temperature, density, and collision number profiles for the constant γ, free jet case, and a qualitative analysis of the molecular dynamics that determines the measured root mean square amplitudes of vibration. In a subsequent paper we shall treat the case of bimolecular associations that require either binary or ternary collisions. An approximate treatment for the latter case (the dimerization of alkali atoms) was presented by Gordon, Lee, and Herschbach.[35] At this stage it is evident that, while approximate corrections for the cooling effect in electron diffraction jets can and should be made, further developments in gas dynamics and measurement of chemical kinetic parameters are needed to provide an accurate description of what takes place in the flow regime between the reservoir and the electron beam for floppy or sticky molecules.

Calculations

The numerical method of characteristics was used to compute the flow fields for an inviscid, near-sonic, axially symmetric, irrotational free jet directed into a vacuum. The restrictions on the fluid are (a) that its equation of state be of the form $p = \rho RT$; (b) that over the operational temperature range its specific enthalpy be expressible as $h(T) = h_0 + c_p T$, with c_p and γ ($\equiv c_p/c_v$) independent of T. The procedure used was first described by Owen and Thornhill;[12] it is essentially the same as those developed by Wolf[36] and Anderson.[37] The method of characteristics leads to the flow Mach number (M) as a function of *dimensionless* coordinates $\chi \equiv x/D$ and $\boldsymbol{R} \equiv R/D$ (x is the axial distance from the nozzle tip, R is the perpendicular (radial) distance from the nozzle axis, and D is the nozzle diameter).

Details to supplement the following brief description are available in a number of sources.[12,38-42] The method of characteristics is a "boot strap" procedure which leads to a lattice of points, P_{ij}, defined by the intersection of two families of characteristic lines (ϵ and η in Figure 1), at which the flow Mach numbers (M) are computed as a function of the χ, $\boldsymbol{R}$ dimensionless coordinates. In supersonic flow, if flow conditions are known at two points, $P_{i,j+1}$ and $P_{i+1,j}$, flow conditions may be calculated for $P_{i+1,j+1}$, at the intersection of the two "characteristic lines" originating from the known points.

The computation begins by finding the Mach number and the direction of flow (θ) with respect to the nozzle axis, at $(n + 1)$ equally spaced points (we used $n = 400$) $P_{1,j}$ ($j = 0, 1, 2, \ldots, n$) along the leading characteristic line, which is the first of the η family. $P_{i,0}$ ($i = 1, 2, \ldots$) designates a set of equally spaced two-dimensional expansion rays that originate at the nozzle lip, and specify the initial flow conditions for all η lines. No solution is available for the case when $M = 1$ at the leading characteristic (in which case it would be perpendicular to the nozzle axis). Hence a Mach number slightly greater than one is chosen (we used $M_0 = 1.01$). The leading characteristic is then a line of points extending from $P_{1,0}$ at the nozzle lip to $P_{1,n}$ at the nozzle axis with $\chi_{1n} = \frac{1}{2}(M_0^2 - 1)^{1/2}$.

With M (χ; $\boldsymbol{R}$) known, the interesting gas kinetic parameters can be calculated at any point.

$$\frac{T(\chi; \boldsymbol{R})}{T_0} = \frac{1}{1 + [(\gamma - 1)/2]M^2} \tag{1}$$

(where the subscript zero corresponds to conditions at $\chi = 0$; the flow is just sonic at the plane of the nozzle exit).

$$\rho(\chi; \boldsymbol{R})/\rho_0 = (T/T_0)^{1/(\gamma-1)} \tag{2}$$

$$Z_{11}/Z_{11}^{\circ} = (\rho/\rho_0)(T/T_0)^{1/2} \tag{3}$$

$Z_{11} = (1/\sqrt{2})\pi n \sigma^2 \bar{v}$, is the hard sphere approximation (mean radius σ) for the number of (self) collisions *per* second per unit volume, when the number density is n; the thermal velocity if $\bar{v} = (8RT/\pi M)^{1/2}$. On dividing Z_{11} by the local streaming velocity one obtains $\langle Z \rangle$, the mean

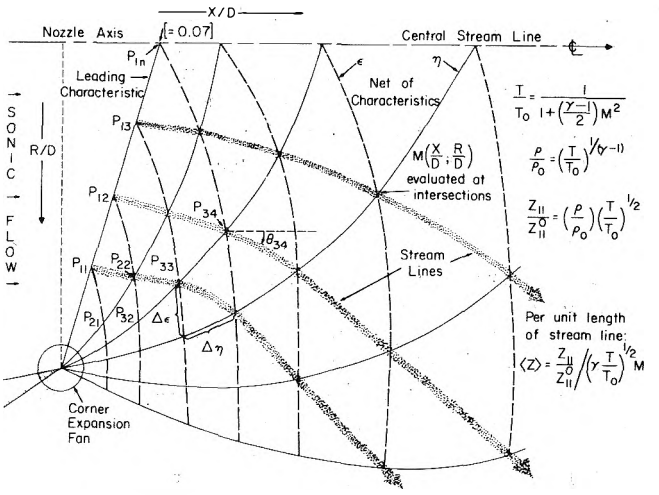

Figure 1. Schematic of ϵ, η net of characteristics for computing $M(x/D; R/D)$ in a supersonic expansion flow field.

number of collisions per unit length of travel along that stream line; in dimensionless units

$$\left(\frac{Z_{11}}{Z_{11}^0}\right)\Big/\left(\gamma\frac{T}{T_0}\right)^{1/2} M$$

$$Z_{tot}' \equiv \int_{streamline}\left(\frac{Z_{11}}{Z_{11}^0}\right)dl' \approx \sum_{streamline}\left(\frac{Z_{11}}{Z_{11}^0}\right)\Delta l' = \frac{Z_{tot}}{Z_{11}^0(D\sqrt{M/RT_0})} \quad (4)$$

Z_{tot}' $(\chi; \boldsymbol{R})$ measures the total number of collisions which an average molecule at $(\chi; \boldsymbol{R})$ has undergone after leaving the leading characteristic line.

$$dl' \equiv \frac{dl}{D\sqrt{M/RT_0}} \approx \left[\Delta\left(\frac{x}{D}\right)^2 - \Delta\left(\frac{R}{D}\right)^2\right]^{1/2}\Big/\left(\gamma\frac{T}{T_0}\right)^{1/2} M \quad (5)$$

dt' is a "dimensionless time" element. The numerator in the right member of (5) is the distance between successive points on a given streamline. Thus Z_{tot}' is a "dimensionless total collision number."

The contours shown in Figures 2–6 are "universal solutions," valid in the region upstream from the Mach disk, as long as the pressure within the jet is an order of magnitude greater than the background pressure. Of course, the source pressure must be sufficiently high so that the molecular mean free path at the nozzle lip is an order of magnitude less than the nozzle diameter (invicid fluid flow).[37] (The last restriction may not be satisfied under all experimental conditions used for electron diffraction experiments, because of low source pressures.) An experimental check on this calculation for N_2,[39] with D = 0.795 mm and p_0 = 10 Torr, showed that the Mach number generated along the axis agreed with the theory up to $\chi \approx 3$. That point, our calculations show, corresponds to the end of the continuum → free flow transition.

The final question to consider relative to nozzle flow is the pressure drop produced by the internal structure of the nozzle. It is good to maximize conductance up to the nozzle lip by using a conical bore; the internal contour of the nozzle is an important feature. However, since hypodermic needles are used in many laboratories, we applied the Poiseuille relation to estimate the pressure drop suffered by a fluid with viscosity coefficient $\eta = 100 \times 10^{-6}$ P, upon transporting 1×10^{-4} mol in 10 sec from a reservoir at 10 Torr through a channel 0.2 cm long, and 0.020 cm in radius. The net drop is ≈4 Torr; *i.e.*, the mean free path at the nozzle lip is no more than twice that in the reservoir.

Thermochemical and Kinetic Considerations

The application of the computed temperature and density profiles to the electron diffraction sampling problem is best illustrated by considering several typical examples. By far the largest group of molecules that have been investigated are those which exist in a single conformation but incorporate a significant range in characteristic frequencies, at one extreme associated with tightly bound atom pairs, and at the other with low-frequency torsional motions. This is illustrated by C_2F_6 (D_{3d}) ($\nu_7 \approx \nu_{10}$ = 1250 cm^{-1} correspond to the C–F stretching motions while $\nu_4 \approx$ 68 cm^{-1} is listed for the torsional libration).[43] A full set of force constants was selected, a normal mode analysis was completed, and the root mean square amplitudes calculated[44] (sho, rigid rotator approximation) for gas samples at 0, at 200, 300, and 400°K. These are plotted in Figure 7. As anticipated, due to the contribution from the zero-point vibrational amplitudes only the magnitudes of the l_{ij} associated with the motion of the gauche atom pairs are affected over this range of temperatures. Since the heat capacity ratio for C_2F_6 is temperature dependent (γ = 1.085 and 1.113 at 300 and 200°K, respectively) consider a mean value, γ = 1.10. Then, the gas encountered by a beam of electrons between χ = 0.5 to 0.7 is at a translational temperature $T \approx$ 255°K, for the densest part of the sample (Figure 5a). Most electron diffraction units operate with the electron beam covering χ = 0.9 to 1.1; then $T \approx$ 225°K. That the distance between the nozzle lip and the beam is a critical experimental parameter which determines the translational temperature of the sample is not generally appreciated by electron diffraction practitioners. While a variable γ has not been incorporated in the free expansion flow analysis, one may estimate the effect of varying its magnitude over the range 1.06 → 1.15 by the comparing profiles in Figures 4–6; the changes are not large. Reference to Figure 7 underscores the point that estimation of the vibrational temperature is of importance only for some of the l_{ij}'s in C_2F_6; *i.e.*, with respect to the F ··· $F_{(gauche)}$ atom pairs.

To assess whether the vibrational temperature closely follows the gas dynamic translational temperature, one must estimate the average number of collisions required to vibrationally deexcite C_2F_6. At 298°K sound dispersion data show Z_{10} = 12.[45] For a source pressure of 10 Torr at 300°K, σ = 4.0 Å, and a nozzle diameter of 0.7 mm, inspection of the ρ/ρ_0 and Z_{tot} profiles (γ = 1.10) indicates that the molecules in the dense core of the sample suffered ≈40 collisions; those in the outer ring a smaller number (27–15). Since this is more than adequate to maintain vibration–translation equilibrium, we conclude that the appropriate temperature for comparison with experiment is 250–225°K depending on the magnitude of χ (beam axis). Details of a reanalysis of the structure and dynamics of C_2F_6 are given by Gallaher, Yokozeki, and Bauer.[46] We conclude that even though no fully satisfactory analysis has yet been presented for the coupled gas dynamic-reaction rate limited case, it is clear that for molecules such as C_2F_6 there is no serious difficulty in estimating a meaningful sample vibrational tem-

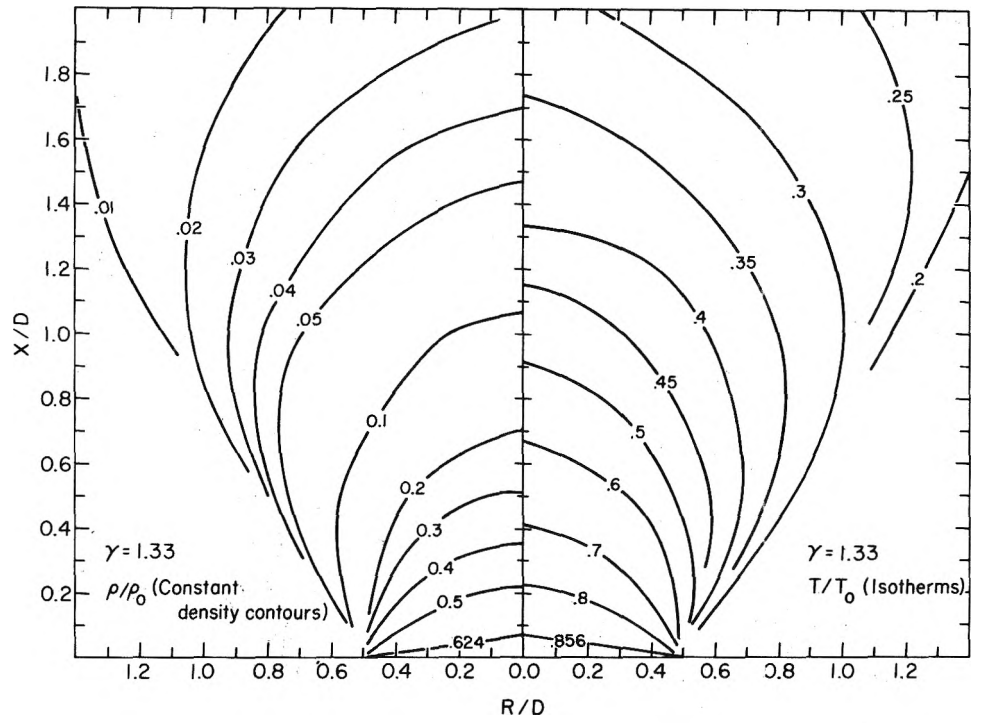

Figure 2. Dimensionless temperature and density contours for $\gamma = 1.33$.

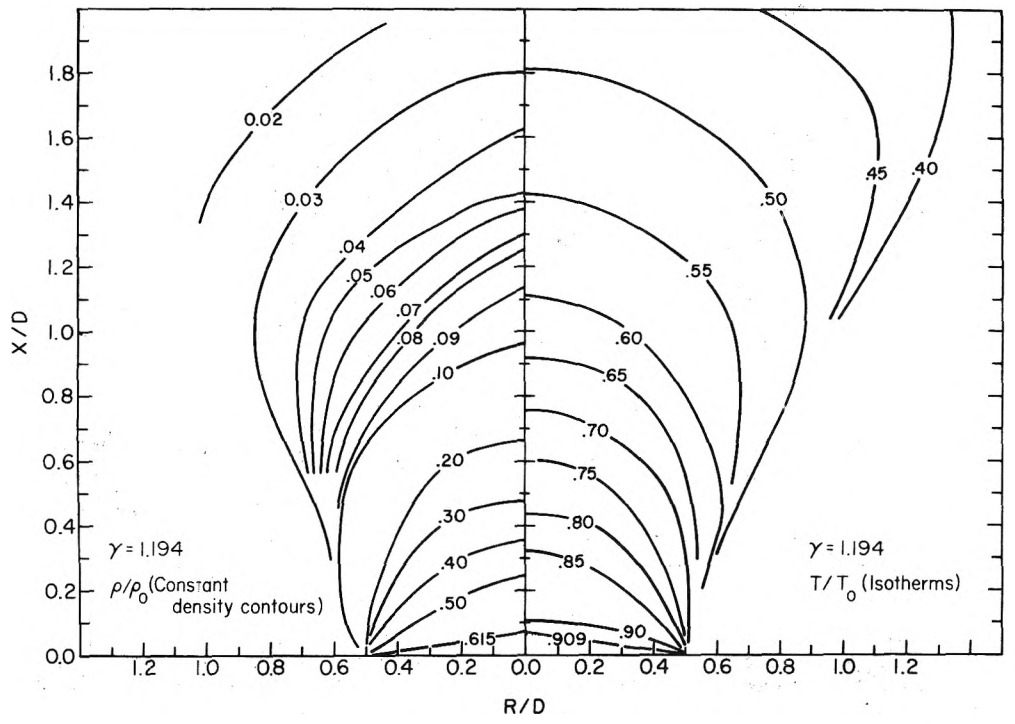

Figure 3. Dimensionless temperature and density contours for $\gamma = 1.194$.

perature for comparing calculated with observed l_{ij}'s. However, we do not claim that l_{ij}'s estimated from electron diffraction patterns are reliable measures of vibrational temperatures.

When the molecules present in the sample may exist in more than one conformation the problem becomes considerably more complex. Obviously, the sample composition is maintained when the conformations in equilibrium at the source temperature are separated by a barrier such that the characteristic time for chemical equilibration to the lower temperature is significantly larger than the transit time from the stagnation condition within the nozzle to the electron beam axis [≈1 msec]. In contrast, when the barrier is so low such that the chemical relaxation time is less than the transit time, the gas mixture in the jet remains in *local* chemical equilibrium throughout the flow, until the freezing condition is reached; *i.e.*, when the density drops to a magnitude at which essentially no further collisions occur.

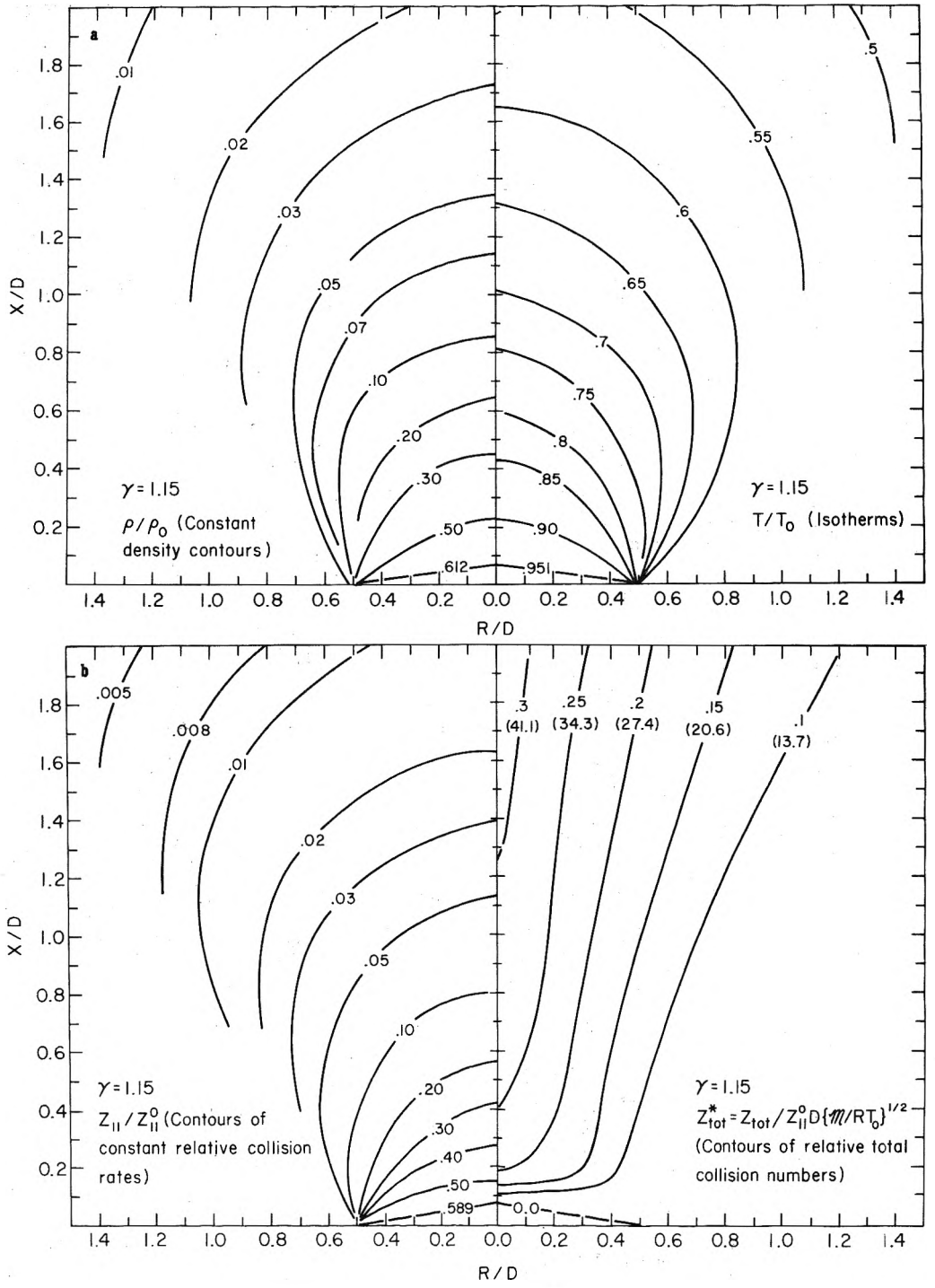

Figure 4. (a) Dimensionless temperature and density contours for $\gamma = 1.15$. (b) Dimensionless local collision rates and total collision numbers for $\gamma = 1.15$. In the right diagram, the numbers in parentheses indicate the average total collision numbers for a source pressure of 10 Torr, at $T = 300°K$, with $\sigma = 4$ Å.

The intermediate case for rate controlled flow within the nozzle and in the free jet has not been solved, but approximate flow fields may be inferred from calculations for wide angle nozzle flows.[47] One procedure, successfully followed by Fenn and Gallagher[48] and used below, is to assume that the relaxation processes did not markedly perturb the translational temperature and density from their equilibrium values, and to integrate the relaxation equations along the center line for an assumed sequence of relaxation collision numbers. By comparing their experimental (T_{tr} *vs.* P_{source}) profiles with their computed curves they interpolated mean collision numbers for rotational relaxation which were in excellent agreement with values derived from other techniques: for H_2 ($Z_{rot} = 300$), CH_4 ($Z_{rot} = 15$), CO_2 ($Z_{rot} = 2.5$), etc.

Before one can estimate a chemical relaxation time he must ascertain whether the reaction follows first- or second-order kinetics, or possibly, if it occurs in the "fall-off" regime. In the following discussion we considered a simple model for a species characterized by a double minimum potential, of unequal depths (*i.e.*, internal rotation or inversion). We assumed that the gas was in equilibrium at the

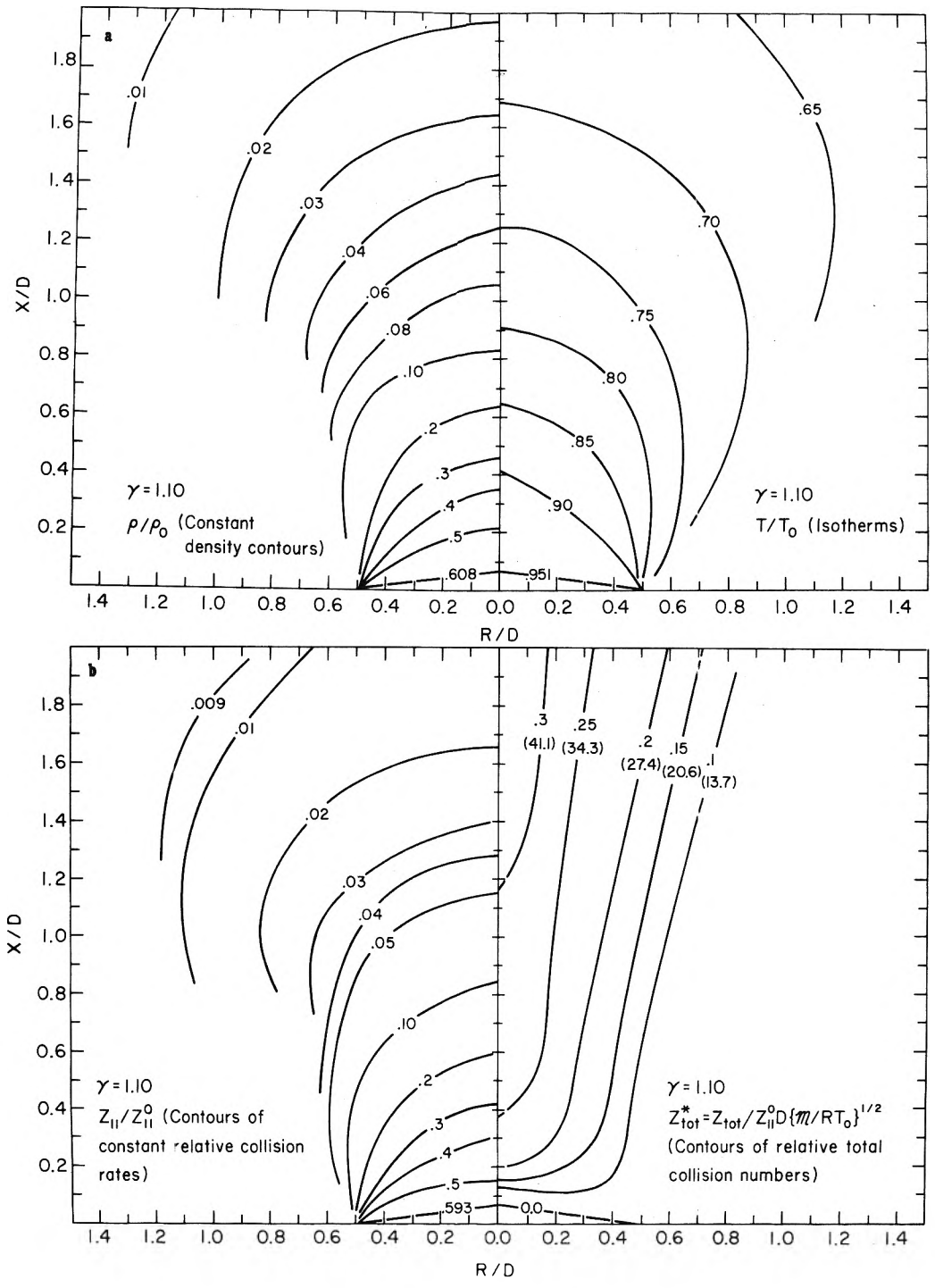

Figure 5. (a) Dimensionless temperature and density contours for $\gamma = 1.10$. (b) Dimensionless local collision rates and total collision numbers for $\gamma = 1.10$. In the right diagram, the numbers in parentheses indicate the average total collision numbers for a source pressure of 10 Torr, at $T = 300°K$, with $\sigma = 4$ Å.

nozzle temperature when it started its forward motion toward the beam. Let ϵ be the difference between the zero-point vibrational levels in the two conformers (A, B), and ξ the "barrier" height, measured from the zero-point level of the less stable conformer (B) to the zero-point level at the top of the potential maximum. Further, let g_A and g_B specify their respective degeneracies; ν_A, ν_B their characteristic frequencies (assuming that the oscillators remain simple harmonic up to the top of the barrier); and φ_A, φ_B the relative fractions of phase space along the reaction coordinate occupied by those species which can be recognized as either A or B, in the level that just skims the top of the barrier ($\varphi_A + \varphi_B = 1$); $\beta \equiv 1/kT$. While this is an oversimplified model it does incorporate all the essential features. Note, that the molecules of current interest (ethylene chlorohydrin, substituted 1,4-dioxenes,[49] etc.) contain eight or more atoms and execute low-frequency vibrations. Hence in applying conventional unimolecular reaction rate theory, one may assume that the "strong collision" energization condition applies, and that the flow of energy between the "effective" oscillators is rapid ($\tau\{\text{intravib}\} \lesssim 10^{-12}$ sec). The number of equivalent classical oscillators may be estimated *via* the

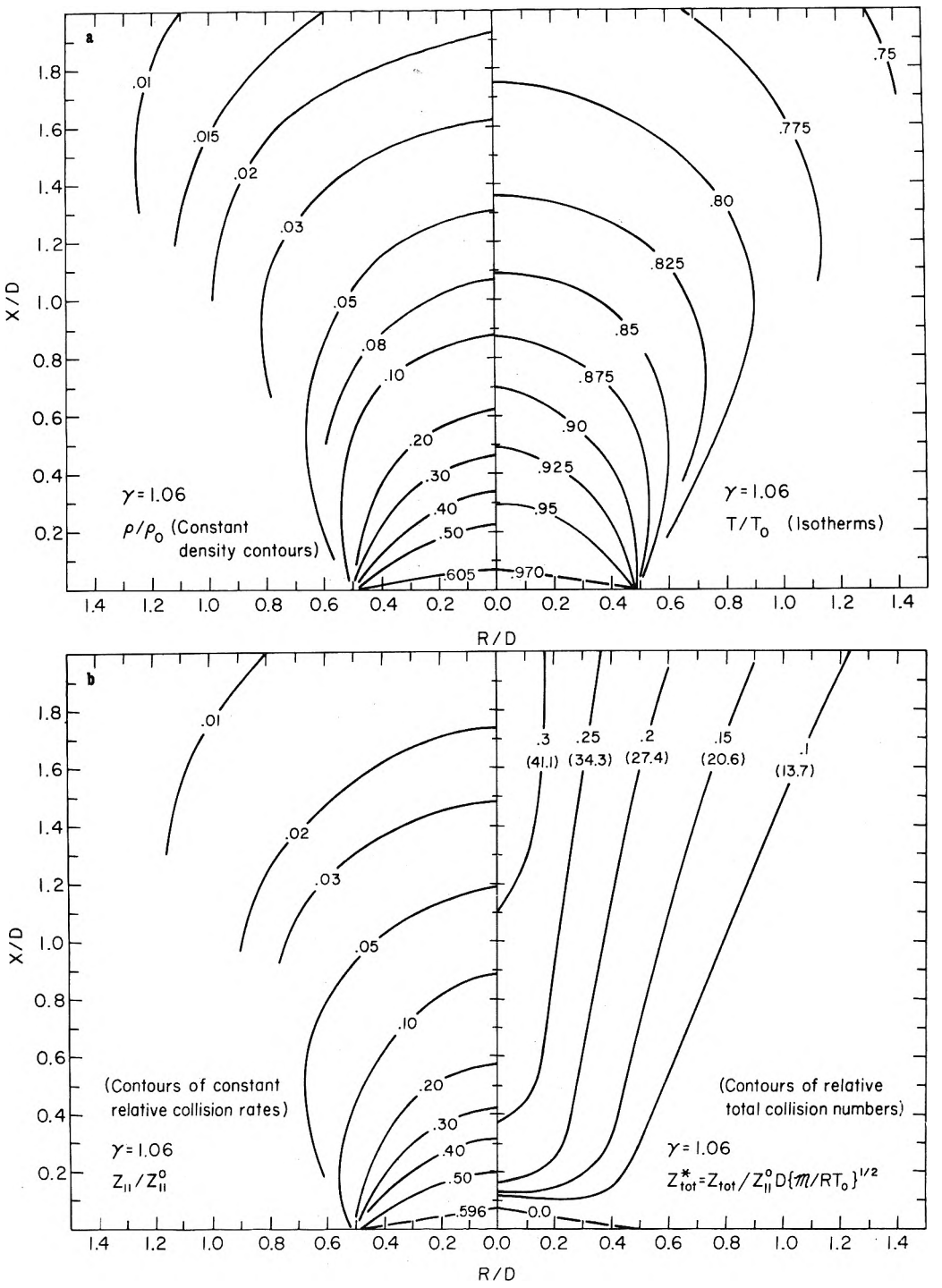

Figure 6. (a) Dimensionless temperature and density contours for $\gamma = 1.06$. (b) Dimensionless local collision rates and total collision numbers for $\gamma = 1.06$. In the right diagram, the numbers in parentheses indicate the average total collision for a source pressure of 10 Torr, at $T = 300°K$, with $\sigma = 4$ Å.

Golden–Solly–Benson correlation[50]

$$s_{uni}(\text{classical equiv}) = C_{vib}/R = [C_{v,total} - C_{tr,rot}]/R \cong 5\text{–}7 \quad (6)$$

based on the reported C_p's at 300°K for the compounds of interest, which range from 18 to 22 cal mol^{-1} deg^{-1}; the corresponding γ's range from 1.08 to 1.14. The high-pressure limit (first order) regime is reached when the mean lifetime, τ_{mlf}, of critically energized molecules is substantially longer than the time between collisions ($\approx 2 \times 10^{-8}$ sec for typical jets used in electron diffraction units). Let E_m be the mean energy of those molecules which do react; then

$$\tau_{mlf}^{-1} = k(E_m) \approx \lambda(1 + \beta E_a/s_u)^{1-s_u} \qquad \lambda \approx 10^{13}\ \text{sec}^{-1} \quad (7)$$

Here s_u is the effective number of oscillators and E_a, the critical energy (identified with the activation energy). Since the temperature in the gas is lowered on passage from the reservoir through the jet, net conversion occurs from B → A. Hence $E_a \lesssim \xi$. Substitution in the above equation, or use of the more elaborate set of graphs and tables given by Siv-

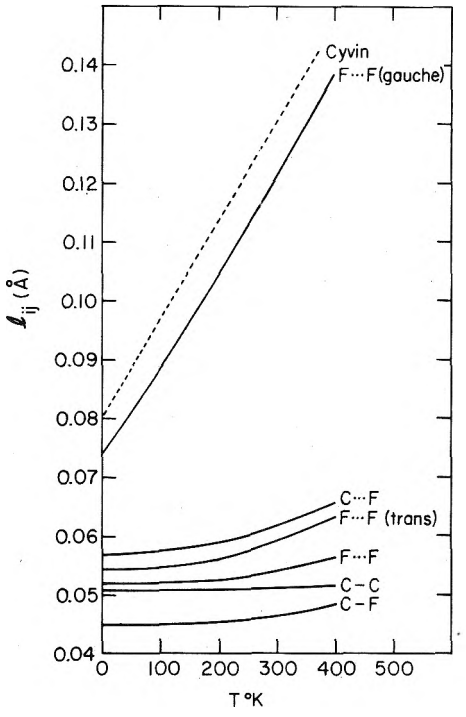

Figure 7. Computed root mean square amplitudes for C_2F_6 as a function of temperature.

ertz and Goldsack[51] shows that for $s \lesssim 8$, even when $(\beta\xi)$ is as high as 13, $\tau_{mlf} \lesssim 10^{-10}$ sec; for $s \lesssim 10$, $(\beta\xi) \approx 11.5$ gives the same mean lifetime. Thus, the appropriate kinetics for reaction in the nozzle exit and in the jet is that for the *limiting low-pressure* regime, wherein the rate of conversion is determined by the rate of energy transfer in bimolecular collisions.

To estimate, at the computed translational temperature, the fraction of bimolecular encounters between species each with s_u effective oscilators, which contain a total internal energy Ξ or greater, one may use the Sivertz–Goldsack[51] graphs for their function: $e^{-x^*} F(x^*; s - 1)$, where $x^* \equiv \beta\Xi$ and $s \simeq 2s_u$. (Actually, this *underestimates* s, since the relative kinetic energy of translation and rotation are not counted.) Essentially the same result is obtained from the classical form

$$\mathbf{P}(E \geq \Xi) = e^{-\beta\Xi}\left\{\frac{(\beta\Xi)^{s-1}}{(s-1)!} + \frac{(\beta\Xi)^{s-1}}{(s-2)!} + \ldots 1\right\} \quad (8)$$

For $(s - 1) = 10$, $\beta\Xi = 10$, $\mathbf{P}(E \geq \Xi) = 0.58$. For $(s - 1) = 10$, $\beta\Xi = 5$, $\mathbf{P}(E \geq \Xi) = 0.98$. Hence, even for $(\epsilon + \xi)$ as high as 17 kcal/mol, there is sufficient vibrational energy in the majority of binary collisions at room temperature to induce the conformational change B → A, provided the "strong collision" condition and short τ(intravib) prevail. The dubious points pertain to the efficiency of energy transfer per collision, and the degree of coupling between oscillators in molecules to which a normal mode analysis is applicable.

Inspection of the summary and correlations presented by Lambert[52] shows that for unsymmetric molecules with more than five atoms, which do not contain hydrogen, the efficiency of energy transfer is $\gtrsim 0.1$ when their lowest molecular frequency is $\lesssim 200$ cm^{-1}; when hydrogen is present the efficiency is $\gtrsim 0.1$ when the lowest molecular frequency is ≤ 300 cm^{-1}. On this basis, one may argue that after suffering hundreds of collisions within the nozzle near the exit, during the time the flow Mach number grows from near zero to unity, and additional 30–50 collisions in the jet prior to reaching the probing electron beam, the molecules under consideration will have their vibrational temperatures essentially relaxed. However, vibrational relaxation does not guarantee chemical relaxation. An upper estimate for the latter is given by classical kinetics. For the reaction

$$B + \{B \text{ or } A\} \underset{k_f}{\overset{k_r}{\rightleftharpoons}} A^* + \{B \text{ or } A\} \quad (9)$$

$$\tau_{chem}^{-1} = k_f\{\overline{[B]} + \overline{[A;B]}\} + k_r\{\overline{[A]} + \overline{[A;B]}\} \quad (10)$$

$$k_f = Z_{B,A}\, p \left\{\frac{(\beta\xi)^{s-1}}{(s-1)!} + \ldots\right\} e^{-\beta\xi}; \text{ and } k_f/k_r = K_{eq} \quad (11)$$

For $M = 80$, $\sigma = 4$ Å, at $T = 300$°K, $Z_{B,A} \simeq 2 \times 10^{14}$ (concentration units in mols cm^{-3}). Assume a mean density for both B and A at about 5 Torr; then, for the case $\beta\xi = 5$, $(s - 1) = 10$, and $p = 0.1$, $\tau_{chem} \simeq 10^{-7}$ sec, which is about a factor of 10 lower than the time from the nozzle exit to the beam center (10^{-6} sec). This suggests extensive chemical relaxation, but the conclusion is dependent on the assumed applicability of the classical kinetic expression for k_f. However, a quantum-statistical model for the trans ↔ gauche interconversion led to essentially the same conclusion. At 300°K, for a plausible set of molecular frequencies, and an assumed barrier of 3 kcal/mol, a complete RRKM calculation of the *effective* unimolecular rate constant showed that it was proportional to the pressure, when $p \leq 10$ Torr (*i.e.*, system is in the bimolecular regime). At $p = 5$ Torr, $k_{uni} = 6 \times 10^{-6}$ sec^{-1} ($\tau_{chem} \simeq 1.5 \times 10^{-7}$ sec). For barriers of 1 and 5 kcal/mol, $\tau_{chem} \simeq 5 \times 10^{-8}$ and 1×10^{-6} sec, respectively.

The Relaxation Model

The opposite extreme of strongly coupled intramolecular oscillators, assumed in the classical and RRKM theories, is a model in which the motion along the reaction coordinate (here, the rotational angle about the C–C bond) is completely decoupled from the rest of the molecule. Then, the accumulation of sufficient energy for interconversion is a consequence of energetically favorable binary collisions, *i.e.*, the molecule executes a random walk up a single vibrational ladder. We shall neglect the role of the large number of collisions with large impact parameters in which very little energy is transferred between the colliding species, but which, none the less, perturb the internal oscillators sufficiently to "coupled them," so that there is a finite probability that some of the vibrational energy gets localized in the reaction oscillator. This section is devoted to an analysis of the chemical relaxation process along the central stream line by integrating the master equation for the population of the states associated with a single vibrator, along the reaction coordinate in the B species (designated n_v) and in the A species (designated n_w), assuming as did Gallagher and Fenn[48] that the density and translation temperature profiles are not significantly distorted by the B ⇄ A transformation. Introduce the notation: $\varkappa_{1,0} = p_{1,0}Z(\chi)$, for the product of the deexcitation probability for $v = 1 \rightarrow 0$ (or $w = 1 \rightarrow 0$) per collision, by the number of collisions B (or A) molecules suffers *per unit length* along the stream line. In dimensionless parameters $Z(\chi)$ is given by $[Z_{11}/Z_{11}^0]/[\gamma(T/T_0)]^{1/2} M$. Thus $\varkappa_{1,0}$ is position dependent, but completely specified for each γ. Note that

while $p_{1,0}$ is temperature dependent, its coefficient is quite small (and is negligible) for the molecules under consideration. Microscopic reversibility requires that $p_{0,1}{}^{B} = p_{1,0}{}^{B} \exp(-\beta h \nu_B)$, etc. Also, for simple harmonic oscillators $p_{v,v-1} = v \cdot p_{1,0} \leq 1$, and transitions between adjacent levels dominate. Finally, we shall refer to the highest B level below the barrier maximum as v^*; that for A, w^*; the first common level above the potential peak is $u \equiv w^* + 1$. The following differential equation describes the evolution of populations for any v, w, or $u > (w^* + 1)$ level [except v^*, w^*, $u = w^* + 1$]

$$\frac{dn_v}{d\chi}\left(\frac{dx}{dt}\right) = \kappa_{v+1,v} n_{v+1} + \kappa_{v-1,v} n_{v-1} - (\kappa_{v,v-1} + \kappa_{v,v+1}) n_v \quad (12)$$

$$\frac{dn_v}{d\chi}\left(\frac{dx}{dt}\right) = p_{1,0} Z(\chi) n_v \left[(v+1)\frac{n_{v+1}}{n_v} + v e^{-\beta h \nu_B} \frac{n_{v-1}}{n_v} - v - (v+1) e^{-\beta h \nu_B}\right] \quad (13)$$

Here β refers to the *local translational* temperature. At equilibrium (for example, within the nozzle where there is no forward motion): $n_{v+1}/n_v]_{eq} = e^{-\beta h \nu_B}$; $n_{v-1}/n_v]_{eq} = e^{+\beta h \nu_B}$ and the bracket in (13) vanishes. However, when the temperature along the streamline decreases rapidly enough, the terms which specify the vibrational level populations *lag* behind those which specify the transition probabilities. To evaluate the evolving composition changes, we integrated incremently along the central stream line, starting within the nozzle, at essentially the stagnation condition ($M = 0.1$).

The corresponding expressions for the population changes in the levels w^* and v^* and $(w^* + 1)$ include factors which are not evident in eq 12. Thus

$$dn(w^*)/d\chi(dx/dt) = \kappa_{w^*+1,w^*}\varphi_A n_{w^*+1} + \kappa_{w^*-1,w^*} n_{w^*-1} - (\kappa_{w^*,w^*-1} + \kappa_{w^*,w^*+1}) n_{w^*} \quad (14)$$

The expression for $dn(v^*)/d\chi$ is similar, with φ_B in the first term.

$$dn(w^* + 1)/d\chi(dx/dt) = \kappa_{w^*+2,w^*+1} n_{w^*+2} + \kappa_{w^*,w^*+1} n_{w^*} + \kappa_{v^*,v^*+1} n_{v^*} - (\kappa_{w^*+1,w^*}\varphi_A + \kappa_{w^*+1,v^*}\varphi_B) n_{w^*+1} \quad (15)$$

The phase space factors, φ_A and φ_B, account for the proper partition of species upon their deexcitation from the common conformation into either valley. The following are the *equilibrium* distributions

$$\left.\frac{n_w}{n}\right]_{eq} = g_A e^{-\beta h \nu_A w}/\Sigma \qquad \left.\frac{n_v}{n}\right]_{eq} = g_B e^{-\beta[\epsilon + h\nu_B v]}/\Sigma \quad (16)$$

$$\left.\frac{n_u}{n}\right]_{eq} = (g_A + g_B) e^{-\beta[\epsilon+\xi+h\nu_u u]}/\Sigma$$

$$\Sigma \equiv \sum_{v=0}^{v^*} n_v + \sum_{w=0}^{w^*} n_w + \sum_{u=1}^{\infty} n_u$$

Here $u = 1$ for $(w^* + 1)$: 2 for $(w^* + 2)$, etc. Were local equilibrium maintained for all χ

$$[B]/[A] \longrightarrow \left.\frac{\Sigma n_v + \varphi_B \Sigma n_u}{\Sigma n_w + \varphi_B \Sigma n_u}\right]_{eq}$$

For an illustrative case we selected parameters which match ethylene chlorohydrin. The integration was started at a point within the nozzle, arbitrarily set at 1.8 mm ($\chi = -9$) upstream from the lip, where the Mach number was taken to be 0.10. Further, we assumed that the Mach number increased linearly along the central streamline from zero at $\chi = -10$ to $\chi = +0.07$ where $M = 1.01$. The fidelity of this representation is determined by the inner contour of the nozzle. Finally, we assumed that the flow was sufficiently rapid, such that there was no significant heat transfer from the walls to the gas (thermal boundary layer). The estimated travel time through the 2-mm channel is $\approx$1 msec. As anticipated, this model indicates that chemical relaxation is incomplete.[53]

Our analysis demonstrated that for nozzles as currently in use in most electron diffraction units, when the reservoir pressure is greater than 1 Torr, for unsummetrical molecules with more than five atoms, vibrational relaxation occurs in the jet. Then, the appropriate temperature to use for calculating l_{ij}'s is that read from contour maps, such as Figures 2–6. When the objective is to determine the proportion of low-energy conformers as a function of source temperature, and thus to estimate enthalpy and entropy increments for the corresponding conversions, serious questions remain. It is difficult to estimate whether chemical relaxation occurs, since that is determined by an unspecified internal contour of the nozzle and unknown degree of intramolecular vibrational coupling. Indeed, the molecular beam method demonstrated by Novick, Lehn, and Klemperer,[16] or an extension of the impact tube technique to low pressures and large pressure ratios,[54] or the technique of beam velocity spectroscopy[48] appear more promising.

For systems with heat capacity ratios other than 1.15, 1.10, and 1.06 appropriate values for the local temperature may be selected by interpolating for the mean value of γ among Figures 4–6, after taking special care to estimate the location of the beam above the nozzle lip. Of course, care must be taken in estimating γ's for reacting systems; for some γ is both temperature and density dependent. When the fraction of A is θ and of B, $(1 - \theta)$, with the reaction written B $\rightarrow$ A

$$\langle C_p \rangle = C_p{}^{(B)} + \theta[C_p{}^{(A)} - C_p{}^{(B)}] + (H_A - H_B)[\delta\theta/\delta T]_{const\ p} \quad (17)$$

A similar expression applies for $\langle C_v \rangle$, and there is the second law constraint: $K_{eq}(T) = (1 - \theta)/\theta$. For a monomer–dimer case, the magnitudes of both $\langle C_p \rangle$ and $\langle C_v \rangle$ may be very large, and $\gamma \rightarrow 1$; then there is very little change in temperature within nozzle flow. On the other hand, such an equilibrium relaxes more rapidly than a conformational change, since the predominant process is association, with high collision cross sections.

Acknowledgments. We sincerely thank Professor James B. Anderson, Engineering and Applied Science at Yale, for the copy of the method-of-characteristics computer program, Dr. David M. Golden (SRI) for the RRKM calculations, and Professor K. Hedberg for a careful and helpful review of this manuscript. This work was supported in part by the National Science Foundation under Grant No. GP-34060.

References and Notes

(1) R. B. Harvey, F. A. Keidel, and S. H. Bauer, *J. Appl. Phys.*, **21**, 860 (1950).
(2) I. L. Karle and J. Karle, *J. Chem. Phys.*, **18**, 963 (1950).
(3) S. H. Bauer and P. Jeffers, *J. Phys. Chem.*, **69**, 3317 (1965).
(4) Y. Morino and Y. Murata, *Bull. Chem. Soc. Jap.*, **38**, 114 (1965).
(5) K. Kuchitsu, *Bull. Chem. Soc. Jap.*, **32**, 748 (1959).

(6) J. B. Anderson and J. B. Fenn, *Phys. Fluids*, **8**, 780 (1965).
(7) P. V. Marrone, *Phys. Fluids*, **10**, 521 (1967).
(8) D. Golomb and R. E. Good, *J. Chem. Phys.*, **52**, 1545 (1970).
(9) A. R. Vick, E. H. Andrews, Jr., J. S. Dennad, and C. B. Cruidon, *NASA Tech. Note*, **D-2327** (1964).
(10) A. B. Bailey, M. R. Busby, and R. Dawbar, Arnold Engineering and Development Center, Technical Report No. 72-32.
(11) H. Ashkenas and F. S. Sherman in "Rarefied Gas Dynamics," Vol. II, J. H. de Leevw, Ed., Academic Press, New York, N.Y., 1966, p 84.
(12) P. L. Owen and G. K. Thornhill, Aeronautical Research Council; (Great Britain) R & M, 2612 (1948).
(13) B. Raoult and J. Farges, *Rev. Sci. Instrum.*, **44**, 430 (1973); J. Farges, B. Raoult, and G. Torchet, in press.
(14) G. D. Stein, work in progress. See also G. D. Stein and J. A. Armstrong, *J. Chem. Phys.*, **58**, 1999 (1973).
(15) W. G. Dorfeld and J. B. Hudson, *J. Chem. Phys.*, **59**, 1253, 1261 (1973).
(16) S. Novick, J. M. Lehn, and W. Klemperer, *J. Amer. Chem. Soc.*, **95**, 8189 (1973).
(17) K. Kuchitsu in "Molecular Vibrations and Structure Studies," S. J. Cyvin, Ed., Elsevier, Amsterdam, 1972, Chapter 10.
(18) L. S. Bartell in "Physical Methods in Chemistry," Vol. 4, A. Weissberger and B. W. Rossiter, Ed., Interscience, New York, N.Y., 1971.
(19) A. Almenningen, S. P. Arnesen, O. Bastiansen, H. M. Seip, and R. Seip, *Chem. Phys. Lett.*, **1**, 569 (1968).
(20) B. W. McClelland, G. Gundersen, and K. Hedberg, *J. Chem. Phys.*, **56**, 4541 (1972).
(21) R. R. Ryan and K. Hedberg, *J. Chem. Phys.*, **50**, 4986 (1969).
(22) S. J. Cyvin, "Molecular Vibrations and Mean Square Amplitudes," Elsevier, Amsterdam, 1968, Chapter 12.
(23) K. Hedberg and M. Iwasaki, *J. Phys. Soc. Jap.*, **17**, Suppl. B-II, 32 (1962).
(24) S. Konaka, Y. Murata, K. Kuchitsu, and Y. Morino, *Bull. Chem. Soc. Jap.*, **39**, 1134 (1966).
(25) S. Konaka, *Bull. Chem. Soc. Jap.*, **43**, 3107 (1970).
(26) Y. Morino, T. Ukaji, and T. Ito, *Bull. Chem. Soc. Jap.*, **39**, 71 (1966).
(27) J. Janzen and L. S. Bartell, *J. Chem. Phys.*, **50**, 3611 (1969).
(28) A. Almenningen, O. Bastiansen, and T. Motzfeldt, *Acta Chem. Scand.*, 23, 2848 (1969).
(29) R. K. Bohn and S. H. Bauer, *Inorg. Chem.*, **6**, 304 (1967).
(30) K. Hagen and K. Hedberg, *J. Amer. Chem. Soc.*, **95**, 1003, 4796 (1973).
(31) A. Almenningen, O. Bastiansen, L. Fernholt, and K. Hedberg, *Acta Chem. Scand.*, **25**, 1946 (1971).
(32) A. H. Lowrey, C. George, P. D'Antonio, and J. Karle, *J. Amer. Chem. Soc.*, **93**, 6399 (1971).
(33) A. L. Andreassen and S. H. Bauer, *J. Mol. Struct.*, **12**, 381 (1972).
(34) P. C. Waterman and S. A. Stern, *J. Chem. Phys.*, **31**, 405 (1959), reported the separation of N_2 and C_2H_4.
(35) R. J. Gordon, Y. T. Lee, and D. R. Herschbach, *J. Chem. Phys.*, **54**, 2393 (1971); see also H. Pauly and J. P. Toennies, *Advan. Exp. Phys.*, **7A**, 251 (1968).
(36) (a) Calculations of W. S. Wolf, Lockheed Missiles and Space Company, Palo Alto, Calif., 1962, reported by (b) H. Askhenas and F. S. Sherman, "Rarefied Gas Dynamics," Vol. 2, J. H. de Leevw, Ed., Academic Press, New York, N.Y., 1966, pp 106–127.
(37) J. B. Anderson, Project SQUID, Purdue University, Lafayette, Ind., Technical Report No. PR-122-PU, 1972.
(38) A. R. Vick, E. H. Andrews, Jr., J. S. Dennard, and C. Cruidon, *NASA Tech. Note*, **TN D-2327**, in press.
(39) F. S. Sherman in "Rarefied Gas Dynamics," Vol. 2, J. H. Laurmann, Ed., Academic Press, New York, N.Y., 1963, p 250.
(40) H. W. Liepmann and A. Roskho, "Elements of Gas Dynamics," Wiley, New York, N.Y., 1957, Chapter 12.
(41) A. B. Cambel and B. H. Jennings, "Gas Dynamics," McGraw-Hill, New York, N.Y., 1954, Chapter 10.
(42) R. Sedney in "Non-Equilibrium Flows," Vol. 1, P. P. Wegener, Ed., Marcel Dekker, New York, N.Y., 1970, Part 2, pp 174–182.
(43) T. Shimanouchi, *Nat. Ref. Data Ser., Nat. Bur. Stand.*, **No. 39**, 95 (1972).
(44) We thank Dr. A. Yokozeki for these calculations. His values are close but not equal to those published by S. J. Cyvin, *et al.*, *Acta Chem. Scand.*, **21**, 2405 (1967).
(45) J. D. Lambert and R. Salter, *Proc. Roy. Soc., Ser. A*, **253**, 277 (1959).
(46) K. L. Gallaher, A. Yokozeki, and S. H. Bauer, *J. Phys. Chem.*, **78**, 2389 (1974).
(47) K. N. C. Bray in ref 42, Chapter 43.
(48) R. J. Gallagher and J. B. Fenn, Technical Report No. YALE-4-PU, Dec 1973.
(49) R. H. Larking and R. C. Lord, *J. Amer. Chem. Soc.*, **95**, 5129 (1973).
(50) D. M. Golden, R. K. Solly, and S. W. Benson, *J. Phys. Chem.*, **75**, 1333 (1971).
(51) C. Sivertz and D. Goldsack, *J. Chem. Phys.*, **36**, 569 (1962).
(52) J. D. Lambert, *J. Chem. Soc., Faraday Trans. 2*, **68**, 364 (1972).
(53) At about the time we received the galley proof for this manuscript we discovered an error in the program used to solve the finite difference equations. Hence the results previously obtained have been deleted and new computations (which are extensive) will be reported after their completion. The error was such as to make the correct relaxation model closer to the equilibrium profile than we had previously found.
(54) S. H. Bauer and M. R. Gustavson, *Discuss. Faraday Soc.*, **7**, 69 (1954).

Reinvestigation of the Structure of Perfluoroethane by Electron Diffraction

K. L. Gallaher, A. Yokozeki, and S. H. Bauer*

Department of Chemistry, Cornell University, Ithaca, New York 14850 *(Received May 17, 1974)*

Gas-phase electron diffraction patterns of C_2F_6 were recorded with the sample reservoir at room temperature. Least-squares analysis of the reduced intensity data gave (D_{3d} symmetry) r_g(C–C) = 1.545 (6) Å, r_g(C–F) = 1.326 (2) Å, and ∠CCF = 109.7$_5$(0.12)°, with the indicated error estimates. These values were compared with corresponding distances reported for analogous compounds. Analysis of the torsional oscillation about the C–C bond axis led to a mean dihedral angle of 67.3(2.7)° (60° = staggered), which corresponds to an effective shrinkage of 0.004 Å for the longest F- - - F distance. A barrier height to internal rotation of 3.7 kcal/mol was derived from the present diffraction data by taking into account sample cooling due to the rapid expansion in the jet.

Introduction

The study of fluorine substitution (C/F and C/F/H) effects on molecular structure and reactivity has been a topic of continuing interest in our laboratory. In the case of the substituted methanes and ethanes, the C–F bond length correlates with the number of F substitutions: 1.38–1.39 Å, 1.34–1.36 Å, and 1.32–1.33 Å for the attachment of one, two, and three fluorines, respectively. The substitution effect upon the adjacent C–C bond length, however, is uncertain. For example, the C–C separation reported from the previous electron diffraction study of hexafluoroethane,[1]

because of its large uncertainty (0.03 Å), is not significantly different from that in ethane.[2] One of the purposes of the present investigation was to redetermine the C–C bond length. Calculations of normal vibrations and their root mean square amplitudes are also available;[3-5] these have been checked and slightly revised.

The barrier height to internal rotation for C_2F_6 has been estimated from thermodynamic (3.92 kcal/mol)[6] and electron diffraction (4.3 kcal/mol) data.[7] While the latter is somewhat larger than the former, which is a revised value from the original estimate (4.35 kcal/mol),[8] they are essentially equal within their respective error limits. The value derived from the diffraction study, however, may prove to be smaller than the quoted magnitude, when account is taken of the effect of sample cooling during the experiment, as was demonstrated in our recent paper.[9] Accordingly, our present study was extended to examine the effect of sample temperature on the deduced barrier height.

Experimental Details and Structural Analysis

An ir spectrum of a commercially prepared sample indicated that no significant impurities were present; the gas was used without further purification. Two sets of diffraction photographs were recorded on Kodak Electron Image plates. The data covered the q range $5 \leq q \leq 127$ Å^{-1}; [$q \equiv (40/\lambda) \sin \theta/2$]. The wavelength and sample-plate scale factors were determined from measurements of MgO powder patterns taken concurrently with the sample. Each of the selected plates was scanned at least three times with our modified Jarrel-Ash densitometer. All data reductions and structure analysis were carried out on an augmented *DEC* PDP-9 computer,[10-12] following our standard procedures.

The intensity data and final backgrounds are shown in Figure 1. The background was chosen on the basis of smoothness and of the positivity criterion proposed by Karle.[13] Throughout this study an analytical fit of the elastic and inelastic scattering factors of Tavard,[14] *et al.*, were used, along with the phase shift approximation of Bonham and Ukaji.[15]

A preliminary set of parameters was obtained from a resolution of the radial distribution curve. Final structural parameters were found from least-squares fitting of the $qM(q)$ function, using a diagonal weight matrix. The refined radial distribution function and $qM(q)$ function are shown in Figures 2 and 3, respectively. Two models were examined. Model I was constrained to the D_{3d} (staggered) configuration whereas in model II the torsional angle was allowed to assume an optimum value (D_3 symmetry). The results are shown in Table I and Figure 4.

Since the correlation between r(C–C) and ∠CCF was −0.97, the range of ambiguity in the C–C distance was investigated by setting r(C–C) at a sequence of values between 1.51 and 1.58 Å, and repeating the least-squares reduction for model I. In this sequence, the six l_{ij}'s and the remaining two geometric parameters were simultaneously varied. A plot of the resulting R factors *vs.* r(C–C) is shown in Figure 5. On applying Hamilton's criterion for the $\boldsymbol{R}$ ratios,[16] the 99.5% confidence interval confines r(C–C) within the limits 1.541 and 1.552 Å; hence we propose the value 1.545 ± 0.006. The corresponding converged values for C–F are 1.326 and 1.325 Å, respectively.

Discussion

Structure. The geometric parameters obtained in this study agree with those of Swick and Karle[1] to within their quoted error limits; the present error limits are considerably smaller, and the new C–C bond distance fits more comfortably with magnitudes listed for related compounds (Table II). It has long been recognized that in the methanes, F for H substitution leads to successively shorter C–F separations. The same trend is evident in the ethanes[17] (Table II); the progression is not as uniform, possibly because of optimistically estimated error limits for the latter compounds and lack of consistency in the definition of distances. With respect to the mean C–C internuclear distances, the only significant departures from the 1.533 Å reference (C_2H_6)[2] appear in C_2F_6 and C_2Cl_6. However, this structural parameter does not correlate with the reported values for the height of the potential barrier for rotation about C–C bonds.

Insertion of τ as an additional variable in model II has the expected effect. The derived value for τ corresponds to the thermal average deviation (7.3 ± 2.7°) from the staggered conformation; the torsion sensitive $l\{\mathrm{F}\cdots\mathrm{F}\}_{\text{gauche}}$ decreases while the torsional deviation produces an effective shrinkage of 0.0036(−0.002, +0.003) with respect to the trans F · · · F distance.

Mean Amplitudes. In contrast to the structural parameters, the magnitudes of the mean amplitudes deduced from diffraction data are subject to systematic errors for which corrections cannot be made with confidence. There are two types: (a) the effects of finite sample size, extraneous scattering, photographic density calibration, inaccuracies in atomic scattering factors, etc., and (b) the effect of sample cooling due to expansion. While type a errors tend to increase the deduced mean amplitudes, type b causes some of them to decrease, particularly for atom pairs which mutually vibrate with low frequencies. The easiest way to correct for the apparent increase in the mean amplitudes due to type a is to use a standard sample (CO_2, CS_2, etc.) under similar experimental conditions. Our recent studies with CO_2 indicated a correction of about 8%[18] but those experimental conditions were not precisely duplicated in the present experiments. We therefore tested a spread of empirical corrections from 3 to 8%; the observed amplitudes are compared with calculated values in Table III. The root mean square amplitudes were estimated for sample temperatures of 300, 250, and 200°K, on the basis of a simple Urey–Bradley force field, with constants derived from analogous molecules.[3,19] Our computed values are consistent with those published by Cyvin, *et al.*,[4] as compared in Table III.

The calculated l_{ij}'s, except for $l(\mathrm{F}\cdots\mathrm{F})_{\text{gauche}}$, are almost independent of temperature and agree with the values derived from diffraction data to within the experimental error. The mean amplitudes of the gauche pair do have a large temperature dependence, which might be used to gauge the vibrational temperature of the sample in the jet, were the experimental errors significantly reduced. In this connection, according to a recent kinetic and gas dynamics study in this laboratory,[9] sample cooling due to jet expansion between the nozzle lip and its intersection by the electron beam should be appreciable. For a heat capacity ratio of 1.10 the translational temperature at the beam was estimated to be about 250°K.[9]

Potential Barrier to Internal Rotation. Several methods are available for estimating a barrier height from electron diffraction data. One is based on the harmonic approximation, which assumes the torsional motion to be an infinites-

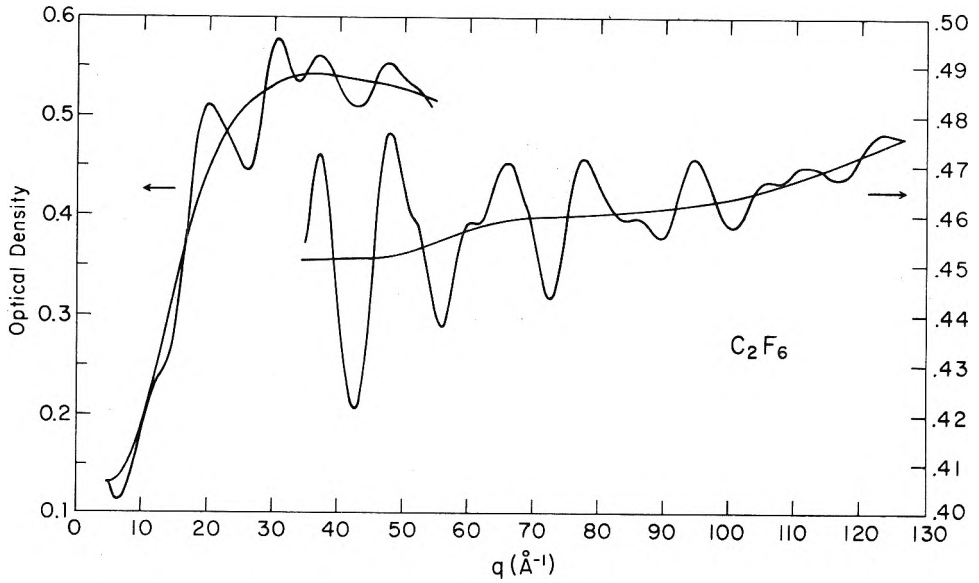

Figure 1. Photographic densities *vs.* *q*, with refined backgrounds drawn in.

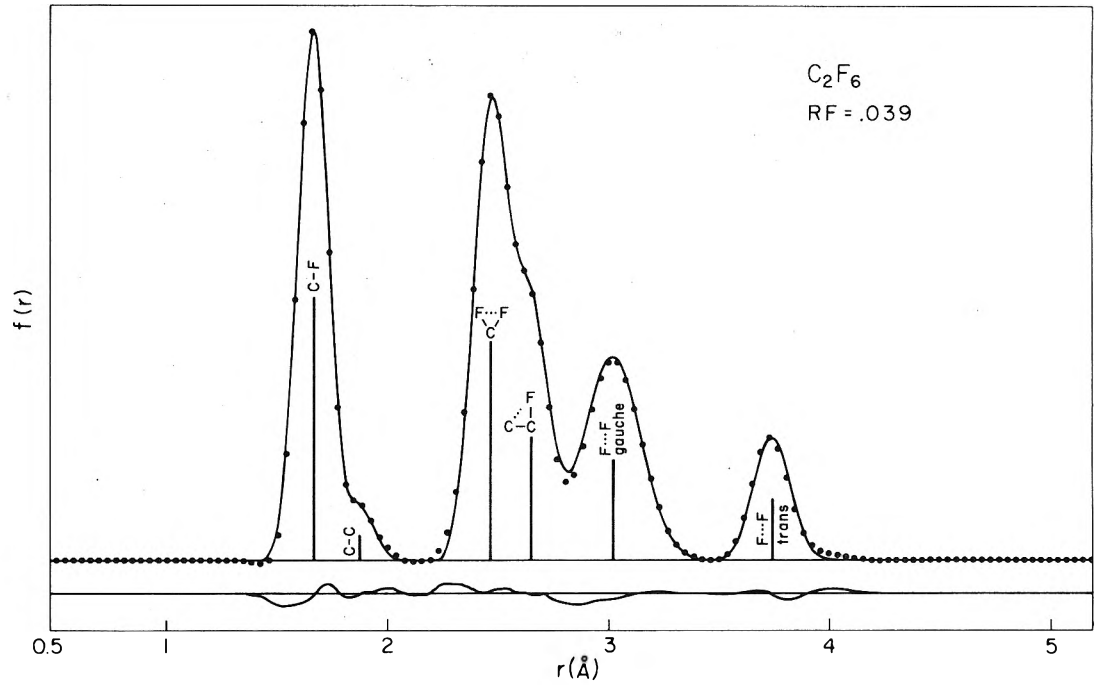

Figure 2. The experimental radial distribution function compared with that calculated for the best model.

TABLE I

	Model I (D_{3d})	Model II (D_3)
C–C	1.545(3)[a]	1.545(3)
C–F	1.326(2)	1.326(2)
∠CCF	109.75(0.12)	109.76(0.11)
τ	60.0(fixed)	67.3 (2.7)
l_{ij}(C–C)	0.039(8)	0.039(8)
l_{ij}(C–F)	0.046(1)	0.046(1)
l_{ij}(F···F / C)	0.057(1)	0.057(1)
l_{ij}(C···F)	0.066(2)	0.066(2)
l_{ij}(F···F((gauche)	0.122(5)	0.102(19)
l_{ij}(F···F)(trans)	0.067(5)	0.067(5)
σ	0.0209	0.0197

[a] Values in parentheses, in 10^{-3} Å or degrees, are 3σ, as obtained from least-squares analysis of the $qM(q)$ function, or 0.15% of the respective parameter, whichever is larger.

imal oscillation around the equilibrium (*i.e.*, the staggered) conformation. Under these conditions, the barrier height (V_0) of this ethane-type molecule [$V(\tau) = (V_0/2)(1 + \cos 3\tau)$] is related to the effective shrinkage, δ_g, of the "trans" pair distance.[1,20]

$$\delta_g = a^2 kT/9V_0 r_g(\text{trans}) \qquad a = r_{CF} \sin(\angle CCF) \tag{1}$$

In the second, the mean amplitude of the "gauche" conformation is used, based on following equation[21,22]

$$l_{obsd}^2 = l_f^2 + a^4 kT/6V_0 r_g^2(\text{gauche}) \tag{2}$$

where l_f is the mean amplitude of framework vibrations only; it was calculated by a normal mode analysis.

In the third method the experimental radial distribution curve, f(*r*), is approximated by treating the internal rota-

TABLE II: Bond Distances in Related Compounds

	C–F	C–C	C–H	∠FCF	Method	Ref	V_0, kcal/mol^{-1}
H_3C-CH_3		1.533(2)	1.111(2)		ED	*a*	2.928(25)[n]
$F-CH_3$	1.38527(5) 1.391(5)		1.106(1) 1.095(10)		MW ED(visual)	*b* *k*	
FCH_2-CH_3	1.398(5)	1.505(4)	1.095(2) 1.090(2)		MW	*c*	3.30(3)[m]
FCH_2-CH_2F (gauche)	1.394(1)	1.535(2)	1.12(1)		ED	*d*	4.6 g-g[l] 2.0 g-t
F_2CH_2	1.358(1) 1.360(5)		1.092(3) 109(3)	108.3(1) 108.2(8)	MW ED(visual)	*e* *k*	
F_2CH-CH_3	1.343(1)	1.54(assumed)	1.1(assumed)	109.1(1)	MW	*f*	3.6(6)[f] 3.18–3.20[m]
F_3CH	1.332(1) 1.334(5)		1.098(20)	108.8 108.5	MW ED(visual)	*g* *k*	
F_3C-CH_3	1.335(5)	1.530(5)	1.085(8)	107.9[m]	MW	*h*	3.48[g]
F_3C-CF_2I	1.338(2)	1.523(27)		109.0(2) 109.7(2)	ED	*i*	5.8[i] 7.09[g]
F_3C-CF_3	1.326(2)	1.545(6)		109.1	ED	This work	3.88(this work)
CF_4	1.323(5)			109.5	ED(visual)	*k*	
Cl_3C-CCl_3		1.564(14)			ED		10.8[o]

[a] Reference 2. [b] F. A. Andersen, B. Bak, and S. Brodersen, *J. Chem. Phys.*, **24**, 989 (1956). [c] L. Nygaard, *Spectrochim. Acta*, **22**, 1261 (1966). [d] E. J. M. Van Schaick, H. J. Deise, F. C. Mijlhoff, and G. Renes, *J. Mol. Struct.*, **16**, 23 (1973). [e] D. R. Lide, Jr., *J. Amer. Chem. Soc.*, **74**, 3548 (1952). [f] N. Solimene and B. P. Dailey, *J. Chem. Phys.*, **22**, 2042 (1954). [g] S. N. Ghosh, R. Trumbarulo, and W. Gordy, *ibid.*, **20**, 605 (1952). [h] W. F. Edgell, G. B. Miller, and J. W. Amy, *J. Amer. Chem. Soc.*, **79**, 2391 (1957). [i] A. L. Andreassen and S. H. Bauer, *J. Chem. Phys.*, **56**, 3802 (1972). [j] A. Almenningen, B. Andersen, and M. Traettenberg, *Acta Chem. Scand.*, **18**, 603 (1964). [k] C. G. Thornton, University Microfilms, Ann Arbor, Michigan, Publication No. 7746; *Diss. Abstr.*, **14**, 604, and private communication from L. O. Brockway as reported in *Chem. Soc., Spec. Publ., No. 11* (1941). [l] S. S. Butcher, R. A. Cohen, and R. C. Rounds, *J. Chem. Phys.*, **54**, 4123 (1971). [m] A. Finch, "Chemical, Applications of Far Infrared Spectroscopy," Academic Press, New York, N.Y., 1970, Chapter 4. [n] S. Weiss and G. E. Leroi, *J. Chem. Phys.*, **48**, 962 (1968). [o] Reference 22.

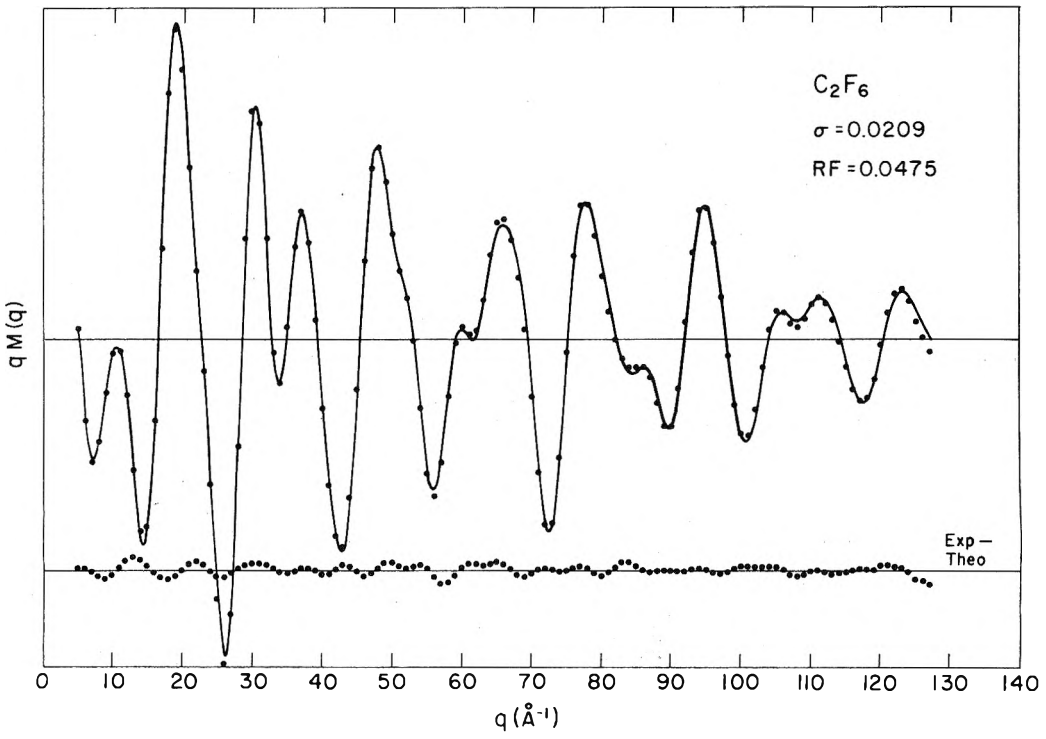

Figure 3. Comparison of the theoretical and experimentally derived $qM(q)$ functions for the best model.

tion separately from the frame vibrations. A classical average of the Gaussian distributions corresponding to the frame motions is taken over all the possible conformations specified by the torsional angle, τ[12,21]

$$f(r) = \int_{-\pi/3}^{\pi/3} f[r(\tau), \ell(\tau)]w(\tau)\,d\tau$$
$$w(\tau) = \exp\{-V(\tau)/kT\}/\int_{-\pi/3}^{\pi/3} \exp\{-V(\tau)/kT\}\,d\tau \quad (3)$$

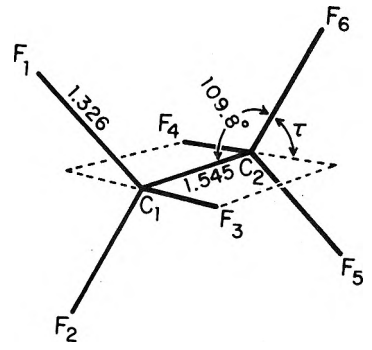

Figure 4. Structure of C_2F_6.

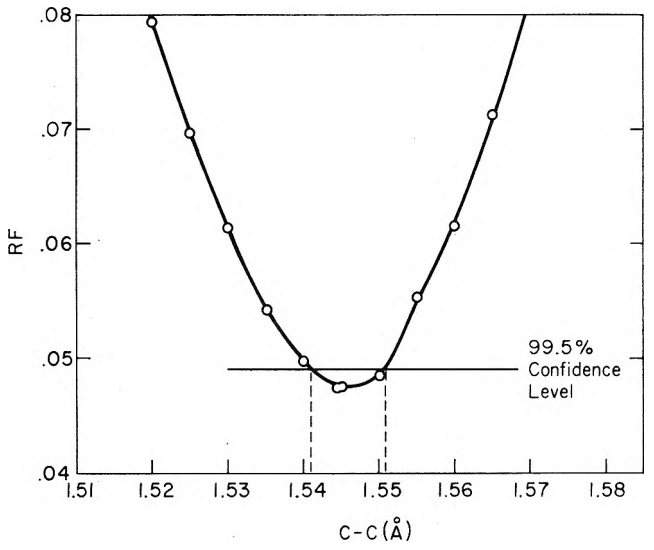

Figure 5. Residuals from least-squares reductions for a sequence of models with r(C–C) fixed at the indicated values. The 99.5% confidence level is indicated, along with the corresponding range in r(C–C).

TABLE III: Comparison of Root Mean Square Amplitudes for C_2F_6 (Å)

	Obsd[a]	Calcd (300°K)[b]	Calcd (250 °K)[b]
l(C–F)	[0.045–0.043]	0.046(0.045)[c]	0.046
l(C–C)	[0.038–0.036]	0.051(0.052)	0.051
l(F···F)	[0.055–0.053]	0.054(0.056)	0.053
l(F···F)$_{gauche}$	[0.118–0.112]	0.122(0.130)	0.112
l(F···F)$_{trans}$	[0.065–0.062]	0.060(0.062)	0.058

[a] Observed values (from Table I) with 3–8% reduction for sample spread (see text). [b] Calculated values (see text). [c] Values calculated by Cyvin, *et al.* (ref 4).

The magnitude of V_0 is then systematically varied to obtain the best-fit function in eq 3.

As is well known, eq 1 and 2 are valid only for high barrier cases [$V_0/RT \approx 15$] whereas eq 3 is applicable for low barriers (for example, large torsional amplitude motions). For an intermediate height one may estimate the barrier by an extension of the above procedures. If the magnitude derived from the high barrier equations agrees with that based upon the low barrier method one may have confidence in the result. For C_2F_6, the estimated barrier is, indeed, in the intermediate catagory since the deviation (7.3 ± 2.7°) of the torsional angle from the staggered position was neither too large nor too small.

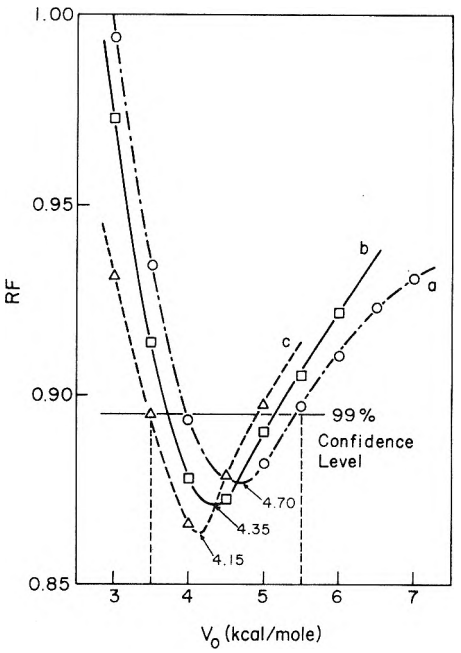

Figure 6. The R factor for the radial distribution function of C_2F_6 plotted as a function of the barrier to internal rotation, based on eq 3. These curves apply to T_{sample} = 300°K; a similar set was obtained for T_s = 250°K. The three curves show the effect of varying $l_{ij}(\tau)$: (a) Cyvin's value; (b) Cyvin reduced by 10%; (c) reduced by 20%.

On applying the above procedures to this molecule the following values were used: r_g(trans) = 3.490_8 Å; r_g(gauche) = 2.741_2 Å; δ_g = 0.0036 (−0.002, +0.003) Å. Then on the basis of eq 1, V_0 = 6.84 (−3.1, +5.2) at 250°K, and increases to 8.21 (−3.7, +6.2) at 300°K. In view of these large error limits, eq 1 is not useful. In eq 2 we used l_{obsd} = 0.122 (−0.015, +0.005) and tested l_f (0.090; 0.094). The various combinations led to V_0 = 3.9_4 (−0.61, +4.04) at 250°K and to 5.30 (−0.90, +6.98) at 300°K. Here, also, the large error limits preclude the assignment of a meaningful value to V_0. For eq 3 the mean amplitudes of the frame vibrations, $l(\tau)$, were taken from ref 4 and 5. Typical results derived from eq 3 are graphed in Figure 6. The final values for 250 and 300°K are V_0 = 3.6_7 (−0.75, +0.91) and 4.4_0 (−0.90, +1.10), respectively. Thus, for either temperature the mean barrier heights estimated according to the three methods generally agree with one another, but only the one based on eq 3 has small enough error limits to be informative. The magnitude thus obtained for a 250°K sample is in slightly better agreement with the 3.92 kcal/mol value derived from thermodynamic data (and rechecked in light of our new structural parameters) than the value found for a 300°K sample, but the error limits are still too large to permit a firm discrimination. Nevertheless, if a 50° drop in sample temperature leads to ≈1 kcal/mol lowering of the estimated barrier height, then the real gas temperature should be used in applying eq 1–3.

Acknowledgments. This work was supported by the National Science Foundation under Grant No. GP-34060.

Appendix I

Optical Densities for Integral q's for C_2F_6.

Q	Intensity	Q	Intensity	Q	Intensity	Q	Intensity
λ = 0.05321 Å							
L = 253.26 mm							
5	0.1332	31	0.5731	57	0.4426	82	0.4610
6	0.1155	32	0.5547	58	0.4503	83	0.4594
7	0.1158	33	0.5376	59	0.4561	84	0.4589
8	0.1321	34	0.5340	60	0.4586	85	0.4594
9	0.1564	35	0.5435	61	0.4583	86	0.4595
10	0.1830	36	0.5556	62	0.4590	87	0.4587
11	0.2090	37	0.5605	63	0.4623	88	0.4571
12	0.2298	38	0.5547	64	0.4667	89	0.4557
13	0.2416	39	0.5418	65	0.4700	90	0.4559
14	0.2559	40	0.5284	66	0.4708	91	0.4587
15	0.2870	41	0.5169	67	0.4687	92	0.4633
16	0.3396	42	0.5097	68	0.4645	93	0.4681
17	0.4060	43	0.5077	69	0.4610	94	0.4714
18	0.4656	44	0.5137	70	0.4546	95	0.4712
19	0.5007	45	0.5270	71	0.4481	96	0.4692
20	0.5107	46	0.5425	72	0.4436	97	0.4658
21	0.5042	47	0.5520	73	0.4443	98	0.4622
22	0.4921	48	0.5519	74	0.4499	99	0.4592
23	0.4791	49	0.5450	75	0.4590	100	0.4578
24	0.4657	50	0.5375	76	0.4670	101	0.4580
25	0.4503	51	0.5323	77	0.4712	102	0.4598
26	0.4445	52	0.5271	78	0.4712	103	0.4627
27	0.4611	53	0.5200	79	0.4684	104	0.4655
28	0.5007	54	0.5102	80	0.4656	105	0.4669
29	0.5463	55	0.5019	81	0.4629	106	0.4673
30	0.5732	56	0.4378				
λ 0.4918 Å							
L = 124.72 mm							
35	0.4545	46	0.4617	107	0.4668	118	0.4681
36	0.4663	47	0.4738	108	0.4671	119	0.4695
37	0.4724	48	0.4764	109	0.4679	120	0.4723
38	0.4671	49	0.4720	110	0.4695	121	0.4743
39	0.4552	50	0.4655	111	0.4702	122	0.4757
40	0.4415	51	0.4609	112	0.4701	123	0.4767
41	0.4300	52	0.4586	113	0.4697	124	0.4767
42	0.4226	53	0.4536	114	0.4694	125	0.4761
43	0.4215	54	0.4465	115	0.4682	126	0.4759
44	0.4292	55	0.4398	116	0.4674	127	0.4754
45	0.4446			117	0.4675		

Appendix II

Error Matrix C_2F_6; Model I

	(C–C)	(C–F)	∠CCF	l(C–C)	l(C–F)	l(C···F)	l(F···F)	l(F···F)$_g$	l(F···F)$_t$
(C–C)	0.0011								
(C–F)	−0.0004	0.0002							
∠CCF	−0.0067	0.0025	0.0401						
l(C–C)	−0.0000	0.0002	0.0005	0.0026					
l(C–F)	−0.0001	−0.0001	−0.0001	−0.0004	0.0003				
l(C···F)	0.0003	−0.0000	−0.0007	0.0002	−0.0001	0.0004			
l(F···F)	−0.0004	0.0000	0.0028	−0.0002	0.0000	0.0002	0.0008		
l(F···F)$_g$	−0.0005	−0.0000	0.0013	−0.0001	0.0000	−0.0002	−0.0003	0.0016	
l(F···F)$_t$	0.0001	−0.0000	−0.0006	−0.0001	0.0000	−0.0000	−0.0001	−0.0000	0.0017

Correlation Matrix C_2F_6; Model I

(C–C)	1.0000								
(C–F)	−0.5806	1.0000							
∠CCF	−0.9685	0.6823	1.0000						
l(C–C)	−0.0002	0.0434	0.0024	1.0000					
l(C–F)	−0.0109	−0.0383	−0.0016	−0.2383	1.000				
l(C···F)	0.1778	−0.0122	−0.0286	0.0268	−0.0268	1.0000			
l(F···F)	−0.1852	0.0030	0.2303	−0.0231	0.0100	0.0761	1.0000		
l(F···F)$_g$	−0.1439	−0.0000	0.0255	−0.0007	0.0030	−0.0379	−0.0721	1.0000	
l(F···F)$_t$	0.0018	−0.0052	−0.0058	−0.0042	0.0039	−0.0025	−0.0037	−0.0005	1.0000

References and Notes

(1) D. A. Swick and I. L. Karle, *J. Chem. Phys.*, **23**, 1499 (1955).
(2) K. Kuchitsu, *J. Chem. Phys.*, **49**, 4456 (1968).
(3) R. Carney, E. A. Piotrowski, A. G. Meister, J. H. Braun, and F. F. Cleveland, *J. Mol. Spectrosc.*, **7**, 209 (1961).
(4) S. J. Cyvin, I. Elvebredd, B. N. Cyvin, J. Brunvoll, and G. Hagen, *Acta Chem. Scand.*, **21**, 2405 (1967).
(5) S. J. Cyvin and J. Brunvoll, *Acta Chem. Scand.*, **22**, 2718 (1968).
(6) D. E. Mann and E. K. Plyler, *J. Chem. Phys.*, **21**, 1116 (1953).
(7) J. Karle, *J. Chem. Phys.*, **45**, 4149 (1966).
(8) E. L. Pace and J. G. Aston, *J. Amer. Chem. Soc.*, **70**, 566 (1948).
(9) K. L. Gallaher and S. H. Bauer, **78**, 2380 (1974).
(10) A. L. Andreassen, D. Zebelman, and S. H. Bauer, *J. Amer. Chem. Soc.*, **93**, 1148 (1971).
(11) Y. C. Wang and S. H. Bauer, *J. Amer. Chem. Soc.*, **94**, 5651 (1972).
(12) S. H. Bauer and A. L. Andreassen, *J. Phys. Chem.*, **76**, 3099 (1972).
(13) I. L. Karle and J. Karle, *J. Chem. Phys.*, **17**, 1052 (1949).
(14) C. Tavard, D. Nickolas, and M. Rouault, *J. Chem. Phys.*, **64**, 540 (1967).
(15) R. A. Bonham and T. Ukaji, *J. Chem. Phys.*, **36**, 72 (1962).
(16) W. C. Hamilton, *Acta Crystallogr.*, **18**, 502 (1965).
(17) S. H. Bauer, "Diffraction of Electrons by Gases," in "Physical Chemistry, An Advanced Treatise," Vol. 4, H. Eyring, *et al.*, Ed., Academic Press, New York, N.Y., 1970, p 790.
(18) A. Yokozeki and S. H. Bauer, to be submitted for publication.
(19) T. Shimanouchi, *Nat. Stand. Ref. Data Ser., Nat. Bur. Stand.*, **No. 39** (1972).
(20) J. Karle and H. Hauptman, *J. Chem. Phys.*, **18**, 875 (1950).
(21) Y. Morino and E. Hirota, *J. Chem. Phys.*, **28**, 185 (1958).
(22) D. A. Swick and I. L. Karle, *J. Chem. Phys.*, **22**, 1242 (1954).

The Crystal Structure of Hydrated Thallium-Exchanged Zeolite X

J. J. de Boer* and I. E. Maxwell

Koninklijke/Shell-Laboratorium, Amsterdam (Shell Research B.V.), Holland *(Received December, 1973; Revised Manuscript Received June 4, 1974)*

Publication costs assisted by Koninklijke/Shell-Laboratorium

The crystal structure of hydrated Tl^+-exchanged zeolite X has been determined by single-crystal X-ray diffraction techniques. The compound crystallizes in space group $Fd3m$ (a = 25.089 (5) Å). Reflection data were collected with Cu Kα (λ 1.54182 Å) radiation using a synthetic crystal with a maximum dimension of approximately 0.1 mm. A total of 281 observed reflections was obtained by counter methods and the structure was refined by least-squares techniques to a final conventional R factor of 0.13. Tl^+ ions are located inside the sodalite cages in front of the hexagonal prisms (site I′) and in front of the six-membered ring face of the sodalite cage on the supercage side (site II). No water molecules and only 52% of the cations could be located. Unlocated cations and water molecules were included as uniformly distributed spheres. The shortest Tl^+–O distances are 2.64 (5) and 2.79 (5) Å.

I. Introduction

In recent years many X-ray diffraction studies have been made of the siting of cations in zeolites with the faujasite framework structure.[1] However, particularly in monovalent cation-exchanged forms, there is always a proportion of cations that are not located by X-ray analysis (so-called site III cations). This proportion is largest in hydrated X-type zeolites (*e.g.*, Na–X, 53% unlocated;[2] K–X, 54% unlocated[3]). Possible sites for these cations have been indicated by several authors.[1-4] The most favored sites are those in the vicinity of the four-membered rings of oxygen atoms in the supercage (see Figure 1). If there is indeed any ordering of these cations then they are on symmetry sites with low occupancy factors or they are spread over general (nonsymmetry) crystallographic positions. However, they may be observed in cases where the monovalent cation has a high atomic number, such as Tl^+. Furthermore, the ion-exchange isotherm for the system (Tl,Na)–X shows that the selectivity of the zeolite for Tl^+ is high over the entire range of the exchange reaction.[5] This suggests that Tl^+ is strongly interacting with the zeolite surface even in the hydrated form. The ion-exchange system (Tl,Na)–A shows a similar effect and indeed 92% of the Tl^+ ions were found by X-ray analysis to be strongly bound to the zeolite surface in hydrated Tl^+-exchanged zeolite A.[6]

We have now studied the crystal structure of hydrated Tl^+-exchanged zeolite X in the hope of locating the site III type cations.

II. Experimental Section

Crystals of zeolite X suitable for single-crystal X-ray analysis were prepared by the method of Charnell.[7] Since some zeolite A cocrystallized, the Si/Al ratio for zeolite X could not be accurately determined by chemical analysis. We have therefore assumed the Si/Al ratio to be 1.18, the value found by Olson[2] for similarly prepared synthetic zeolite X crystals. For X-ray examination zeolite X and A crystals were easily separated owing to the differences in crystal product morphology.

The crystalline product was contacted for several weeks with 20 ml of a 0.1 M solution of $TlNO_3$ at room temperature and subsequent chemical analysis indicated that exchange was complete. A roughly octahedrally shaped crystal of zeolite X, approximately 0.1 mm on edge, was selected for X-ray examination. Preliminary precession photographs confirmed the space group to be $Fd3m$ and no spu-

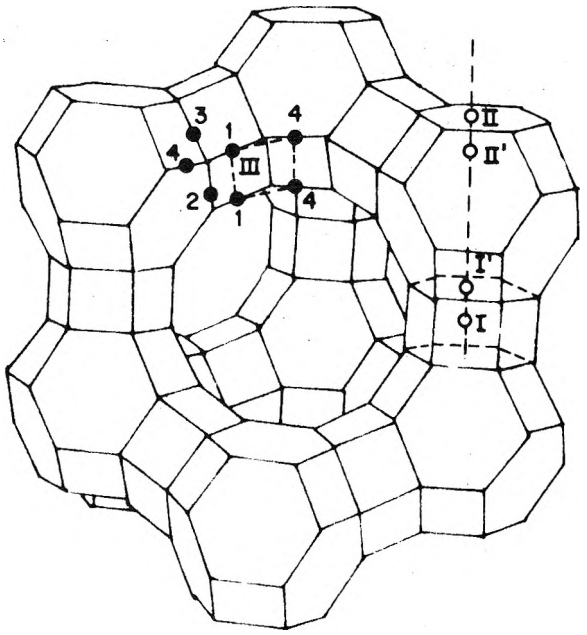

Figure 1. Faujasite framework and cation siting (roman numerals indicate cation sites, arabic numbers show oxygen atom numbering scheme).

rious reflections were evident on the films. For data collection the crystal was then mounted about the [110] direction on a three-circle Nonius automatic diffractometer equipped with scintillation counter and pulse height discriminator. Least-squares refinement based on θ, $-\theta$ ($\theta \leq 15°$) values measured for several reflections using Cu Kα radiation (λ 1.54182 Å) gave a = 25.089 (5) Å. Approximately eight equivalent data sets were collected, with Ni-filtered Cu Kα radiation ($\theta \leq 50°$). The θ–2θ scan method was employed with a scanning speed of 0.6°/min (in θ) and a scan range of 0.7°.

Backgrounds were measured for half of the scan time on each side of the scan. As a check on electronic and crystal stability, a control reflection was monitored at regular intervals. No significant variation in intensity of this reflection was observed during data collection. The initial standard deviation, $\sigma(I)$, of an intensity, I, was estimated from the expression $\sigma(I)$ = (total counts + total background counts + (0.035 × net counts)^2)$^{1/2}$. The standard deviation, $\sigma(F)$, of a structure amplitude F was then taken to be $\sigma(F^2)/(2F)$ and weights, ω, for the least-squares refinements were $\sigma^{-2}(F)$. Lorentz, polarization, and absorption corrections ($\mu_{CuK\alpha}$ = 46.5 mm^{-1}) were applied, the latter by means of a semiempirical method as described by Furnas.[8] The φ-dependent absorption corrections were obtained from measurements of the $hh0$ reflections (h = 2, 4, 6 . . .). These corrections were then applied to zones of the type (h + k)/2 = 1, 2, 3 . . . ; corrections for the odd-numbered zones were found by interpolation. As suggested by North, *et al.*,[9] a θ-dependent absorption correction was also applied, assuming a cylindrical diameter of 0.1 mm. Applied empirical absorption correction factors ranged from 0.74 to 1.24. The data were then scaled and averaged to yield 281 unique reflections with an estimated conventional R factor of 0.10, where

$$R = \sum_{j=1}^{N_0} \left\{ \sum_{i=1}^{m} \left(\frac{|F_0| - |\bar{F}|}{m|\bar{F}|} \right) \right\} / N_0$$

in which N_0 = number of unique reflections, m = number of equivalent reflections, $|F_0|$ = observed structure factor amplitude, and $|\bar{F}|$ = average structure factor amplitude = $\Sigma_{i=1}{}^{m}(|F_0|)/m$.

At the completion of the data collection and structure analysis, the crystal was mounted, for demonstration purposes, on a Philips PW1100 four-circle automatic diffractometer. By means of the computer-controlled random reciprocal lattice search routine it was discovered that the crystal contained a small twin intergrowth. The twin planes were shown to be of the type (11$\bar{1}$),(011) and ($\bar{1}$11),(0$\bar{1}$1) for the main and intergrowth crystals, respectively. However, the agreement between equivalent reflections likely to be affected by twinning was found to be good. Furthermore, the intensities of unique reflections from the intergrowth were shown to be weak. Thus, the effects of the twin on the results of the structural analysis are believed to be small.

III. Structure Determination

Initial full matrix refinement was carried out with the framework parameters of hydrated Na–X.[2] Difference Fourier syntheses revealed the position of Tl$^+$ cations at sites I′ and II.[10] There was no significant electron density inside the hexagonal prism (site I). Subsequent refinement of Tl$^+$ cations in this position led to an occupancy factor of zero within the limits of error.

The located cations were included in further refinement, which led to an R_1 value of 0.17 (where $R_1 = \Sigma||F_0| - |F_c||/\Sigma|F_c|$). Unfortunately, at this stage there was no evidence from difference syntheses of electron density due to Tl$^+$ ions inside the supercages other than those at site II. Examination of the data showed that agreement between observed and calculated structure factor amplitudes was rather poor for low-angle reflections. To account for the relatively high percentage of unlocated electron density, a function of the type used by Simpson and Steinfink[11] was introduced. This function modifies the form factor, f, of a given atom such that $f' = f[3/(\mu R)^3][\sin(\mu R) - \mu R \cos(\mu R)]$, where $\mu = 4\pi(\sin\theta)/\lambda$ and R is the radius of the sphere for the uniformly distributed atom. Unlocatable Tl$^+$ ions and water molecules were included as uniformly distributed spheres at the center of the supercage with radii of 6.1 and 6.2 Å, respectively. A further contribution from water inside the sodalite cage was included with a spherical radius of 2.3 Å. These radii were found to give the best agreement between observed and calculated structure factor amplitudes with the low angle data.

In view of the high degree of correlation between the scale factor and the occupancy and temperature factors of the Tl$^+$ ions, these parameters were varied separately in alternating refinement cycles. In the final stages of refinement all shifts in parameters were less than 20% of their corresponding standard deviations. No significant anisotropic thermal motion was evident from a difference synthesis. Thus, on account of the limited amount of data and the high degree of correlation between the scale and temperature factors, refinement of anistropic temperature factors was not attempted.

A plot of $\langle(|F_0| - |F_c|)^2\rangle$ in ranges of $(\sin\theta)/\lambda$ indicated that the initial weighting scheme was incorrect. The estimated standard deviations were accordingly modified such that for $(\sin\theta)/\lambda < 0.1699$; $\sigma(F) = 4.4$; for F_0/scale factor > 380, $\sigma(F) = 6.6$; otherwise $\sigma(F) = 2.2$. This weighting scheme gave a final value for the error in an observation of unit weight of 0.98. Final values for the residuals were R_1 =

TABLE I: Positional, Thermal, and Occupancy Parameters for Hydrated Thallium-Exchanged Zeolite X

Atom	Position[a]	Occupancy factor[b]	X	Y	Z	B, Å²
(Si, Al)	192(i)	1.0	0.0351 (6)	0.3031 (6)	0.1239 (5)	3.6 (3)
O(1)	96(h)	1.0	0.0	−0.106 (2)	0.106 (2)	2.6 (9)
O(2)	96(g)	1.0	0.004 (3)	−0.144 (2)	0.004 (3)	4.0 (1.0)
O(3)	96(g)	1.0	0.077 (3)	−0.033 (2)	0.077 (3)	4.2 (1.1)
O(4)	96(g)	1.0	0.072 (4)	0.325 (3)	0.072 (4)	7.5 (1.8)
Tl(I′)	32(e)	0.71 (1)	0.0722 (5)	0.0722 (5)	0.0722 (5)	2.7 (2)
Tl(II)	32(e)	0.72 (1)	0.0053 (3)	−0.2553 (5)	0.0053 (5)	2.8 (2)

[a] Origin at center ($\bar{3}m$). [b] Standard deviations, in parentheses, are given in units of the least significant digits of the corresponding parameter.

TABLE II: Cation Siting in Hydrated Na^+-, K^+-, and Tl^+-Exchanged Forms of Zeolite X

Formula per unit cell	Occupancy factor[a]			Unlocated cations (site III)
	Site I	Site I′	Site II	
$Na_{88}(AlO_2)_{88}(SiO_2)_{104}$[c]	9.0 (6)[b] Na^+	8.0 (13) Na^+	24.0 (3) Na^+	47.0 Na^+
$K_{86.5}(AlO_2)_{86.5}(SiO_2)_{105.5}$[d]	8.9 (6) K^+	7.2 (9) K^+	23.2 (6) K^+	47.2 K^+
$Tl_{88}(AlO_2)_{88}(SiO_2)_{104}$		22.7 (3) Tl^+	23.0 (3) Tl^+	42.3 Tl^+

[a] All occupancy factors are given as the number of cations per unit cell. [b] Standard deviations, in parentheses, are given in units of the least significant digits of the corresponding parameter. [c] Reference 2. [d] Reference 3.

TABLE III: Interatomic Distances and Angles[a] for Hydrated Thallium-Exchanged Zeolite X

Distances[b]			
(Si,Al)–O(1)	1.67 (3)	O(2)–O(3)	2.74 (5)
(Si,Al)–O(2)	1.64 (2)	O(2)–O(4)	2.75 (6)
(Si,Al)–O(3)	1.70 (2)	O(3)–O(4)	2.74 (11)
(Si,Al)–O(4)	1.69 (3)	Tl(I′)–O(3)	2.64 (5)
O(1)–O(2)	2.73 (8)	Tl(I′)–O(2)	3.25 (8)
O(1)–O(3)	2.76 (7)	Tl(II)–O(2)	2.79 (5)
O(1)–O(4)	2.67 (3)	Tl(II)–O(4)	3.26 (11)
Angles[c]			
O(1)–(Si,Al)–O(2)	111 (4)	(Si,Al)–O(3)–(Si,Al)	144 (3)
O(1)–(Si,Al)–O(3)	110 (3)	(Si,Al)–O(4)–(Si,Al)	138 (5)
O(1)–(Si,Al)–O(4)	105 (4)	O(3)–Tl(I′)–O(3)	95 (3)
O(2)–(Si,Al)–O(3)	110 (3)	O(3)–Tl(I′)–O(2)	128 (3)
O(2)–(Si,Al)–O(4)	111 (4)	O(2)–Tl(I′)–O(2)	108 (1)
O(3)–(Si,Al)–O(4)	108 (5)	O(2)–Tl(II)–O(2)	89 (3)
		O(2)–Tl(II)–O(4)	53 (1)
(Si,Al)–O(1)–(Si,Al)	139 (5)	O(2)–Tl(II)–O(4)	121 (3)
(Si,Al)–O(2)–(Si,Al)	145 (4)	O(4)–Tl(II)–O(4)	106 (2)

[a] Standard deviations, in parentheses, are given in units of the least significant digits of the corresponding parameter. [b] Distances are in ångströms. [c] Angles are in degrees.

0.13 and $R_2 = 0.15$ (where $R_2 = [\Sigma\omega(|F_o| - |F_c|)^2/\Sigma|F_o|^2]^{1/2}$).

The refined positional, occupancy, and temperature factors are given in Table I, and the observed and calculated structure factors are available elsewhere.[12,13]

IV. Discussion

In hydrated thallium-exchanged zeolite X, Tl^+ ions are located at sites I′ and II (see Figure 1). Surprisingly, there are no Tl^+ cations (or residual Na^+ cations) inside the hexagonal prisms (site I). Partial occupancy of this site might be expected for an even charge balance distribution to be maintained over the zeolite framework. Such is the case for both hydrated Na^+ [2] and K^+ [3] exchanged forms of zeolite X, where cations are located at sites I, I′, and II (see Table II). Distance calculations show that the hexagonal prism (centered at the origin) is in fact sufficiently large to accommodate a Tl^+ (origin · · · O(3), 2.86(7); origin · · · O(2), 3.62 (5) Å). Moreover, the calculated angles [O(3)–origin–O(3′), 86(3)°; O(3)–origin–O(3″), 94(3)°] indicate that the coordination geometry would be very close to octahedral. However, Tl^+ ions must diffuse through the single six-membered rings forming the entrances to the sodalite cage in order to be located at site I′. Furthermore, the minimum diameters of these two crystallographically different six-membered rings are very similar (hexagonal prism six-ring diameter, O(3) · · · O(2), 5.29 (9); $r_{Tl^+} + r_{O^{2-}}$, 5.6 Å;[14] sodalite cage six-ring diameter, O(2) · · · O(4), 5.28 (11) Å).

There are two possible reasons for the absence of Tl^+ ions at site I. First, this site may be thermodynamically unfavorable; second, the six-membered ring entrance to the hexagonal prism inhibits diffusion. The structural data alone do not allow us to distinguish between these two possibilities. However, in view of the potentially favorable coordination geometry at site I for a Tl^+ ion, and the occupancy of this site by other monovalent cations such as Na^+ and K^+ (see Table II), the thermodynamic argument seems less likely. In this case the double six-ring structural unit could conceivably be more rigid than a single six-mem-

TABLE IV: Deviations of Atoms from {111} for Hydrated Thallium-Exchanged Zeolite X

Atom(s) defining plane	Atom not in plane	Distance from plane, Å[a]
O(3)	Tl(I′)	1.37
O(3)	O(2)	0.21
O(2)	Tl(II)	1.65
O(2)	O(4)	0.41

[a] All deviations are positive, indicating that the atoms all lie on the opposite side of the plane to the origin.

bered ring and thereby increase the activation energy for diffusion of Tl^+ ions into the hexagonal prisms.

Furthermore, there is good evidence from ion-exchange isotherm studies[15] that for large ionic radii monovalent cations such as Rb^+ and Cs^+ diffusion through six-membered ring systems in zeolites X and Y cannot occur at room temperature under equilibrium conditions, whereas for small ionic cations such as K^+, Na^+, and Li^+ diffusion into the dense cage system readily occurs. It would therefore not be so surprising if Tl^+ (r_{Tl^+} = 1.40 Å) with an ionic radius intermediate between K^+ (r_{K^+} = 1.33 Å) and Rb^+ (r_{Rb^+} = 1.48 Å) was a rather critical case.

As shown in Table III the closest approaches of Tl^+ ions to the framework are Tl(I′)–O(3), 2.64 (5) Å and Tl(II)–O(2), 2.79 (5) Å. At site I′ the cation–oxygen distance is less than the sum of the ionic radii ($r_{Tl^+} + r_{O^{2-}}$ = 1.40 + 1.40 = 2.80 Å[14]), indicating strong bonding to the zeolite framework. Shortest Tl–O distances in the related hydrated Tl–A structure[6] are 2.75 (2), 2.86 (2), and 2.81 (2) Å. These distances decrease to 2.64 (2), 2.82 (3), and 2.60 (3) Å, respectively, on dehydration. The rather short Tl(I′)–O(3) distance in the hydrated Tl–X structure may therefore be indicative of only weak cation–water interactions at this site. The larger ionic radius of the Tl^+ ion is reflected by the protrusion of these ions above the mean plane formed by the six-membered oxygen rings (see Table IV). A similar protrusion of Tl^+ ions above a six-membered ring was observed in the hydrated Tl–A structure.[6] Also from Table IV it can be seen that the single six-membered ring formed by O(2) and O(4) type oxygen atoms is more buckled than the double six-membered ring formed by O(2) and O(3) oxygen atoms.

The distribution of cations in hydrated Tl^+-exchanged zeolite X is compared with that in the Na^+ and K^+ forms in Table II. Clearly, the absence of cations at site I results in a relative increase in the number of cations at site I′ to balance the negative framework charge. However, the total number of Tl^+ cations at site I′ (22.7 (3) per unit cell) is somewhat higher than the sum of the cations at sites I and I′ in the Na^+- and K^+-exchanged forms (Na^+, 17.0; K^+, 16.1 per unit cell). Nevertheless, the number of cations located at site II is very similar for all three monovalent exchanged forms. The high occupancy of site I′ in the Tl^+-exchanged form corresponds to approximately three Tl^+ ions per cubo-octahedron; the closest Tl(I′) ··· Tl(I′) approach inside this cage is therefore 3.75 (4) Å.

The ion-exchange isotherms for the systems (Tl,Na)–X and (Tl,Na)–Y (25° and 0.1 total normality) measured by Sherry[5] are shown in Figure 2. As previously discussed, in zeolite X the Na^+ ions can be completely exchanged for Tl^+ and a high selectivity for Tl^+ is demonstrated throughout the exchange reaction. The selectivity was attributed to the high polarizability of Tl^+ and considered to be indicative of strong binding onto the zeolite surface. This is in agreement with the rather high occupancy factor of site I′ and the short framework–cation distance, Tl(I′)–O(3), 2.64 (5) Å (Table III).

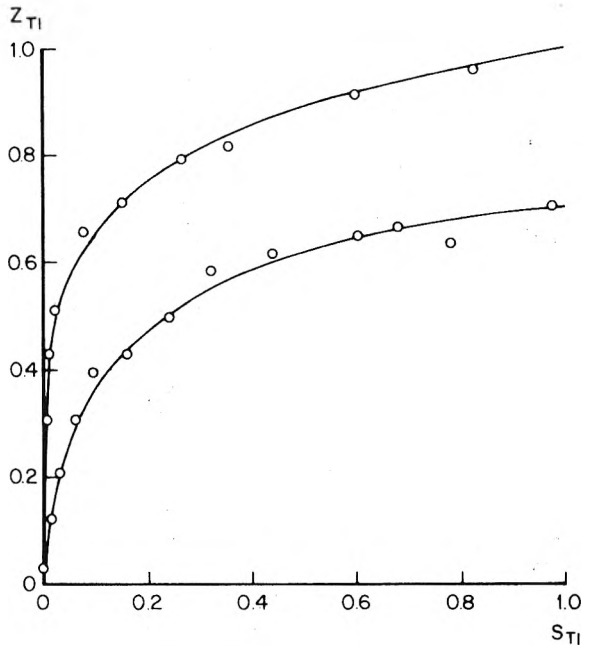

Figure 2. Tl^+–Na^+ isotherms at 25°, 0.1 total normality: top curve, zeolite X; bottom curve, zeolite Y.

In the system (Tl,Na)–Y exchange of Na^+ for Tl^+ ions was found to be incomplete at 25° (see Figure 2). A maximum Tl^+ exchange level of only approximately 65% was attainable. In the zeolite Y structure this corresponds to 16 Na^+ cations per unit cell which remain unexchanged. These cations were presumed[5] to be sited inside the dense cage system (sites I and I′).

Sherry[15] has attributed the incomplete exchange to a slow rate of diffusion of Tl^+ ions through the six-membered ring entrances of the sodalite cage. These rings have a slightly smaller diameter (approximately 0.01 Å) in zeolite Y than in X due to a lattice contraction as the Si/Al ratio is increased. To confirm that this was kinetic, rather than thermodynamic in origin, as was proposed by other workers,[16] Sherry showed[15] that at 100° complete exchange of Na^+ for Tl^+ ions could be achieved in zeolite Y. If a diffusion barrier exists in zeolite X, Tl^+ cations may migrate from site I′ to site I at elevated temperatures.

The fact that approximately 42 Tl^+ ions per unit cell (a total of 3360 electrons) could not be located by X-ray analysis indicates that these cations are very disordered. Conceivably, these cations may be more ordered in the dehydrated form and thus be locatable by X-ray diffraction techniques.

Acknowledgments. Crystals of zeolite X suitable for X-ray analysis were kindly prepared by P. Hendriks and J. Helle. The authors thank Dr. E. Keulen of the Philips Laboratories, Netherlands, for discovering the crystal intergrowth during a demonstration of the PW 1100 four-circle automatic diffractometer.

Supplementary Material Available. A listing of structure factor amplitudes will appear following these pages in the microfilm edition of this volume of the journal. Photocopies of the supplementary material from this paper only

or microfiche (105 × 148 mm, 24× reduction, negatives) containing all of the supplementary material for the papers in this issue may be obtained from the Journals Department, American Chemical Society, 1155 16th St., N.W., Washington, D. C. 20036. Remit check or money order for $3.00 for photocopy or $2.00 for microfiche, referring to code number JPC-74-2395.

References and Notes

(1) J. V. Smith, *Advan. Chem. Ser.*, **No. 101**, 171 (1971).
(2) D. H. Olson, *J. Phys. Chem.*, **74**, 2785 (1970).
(3) W. J. Mortier and H. J. Bosmans, *J. Phys. Chem.*, **75**, 3327 (1971).
(4) D. H. Olson, R. J. Mikovsky, G. F. Shipman, and E. Dempsey, *J. Catal.*, **24**, 161 (1972).
(5) H. S. Sherry, *J. Phys. Chem.*, **70**, 1158 (1966).
(6) P. E. Riley, K. Seff, and D. P. Shoemaker, *J. Phys. Chem.*, **76**, 2593 (1972).
(7) J. F. Charnell, *J. Cryst. Growth*, **8**, 291 (1971).
(8) T. C. Furnas, "Single Crystal Orienter Instruction Manual," General Electric Co., Milwaukee, Wisc., 1957.
(9) A. C. T. North, D. C. Phillips, and F. S. Mathews, *Acta Crystallogr., Sect. A*, **24**, 351 (1968).
(10) The site nomenclature is as follows: site I, center of hexagonal prism; site II, six-membered ring face of sodalite cage on the supercage side; sites I′ and II′ lie on the other sides of the six-membered rings, opposite sites I and II, respectively, inside the sodalite cage (see also Figure 1).
(11) H. D. Simpson and H. Steinfink, *J. Amer. Chem. Soc.*, **91**, 6225 (1969).
(12) See paragraph at end of text regarding supplementary material.
(13) Scattering factors used for all atoms were taken from the "International Tables for X-Ray Crystallography," Vol. III, Kynoch Press, Birmingham, England 1969. The anomalous dispersion correction for Tl^+ was also included. The following computer programs were used: full-matrix least-squares refinement, J. Ibers' modification of ORFLS, Busing, Martin, and Levy Report No. ORNL-TM-305, Oak Ridge National Laboratory, Oak Ridge, Tenn., 1964; Fourier synthesis, J. Ibers' modification of FORDAP, written by A. Zalkin (1962); Errors distances and angles, ORFFE, Busing, Martin, and Levy, No. ORNL-TM-306, Oak Ridge National Laboratory, Oak Ridge, Tenn., 1964.
(14) L. Pauling, "The Nature of the Chemical Bond," 3rd ed, Cornell University Press, Ithaca, N.Y., 1960, p 518.
(15) H. S. Sherry, *Advan. Chem. Ser.*, **No. 101**, 350 (1971).
(16) R. M. Barrer, J. A. Davies, and L. V. C. Rees, *J. Inorg. Nucl. Chem.*, **30**, 3333 (1968).

Insertion Compounds of Transition Element Disulfides

J. V. Acrivos[1]

W. W. Hansen Laboratories, Stanford University, Stanford, California 94305

(*Received May 20, 1974*)

The Hückel one electron approximation has been applied to explain the process of intercalating atoms and molecules between the layers of transition element dichalcogenides of groups Vb and VIb of the periodic table. The wave vector for the Bloch functions representing the lowest unoccupied and highest occupied levels of these compounds are known from the optical data reported in the literature. Thus the power of the simple Hückel approximation is shown by the explanation obtained for the bonding and for the process of intercalation using the highest occupied and lowest unoccupied levels in the dichalcogenide and intercalate molecules. The prediction that 2H–MoS_2 intercalated with the strong acceptor tetracyanoquinodimethane should behave as the neighbor Vb compound 2H–NbS_2 is suggested by the observed onset of a superconducting transition below 2 K.

I. Introduction

Recent studies on the chemical and physical properties of insertion compounds into layer transition element dichalcogenides are of some importance for the following reasons: *one*, molecular complexes of well determined stoichiometry are usually formed,[2,3] and, *two*, the transport and optical properties show that metal superconductors (*e.g.*, $NbSe_2$) are transformed into semimetals by the intercalation of sodium atoms,[4] whereas semiconductors (*e.g.*, MoS_2) are transformed into superconducting metals by the intercalation of Na–NH_3.[4,5]

The process of intercalation is described by the chemical reaction

$$TX_2(\text{xtal}) + x\text{I(g)} = TX_2{\cdot}I_x(\text{xtal}), \qquad \Delta H_I < 0 \quad (1)$$

where I is the intercalate atom or molecule and TX_2 is the laminar solid which consists of stacked macromolecules $(TX_2)_N$, $N \gtrsim 10^5$, held together by X–X′ van der Waals bonds between neighboring layers. These weak bonds are easily broken to accommodate the guest atoms and molecules in the so-called van der Waals gap of the solids shown in Figure 1a. The change in enthalpy is typical of the formation of a molecular comples.[6,7] Thus

$$\Delta H_I = E_{vdW} + E_{steric} + p\Delta V - \langle|\beta|^2/\Delta\rangle_{av} \quad (2)$$

where both E_{vdW} and E_{steric} are positive terms which represent the energy necessary to break the van der Waals bonds in the original solid and to repolarize the system and to orient the intercalate molecules, respectively. The work due to volume changes at constant pressure $p\Delta V < 0$ is negligible. The last term represents the resonance energy contribution for the electron donor acceptor complex (EDA) when $|\beta| \ll \Delta$.[6,7] Here $\Delta = I_p - E + \delta E_C$, I_p is the ionization energy of the donor level, E is the electron affinity, and δE_C is the change in Madelung energy between the ground and excited states of the complex. Already the shifts produced by intercalation on the optical absorbancy of dichalcogenides of elements in groups IVb and VIb indicate that EDA complexes are formed by reaction 1.[8,9]

The purpose of this work is to examine the stoichiometry

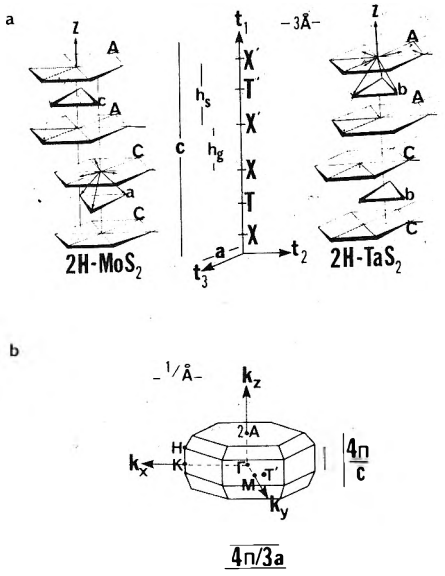

Figure 1. Structure of 2H-MoS_2 and 2H-TaS_2 in the hexagonal closed-packed lattice: (a) positions of the atoms generated by the primitive translations $\mathbf{t}_1 = (0, 0, c)$, $\mathbf{t}_2 = (a, 0, 0)$ and $\mathbf{t}_3 = -(1, 3^{-1/2}, 0)a/2$ and (b) first Brillouin zone for the 2H compounds according to ref 9 and 12.

of (1) in light of the LCAO tight binding approximation for solids,[10] and to apply the predictive power of the Hückel MO approximation[11] to the intercalation reactions.

II. Interacting LCAO-MO of Solid and Intercalate

Symmetry based rules have been derived for the reactions of aromatic compounds using the Hückel-MO one electron approximation for π orbitals.[11] These are one electron Bloch functions over the finite molecular frame, *e.g.*, the benzene π orbitals are

$$\phi_m = 6^{-1/2}\sum_{n=1}^{6} \exp[imn(\pi/3)]C_n{:}2p_z(\mathbf{r} - \mathbf{R}_n) \quad (3)$$

where $m = 0, \pm1, \ldots$ and $C_n{:}2p_z(\mathbf{r} - \mathbf{R}_n)$ is the atomic orbital centered at $\mathbf{r} = \mathbf{R}_n$. Similarly the chemical reactivity of the solid should be predictable using the two dimensional Bloch functions which describe the dichalcogenide macromolecule $(TX_2)_N$, *e.g.*

$$b_{k\nu}(\mathbf{r}) = N^{-1/2}\sum_{n=1}^{N} \exp[i\mathbf{k}\cdot\mathbf{R}_n\phi_\nu(\mathbf{r} - \mathbf{R}_n)] \quad (4)$$

where $\mathbf{k}$ is a reduced wave vector within the first Brillouin zone shown in Figure 1b;[12] $\phi_\nu(\mathbf{r} - \mathbf{R}_n)$ is an atomic or LCAO-MO wave function centered at $\mathbf{r} = \mathbf{R}_n$ and ν represents the irreducible species representation within the D_{3h} point group symmetry of the single TX_2 complex.[9,13] Recent optical data[14,15] and band calculations[16-19] for the unintercalated centrosymmetric structures shown in Figure 1a indicate that the wave vectors for highest occupied levels in 2H-MoS_2 are in the neighborhood of $\mathbf{k} = \mathbf{K}$ whereas those for the lowest unoccupied levels in 2H-TaS_2 are in the neighborhood of $\mathbf{k} = \mathbf{M}$ within the "d_{z^2}" band, when interlayer interactions are neglected as would be expected when the separation between the layers increases beyond the van der Waals value.

The chemical reactivity of the solid must be described, however, in the real space representation and the LCAO wave functions which satisfy the $D_{6h}{}^4$ space group symmetry of the solid are orthonormal linear combinations of (4) for all equivalent momentum coordinates $\mathbf{k}$. Thus the reactivity of 2H-TaS_2 with a half-filled "d_{z^2}" band should be described by real space orbitals in the neighborhood of

$$b_{M1\nu}(\mathbf{r}) = (1/3N)^{1/2}\sum_{N}[\cos(2\pi y_n/3^{1/2}a) + 2\cos(\pi x_n/a)\cos(\pi y_n/3^{1/2}a)]\phi_\nu(\mathbf{r} - \mathbf{R}_n)$$

$$b_{M2_1\nu}(\mathbf{r}) = (2/3N)^{1/2}\sum_{n}[\cos(2\pi y_n/3^{1/2}a) - \cos(\pi x_n/a)\cos(2\pi y_n/3^{1/2}a)]\phi_\nu(\mathbf{r} - \mathbf{R}_n)$$

$$b_{M2_2\nu}(\mathbf{r}) = (2/N)^{1/2}\sum_{n}\sin(\pi y_n/3^{1/2}a)\sin(\pi x_n/a)\phi_\nu(\mathbf{r} - \mathbf{R}_n) \quad (5)$$

and that for 2H-MoS_2 (with a completely filled "d_{z^2}" band) should be described by space orbitals in the neighborhood of b_{K2} where

$$b_{K1\nu}(\mathbf{r}) = (2/9N)^{1/2}\sum_{n}[\cos(4\pi x_n/3a) + 2\cos(2\pi x_n/3a)\cos(2\pi y_n/3^{1/2}a)]\phi_\nu(\mathbf{r} - \mathbf{R}_n)$$

$$b_{K2_1\nu}(\mathbf{r}) = (2/N)^{1/2}\sum_{n} 1/3[\cos(4\pi x_n/3a) - \cos(2\pi x_n/3a)\cos(2\pi y_n/3^{1/2}a)]\phi_\nu(\mathbf{r} - \mathbf{R}_n)$$

$$b_{K2_2\nu}(\mathbf{r}) = (2/N)^{1/2}\sum_{n}[(2/3^{1/2})\sin(\pi x_n/3a)\times \sin(2\pi y_n/3^{1/2}a)\cdot\phi_\nu(\mathbf{r} - \mathbf{R}_n)] \quad (6)$$

$[x_n, y_n] = [n_x a, 3^{1/2}n_y a]$ and $[(2n_x + 1)a/2, 3^{1/2}(2n_y + 1)a/2]$, and $[n_x a, 3^{1/2}(3n_y \pm 1)a/3]$ and $[(2n_x + 1)a/2, 3^{1/2}(6n_y \mp 1)a/6]$ where $n_x, n_y = 0, \pm 1, \ldots$ at sites B, A, and C, respectively, of the hexagonal close packed lattice and $\mathbf{R}_n = (x_n, y_n, z_n)$; a is the magnitude of the crystallographic principal axis in the xy plane of the layers in Figure 1a and the variation along the z direction is explicitly given by ϕ_ν which is mainly a metal d_{z^2} orbital.[17]

The Hückel approximation can now explain the different occupation of sites in the hexagonal close-packed lattice for compounds of groups Vb and VIb. When the wave vector is near $\mathbf{k} = \mathbf{M}$, the coefficients given in Figure 2 indicate that a transition element atom occupying the center of symmetry site B can bond with equal strength to chalcogens at sites A or C leading to the observed stacking AbA/CbC along the $11\bar{2}0$ direction. The stability of the trigonal prism configuration for the single TX_2 complex has already been explained using the one electron approximation[13] and octahedral hybridization sp^3d^2 at the chalcogen atoms explains the relative position of the latter across the van der Waals gap.[9]

However, when the wave vector is near $\mathbf{k} = \mathbf{K}$ the distribution in Figure 2 indicates that if the electron density is nonzero at the center of symmetry site B it will vanish at sites A and C and *vice versa*. The stable energy states must then be described by the b_{K2} term where the transition elements and the chalcogens alternately occupy the sites A and C leading to the stacking AcA/CaC along the $11\bar{2}0$ direction.

The successful explanation given by the Hückel approximation for the observed geometry suggests it may be used to explain the formation of EDA complexes by the intercalation process. The charge density distribution on the xy plane of the macromolecule $(TX_2)_N$ must be compatible

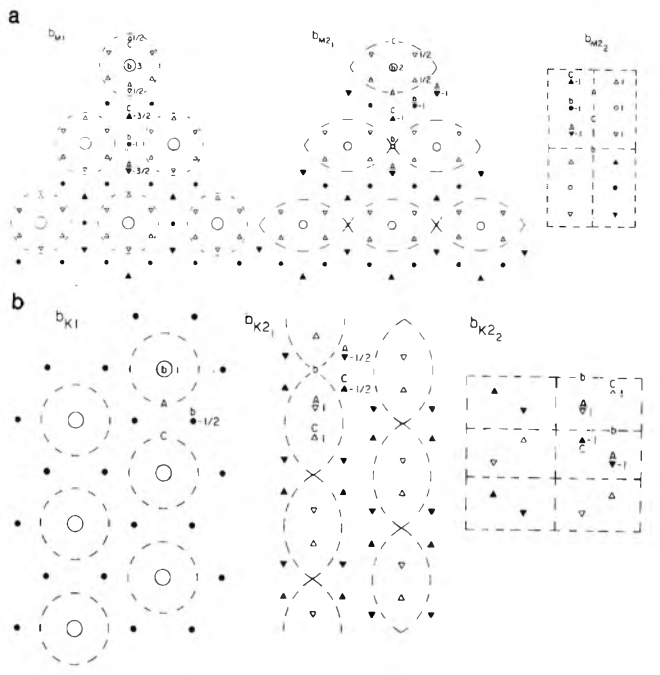

Figure 2. Map of the unnormalized coefficients of ϕ_ν in the LCAO approximation: (a) coefficients of b_M according to eq 5 and (b) coefficients of b_K according to eq 6. The circles represent the center of symmetry site b and the triangles ∇ and Δ the sites A and C, respectively. The dashed lines indicate the lines of nodes in the empty lattice. The charge density in the tight binding approximation is estimated by $|\phi_\nu|^2$ times the square of the normalized coefficients with the normalization constants given by (5) and (6).

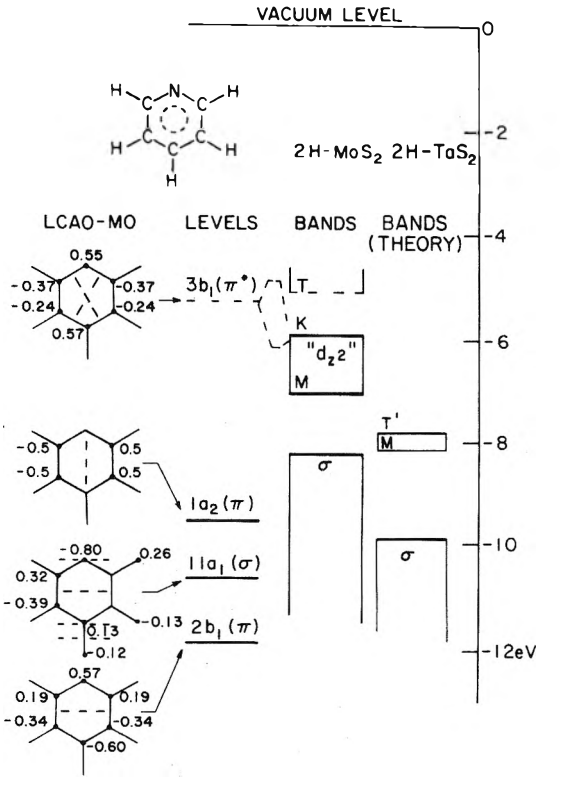

Figure 3. Comparison of the experimentally determined levels of free pyridine (ref 31) with those of the solid (ref 30). The coefficients of the corresponding LCAO-MO (given by ref 11 and 21b) are also shown. The calculated bands for 2H-TaS_2 from ref 17 are also shown.

with that of the donor or acceptor levels of the intercalated molecules in order that the resonance integral will not vanish. In addition, the stoichiometry $x = N_I/N$ (where N_I is the number of intercalate molecules inserted between two macromolecules) will also determine the magnitude of the interaction term because the normalization coefficients in (5) and (6) are indeed small. The complex stability will also increase if by the process of intercalation new delocalized states are produced, thereby increasing the change in entropy ΔS_I for reaction 1 above the value for the two dimensional condensation of the intercalate.

III. Pyridine Complexes

Pyridine intercalation of 2H-TaS_2 and 2H-MoS_2 provides an excellent example to apply the Hückel approximation. The interaction of the intercalate donor and acceptor levels with those of the solid macromolecule $(TX_2)_N$ is determined as follows.

The stoichiometry measurements indicate that the Vb complex is 2H-TaS_2 · pyridine$_{1/2}$ to within ±0.007 (1.5%) accuracy.[3] X-Ray diffraction measurements show that two stable configurations are possible. The plane of symmetry of the intercalate molecules can be aligned either normal or parallel to the xy plane of the solid.[3] Two layers of stoichiometry $x = 1/4$ each give the total stoichiometry. In both models the molecules in these two layers must align with parallel aromatic nuclei but antiparallel dipoles in order to fit into the lattice and to lower the energy. The center of symmetry will be preserved if the stacking in the dichalcogenide layers is shifted to nearly AcA/AbA.[20] This effect has been observed for pyridine[20a] and for ammonia and ethylenediamine[20b] intercalates of 2H-TaS_2. The shifts observed in the optical absorption spectra of the complex indicate that pyridine is a weak donor.[9]

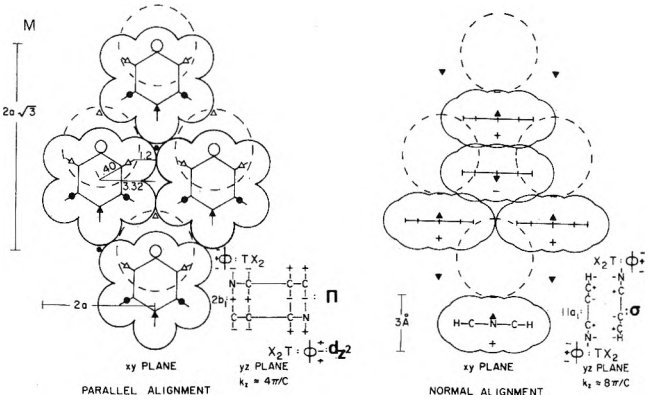

Figure 4. Superposition of a layer of pyridine with stoichiometry $x = 1/4$ with the pyridine plane of symmetry either normal or parallel to the xy plane of the solid on the map of the coefficients of b_{M1} shown in Figure 2. The relative dimensions in ångströms are from ref 14 and 35 and the van der Waals radii are shown to indicate the relative fit. The compatibility of the b_{M1} functions (ϕ_ν = metal d_{z^2} atomic orbital) with the pyridine $2b_1$ (π orbital) and $11a_1$ (σ orbital) is indicated by the sign variations of the wave functions in the yz plane.

The highest occupied levels for pyridine are shown in Figure 3 together with the LCAO-MO coefficients for the orbitals transforming in the given species representation of the C_{2v} point group.[21] The stoichiometry $x = 1/4$ per layer suggests that interactions between these three levels *can* reproduce the symmetry of an unoccupied Bloch function with wave vector near $\mathbf{k} = \mathbf{M}$ and Figure 4 shows a superposition which favors the interaction between the pyridine $2b_1$ and $11a_1$ levels with the solid b_{MI} level where ϕ_ν is

mainly a transition element d_{z^2} atomic orbital. The pyridine $1a_2$ π orbital can also reproduce the b_{M1} symmetry when the C_2 axis of pyridine is made to coincide with the nodes in the electron density but the resonance integral would be much lower than for the other two pyridine orbitals considered. In Figure 4 the dimension of the intercalate unit cell is 2a by $2 \times 3^{1/2}a$.

The predictive power of the Hückel approximation can also be used to analyze the transport properties of the solid. Recently the most important effect on the transport properties of the unintercalated solid has been identified as a distortion which leads to an increase in the size of the unit cell along the xy plane of the crystal.[22,23] The maximum in the susceptibility[24] and the point of inflection in the resistivity[25] which occur at 80 K have also been associated with the formation of a superlattice in 2H-TaS_2 and the change in the superconducting transition temperature T_c from 0.8 K for 2H-TaS_2 to 4 K for 2H-TaS_2 · $\text{pyridine}_{1/2}$. However, heat capacity measurements indicate that the density-of-states for the normal metal increases only by the order of 5% upon intercalation[3,26] and the optical shifts indicate that the charge transfer contribution $2|\beta/\Delta|^2$ is of the same order of magnitude.[8,9] Since the change in the density-of-state alone can not explain within the framework of the BCS theory[27] the rise in T_c and since the maximum in the susceptibility and the point of inflection in the resistivity *vs.* T disappear upon intercalation,[24,25] the registry of intercalate molecules must be able to prevent the lattice distortion. This is in agreement with the experimental fact that the stacking of the solid layers is determined by the order of the intercalate molecules.[20] Thus the interaction between two pyridine antiparallel dipoles separated by $r \sim 3$ Å, $\mu_1 \cdot \mu_2 / r^3 \simeq -0.1$ eV is stronger than the resonance interaction energy $-\langle|\beta|^2/\Delta\rangle \sim -0.04$ eV,[9] which in turn is stronger than the energy driving the distortion in the solid which is estimated to be of the order $-k_B T = -7 \times 10^{-3}$ eV, when $T \sim 80$ K. This suggests the importance of the electron–phonon coupling constant in the BCS theory.[27]

The predicted charge distribution can also be checked against the experimental results. Recent photoemission studies on 1T-$TaSe_2$, which is a semimetal and shows a superlattice,[22] have been used to determine the charge density distribution in the highest occupied LCAO of the solid *vs.* the azimuthal angle at a constant polar angle of 55°.[28] The angular distribution of the photoemission intensity is shown in Figure 5a superimposed on the map of LCAO coefficients of a Bloch function with wave vector $\mathbf{k} = \Sigma = \mathbf{M}/2$. The observed trigonal symmetry, including the bifurcation of the lobes in the direction of the transition element occupied sites, suggests that the highest occupied levels have wave vectors near $\mathbf{k} = \Sigma$ but not near $\mathbf{k} = \mathbf{M}$, $\mathbf{K}$ or $\mathbf{T} = \mathbf{K}/2$ (see Figures 5b and 2). This is of some importance in trying to understand the phenomena leading to the formation of a superlattice. Recently explanations for this effect have been advanced.[22,23] These should be tested with the observed charge density.[28] The most important observation, however, is that the pyridine complex stoichiometry shown in Figure 4 will not stabilize the charge distributions in Figures 5 or 2b.

The intercalation of pyridine into 2H-MoS_2 produces an effect opposite to that observed for 2H-TaS_2, in the high-energy optical absorption peaks.[9] These shifts are to the blue and increase as the temperature decreases.[29] The schematic energy level diagram shown in Figure 3 constructed using only experimental data[30,31] suggests that pyridine is an acceptor in the complex. The inverse temperature dependence of the shifts in the D absorbancy peak (at 3.16 eV) of 2H-MoS_2 is shown in Figure 6. The shift due to intercalate–solid interactions is

$$\Delta_i \nu_D = \nu_D{}^i - \nu_D{}^0 - \Delta_{vdW}\nu_D \qquad (7)$$

where $\nu_D{}^0$ and $\nu_D{}^i$ are the reported absorption frequencies before and after intercalation at a given temperature,[29] and the correction term for opening the van der Waals gap $\Delta_{vdW}\nu_D \approx -0.1$ eV was estimated from the band calculations.[17] The experimental fact that the shift in the D absorbancy peak of intercalated 2H-MoS_2 increases as $1/T$ indicates that a more stable complex is formed as T decreases either because of a contraction in the crystalline c axis or because there is a different occupancy of the vibrational levels in the complex. Figure 7 shows the charge distribution for a Bloch function with $\mathbf{k} = \mathbf{K}$ and the π^* orbital of one intercalate layer of pyridine. The predicted stoichiometry is $x = \frac{2}{9}$ when two intercalate layers are present.

For 2H-TaS_2 · $\text{pyridine}_{1/2}$ $\Delta H_I = -60 \pm 20$ kJ mol^{-1}.[3b] The standard entropy change can be determined using the

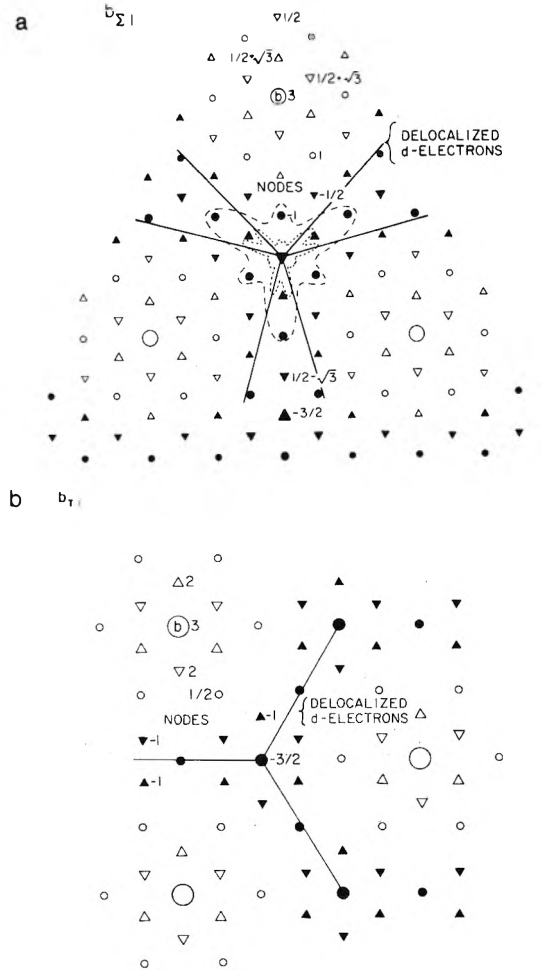

Figure 5. Map of the coefficients of the LCAO at symmetry points within the first Brillouin zone in Figure 1b: (a) superposition of the coefficients of $b_{\Sigma 1}$ and the radial distribution of photoemission intensity of octahedrally coordinated 1T-$TaSe_2$ according to ref 28: (. . .) d band and (- - -) total intensity. (b) Map of the coefficients of b_{T1}. The direction of d-electron delocalization (obtained from the data) and the direction of the nodeless lines connecting the center of symmetry sites b: O, occupied by the Ta, suggests that the exact wave vector is in the neighborhood of Σ.

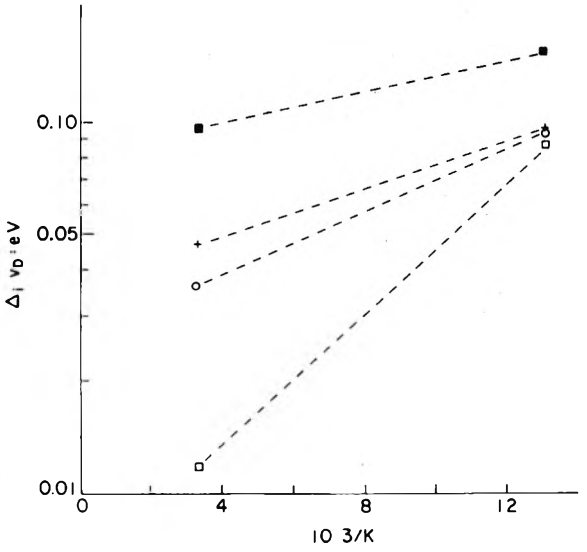

Figure 6. Shift in the 3.41 eV D absorbancy peak of 2H-MoS_2 due to intercalate-solid interaction *vs.* $1/T$ for (●) pyridine, (○) ammonia, (□) cyclopropylamine, and (+) aniline with 2H-MoS_2, using the data in ref 29 corrected for the breaking of the van der Waals bonds in 2H-MoS_2 obtained from ref 17.

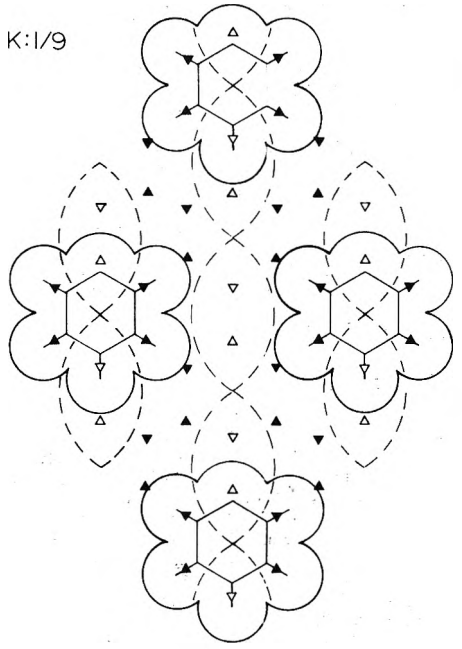

Figure 7. Superposition of the coefficients of b_{K2_1} shown in Figure 2b with a pyridine layer which favors π^* acceptor level interactions with the solid.

tabulated third law entropy data for I(g) and the measured parameters in the Debye-Sommerfeld relation for the heat capacity of TX_2 and $TX_2 \cdot I_x$.[3,20] Thus

$$\Delta S_I^\theta = S_0(TX_2 \cdot I_x) - S_0(TX_2) - xS_T^\theta(I) + \int_0^T [C_p(TX_2 \cdot I_x) - C_p(TX_2)]\, d \ln T' \quad (8)$$

Assuming TX_2 and $TX_2 \cdot I_x$ are "perfect crystalline substances" at absolute zero

$$\Delta S_I^\theta{}_{298K} = -142 \text{ J mol}^{-1}\text{K}^{-1} + \int_0^{298} [C_p(TaS_2 \cdot \text{pyridine}_{1/2}) - C_p(TaS_2)]\, d \ln T' \quad (8')$$

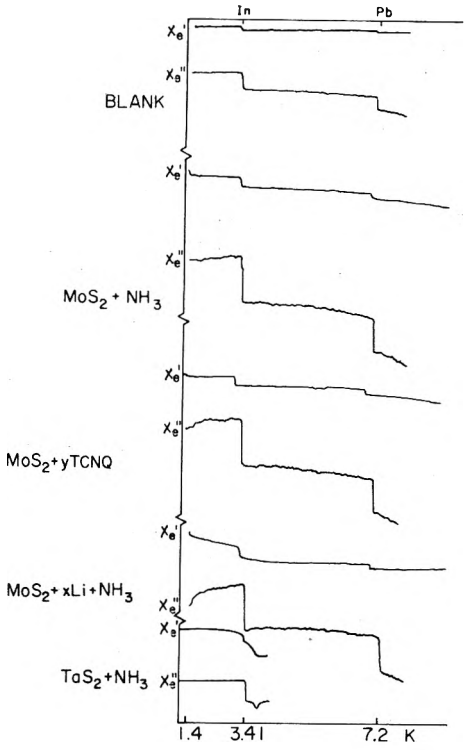

Figure 8. Components of the ac-susceptibility χ_e' and χ_e'' used to determine the superconducting transition temperatures of the given samples. The calibration points are the bath temperature at 1.4 K and the In and Pb superconducting transition temperatures at 3.41 and 7.2 K, respectively. The In and Pb standards are contained inside the apparatus described in ref 33a.

should be compared to the change in entropy for the condensattion of the intercalate, $\frac{1}{2}\Delta S_{298.15K}^\theta${(pyridine (g) = pyridine(solid)} $\simeq -84$ J mol^{-1} K^{-1}.[32] The heat capacity data do not extend to the room temperature region. However the low temperature data[3,26] suggest the integral in (8) is positive. At sufficiently low temperature phonon-assisted hopping across the intercalate layer contributes to the conductivity so that the solid becomes three dimensional and a bulk transition to the superconducting state can occur.

IV. Experimental Results on Superconductivity

The predictive power of the simple LCAO approximation in solids was tested to show that 2H-MoS_2 complexes with strong acceptors such as tetracyanoquinodimethane (TCNQ) would behave as 2H-NbS_2 which is a metal superconductor near 6 K.[3] The TCNQ was introduced from the vapor phase and electrolytically from a solution of LiTCNQ in liquid ammonia. Both the anode and cathode were 2H-MoS_2 single crystals weighting 14 mg cleaved from a large natural single crystal.[9] These were connected by gold wires to the rest of a circuit supplying a constant 1 mA current to give an estimated current density of 0.07 A/cm^2. After the samples were electrolyzed to saturation (~1 hr) they were sealed in ampoules with 10 Torr of He gas by a method described elsewhere.[33] The test for superconductivity was carried out in a high-frequency (~50 kHz) ac-susceptibility apparatus of the self-inductance type.[33a,34] The components of the complex susceptibility for the samples studied are shown in Figure 8. Changes in the skin depth mix the real and imaginary components. Therefore χ_e' and χ_e'' are only signals in quadrature. $-\chi_e'$ is a measure of the change in the oscillator resonance frequency due to

the change in the filling factor produced by the transition and $-\chi_e''$ is a measure of the power loss due to the transition.[33a,34] In Figure 8 ($MoS_2 + NH_3$) gives a negligible contribution to the susceptibility whereas both the cathode and anode crystals ($MoS_2 + x\,Li + NH_3$ and $MoS_2 + y\,TCNQ$, $y \sim 1/16$ by weight gain) give nonzero contributions to the susceptibility at temperatures below 3.7 and 2 K, respectively. Now, since ($MoS_2 + x\,Li + NH_3$, $1 \gtrsim x \gtrsim 0.4$) prepared from 2H–MoS_2 and a Li–NH_3 solution is a bulk superconductor below 3.7 K,[5] the observed signals suggest the onset of superconducting transitions. The bulk superconducting transition for a crystal of 2H–$TaS_2 + NH_3$ of a comparable size is shown in Figure 8 to indicate that complete transitions must occur below 1.4 K. Measurements at $T < 1.4$ K and lower oscillator frequencies would be necessary to determine the exact temperature of the transition. However the changes observed indicate that the original semiconductor 2H–MoS_2 ($\sigma \sim 1$ to $0.1(\Omega\ cm)^{-1}$)[14] becomes a metal when either electrons are added or withdrawn by the process of intercalating a donor (*e.g.*, M–NH_3)[4,5] or an acceptor (*e.g.*, TCNQ). Esr absorption studies[36] show that the TCNQ free radical is oriented with the plane of the aromatic nucleus parallel to the xy plane of the solid.

V. Conclusions

The power of the simple Hückel one electron approximation has been shown to work for solids represented by macromolecules with delocalized electrons in a two-dimensional network. Thus an approximation developed to explain homogeneous chemical reactions of delocalized "π electrons" may be applied to study heterogeneous reactions at the interfaces of two-dimensional solids with delocalized "d_{z^2} electrons."

Acknowledgments. A visiting scientist appointment at Stanford University is acknowledged. The measurement of the superconducting transition temperatures by R. Barr and G. McDavid in the low temperature laboratory of Professor T. H. Geballe is gratefully acknowledged. Also it has been a great pleasure to visit and discuss the results of this work with Professor Geballe. A leave of absence from San José State University and the numerous preprints (*e.g.*, ref 23 and 28) are also gratefully acknowledged.

References and Notes

(1) Address correspondence to Department of Chemistry, San José State University, San José, Calif. 95192. Facilities used for this work were supported at Stanford University by the Air Force Office of Scientific Research, Air Force Systems Command USAF, under Grant No. 73-2435A and at San José State University by a Research Corporation Grant in Aid.

(2) (a) W. Rudorff, *Chimia*, **19**, 489 (1965); (b) A. Weiss and R. Ruthardt, *Z. Naturforsch. B*, **24**, 256 (1969).
(3) (a) F. R. Gamble, J. H. Osiecki, M. Cais, R. Pisharody, F. J. DiSalvo, and T. H. Geballe, *Science*, **174**, 493 (1971); (b) F. DiSalvo, Ph.D. Thesis, Stanford University, 1971; (c) F. J. DiSalvo, R. Schwall, T. H. Geballe, F. R. Gamble, and J. H. Osiecki, *Phys. Rev. Lett.* **27**, 320 (1971).
(4) J. V. Acrivos, W. Y. Liang, J. A. Wilson, and A. Yoffe, *J. Phys. C.*, **4**, L18 (1971).
(5) R. B. Somoano, V. Hadek, and A. Rembaum, *J. Chem. Phys.*, **58**, 697 (1973).
(6) J. V. Acrivos, S. F. Meyer, and T. H. Geballe in "Electrons in Fluids," J. Jortner and N. R. Kestner, Ed., Springer Verlag, New York, N.Y., 1973, p 341; S. F. Meyer, T. H. Geballe, and J. V. Acrivos, *Bull. Amer. Phys. Soc.*, **17**, 519 (1972).
(7) R. S. Mulliken and W. B. Person, "Molecular Complexes," Wiley, New York, N.Y., 1970.
(8) A. R. Beal and W. Y. Liang, *Phil. Mag.*, **27**, 1397 (1973); *J. Phys. C.*, **6**, L482 (1973).
(9) J. V. Acrivos and J. R. Salem, *Phil. Mag.*, in press.
(10) J. C. Slater and G. F. Koster, *Phys. Rev.*, **94**, 1498 (1954).
(11) C. A. Coulson, "Valence," Oxford Univeristy Press, London, 1952; C. A. Coulson and A. Streitwiesser, Jr., "Dictionary of π-Electron Calculations," W. H. Freeman, San Francisco, Calif., 1965.
(12) A. H. Wilson, "The Theory of Metals," Cambridge University Press, New York, N.Y., 1965, p 89.
(13) (a) R. Hultgren, *Phys. Rev.*, **40**, 891 (1932); (b) L. Pauling, *J. Amer. Chem. Soc.*, **53**, 1367 (1932); (c) R. Huisman, R. DeJonge, C. Haas, and F. Jellinek, *J. Solid State Chem.*, **3**, 56 (1971).
(14) J. A. Wilson and A. D. Yoffe, *Advan. Phys.*, **18**, 193 (1969).
(15) A. D. Yoffe, Festkörperprobleme *XIII*, 1 (1973).
(16) R. A. Bromley, R. B. Murray, and A. D. Yoffe, *J. Phys. C.*, **5**, 759 (1969).
(17) L. Mattheiss, *Phys. Rev. Lett.*, **30**, 784 (1973); *Phys. Rev. B*, **8**, 3719 (1973).
(18) R. V. Kasowski, *Phys. Rev. Lett.*, **30**, 1175 (1973).
(19) C. Y. Fong and M. L. Cohen, *Phys. Rev. Lett.*, **32**, 720 (1974).
(20) (a) J. F. Revelli, Ph.D. Thesis, Stanford University, 1972; (b) S. F. Meyer, R. B. Howard, G. Stewart, J. V. Acrivos, and T. H. Geballe, to be submitted for publication.
(21) (a) M. A. El Sayed, M. Kasha, and V. Tanaka, *J. Chem. Phys.*, **34**, 334 (1961); (b) E. Clementi, *ibid.*, **46**, 4731 (1967).
(22) J. A. Wilson, F. J. DiSalvo, and S. Mahajan, *Phys. Rev. Lett.*, **32**, 882 (1974).
(23) H. P. Hughes and W. Y. Liang, *J. Phys. C. Lett.*, in press; P. M. Williams, G. S. Parry, and C. B. Scruby, *Phil. Mag.*, in press.
(24) F. DiSalvo, *Proc. Int. Conf. Low Temp. Phys., 13th, 1972*, **3**, 417 (1973).
(25) A. H. Thompson, F. R. Gamble, and R. F. Koehler, *Phys. Rev. B*, **5**, 2811 (1972).
(26) R. Schwall, Ph.D. Thesis, Stanford University, 1972.
(27) J. Bardeen, L. N. Cooper, and J. R. Schrieffer, *Phys. Rev.*, **108**, 1175 (1957).
(28) N. M. Traum, N. V. Smith, and F. J. DiSalvo, *Phys. Rev. Lett.*, **32**, 1241 (1974).
(29) A. R. Beal, Ph.D. Thesis, Cambridge University, 1973.
(30) J. C. McMenamin and W. E. Spicer, *Phys. Rev. Lett.*, **29**, 1503 (1972); private communication.
(31) (a) J. L. Franklin, J. G. Dillard, H. M. Rosenstock, J. T. Herron, K. Draxl, and F. H. Field, *Nat. Ref. Data Ser., Nat. Bur. Stand.*, **No. 26** (1969); (b) D. W. Turner, C. Baker, A. D. Baker, and C. R. Brundle, "Molecular Photoelectron Spectroscopy," Wiley, New York, N.Y., 1970.
(32) M. Kh. Karapet'yants and M. L. Karapet'yans, "Thermodynamic Constants of Inorganic and Organic Compounds," translated from the Russian by J. Schmorak, Ann Arbor Humphrey Science Publishers, Ann Arbor, Mich., 1970, p 354.
(33) (a) S. F. Meyer, Ph.D. Thesis, Stanford University, 1973; (b) J. V. Acrivos and S. F. Meyer, *Bull. Amer. Phys. Soc.*, **18**, 385 (1973).
(34) M. Strongin and E. Maxwell, *Phys. Lett.*, **6**, 49 (1963).
(35) L. E. Sutton, "Tables of Interatomic Distances," The Chemical Society, London, 1958.
(36) N. B. Handly and J. V. Acrivos, to be submitted for publication.

Cationic Transport Number of Potassium Bromide and Solvation of Ions in Dimethyl Sulfoxide

Ram Gopal* and Jai Shanker Jha

Department of Chemistry, Lucknow University, Lucknow, India *(Received April 12, 1974)*

The cationic transport numbers of potassium bromide in dimethyl sulfoxide have been determined at different temperatures and the data have been used to obtain the ionic mobilities in this solvent from the available electrolyte conductance. Ionic solvation has been estimated from the ionic conductance data using the Nightingale's procedure. The results indicate that cations are more solvated than the anions presumably due to stronger electrostatic interaction between the exposed negative end of the solvent dipole on the oxygen atom and the cations. Among the cations, the smallest (the Li^+ ion) has the largest solvation number and the solvation decreases gradually as the crystal radius of the ion increases.

Introduction

The transport number of ions in solution provides information about ion–solvent interaction and also yields ionic conductances from the experimental electrolyte conductance data. With a view to study ion–solvent interaction in some nonaqueous solvents of high dielectric constant, determinations of the cationic transport number of potassium chloride or potassium bromide were previously undertaken in formamide,[1,2] *N*-methylacetamide,[3] *N*-methylformamide,[4] and *N*-methylpropionamide.[5] Similar studies, although somewhat incomplete, have been reported recently in DMF[6,7] and our present interest in dimethyl sulfoxide prompted the determination of the transport number in this solvent. It may be noted that DMSO has a medium dielectric constant ($\epsilon_{25°}$ = 46.4) and is highly associated through dipolar interaction[8,9] without involving hydrogen bonding.[9] The present communication reports a study of the transport number of ions of potassium bromide in DMSO at different concentrations and temperatures.

Experimental Section

AR grade potassium bromide (British Drug House) was recrystallized from conductivity water and dried under vacuum. DMSO, obtained from Fluka A.G., was dried over freshly ignited quicklime and distilled under reduced pressure until its conductivity was decreased to 10^{-6} mho or less. A transport number cell, similar to that used by MacInnes and Dole,[10] but slightly modified in order to facilitate the removal of the anode and cathode solutions from the cell, was used in the experiments. Solutions of desired concentrations were prepared from freshly distilled DMSO in a drybox. The electrodes were made of stout silver wire and the complete cell, filled with the solution, was thermostated at the desired temperature (fluctuation less than ±0.05°). A current of 2–5 mA was passed for nearly 10–12 hr from a battery of dry cells of 90 V. A copper coulometer was used to measure the flow of electricity. As silver bromide (formed at the anode during electrolysis) is slightly soluble in DMSO,[11] the solution in the cathode compartment was analyzed for bromide ions by conductometric titration. Potassium metal deposited at the cathode did not seem to affect the estimation of bromide ions in the cathodic compartment. The contents of the middle compartment were similarly analyzed. The validity of this method for estimating halide ions in this solvent in dilute solution was checked beforehand with a few samples of known concentrations and the results were found to agree within 0.5%. The transport number of Br^- was calculated by the usual procedure when that of K^+ was obtained. The results were found to be reproducible within experimental error (±0.5%) and are summarised in Table I.

The Longsworth function $t_+^{0'}$ was calculated using the relation

$$t_+^{0''} = \frac{t_+''\Lambda_+' + {}^1/_2\beta\sqrt{C}}{\Lambda_+' + \beta\sqrt{C}} = t_+^0 + BC \qquad (1)$$

from the experimental values of transport number, t_+, obtained with different concentrations and at a fixed temperature. The terms in eq 1 have their usual significance. The values of Λ_0 for KBr, needed to obtain Λ' at various temperatures, were found to be 38.45, 42.31, 50.7, and 59.28 at 25, 30, 40, and 50°, respectively. The values of viscosity and dielectric constant of the solvent, at the corresponding temperatures, were obtained graphically from the data given by Yao and Bennion.[12] The values of $t_+^{0'}$, at various concentrations and at a fixed temperature, were calculated from eq 1 and were plotted against C. The curves were found to be straight lines. Interpolation of the $t_+^{0'}$ *vs.* C curve to zero concentration gives t_+^0, the cationic transport number at infinite dilution, and values of t_+^0 are given in column 1 of Table I.

Discussion

From Table I, it may be observed that the variation of the transport number, t_+, with temperature and concentration follows the same pattern of behavior as in solvents of high dielectric constant and strong hydrogen bonding such as formamide, NMA, NMF, and NMP,[1–5] *i.e.*, it increases with an increase in temperature and decreases with an increase in concentration. The effect of temperature is consistent with the Kohlrausch's law that states that the faster the ion, the smaller the temperature coefficient of its mobility; thus the slower moving K^+ ion has a positive temperature coefficient and t_+ increases with increasing temperature and reverse is true for the faster bromide ion.

TABLE I: Transport Numbers of K^+ in Solutions of KBr in DMSO at Different Temperatures and Concentrations

Molality, m	t_+^0 at 25°	30°	40°	50°
0.00	0.382	0.386	0.393	0.400
0.10	0.349	0.355	0.365	0.372
0.15	0.343	0.349	0.359	0.367
0.20	0.338	0.344	0.354	0.362
0.25	0.333	0.340	0.349	0.357
0.30	0.329	0.335	0.345	0.353

TABLE II: Ionic Mobilities of Some Ions at 25°

Ion	Ionic mobility: This work	Lit. values
Li^+	11.18	11.4[b]
Na^+	14.24	13.8[a] 14.34[c]
K^+	14.69	14.4[a]
Cs^+	16.39	16.1[e]
Me_3PhN^+	14.29	14.1[a]
Me_4N^+	18.89	18.6[b]
Et_4N^+	17.35	17.06[b]
Pr_4N^+	13.71	13.42[b]
Bu_4N^+	11.88	11.59[b] 11.2[a]
Hex_4N^+	10.08	9.79[b]
Hep_4N^+	9.47	9.18[b]
Cl^-	24.12	24.40[b] 23.9[d]
Br^-	23.76	24.06[b] 24.2[a]
I^-	23.51	23.80[b] 23.8[a]
SCN^-	29.90	29.2[a] 29.80[c]
NO_3^-	26.81	27.0[a]
Pi^-	17.01	17.3[a]
ClO_4^-	24.52	24.6[a] 24.42[c]

[a] Reference 13. [b] Reference 14. [c] Reference 12. [d] Reference 16. [e] Reference 15.

Ionic Mobility

Although the mobilities of some ions in DMSO have been obtained by Sears, Lester, and Dawson,[13] using the indirect method, it will be instructive to calculate their values directly from t_+^0 values given in Table I. The conductance data at infinite dilution have been reported by some workers[13-17] and were used to calculate mobilities of various ions as given in Table II. In Table II are also included the ionic conductances reported from indirect methods. It may be noted that the agreement in the values of ionic cnductances given in columns 2 and 3 of Table II is quite satisfactory.

Solvation Numbers of Some Ions in DMSO

Although some attempts have been made earlier to estimate ionic solvation in DMSO,[18,19] the ionic mobilities given in Table II can be used to estimate solvation numbers of ions in a more quantitative manner.

Since the conductance data are mostly known at 25°, the solvation number can be calculated for this temperature only. The methods of Robinson and Stokes[20] and Nightingale[21] give usually almost similar solvation numbers; however, the latter was used here because of greater convenience. Stokes radius, r_s, is given by

$$r_s = 0.82|Z|/\lambda_0\eta_0$$

where the terms used have their usual significance. Now, assuming that the larger ions (the tetraalkylammonium ions, (R_4N^+)) are unsolvated in DMSO,[22] a curve can be drawn between r_s and the crystal radius r_c.[20] Such a curve is given in Figure 1, from which it may be noted that only the tetramethylammonium ion falls off the line, perhaps due to appreciable electrostatic ion–solvent dipole interaction; the rest of the R_4N^+ ions lie on almost a straight line from which on intrapolation, the actual radii r_{HX} of other smaller ions in solution, can be read from the knowledge of the corresponding r_s values. The relative positions of some ions are indicated on the curve. Solvation numbers of a few common ions, along with their r_s and r_{HX} values, are given in Table III. In calculating the solvation number, the volume of the ion itself was subtracted from that of the ion in solution ($\frac{4}{3}\pi r_{HX}^3$). The difference was then divided by the volume of the molecule of DMSO (≈106 Å^3). It appears from Table III that cations are more solvated than anions due to stronger electrostatic interaction between the exposed negative end of the solvent dipole on the oxygen atom and the cation.[13] Among the cations, the smallest (the Li^+ ion) has the largest solvation number and the solvation decreases gradually as the crystal radius of the ion increases. Solvation of the three halide ions is almost the same, perhaps due to a polarization effect of the highly polar DMSO molecule on the larger bromide and iodide ions which counterbalances the effect of the larger size.

TABLE III: Solvation Numbers of Some Ions in DMSO at 25°

Ion	r_c, Å	r_s, Å	r_{HX}, Å	Solvation no.
Li^+	0.60	3.67	5.18	5.5
Na^+	0.95	2.88(3.2)[a]	4.45	3.4(2.4)[b]
K^+	1.35	2.79(3.0)[a]	4.36	3.2(2.4)[b]
Cs^+	1.69	2.50	4.10	2.5
Cl^-	1.81	1.70	3.35	1.3
Br^-	1.95	1.73(1.7)[a]	3.38	1.2(1.1)[b]
I^-	2.16	1.74	3.39	1.1(1.1)[b]
SCN^-		1.37	3.02	1.1(0.7)[b]
NO_3^-		1.53	3.18	1.3

[a] Values calculated by Prue and Sherrington from[6] the data of Dawson, *et al.* [b] Values reported by Gopal and Husain,[19] using the curve given by Robinson and Stokes[20] for water; this was a serious drawback in their procedure.

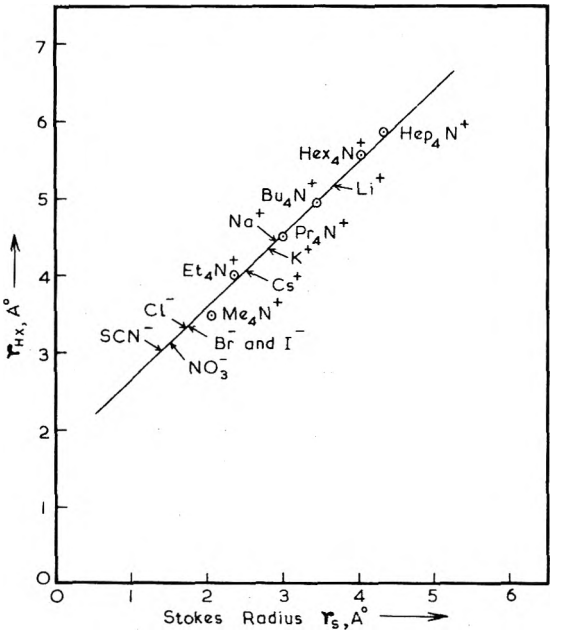

Figure 1.

Acknowledgment. One of us (J.S.J.) is thankful to HMG of Nepal and Government of India for providing a research scholarship under T.C.S. of the Colombo Plan.

References and Notes

(1) R. Gopal and O. N. Bhatnagar, *J. Phys. Chem.*, **68**, 3892 (1964).
(2) J. M. Notley and M. Spiro, *J. Phys. Chem.*, **70**, 1502 (1966).
(3) R. Gopal and O. N. Bhatnagar, *J. Phys. Chem.*, **69**, 2382 (1965).
(4) R. Gopal and O. N. Bhatnagar, *J. Phys. Chem.*, **70**, 3007 (1966).
(5) R. Gopal and O. N. Bhatnagar, *J. Phys. Chem.*, **70**, 4070 (1966).
(6) J. E. Prue and P. J. Sherrington, *Trans. Faraday Soc.*, **57**, 1795 (1961).
(7) R. C. Paul, J. P. Singla, and S. P. Narula, *Indian J. Chem.*, **8**, 63 (1970).
(8) H. H. Szmant in "Dimethyl Sulphoxide," S. W. Jacob, E. E. Rosenbaum, and D. C. Wood, Ed., Marcel Dekker, New York, N.Y., 1971, pp 1–98.
(9) J. B. Kinsinger, M. M. Tannahill, M. S. Greenbery, and A. I. Popov, *J. Phys. Chem.*, **77**, 2444 (1973).
(10) D. A. MacInnes and M. Dole, *J. Amer. Chem. Soc.*, **53**, 1357 (1931).
(11) D. C. Luehns and K. Abate, *J. Inorg. Nucl. Chem.*, **30**, 549 (1968).
(12) N. P. Yao and D. N. Bennion, *J. Electrochem. Soc.*, **118**, 1097 (1971).
(13) P. G. Sears, G. R. Lester, and L. R. Dawson, *J. Phys. Chem.*, **60**, 1433 (1956).
(14) D. E. Arrington and E. Griswold, *J. Phys. Chem.*, **74**, 123 (1970).
(15) A. D. Archer and R. P. H. Gasser, *Trans. Faraday Soc.*, **62**, 3451 (1966).
(16) J. S. Dunnett and R. P. H. Gasser, *Trans. Faraday Soc.*, **61**, 922 (1965).
(17) H. L. Schläfer and W. Schaffernicht, *Angew. Chem.*, **72**, 618 (1960).
(18) A. J. Parker, *Quart. Rev., Chem. Soc.*, **16**, 163 (1962).
(19) R. Gopal and M. M. Husain, *J. Indian Chem. Soc.*, **40**, 981 (1963).
(20) R. A. Robinson and R. H. Stokes, "Electrolyte Solutions," Butterworths, London, 1959, pp 124–126.
(21) E. R. Nightingale, Jr., *J. Phys. Chem.*, **63**, 1381 (1959).
(22) This may not be strictly true. Studies on apparent molal volume indicate the R_4NI–DMSO interaction to be somewhat stronger than that in solvents such as formamide, NMA, and NMP.[23]
(23) R. Gopal, R. Kumar, and D. K. Agarwal, *Bull. Chem. Soc. Jap.*, **46**, 1973 (1973).

Mechanisms of Electronic Energy Transfer in the Gas Phase

R. G. Brown, D. Phillips,* and G. Das Gupta

Chemistry Department, The University, Southampton SO9 5NH, England *(Received January 26, 1973; Revised Manuscript Received May 13, 1974)*

Cross sections and rate constants for the quenching of the excited singlet states of a variety of substituted benzenes by 2-pentanone and biacetyl in the vapor phase are reported. Results are discussed in terms of the size of the molecules and the exchange and dipole–dipole mechanisms of electronic energy transfer. It is suggested that the contribution of the latter to the total cross section for energy transfer may in some cases be significant, confirming earlier reports.

Introduction

Several reviews of the mechanisms by which electronic energy transfer may occur are available.[1–3] Two of the four main processes may be expected to account for virtually all of the observations of electronic energy transfer in the gas phase. Exciton transfer occurs principally in solids. The "trivial" process, reabsorption of the donor molecule's fluorescence emission by the acceptor molecule, may be avoided in the vapor phase with careful experimentation.

Studies of the theory of the electronic energy transfer process (eq 1 where D* is an electronically excited donor

$$D^* + A \xrightarrow{k_Q} D + A^* \qquad (1)$$

molecule and A is the acceptor molecule) have resulted in two distinguishable cases being recognized. The first is a coulombic interaction between donor and acceptor molecules which was first treated by Förster.[4] It was assumed that the interaction can be expressed in terms of the dipole transition moments of D and A, and taking the dipole–dipole term to be large compared to all the other terms, the probability of transfer (n_{D^*-A}) was derived as

$$n_{D^*-A} = \frac{9000K^2 \ln 10}{128\pi^5 N n^4 \tau_D R^6} \int_0^\infty f_D(\nu)\epsilon(\nu)\frac{d\nu}{\nu^4} \qquad (2)$$

where ν is the frequency in wave numbers, $\epsilon(\nu)$ is the molar decadic extinction coefficient of A, $f_D(\nu)$ is the spectral distribution of the fluorescence of D* normalized to unity on a frequency scale, N is Avogadro's number, τ_D is the radiative lifetime of D*, n is the refractive index of the solvent, R is the mutual distance between molecules D* and A, and K^2 is an orientation factor (value approximately $\frac{2}{3}$)

This treatment has been extended by Dexter to also include dipole–quadrupole terms,[5] and rederived by Lin[6] to show isotope effects and the dependence on energy gap and temperature.

The Förster mechanism has been verified many times in solid matrices, and can lead to electronic energy transfer over large intermolecular distances. When large rate constants for electronic energy transfer are obtained in vapor phase studies, the possibility of the involvement of the Förster mechanism must be considered. Eliminating the constants from Förster's equation, one finds the rate constant for energy transfer to be inversely proportional to the radiative lifetime of the donor and to R,[6] and directly proportional to the spectral overlap integral. In fluid media the intermolecular distance, R, cannot be determined. If, however, it is assumed constant on average, which would not be too unreasonable for a series of structurally similar molecules, there should then be a direct correlation between the radiative rate constant and the ratio of the quenching rate constant to the spectral overlap integral.

Dexter has also derived an expression for the probability of energy transfer by an exchange mechanism,[5] where there

is a short range of interaction. The relationship was given as

$$P_{D^*-A} = \frac{2\pi}{h} K^2 \exp(-2R/L) \int_0^\infty f_D(\nu) F_A(\nu)\, d\nu \quad (3)$$

with $f_D(\nu)$ as before, but with the acceptor absorption coefficients also normalized to unity ($F_A(\nu)$). K^2 is a constant with dimensions of energy squared and L is also a constant called the "effective average Bohr radius." Unfortunately, neither K^2 nor L are amenable to experimental determination.

A recent report[7] provides evidence that large cross sections for energy transfer from a series of substituted aromatic molecules to pyrazoline and cyclopentanone in the vapor phase could be indicative of the partial involvement of the Förster long-range process, in keeping with the theoretical predictions of Lin.[6] Investigations in this and other laboratories on the quenching by energy transfer of the first excited singlet states of a range of substituted aromatic molecules by 2-pentanone and biacetyl in the gas phase have also resulted in high measured quenching cross sections. These results are therefore worthwhile investigating in the light of the above energy transfer mechanisms.

Experimental Section

The apparatus used for the quenching measurements was similar to that described in earlier reports,[8-10] consisting of a conventional high-vacuum system, T-shaped fluorescence cell, and an optical system with associated electronics. The vacuum system was evacuated to a pressure of better than 10^{-5} Torr using a combination of rotary and mercury two-stage diffusion pumps. Rotaflo Teflon barrel stopcocks or Springham greaseless stopcocks were used throughout. The fluorescence cell was 6 cm long, of 3 cm diameter, and has a centrally placed 2-cm diameter emission window. The use of this cell has been described in an earlier report.[11]

The light source used in this study was an Osram XBO 150 xenon arc operated from a dc stabilized power supply. Exciting wavelengths were selected with a Bausch and Lomb high-intensity grating monochromator. Transmitted light was measured using an RCA 935 phototube powered by a 110-V dc supply and emitted light was detected by an RCA IP28 photomultiplier tube run off a Farnell EHT 2 power supply. The signal in both cases was displayed on a Victoreen VTE 1 picoammeter. A Corning CS-7-54 filter was interposed between the fluorescence cell and photomultiplier.

Pressures were measured on a mercury manometer or on an Edwards 0–20 Torr CG3 series capsule dial gauge, which was previously calibrated against the mercury manometer. Pressures below 1 Torr were obtained by expansion and assumption of perfect gas laws. Mixing was achieved by flash vaporization and standing for up to 1 hr.

Absorption spectra were taken on a Pye Unicam SP700 spectrometer at 23° using a cell of 6 cm path length. Low-resolution fluorescence emission spectra were measured on a Farrand Mark 1 spectrofluorimeter with a 1-cm square fluorescence cell. Higher resolution fluorescence spectra were obtained (by Mr. M. G. Rockley of this department) using a Hilger Monospek 1000 Monochromator and Brookdeal 5C1 photon-counting set-up.

Fluorescence decay times were measured using the pulse fluorimeter described in earlier reports.[12,13]

TABLE I: Rate Parameters for Quenching of Some Aromatic Compounds by 2-Pentanone and Biacetyl

Compound	λ_{ex}, nm	τ_F,[a] nsec	Slope, Torr^{-1}	$10^{10}k_Q$, M^{-1} sec^{-1}
2-Pentanone Quencher				
o-Xylene	269.5	52.0	1.046	36.8
m-Xylene	270.5	49.0	0.834	31.1
p-Xylene	272.5	44.0	0.880	36.5
p-Fluorotoluene	271.2	14.8	0.205	25.3
Benzotrifluoride	264.4	19.0	0.421	31.5
p-Fluorobenzotrifluoride	264.0	16.2	0.260	32.6
Hexafluoro-*m*-xylene	265.9	20.4	0.330	31.3
Hexafluoro-*p*-xylene	266.8	8.6	0.170	26.6
Benzyl fluoride	265.0	38.6	0.458	21.1
Fluorobenzene	265.0	9.5	0.117	22.4
o-Difluorobenzene	264.5	5.5	0.080	25.2
m-Difluorobenzene	264.0	6.0	0.067	18.7
p-Difluorobenzene	272.5	8.0	0.123	25.8
1,2,4-Trifluorobenzene	270.0	3.1	0.071	41.9
1,3,5-Trifluorobenzene	264.0	3.9	0.075	35.1
1,2,3,4-Tetrafluorobenzene	264.0	1.3	0.019	27.0
1,2,3,5-Tetrafluorobenzene	268.0	1.2	0.016	24.5
1,2,4,5-Tetrafluorobenzene	273.0	2.0	0.060	54.4
Pentafluorobenzene	270.0	1.6	0.015	16.9
Hexafluorobenzene	270.0	1.5	0.013	16.3
Biacetyl Quencher				
p-Fluorotoluene	271.2	14.8	0.274	33.8
Benzotrifluoride	264.4	19.0	0.210	14.8
p-Fluorobenzotrifluoride	264.0	16.2	0.289	29.3
Hexafluoro-*m*-xylene	265.9	20.4	0.240	23.0
Hexafluoro-*p*-xylene	266.8	8.6	0.110	16.9
Benzyl fluoride	265.0	38.6	0.557	25.7
1,3,5-Trifluorobenzene	264.0	3.9	0.066	30.9
Pentafluorobenzene	270.0	1.6	0.023	25.8

[a] Lifetimes taken from ref 12, 14, and 24.

Details of the purity of most materials used have been given in an earlier paper.[14]

Diffusion coefficients were obtained using a method developed by Wakeham and Slater.[15] Essentially the technique consists of injection of a sample of the material into a carrier gas flow in an empty column of a gas–liquid chromatograph. Analysis of the resulting peak width permits evaluation of the diffusion coefficient. From temperature studies, diffusion coefficients for ground-state molecules at room temperatures were obtained by extrapolation using the equation shown below

$$\ln D_{12} = \ln A + S \ln T(\text{Å}) \quad (4)$$

Results

The data concerning the quenching of the first excited singlet states of the various aromatic compounds by 2-pentanone and biacetyl, where not already available in the literature, are presented in Table I. The slope referred to is that derived from a Stern–Volmer type plot of the ratio of the (arbitary) fluorescence quantum yields in the absence (Φ_{f0}) and presence (Φ_f) of quencher against the concentration of quencher. From a simple kinetic scheme

$$\Phi_{f0}/\Phi_f = 1 + k_Q \tau_f [A] \quad (5)$$

and hence the slope of the above-mentioned plot is $k_Q\tau_f$ (τ_f being the fluorescence decay time of the excited aromatic donor). These plots for the new data being presented are shown in Figures 1 and 2.

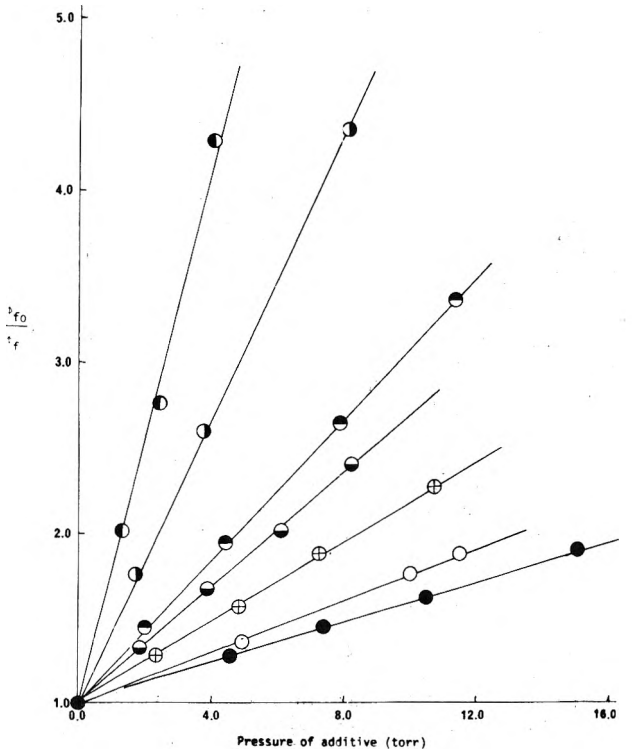

Figure 1. Some Stern–Volmer plots of aromatic compounds quenched by 2-pentanone; ◐, *m*-xylene; ◑, benzotrifluoride; ◓, *p*-fluorotoluene; ◒, hexafluoro-*p*-xylene; ⊕, fluorobenzene; ○, 1,3,5-trifluorobenzene; ●, 1,2,4,5-tetrafluorobenzene.

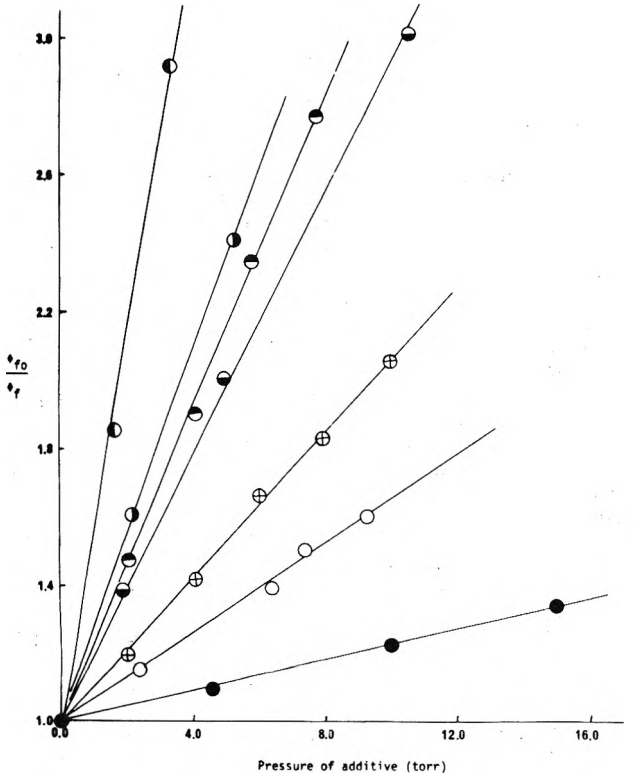

Figure 2. Some Stern–Volmer plots aromatic compounds quenched by biacetyl: ◐, benzyl fluoride; ◑, *p*-fluorotoluene; ◓, hexafluoro-*m*-xylene, ◒, benzotrifluoride; ⊕, hexafluoro-*p*-xylene, ○, 1,3,5-trifluorobenzene; ●, pentafluorobenzene.

In some cases the quenching parameters measured by this quantum yield determination were checked by measurements of fluorescence decay time as a function of pressure of additive. These plots are shown in Figure 3, and data obtained are compared in Table II. The compounds chosen for study in this way were selected on the basis of their having relatively long lifetimes such that after significant quenching the decay time was within the capability of measurement of the apparatus.

TABLE II: Comparison of Quenching Rate Constants for Various Aromatic Compounds Obtained by Static and Lifetime Methods

Compound	$10^{10}k_Q$, M^{-1} sec^{-1} (static)	$10^{10}k_Q$, M^{-1} sec^{-1} (lifetime)
2-Pentanone Quencher		
Fluorobenzene	23.4 ± 2.3	22.1 ± 6.6
m-Fluorotoluene	17.4 ± 1.7	22.5 ± 4.9
Benzotrifluoride	31.5 ± 3.2	29.1 ± 1.4
p-Fluorobenzotrifluoride	32.3 ± 3.2	30.2 ± 2.4
Hexafluoro-*m*-xylene	31.2 ± 3.1	36.9 ± 5.0
n-Pentane Quencher		
Benzotrifluoride	0.78 ± 0.08	0.85 ± 0.19
m-Fluorobenzotrifluoride	0.71 ± 0.07	0.63 ± 0.10

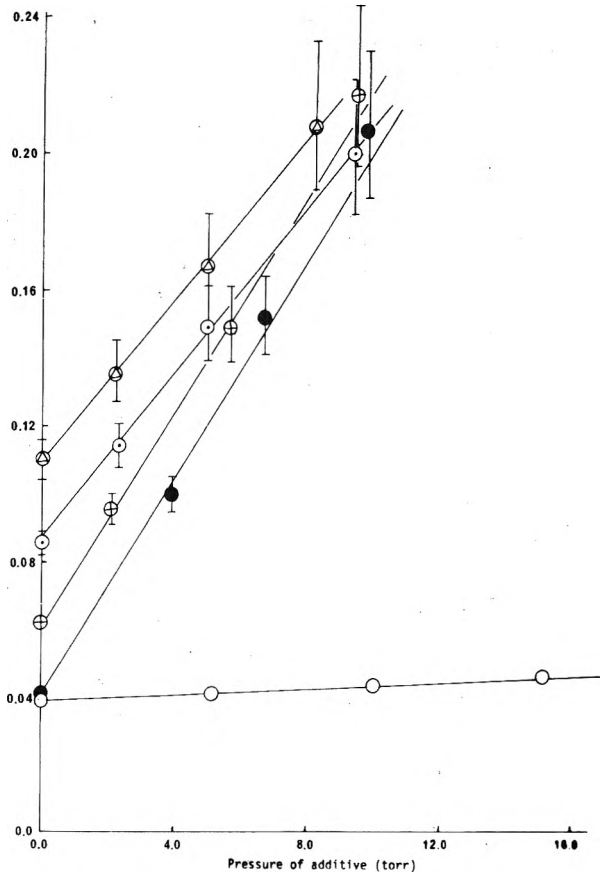

Figure 3. Effect of additives on the fluoroescence lifetime (τ) of some aromatic compounds: ○, fluorobenzene + 2-pentanone; ⊙, *m*-fluorotoluene + 2-pentanone, ⊕, *p*-fluorobenzotrifluoride + 2-pentanone; ●, benzotrifluoride + 2-pentanone; ○, benzotrifluoride + *n*-pentane.

Table III lists apparent quenching parameters for all of the molecules under study when *n*-pentane is used as the additive for comparison with the equivalent parameter for 2-pentanone quenching.

The effect of various pressures of additive upon the fluo-

TABLE III: Comparison of Rate Constants for Various Aromatic Compounds Quenched by 2-Pentanone and *n*-Pentane

Compound	$10^{10}k_Q$, M^{-1} sec^{-1} (2-pentanone)	$10^{10}k_Q$, M^{-1} sec^{-1} (*n*-pentane)
Benzene	14.6	0.12
Toluene	19.5	0.26
o-Xylene	36.8	0.24
m-Xylene	31.1	0.17
p-Xylene	36.5	0.26
Benzyl fluoride	21.1	0.40
o-Fluorotoluene	21.0	0.54
m-Fluorotoluene	17.4	
p-Fluorotoluene	25.3	0.47
Benzotrifluoride	31.5	0.73
o-Fluorobenzotrifluoride	32.8	1.07
m-Fluorobenzotrifluoride	29.8	0.70
p-Fluorobenzotrifluoride	32.6	0.34
Hexafluoro-*m*-xylene	31.3	0.62
Hexafluoro-*p*-xylene	26.6	0.54
Fluorobenzene	22.4	0.36
o-Difluorobenzene	25.2	0.48
m-Difluorobenzene	18.7	0.00
p-Difluorobenzene	25.8	0.78
1,2,4-Trifluorobenzene	41.9	0.58
1,3,5-Trifluorobenzene	35.1	1.50
1,2,3,4-Tetrafluorobenzene	27.0	0.45
1,2,3,5-Tetrafluorobenzene	24.5	0.35
1,2,4,5-Tetrafluorobenzene	54.4	2.13
Pentafluorobenzene	16.9	0.32
Hexafluorobenzene	16.3	0.85

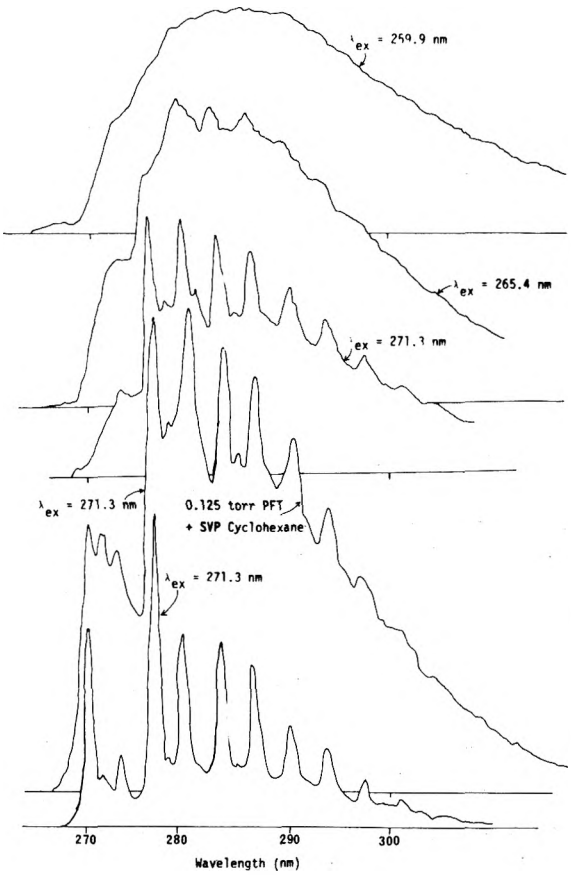

Figure 4. *p*-Fluorotoluene fluorescence spectra at pressures 0.125 (bottom spectrum) and 2.0 Torr (all others).

rescence spectrum of one of the aromatic molecules, *p*-fluorotoluene, is shown in Figure 4.

TABLE IV: Diffusion Coefficients of Some Ground-State Aromatic Molecules at 20°

Compound	ln *A*	*S*	D_{12}	$10^8\sigma_A$,[a] cm
Benzene	−13.59	1.921	0.060	5.63
Toluene	−13.70	1.916	0.052	6.15
o-Xylene	−15.21	2.130	0.038	7.64
m-Xylene	−14.45	2.007	0.041	7.76
p-Xylene	−13.67	1.879	0.044	6.94
Benzyl fluoride	−16.52	2.356	0.037	7.85
m-Fluorotoluene	−13.46	1.861	0.049	6.36
p-Fluorotoluene	−15.29	2.153	0.040	7.35
Benzotrifluoride	−14.19	1.962	0.041	7.02
o-Fluorobenzotrifluoride	−16.71	2.372	0.033	8.16
m-Fluorobenzotrifluoride	−15.38	2.157	0.038	7.46
Hexafluoro-*m*-xylene	−16.95	2.388	0.029	8.91
Hexafluoro-*p*-xylene	−14.12	1.925	0.036	7.56
o-Difluorobenzene	−15.64	2.226	0.043	7.01
m-Difluorobenzene	−14.60	2.048	0.045	6.79
1,2,4-Trifluorobenzene	−13.60	1.890	0.050	6.14
1,3,5-Trifluorobenzene	−15.29	2.162	0.042	6.96
Hexafluorobenzene	−16.38	2.320	0.035	8.61

[a] For method of calculation see text.

TABLE V: Values of the Spectral Overlap Integrals for the Quenching of the Various Aromatic Compounds by 2-Pentanone and Biacetyl for the Förster and Dexter Mechanisms

	2-Pentanone		Biacetyl	
Compound	Förster spectral overlap	Dexter spectral overlap	Förster spectral overlap	Dexter spectral overlap
Benzene	1.00	1.00	1.00	1.00
Toluene	0.99	0.97	0.96	0.93
o-Xylene	0.99	0.96	0.98	0.94
m-Xylene	0.95	0.97	0.90	0.94
p-Xylene	0.99	0.96	0.94	0.94
Benzyl fluoride	0.99	0.97	0.96	0.94
o-Fluorotoluene	0.97	0.95	0.95	0.93
m-Fluorotoluene	0.97	0.95	0.94	0.92
p-Fluorotoluene	0.97	0.89	0.92	0.84
Benzotrifluoride	0.97	0.98	0.98	0.99
o-Fluorobenzofluoride	0.96	0.88	0.86	0.79
m-Fluorobenzotrifluoride	0.94	0.86	0.83	0.75
p-Fluorobenzotrifluoride	0.94	0.86	0.94	0.76
Hexafluoro-*m*-xylene	0.96	0.98	0.98	1.01
Hexafluoro-*p*-xylene	0.96	0.97	0.97	0.96
Fluorobenzene	0.97	0.98	0.98	0.99
o-Difluorobenzene	0.94	0.96	0.95	0.98
m-Difluorobenzene	0.94	0.97	0.98	1.02
p-Difluorobenzene	0.97	0.92	0.91	0.86
1,2,4-Trifluorobenzene	0.95	0.92	0.93	0.90
1,2,5-Trifluorobenzene	0.95	0.91	0.95	0.92
1,2,3,4-Tetrafluorobenzene	0.93	0.94	0.88	0.89
1,2,3,5-Tetrafluorobenzene	0.93	0.93	0.95	0.92
1,2,4,5-Tetrafluorobenzene	0.93	0.96	0.95	0.91
Pentafluorobenzene	0.94	0.94	0.95	0.89
Hexafluorobenzene	0.94	0.93	0.95	0.91

Table IV lists the cross sections for ground-state aromatic molecules where measured for a variety of the molecules studied here. The cross sections tabulated were obtained from diffusion coefficients, measured in argon, making the assumption that the intermolecular aromatic–argon interaction is the same for all aromatics, and thus

TABLE VI: Rate Parameters for the Aromatic Compounds Quenched by 2-Pentanone and Biacetyl

Compound	λ_{ex}, nm	τ_F,[a] nsec	Φ_F[a]	$10^6 k_R$,[a] sec^{-1}	2-Pentanone[b] $10^{10}k_Q$, M^{-1} sec^{-1}	2-Pentanone[b] $10^{-16}\sigma_Q^2$, cm^2	2-Pentanone[b] σ_{QF}^2	Biacetyl[b] $10^{10}k_Q$, M^{-1} sec^{-1}	Biacetyl[b] $10^{-16}\sigma_Q^2$, cm^2	Biacetyl[b] σ_{QF}^2
Benzene	253.7	77.0	0.18	2.46	14.6	18.4	18.4	12.4	15.8	15.8
Toluene	267.0	56.0	0.30	5.36	19.5	28.1	28.3	24.9	31.2	32.6
o-Xylene	269.5	52.0	0.38	7.31	36.8	53.3	53.8	33.4	48.4	49.4
m-Xylene	270.5	49.0	0.35	7.14	31.1	45.0	47.4	27.2	39.4	43.8
p-Xylene	272.5	44.0	0.52	11.80	36.5	52.9	53.4	33.0	47.8	51.4
Benzyl fluoride	265.0	38.6[c]	0.16[d]	4.15	21.0	31.0	31.3	25.7	37.7	39.3
o-Fluorotoluene	266.5	10.5[e]	0.28[c]	27.00	21.0	30.9	31.8	29.5	43.0	45.5
m-Fluorotoluene	267.1	12.5[e]	0.33[c]	26.00	17.4	26.2	27.0	30.1	43.7	46.4
p-Fluorotoluene	271.2	18.4[e]	0.65[c]	36.00	25.3	37.8	39.0	33.8	49.1	53.6
Benzotrifluoride	264.4	19.0	0.16	8.50	31.5	43.3	44.6	14.8	20.2	20.6
o-Fluorobenzotrifluoride	267.4	6.5[e]	0.30[c]	46.00	32.8	54.0	56.0	27.3	45.0	52.3
m-Fluorobenzotrifluoride	267.1	6.4[e]	0.30[c]	47.00	29.8	49.0	51.9	26.6	44.0	53.3
p-Fluorobenzotrifluoride	271.2	16.2[e]	0.13[c]	7.80	32.6	53.7	57.1	29.3	48.5	51.6
Hexafluoro-*m*-xylene	265.9	20.4[e]	0.18[c]	8.60	31.3	45.2	47.2	23.0	33.2	33.8
Hexafluoro-*p*-xylene	266.8	8.6[e]	0.21[c]	25.00	26.6	38.4	40.1	16.9	24.4	25.2
Fluorobenzene	265.0	9.5	0.22	23.00	22.4	31.7	32.7	21.5	27.4	27.9
o-Difluorobenzene	264.5	5.5	0.15	29.00	25.2	35.7	38.0	12.6	16.4	17.2
m-Difluorobenzene	264.0	6.0	0.16	27.00	18.7	26.5	28.2	10.9	14.2	14.5
p-Difluorobenzene	272.5	8.0	0.50	62.50	25.8	36.5	37.6	19.5	25.4	28.0
1,2,4-Trifluorobenzene	270.0	3.1[c]	0.36	116.10	41.9	55.9	58.7	16.5	22.0	23.7
1,3,5-Trifluorobenzene	264.0	3.9[c]	0.039	10.00	35.1	46.9	49.6	30.9	41.3	43.3
1,2,3,4-Tetrafluorobenzene	264.0	1.3[c]	0.19	146.20	27.0	36.1	38.7	16.9	22.6	25.7
1,2,3,5-Tetrafluorobenzene	268.0	1.2[c]	0.029	24.20	24.5	32.8	35.2	18.2	24.8	26.1
1,2,4,5-Tetrafluorobenzene	273.0	2.0[c]	0.34	170.00	54.4	72.8	78.6	57.5	78.3	82.4
Pentafluorobenzene	270.0	1.6	0.025	15.60	16.9	23.7	25.3	25.8	36.2	38.0
Hexafluorobenzene	270.0	1.5	0.010	6.70	16.3	22.9	24.4	22.0	30.8	32.4

[a] Data taken from ref 24 unless stated otherwise. [b] Data not already presented taken from ref 24. [c] Reference 14. [d] R. G. Brown and D. Phillips, unpublished data. [e] Reference 13.

$$(\sigma_{12}^{a})^2/(\sigma_{12}^{b})^2 = (D_{12}^{a}/D_{12}^{b})(\mu^{a}/\mu^{b})^{1/2} \quad (6)$$

where $\sigma_{12}^{a(b)} = \frac{1}{2}(\sigma_A^{a(b)} + \sigma \text{ argon})$, D_{12} = diffusion coefficient of a(b) through argon, μ = reduced mass, and σ_A(benzene) = 5.63 Å and σ_A (argon) = 3.41 Å.

In Table V values for the Förster and Dexter spectral overlaps are given. These were calculated from consideration of the fluorescence emission spectrum of the donor and the absorption spectrum of the acceptor (examples of which are given in Figure 5) and standardized against a value of unity for benzene. As found by Breuer and Lee with cyclopentanone,[7] the value of these integrals varied little over the range of compounds studied, usually remaining less than 10% below the value for benzene. This is not surprising considering the excellent donor–acceptor spectral overlap.

In Table VI the quenching parameters for the compounds being studied are collected. σ_Q^2 is the quenching cross section derived from k_Q by the relationship

$$\sigma_Q^2 = k_Q(8\pi kt)^{-1/2}\mu^{1/2} \quad (7)$$

μ being the reduced mass of the donor and acceptor. This has been divided by the Förster spectral overlap integral to produce σ_{QF}^2.

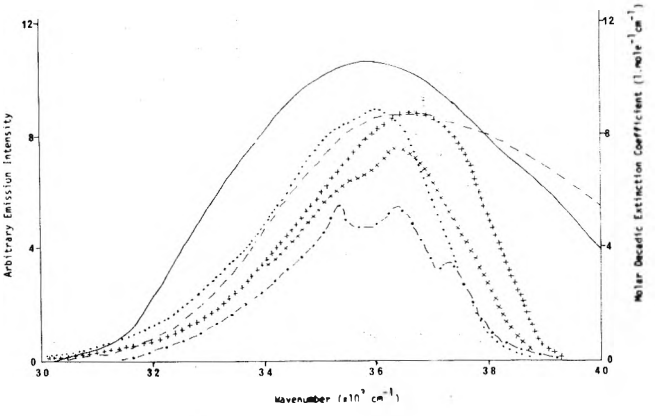

Figure 5. Examples of the spectral overlap between 2-pentanone (—) and biacetyl (- - - -) and various aromatics (benzene (- · - · - ·), *o*-fluorotoluene (· · · ·), *m*-difluorobenzene (+ + +), and hexafluoro-*p*-xylene (× × ×)).

Discussion

The results of the experiments above indicate that the first excited singlet states of the substituted benzenes are quenched efficiently by the ketone species 2-pentanone and biacetyl. It remains therefore to determine by what mechanism such quenching occurs. The energy levels of the first excited singlet state of 2-pentanone, and the second excited singlet state of biacetyl (3.7 and 4.1 eV, respectively), are such that exothermic singlet–singlet energy transfer from all of the aromatic donor molecules to these ketones is possible, and the good spectral overlap between donor fluorescence and acceptor absorption (see Figure 5 for examples) would further indicate that this is a probable mechanism.

In the absence of observation of some property characteristic of the excited singlet states of the ketone molecules (*e.g.*, fluorescence, decomposition), however, it cannot be *proved* that this is the quenching mechanism. In the present case energy transfer is *assumed* because of favorable energetics and spectral distributions, and because of the similarity of the observed quenching characteristics to those of other substituted benzenes by cyclopentanone and

pyrazoline where energy transfer has been definitely established.[7]

Before proceeding to a discussion of the nature of the electronic energy transfer mechanism, it is necessary to consider what effect collisional vibrational redistribution and relaxation might have upon the molecules considered here. Certainly for benzene at very low pressures it has been shown that vibrational relaxation[16] can have an important effect, since change in the nature of the emitting levels can cause quantum yield and lifetime changes, which must not be confused with changes due to electronic quenching. There are important differences between the experimental conditions used in those experiments and in the present case however. In the study on the effects of competition between electronic relaxation and vibrational relaxation of single vibronic levels of benzene, it is important to realize that only one fluorescence band was monitored which was characteristic of the initially populated level of the singlet state. The "quenching" parameters quoted therefore refer to the relaxation only of the initial state, and the subsequent fate of other vibronic levels populated by vibrational relaxation is ignored. In the present case, total fluorescence is monitored, and vibrational relaxation effects would be expected to have a minimal effect on quenching parameters measured here, provided that the initial states populated upon absorption do not differ appreciably from a relaxed system. There is evidence to support this argument. It can be seen from Table III that the apparent quenching caused by *n*-pentane, which must in fact be due to vibrational relaxation, is for most molecules only a few per cent of that caused by 2-pentanone. Moreover, results for quenching of various aromatic molecules obtained by the method of monitoring relative quantum yields are within 10% of those obtained by monitoring fluorescence decay times directly, Table II. Since in the former case measurement is made of the quantity Φ_f which is a ratio of rate constants

$$\Phi_f = \frac{k_R}{k_R + k_{NR} + k_Q[Q]}$$

and in the latter case, of τ, where

$$\tau^{-1} = k_R + k_{NR} + k_Q[Q]$$

should vibrational relaxation to states with very different values of k_R and k_{NR} be of importance, it would not be expected that the two different sets of measurements would yield the same result within experimental error. Finally, it is evident that at the comparatively high pressures of aromatic molecule used in these experiments, vibrational relaxation to the Boltzmann distribution is almost complete. For many molecules, the initial step in this process appears to be the fast unimolecular redistribution of vibrational energy from the optically pumped level to the set of isoenergetic levels in the singlet state which are inaccessible from the ground state because of symmetry restrictions or unfavorable Franck–Condon factors.[17] This is followed by collisional relaxation. The effects are illustrated in Figure 4 for *p*-fluorotoluene. In the lower diagram, the fluorescence spectrum arising from the zero-point level of the first excited singlet state is shown to be highly structured under isolated molecule conditions. In the presence of saturated vapor pressure of cyclohexane, and excitation in the 0–0 band, a dense continuum results, with some band structure superimposed. It is evident that the envelope of the fluorescence resulting from the relaxed molecule is very similar to that resulting from excitation of 2 Torr of *p*-fluorotoluene above, except that resonance bands are reduced in intensity because of the effects of reabsorption. For excitation at 265.4 nm at 2 Torr pressure (used in the present quenching study), the envelope differs a little from that obtained for excitation of the same pressure at 271.3 nm, in that band maxima are less prominent, but it is evident that the effects of collisional relaxation would be expected to be small for excitation at this wavelength. For excitation to higher vibrational levels, the effects would be more dramatic, and a discussion of relaxation in such compounds for higher energy excitation has been given earlier.[18] We thus conclude that for the molecules studied here in which excitation near the zero–zero band and comparatively high pressures of aromatic molecule are used, the observed reduction in quantum yield of fluorescence is accounted for to an extent not less than 90% but in most cases almost exclusively by electronic quenching.

The magnitude of the quenching cross sections shown in Table VI clearly indicates an efficient transfer process. It is necessary to interpret the variation in cross sections in the present case. For a collisional short-range process *via* the exchange mechanism, the kinetic theory of gases provides a convenient basis for discussion. As Breuer has pointed out,[19] the value of σ_d for gas kinetic collisions can be obtained for the Lennard-Jones 6–12 potential from viscosity measurements, and for benzene, toluene, and mesitylene the values given[20] are 5.628 or 5.270, 5.932, and 7.706, respectively. By assuming that the collisional cross section for donor–acceptor pairs σ_{da} is given by $(\sigma_a + \sigma_d)/2$, and making reasonable guesses at σ_a, realistic gas-kinetic cross sections can be obtained. Thus for cyclopentanone as the acceptor with the three donors mentioned above, gas-kinetic cross sections σ_{da}^2 have been given as 30, 33.5, and 44 $\times$ 10^{-16} cm^2, respectively.[19] The cross sections obtained from diffusion coefficient measurements in the present work are given in Table IV. It is clear that the effects of size of the aromatic molecule can be large, and that cross sections up to twice that for bezene could result from such effects. For the results of quenching of the trifluoromethylbenzenes, the variation in quenching cross section appears to correlate quite well with the size of the molecule, and this may partly account for the effects in the fluorotoluenes and methylbenzenes. In the case of the fluorobenzenes, however, inspection of Table VI reveals that some of the larger members of the series have the smallest quenching rate constants, and thus size appears not to be the only significant factor in determining quenching efficiency. Breuer and Lee[7] have interpreted similar results in terms of contributions to the overall quenching efficiency of long-range dipole–dipole interactions. Lin has shown that exchange and resonance interactions additively result in the overall cross section.[6] Lee has shown that dipole–dipole interactions are revealed by a correlation of quenching efficiencies, corrected for spectral overlap, with the radiative rate constant of the donor molecule. Before testing this for the case of the fluorobenzenes and methylbenzenes, it is as well to comment upon the accuracy of estimates of k_R, which are obtained by fluorescence decay time measurement and quantum yields. For some of the fluorinated benzenes used in this study, measured decay times are very short, and thus inaccuracies can be large. In order to provide a check on the results, we compare measured values of k_R with those anticipated on the basis of calculations of Petruska,[21] considering the second-order inductive effect of the sub-

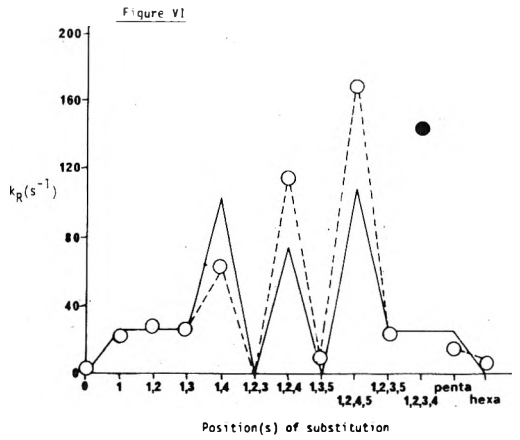

Figure 6. Correlation of the radiative rate constant with theory for fluorobenzenes in the gas phase. The solid line represents the variation of the values predicted from analysis of the second-order inductive effect by Petruska (ref 21) and the experimental values are the circles joined by the dashed line. The abberant value for 1,2,3,4-tetrafluorobenzene is the filled circle.

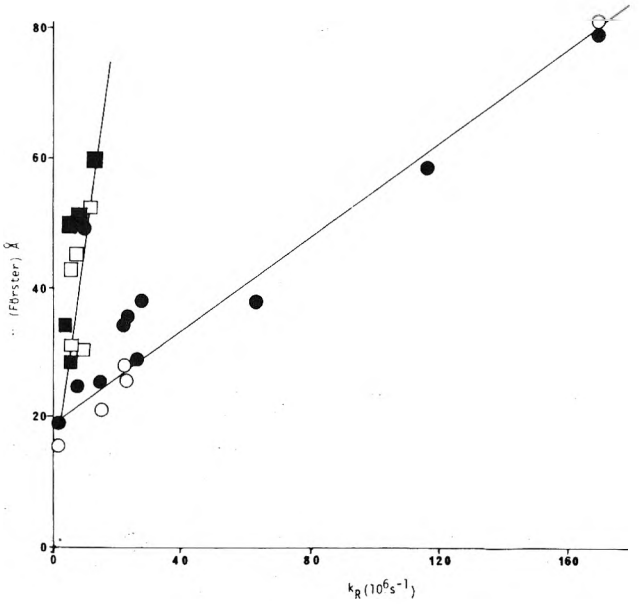

Figure 7. Variation of σ_{QF}^2 with k_R for the fluorobenzenes (circles) and the methylbenzenes (squares). Biacetyl values are open points and 2-pentanone filled.

stituent on the oscillator strength for the radiative transition. Despite the simplicity of the treatment, excellent correlations have been found for the methylbenzenes.[22,23] That for the fluorobenzenes is shown in Figure 6. It can be seen that the expected pattern is approximately obtained, with one notable exception, that of 1,2,3,4-tetrafluorobenzene, for which the measured rate constant differs by more than a factor of 6 from that expected on the basis of the simple theory. It seems justifiable on this basis to ignore the results obtained for this compound.

In Figure 7 we show the value of the cross section for quenching of the methylbenzenes and fluorobenzenes by 2-pentanone and biacetyl corrected for spectral overlap as a function of the radiative rate constant of the benzene molecule. Despite the scatter in the data, some evidence of correlation is present, but the relationship is not universal, since data for the methyl- and fluorobenzenes fall on distinctly different lines, which may reflect the effect of dif-

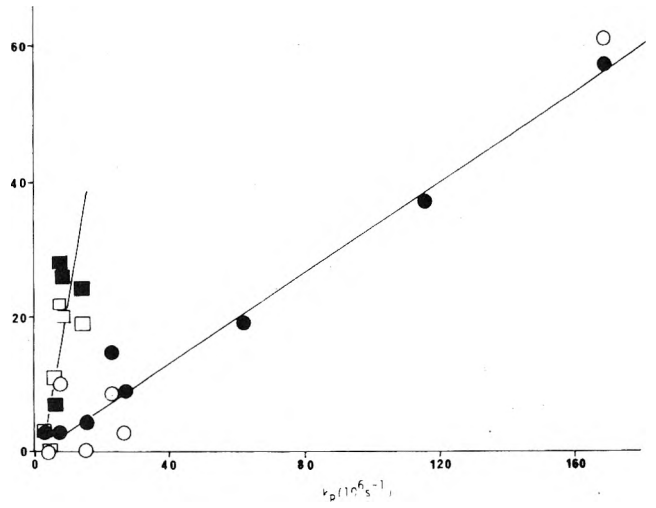

Figure 8. Variation of $(\sigma_{QF}^2 - \sigma_Q^2(\text{oxygen}))$ with k_R for the fluorobenzenes (circles) and methylbenzenes (squares). Biacetyl values are open points and 2-pentanone filled.

ferent sizes of the substituent group in each case. One may attempt to account for the size factor by a consideration of oxygen quenching parameters.[14] The quenching of fluorescence of benzene by molecular oxygen has been accounted for by the overall process 8 and application of the Wigner

$$^1A + {}^3O_2 \longrightarrow {}^3A + {}^3O_2 \qquad (8)$$

spin conservation law for the exchange mechanism reveals that this process has a spin statistical factor of unity. Since long-range effects cannot occur in this case, it may be taken that the rate constant for quenching by oxygen represents the maximum value for the exchange interaction. Cross sections for quenching of the substituted benzenes used here by oxygen have been measured,[14] and it was shown that for aromatic molecules with an ionization potential of less than 9.0 eV quenching occurs with a gas kinetic rate constant. For aromatic molecules with ionization potential greater than 9.0 eV, the oxygen quenching is less efficient. The average value of the cross section for quenching by oxygen of the aromatic molecules of low ionization potential is 21.7×10^{-16} cm^2, which is close to the intercept value shown in Figure 7. If we therefore take the oxygen quenching cross section as representing the magnitude of the exchange interaction, using the average value of 21.7×10^{-16} when dealing with aromatic molecules of large ionization potential, subtraction[6] of this value from the measured cross sections for quenching by 2-pentanone and biacetyl should give a measure of the contribution to overall efficiency of the long-range process, and this should correlate with k_R for the donor. The results of this procedure are shown in Figure 8, from which it can be seen that within the limits of experimental error, the expected correlation is observed.

These data provide the only evidence in all compounds studied that long-range effects may be of importance, since in all other cases the range of values of k_R is small, and variation of molecular size large. For the fluorobenzenes, however, molecules with a large range of values of k_R are available within this series. It is noticeable that differences in cross sections for quenching by 2-pentanone and oxygen of pentafluorobenzene and hexafluorobenzene, of large size, but small k_R, are in fact small, suggesting that long-

range effects rather than size alone must be invoked in the overall quenching mechanisms in this series of compounds.

Acknowledgments. We wish to thank the Science Research Council and the Royal Society for equipment grants. Helpful discussions with Dr. G. M. Breuer are gratefully acknowledged.

References and Notes

(1) F. Wilkinson, *Quart. Rev., Chem. Soc.*, **20**, 403 (1966).
(2) R. G. Bennett and R. E. Kellogg, *Progr. React. Kinet.*, **4**, 215 (1967).
(3) A. A. Lamola, *Tech. Org. Chem.*, **14**, 17 (1969).
(4) Th. Förster, *Discuss. Faraday Soc.*, **27**, 7 (1959); *Naturwissenschaften*, **33**, 166 (1946).
(5) D. L. Dexter, *J. Chem. Phys.*, **21**, 836 (1953).
(6) S. H. Lin, *Mol. Phys.*, **21**, 853 (1971); S. H. Lin, *Proc. Roy. Soc., Ser. A*, **335**, 51 (1973).
(7) G. M. Breuer and E. K. C. Lee, *Chem. Phys. Lett.*, **14**, 407 (1972).
(8) Kh. Al-Ani and D. Phillips, *J. Phys. Chem.*, **74**, 4046 (1970).
(9) D. Phillips, *J. Chem. Phys.*, **46**, 4679 (1967).
(10) D. Gray and D. Phillips, *J. Phys. Chem.*, **76**, 823 (1972).
(11) D. Phillips, D. Gray, and Kh. Al-Ani, *J. Chem. Soc. A.*, 905 (1971).
(12) G. M. Breuer, P. A. Hackett, D. Phillips, and M. G. Rockley, *J. Chem. Soc., Faraday Trans. 2*, **68**, 1995 (1972), and references therein.
(13) M. G. Rockley and D. Phillips, *J. Phys. Chem.*, **78**, 7 (1974).
(14) R. G. Brown and D. Phillips, *J. Chem. Soc., Faraday Trans. 2*, **70**, 630 (1974).
(15) W. A. Wakeham, and D. H. Slater, *J. Phys. B.*, **6**, 886 (1973).
(16) K. C. Janda, J. M. Koert, and F. S. Wettack, *J. Photochem.*, 1 345 (1973).
(17) M. G. Rockley, Ph.D. Thesis, University of Southampton, 1974.
(18) Kh. Al-Ani and D. Phillips, *J. Phys. Chem.*, **76**, 2967 (1972).
(19) G. M. Breuer, Ph.D. Thesis, University of California, Irvine, 1972.
(20) J. O. Hirschfelder, C. F. Curtiss, and R. B. Bird, "Molecular Theory of Gases and Liquids," Wiley, New York, N.Y., 1964.
(21) J. Petruska, *J. Chem. Phys.*, **34**, 1120 (1961).
(22) A. Reiser and L. Leyshon, *J. Chem. Phys.*, **56**, 1011 (1972).
(23) P. A. Hackett, D. Phillips, and M. G. Rockley, *J. Photochem.*, **2**, 71 (1973–1974).
(24) D. Phillips, *J. Photochem.*, **1**, 97 (1972–1973).

COMMUNICATIONS TO THE EDITOR

Yield of Solvated Electrons in the Aliphatic Alcohols at Picosecond Times

Publication costs assisted by the Medical Research Council of Canada

Following the discovery of hydrated electrons in water, solvated electrons have been studies in a large number of solvents ranging in polarity from the aliphatic alcohols[1] to the hydrocarbons.[2] The yield of solvated electrons, e_{sol}^-, that escape from the local concentration of reactive species along the radiation tracks are called the free ion yield of electrons, $g(e_{sol}^-)_{fi}$. The yields have been measured in many solvents. Recently, the yield of e_{sol}^- in alcohols has been measured in times as short as 5 nsec following a short pulse of radiation.[3] The e_{sol}^- decays in alcohols in nanosecond times are similar to those in water[4-6] in which the 5-nsec e_{sol}^- yields, $g(e_{sol}^-)_{5nsec}$, are considerably higher than the corresponding $g(e_{sol}^-)_{fi}$.[3,4]

The conventional spur diffusion model as developed by Samuel and Magee[7] and improved by Kuppermann[8] and Schwarz[9] has been applied in detail to the radiolysis of water and aqueous solutions. The yield of e_{aq}^- at picosecond times as predicted by this model is not in agreement with the observations.[5,6,10] Modification of the parameters for the model was required to reconcile the discrepancy. It is expected that the radiolysis of alcohols should exhibit similar spur decay patterns as that of water with only minor changes due to the differences in physical properties between alcohols and water. The spur diffusion model has not yet been applied to the alcohols. However, a knowledge of the yield of e_{sol}^- at picosecond times should help to develop any model concerning the radiolysis of alcohols.

When the yield of e_{aq}^- at 30 psec was first determined by Bronskill, *et al.*,[11] and Wolff, *et al.*,[10] the yields of solvated electrons, e_{sol}^-, in simple aliphatic alcohols were also measurred relative to that of e_{aq}^- using extinction coefficients obtained by Sauer, *et al.*[12] The values obtained were 1.6 ± 0.2 in both methanol and ethanol, 1.8 ± 0.2 in 1-propanol, and 1.5 ± 0.2 in 2-propanol.[10] Thus, the apparent initial yields of e_{sol}^- in alcohols were much lower than in water. However, after these preliminary results were published, new observations in our laboratory and new data from literature were available and we decided to study the picosecond absorption spectra of e_{sol}^- and to obtain a more accurate value of $g(e_{sol}^-)$ at picosecond times.

Recently, we were able to study absorption signals in the infrared up to 1100 nm using a solid state detector, PIN-10, from United Detector Technology Inc. The spectral region used for previous picosecond studies of Bronskill, *et al.*,[11] and Wolff, *et al.*,[10] using photomultipliers was limited to wavelengths of about 250 to about 750 nm. In this wavelength region, the spectra in water and aliphatic alcohols at the time period from 30 to 350 psec are very similar to those observed at microsecond times. Because of this, they concluded that the e_{aq}^- and e_{sol}^- are formed by 30 psec. However, studies in the 800–1100-nm region shown here revealed that while the spectrum of e_{aq}^- at 30 psec resembles that in microsecond times, it was not true for the e_{sol}^- in alcohols. For all the alcohols studies, namely, methanol, ethanol, 1-propanol, and 2-propanol, there were large absorp-

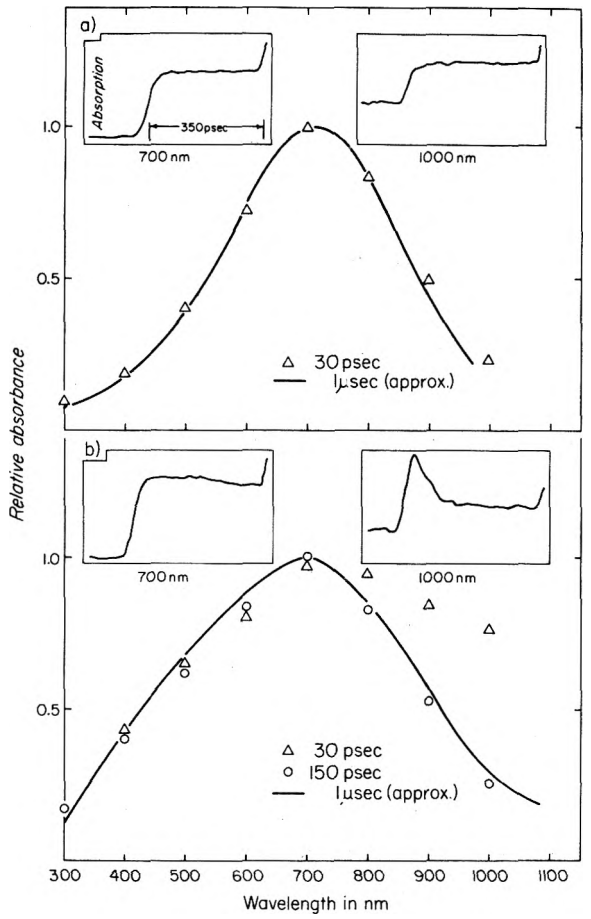

Figure 1. Picosecond spectral changes for e_{sol}^- for water (a) and ethanol (b) at room temperature. The microsecond spectra are taken from L. M. Dorfman and M. S. Matheson, *Advan. Chem. Ser.*, **No. 50,** 38, 46 (1968).

tion signals in the infrared region after 30 psec. These signals decay in a time of about 30–250 psec, leaving absorption signals whose spectra resemble those of the normal e_{sol}^- in these alcohols. Similar spectral changes have been obtained in the cold alcohols at nanosecond times by Baxendale and Wardman.[13,14] The time-dependent spectral changes for ethanol and water are shown in Figure 1.

These fast decaying signals in the infrared wavelength have been attributed to a precursor of e_{sol}^-, e_{damp}^-, in these alcohols.[13,14] These e_{damp}^- are presumably electrons in a solvent environment in which the neighboring molecules have not oriented to give the electron the most stable state. In other words, the electrons are in shallow traps in the medium. When the neighboring molecules orient themselves, spectral changes take place until the solvated electrons are stabilized into deeper traps.

Since the absorption spectra at 30 psec of the radiolytic species for these alcohols were not those of the normal e_{sol}^- in these alcohols, determination of g values of e_{sol}^- at 30 psec was obviously not possible. However, the initial spectra transform quickly into those of e_{sol}^- within 350 psec in all these alcohols, so we could determine the $g(e_{sol}^-)$ after the spectral changes were over. Typical kinetic traces are shown in Figure 2. It is observed that the spectral changes were completed in 150 psec in both methanol and ethanol and in 250 psec in 1-propanol and 2-propanol, so determination of g values could be made at these times. Hydrated electron dosimetry was used assuming an $\epsilon_{575}(e_{aq}^-)$ of 1.04

TABLE I

Solvent	Time, psec	Rel absorption[a] signals	$g(e_{sol}^-)$ using ϵ^b from ref 9	$g(e_{sol}^-)$ using ϵ^b from ref 12
H_2O	30	1.00		
Methanol	150	0.77	2.0 ± 0.2	3.3 ± 0.3
Ethanol	150	0.61	2.0 ± 0.2	3.2 ± 0.3
1-Propanol	250	0.59	2.3 ± 0.2	
2-Propanol	250	0.48	1.9 ± 0.2	

[a] The absorption signals at 575 nm of e_{sol}^- divided by signals of e_{aq}^-, and corrected for the dosimetry noted in the text. [b] The observed g values in the alcohols are relative to value of 4.0/100 eV for H_2O at 30 psec.[10]

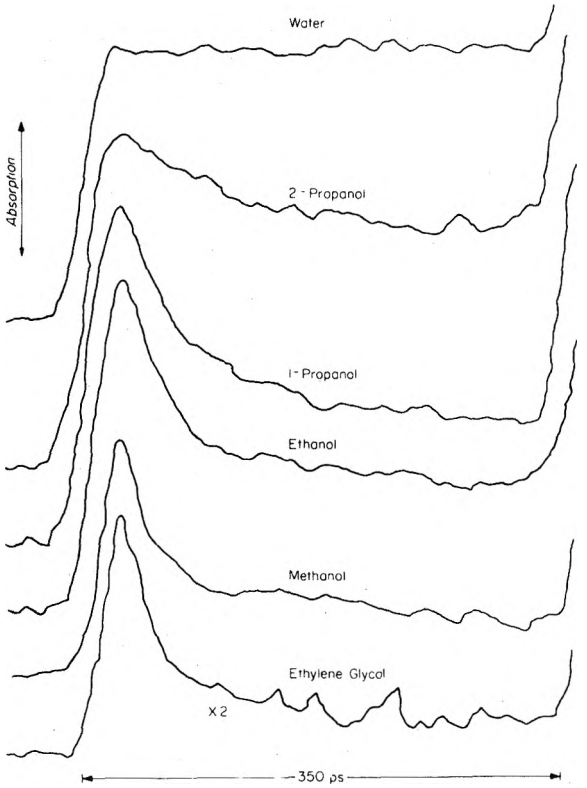

Figure 2. Kinetic traces of the absorption signals in various media at 1000 nm at room temperature. Since all these signals do not decay back to zero at 350 psec, they all ride on some background absorptions which are different from solvent to solvent.

$\times 10^4\ M^{-1}\ cm^{-1}$ [15] and $g(e_{aq}^-)$ at 30 psec = 4.0 ± 0.2.[10] As the dose absorbed in the solvents is approximately proportional to the number of electron per unit volume, corrections for the electron density per unit mass and the physical density of the solvents were made. It should be noted that in one early determination of $g(e_{sol}^-)$ at 30 psec,[10] it appears that the physical density corrections have not been included in the calculations. Consequently, these yield values were ~20% lower than the present values in this letter.

There is still some uncertainty, however, in the values of the extinction coefficients of the solvated electrons in some alcohols. Using electron scavengers such as biphenyl and phenylanthracene in microsecond pulse radiolysis, Sauer, *et al.*,[12] measured $g(e_{sol}^-) = 1.1$, $\epsilon_{575}(e_{sol}^-)$ $1.55 \times 10^4\ M^{-1}\ cm^{-1}$, in methanol and $g(e_{sol}^-) = 1.1$, $\epsilon_{575}(e_{sol}^-)$ $1.2 \times 10^4\ M^{-1}\ cm^{-1}$, in ethanol. Recently, using observations from conductivity and optical measurements, Jha, *et al.*,[16] sug-

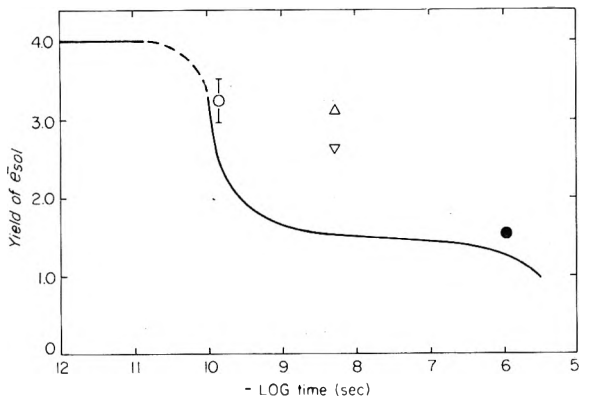

Figure 3. Yield of e_{sol}^- in ethanol as a function of time. The solid line is based on the calculations of Freeman.[13] The experimental observations are: O, this work; △, ref 3; ▽, J. H. Baxendale and P. Wardman, *Chem. Commun.*, **429** (1971) as quoted in ref 3 and 13; ●, ref 16.

gested that the free ion yield of e_{sol}^- in methanol and ethanol should be 2.0 and 1.7, respectively. These values are in good agreement with the nonhomogeneous kinetic model[17] for the reactions of ions produced during radiolysis of liquids. Similar values have also been reported in other laboratories using conductivity techniques.[18-20] Consequently, Jha, *et al.*,[16] proposed a new set of extinction coefficients for e_{sol}^-: $\epsilon_{\lambda_{max}}$ $(10.2 \pm 0.4) \times 10^3\ M^{-1}\ cm^{-1}$ and $\epsilon_{\lambda_{max}}$ $(9.4 \pm 0.4) \times 10^3\ M^{-1}\ cm^{-1}$ in methanol and ethanol, respectively. However, new extinction coefficients for e_{sol}^- in 1-propanol and 2-propanol have not been proposed. With this uncertainty in the extinction coefficients of e_{sol}^-, the g values measured using the extinction coefficients of both Sauer, *et al.*,[12] and Jha, *et al.*,[16] are summarized in Table I.

Freeman's nonhomogeneous kinetic model[17] has been applied to the estimation of lifetimes of solvated electrons in water, ethyl alcohol, acetone, and cyclohexane. However, his calculation was somewhat semiempirical in which he assumed a tight spacial distribution of ions formed by the radiation. A comparison with the observed yield values in ethanol has been made as shown in Figure 3. The total ionization yield has been taken to be 4 as in Freeman's model. It can be observed that the e_{sol}^- yield decreases much less rapidly with time than the model predicts. This discrepancy is similar to the one in water with the spur diffusion model.[5,6,10] In addition, reactive precursors of e_{sol}^- have been observed in the alcohols at room temperature[21] and it appears that an accurate theoretical treatment of the radiolysis of alcohols must include the precursors as well.

Acknowledgments. The authors thank M.J. Bronskill, E. Rasburn, and S.G. Chenery for their suggestions in this work, and A. Worthington for his technical assistance. We also thank, Mr. T. Horrigan and the staff of the Linac Laboratory of the University of Toronto for their cooperation, and the National Research Council for its financial support. The experimental work was supported by the Medical Research Council of Canada and the National Cancer Institute of Canada.

References and Notes

(1) L. M. Dorfman, *Advan. Chem. Ser.*, **No. 50,** 36 (1968).
(2) G. R. Freeman and J. M. Fayadh, *J. Chem. Phys.*, **43,** 86 (1965).
(3) R. R. Hentz and G. A. Kenney-Wallace, *J. Phys. Chem.*, **78,** 1514 (1974).
(4) J. K. Thomas and R. V. Bensasson, *J. Chem. Phys.*, **46,** 4147 (1967).
(5) J. W. Hunt, R. K. Wolff, M. J. Bronskill, C. D. Jonah, E. J. Hart, and M. S. Matheson, *J. Phys. Chem.*, **77,** 425 (1973).
(6) C. D. Jonah, E. J. Hart, and M. S. Matheson, *J. Phys. Chem.*, **77,** 1838 (1973).
(7) A. H. Samuel and J. L. Magee, *J. Chem. Phys.*, **21,** 1080 (1953).
(8) A. Kuppermann, *Proc. Int. Congr. Radiat. Res., 3rd, 1966,* 212 (1967).
(9) H. A. Schwartz, *J. Phys. Chem.*, **73,** 1928 (1969).
(10) R. K. Wolff, M. J. Bronskill, J. E. Aldrich, and J. W. Hunt, *J. Phys. Chem.*, **77,** 1350 (1973).
(11) M. J. Bronskill, R. K. Wolff, and J. W. Hunt, *J. Chem. Phys.*, **53,** 4201 (1970).
(12) M. C. Sauer, S. Arai, and L. M. Dorfman, *J. Chem. Phys.*, **42,** 708 (1965).
(13) J. H. Baxendale and P. Wardman, *Nature (London)*, **230,** 449 (1971).
(14) J. H. Baxendale and R. Wardman, *J. Chem. Soc., Faraday Trans. 1,* **69,** 584 (1974).
(15) E. M. Fielden and E. J. Hart, *Radiat. Res.*, **32,** 564 (1967).
(16) K. N. Jha, G. L. Bolton, and G. R. Freeman, *J. Phys. Chem.*, **76,** 3876 (1972).
(17) G. R. Freeman, *J. Chem. Phys.*, **46,** 2823 (1967).
(18) P. Fowles, *Trans. Faraday Soc.*, **67,** 428 (1971).
(19) J. Rabani, M. Grätzel, and S. A. Chandhri, *J. Phys. Chem.*, **75,** 3893 (1971).
(20) J. Lilie, S. A. Chandhri, A. Mamon, M. Grätzel, and J. Rabani, *J. Phys. Chem.*, **77,** 597 (1973).
(21) K. Y. Lam and J. W. Hunt, *Int. J. Radiat. Phys. Chem.*, in press.
(22) Address correspondence to this author at The Ontario Cancer Institute.

Department of Medical Biophysics **K. Y. Lam*** [22]
University of Toronto **J. W. Hunt**
and the Physics Division
The Ontario Cancer Institute
Toronto, Ontario, Canada M4X 1K9

Received July 10, 1974

Journal of Chemical and Engineering Data

OCTOBER 1974, Vol. 19, No. 4

TABLE OF CONTENTS

■ Supplementary material for this paper is available separately, in photocopy or microfiche form. Ordering information is given in the paper.

Responsible for environmental management and pollution control?

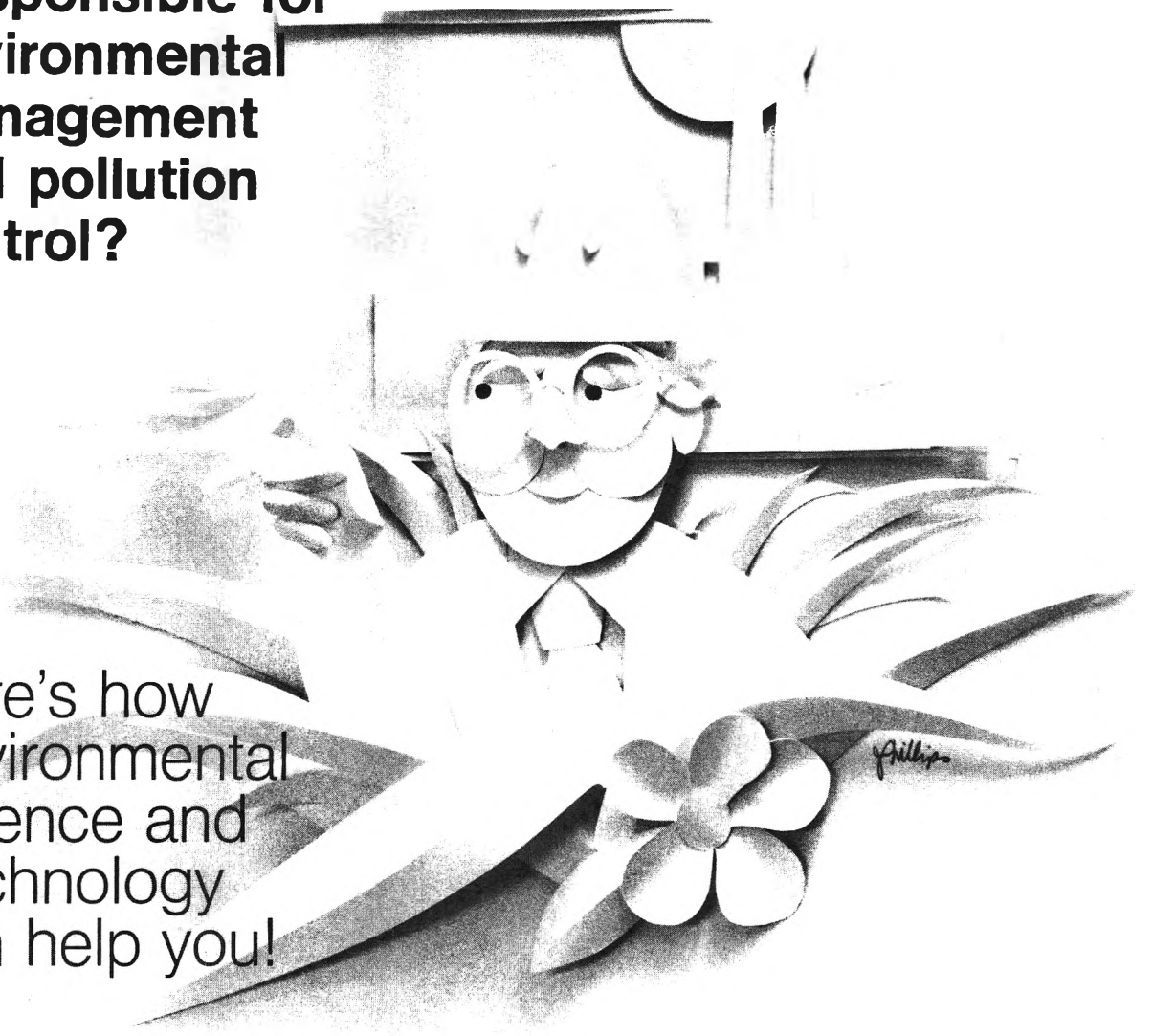

Here's how Environmental Science and Technology can help you!

ES&T brings you the *new technology*. These are the techniques to avoid contamination of air, water, and land. And it brings you up-to-the-minute information of the *economics, laws,* and *feasibility* of many of these new techniques.

Utilizing the American Chemical Society's world-wide contacts, ES&T includes each month:

- ☐ Current government pollution legislation and guidelines.
- ☐ More efficient engineering techniques.
- ☐ Important fundamental research.
- ☐ First word of more productive equipment coming on the market.
- ☐ Case history studies of how others are overcoming the same problems as yours.

Complete the form and mail it back today. You can start benefiting from ES&T's coverage immediately! INCLUDED with your SUBSCRIPTION IS THE VALUABLE *1973-74 POLLUTION CONTROL DIRECTORY.*

Environmental Science & Technology
American Chemical Society
1155 Sixteenth Street, N.W.
Washington, D.C. 20036

	U.S.	**Canada, PUAS	**Other Nations
One Year Subscription:			
*ACS Member:	☐ $ 6.00	☐ $10.00	☐ $11.00
Nonmember:	☐ $ 9.00	☐ $13.00	☐ $14.00
Three Year Subscription:			
*ACS Member:	☐ $15.00	☐ $27.00	☐ $30.00
Nonmember:	☐ $22.00	☐ $34.00	☐ $37.00

☐ Payment enclosed. ☐ Bill me. ☐ Bill company. *Air freight rates available on request.*

Name _____ Position _____

Your Employer _____

Address ☐ Home ☐ Business _____

City _____ State _____ Zip _____

Employer's Business: ☐ Manufacturing ☐ Government ☐ Academic ☐ Other _____

If Manufacturer, Type of Products Produced _____

*NOTE: Subscriptions at ACS member rates are for personal use only. **Payment must be made in U.S. currency, by international money order, UNESCO coupons, U.S. bank draft, or order through your book dealer.

GET THE CHEMTECH HABIT

and you won't be able to break it!

and you won't want to either . . . . because CHEMTECH is the lively, stimulating, innovative magazine that you'll read and use and refer to again and again . . .

You'll keep abreast of your own chemical discipline while being informed about others . . .

You'll be exposed to challenging new viewpoints and plain exciting concepts . . .

You'll hear from specialists and learn about their objectives and problems . . .

You'll have months of enjoyable and valuable reading . . .

and all for a very nominal sum.

You can start the rewarding CHEMTECH habit by just checking and returning the order form below. Sign up for three years and you'll save $14.00 and protect yourself against future price raises during the next three years.

Act today!

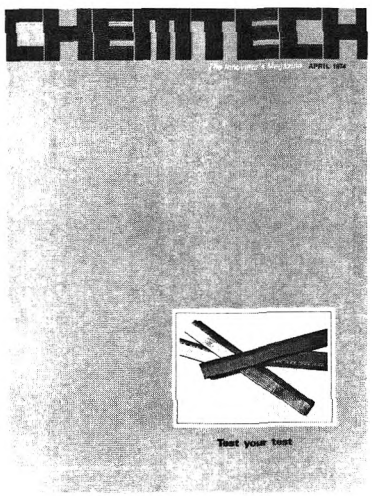

CHEMTECH
American Chemical Society
1155 16th Street, N.W., Wash., D.C. 20036

	U.S.	Canada, PUAS	Other Nations
* ACS Member, 1 year	☐ $9.00	☐ $13.00	☐ $14.00
Student	☐ $4.50	☐ $8.50	☐ $9.50
Nonmember, 1 year	☐ $18.00	☐ $22.00	☐ $23.00
Nonmember, 3 years	☐ $40.00	☐ $52.00	☐ $55.00

Name _____

Address ☐ Home ☐ Office _____

City _____ State _____ Zip _____

☐ Check enclosed ☐ Bill Company ☐ Bill Me

*ACS member rates are for personal use only.